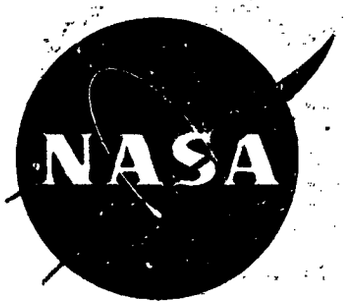

NASA CR-112119-3

EVALUATION OF COATED COLUMBIUM ALLOY HEAT SHIELDS FOR SPACE SHUTTLE THERMAL PROTECTION SYSTEM APPLICATION

VOLUME III

PHASE III FULL SIZE TPS EVALUATION

March 1974

J. W. Baer and W. E. Black

GENERAL DYNAMICS
Convair Aerospace Division

NASA-CR-112119-3

EVALUATION OF COATED COLUMBIUM ALLOY HEAT SHIELDS FOR SPACE SHUTTLE THERMAL PROTECTION SYSTEM APPLICATION

VOLUME III

PHASE III - FULL SIZE TPS EVALUATION

March 1974

By

J. W. Baer and W. E. Black

Prepared Under
Contract NAS1-9793

Prepared by
CONVAIR AEROSPACE DIVISION OF GENERAL DYNAMICS
San Diego, California

for

National Aeronautics and Space Administration
LANGLEY RESEARCH CENTER
Hampton, Virginia

FOREWORD

This report was prepared by Convair Aerospace Division of General Dynamics — San Diego Operation under Contract NAS1-9793 for the National Aeronautics and Space Administration, Langley Research Center, Hampton, Virginia. It was administered under the direction of the Materials Division, Materials Research Branch, with Mr. D. R. Rummler acting as the Technical Representative of the Contracting Officer. The Convair program manager and principal designer through Phase I and Phase II was W. E. Black. Mr. Black served as program manager during Phase III until his resignation. J. W. Baer was appointed program manager for the completion of the contract. Mr. Baer had previously served as deputy program manager and in program process development. Other Convair personnel who participated in this program were R. S. Wilson (structural analysis), A. M. Roberge (thermodynamics analysis), R. W. Gilbert (environmental testing), O. H. Moore (acoustic testing), and G. L. Getline (acoustic fatigue analysis). In addition the subcontract support is acknowledged for W. G. Burnett (Burnett Industries - TPS component machining), L. J. Robles (Electron Beam Welding, Inc., - TPS component welding), L. Sama (HiTemCo - coating application), and S. J. Gerardi (Vac-Hyd Processing Corporation - coating application).

This report covers the Phase III performance period from February 1973 to March 1974.

CONTENTS

FIGURES

Page

TABLES

1 SUMMARY

This report concludes a three-phase study program to develop and evaluate coated columbium alloy heat shields for the reentry environment of a Space Shuttle orbiter. Based on the alloy assessment and selection of Phase I and the material system and heat shield configuration evaluation of Phase II, a full-scale, vehicle-applicable thermal protection system (TPS) was designed into test hardware.

The configuration evaluated herein consisted of one primary heat shield thermally and structurally isolated from the test fixture by eight peripheral guard panels all encompassing an area of approximately 12 ft^2 (1.1 m^2). The TPS consisted of tee-stiffened Cb-752/R-512E heat shields, bi-metallic support posts, panel retainers, and high-temperature insulation blankets. The vehicle primary structure was simulated by a titanium skin, frames, and stiffeners.

Standard manufacturing processes were used to fabricate all of the components. Extensive use was made of electron beam welding which significantly reduced the amount of raw material required when compared with the similar components of Phase II. The total system cost, including heat shields, support system, and insulation, was $500/lb ($1101/kg). The unit weight of the test hardware with Fiberfrax H insulation was 4.88 lb/ft^2 (0.21 kg/m^2) or 19-percent under the limit of 6.0 lb/ft^2 (0.26 kg/m^2) established at the beginning of the program. The unit weight could be further reduced for flight-ready TPS to 4.72 lb/ft^2 (0.199 kg/m^2) when the hardware is sized using the improved thermal properties of Fiberfrax H insulation over Dyna-Flex. When projected for one ship set of 24 heat shields and associated components, a cost of $342/lb ($753/kg) is indicated.

Testing of the nine-panel TPS array consisted of 100 boost acoustic cycles to 158 dB overall sound pressure level (OASPL) and 50 reentry thermal cycles to a programmed 2400°F (1589°K) surface temperature at reduced pressures. The specimen successfully completed 50 pre-thermal and 50 post-thermal acoustic tests without experiencing any failures attributable to the acoustic pressure loading. After completing 50 thermal cycles, the test specimen was determined to be in excellent condition with no problems related to thermal/structural design. Several oxidation sites were evident and were readily identifiable, and were repaired. Components such as retainers, bolts, and heat shields were removed without difficulty enabling inspection, refurbishment, repair or replacement.

Similar to Phase II, the methods of analysis employed proved highly reliable. Calculated margins of safety were verified under acoustic exposure. The temperature distribution analysis was accurate and slightly conservative. With an average heat shield surface temperature at the center of the array of 2408°F (1593°K), the corresponding titanium skin sustained 525°F (547°K).

Clearly, major questions of TPS accessability, refurbishability, and durability have been affirmatively answered during this program. Those problems which did arise during the test program were largely design, manufacturing and quality control omissions, attributed mainly to the emphasis on program cost reduction. Most of these were peculiar to the test specimen and test conditions and have no relationship to flight hardware.

2 INTRODUCTION

The economical development of manned systems for outer space depends on the development of low-cost, lightweight, reliable systems employed on reusable reentry spacecraft. The NASA approach to this development is to provide vehicles capable of earth landings and possessing the aerodynamic maneuvering characteristics of aircraft and yet able to withstand spacecraft reentry temperatures. This system has been designated the Space Shuttle. ...

The key element in the success of these vehicles is the thermal protection system (TPS). It must be capable of withstanding the structural static and dynamic loads as well as dissipating the frictional heat in aerodynamically slowing down the vehicle. One promising TPS concept from a reliability, inspectability, cost, and reusability standpoint utilizes metallic radiative heat shields. It is toward columbium alloys as applied to heat shields operating in the temperature range of 2000 to 2400° F (1366 to 1589° K) that this study has been directed.

The principal objective has been to evaluate coated columbium alloy thermal protection systems by a logical sequence of analytical and experimental investigations involving simulated mission and environmental conditions. These efforts were directed toward the selection, characterization, and design of one material system (i. e., one columbium alloy with one coating), one heat shield configuration, and one support system with insulation. Reported herein are the results of the final phase of this three phase study.

Phase I (Reference 1a) was initiated by selecting a model vehicle with an associated total environment from prelaunch to landing. This vehicle and environment would be the basis for the design conditions, design criteria, and test conditions used throughout the program. This selection was followed by an experimental and analytical evaluation of the properties of the material systems as applied to heat shields. Phase I culminated with the selection of two material systems (Cb-752/R-512E and C-129Y/R-512E) for further application and evaluation in Phase II (Reference 1b). . . .

Phase II consisted of two parts involving two types of panels. Part 1 entailed the analytical investigation of several heat shield configurations. The two most promising concepts were selected for subsize panel fabrication and testing. From this was selected the better performing of the two material systems (Cb-752/R-512E) for further, larger scale evaluation. A complete TPS (i. e., heat shields, support structure, and insulation) was then fabricated for each of the two configurations for testing under hot gas flow and radiant heat with applied loads at reduced pressures with supplemental acoustic testing. Also investigated were the forming, machining, and joining methods to be used for the fabrication of complete thermal protection systems. Based on the total performance of the two TPS configurations, one concept was selected for full-scale, full-size system evaluation in Phase III.

Two types of TPS were designed, fabricated, and tested during Phase III. One was designed for testing in the NASA Langley Research Center Thermal Protection System Facility (TPSTF). This specimen is intended to study the effects of hot gas flow on parallel and transverse heat shield joints. Testing of this specimen will be undertaken independently by NASA after completion of this program. The second specimen was a full-scale, nine-panel configuration representative of an orbiter vehicle lower surface. This specimen was exposed to simulated mission duty cycles consisting of combined thermal and acoustic testing to verify structural adequacy. Phase III demonstrated the structural and thermal adequacy and the manufacturability of full-sized, coated columbium alloy thermal protection systems and provided data necessary to project the performance and cost of these systems for Space Shuttle vehicles.

3 TPS DESIGN

No significant changes were made in TPS configuration as a result of the Phase II test series. Those modifications that were made primarily were for fabrication expediency. Much more use was made of welding in order to minimize the amount of material scrap resulting from the extensive machining employed in the small size TPS fabrication. An exploded assembly view of the heat shield and support system is shown in Figure 3-1.

3.1 Nine-Panel Test Specimen

The nine-panel specimen was designed to completely isolate one panel from extraordinary thermal/structural influence of the holding frame. This heat shield and the two adjacent transverse panels had nominal dimensions 12.00 in. (30.48 cm) by 16.00 in. (40.64 cm). All other panels had modifications of the forward or aft flanges to accommodate the holding frame. The total array was 40.90 in. (103.89 cm) by 54.00 in. (137.03 cm) by 6.43 in. (16.33 cm). The fully assembled nine-panel specimen is shown in Figure 3-2.

Two views of the holding fixture are shown in Figures 3-3 and 3-4. The edge members and clips were formed from cobalt base alloy (HS-188) sheet stock. Simulating the primary structure were titanium alloy (Ti-6Al-4V) skin and stringers, and unalloyed titanium frame members. Standard aerospace assembly methods were used on this fixture.

The support posts separating the heat shields from the primary structure were designed such that the maximum temperature of the cobalt alloy, HS-25 (L-605), lower post was to be 2000° F (1366° K). These posts were internally fitted with discs of blanket insulation to minimize radiant heat transfer. The upper posts were of Cb-752 attached to the lower posts by two dispersion strengthened nickel-20% chromium alloy (TD NiCr) screws. The heat shields are assembled in a shingled manner in the fore and aft directions. A panel is fixed to a center support post at a point at the center of trailing edge and permitted to expand in the forward direction. The center retainer is attached to the posts by a TD NiCr bolt. Tee-member longitudinal edge retainers restrict air passage and permit free expansion of the heat shields and are attached to the corner posts by a TD NiCr bolt. A Cb-752 plug is inserted into each of the six posts and threaded onto the TD NiCr bolt. All of the TD NiCr fasteners were coated with a proprietary aluminide to minimize any potential reaction with the R-512E silicide coating (Si-20Cr-20Fe) of the Cb-752. The system is insulated with 15 layers of nominal 0.25-inch (0.64 cm) thick Fiberfrax H blanket insulation located between the outer heat shield and the skin of the primary structure. The assembly drawing of the nine-panel array (76C0104) and the major component detail drawings (76C0103, 76C0105, 76C0106, and 76C0108) are shown in Figures 3-5, 3-6, 3-7, 3-8, and 3-9.

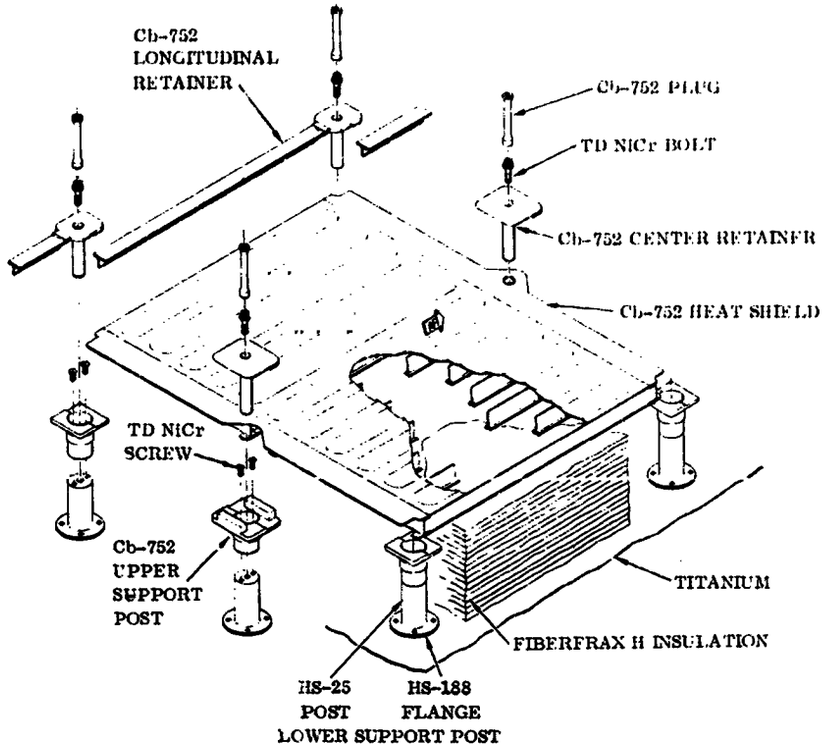

Figure 3-1. Tee-Stiffened TPS Exploded Assembly

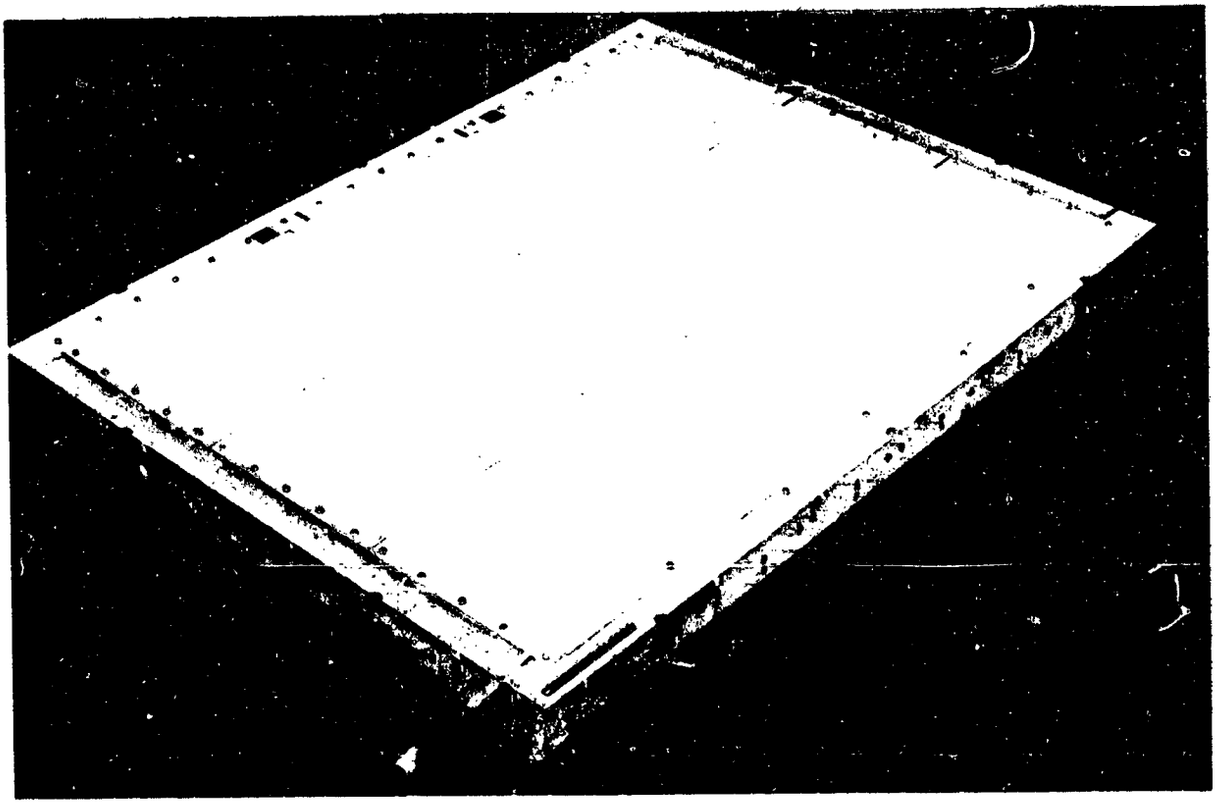

Figure 3-2. Nine-Panel TPS Test Specimen and Holding Fixture (137397)

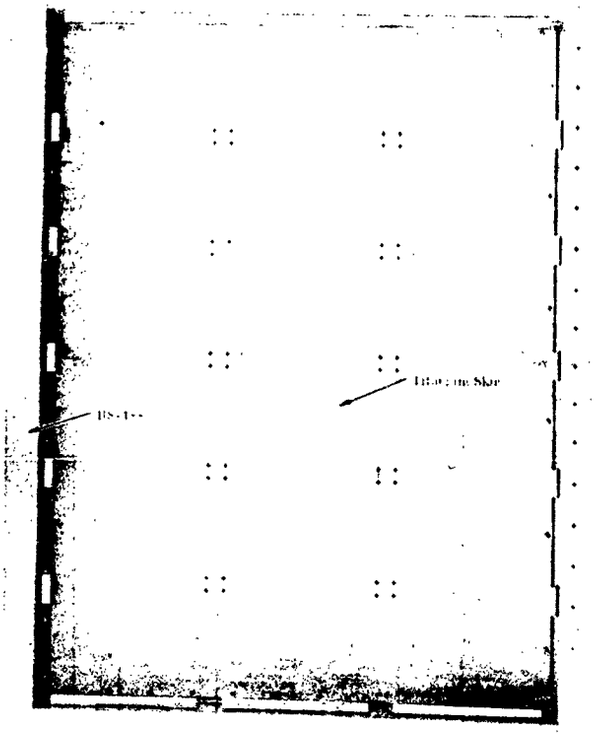

Figure 3-3. View Looking Down on Nine-Panel Array Holding Fixture (133648B)

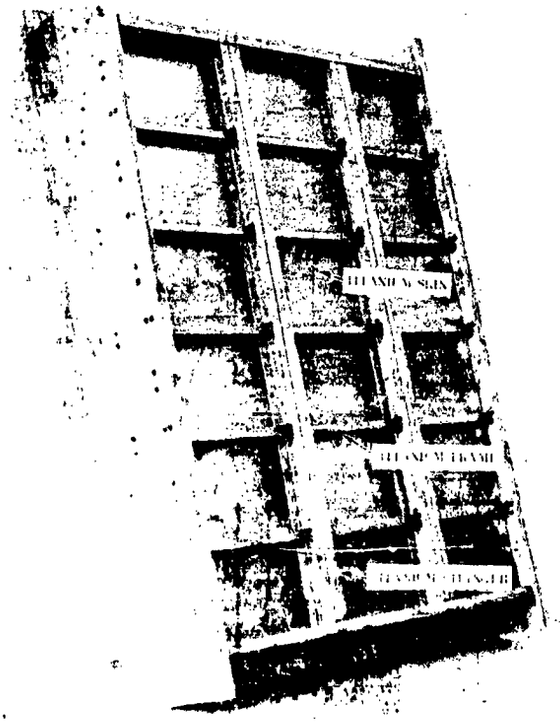

Figure 3-4. Exterior View of Nine-Panel Array Holding Fixture-Cooling Tubes for HS-188 Frame Not Shown (133649B)

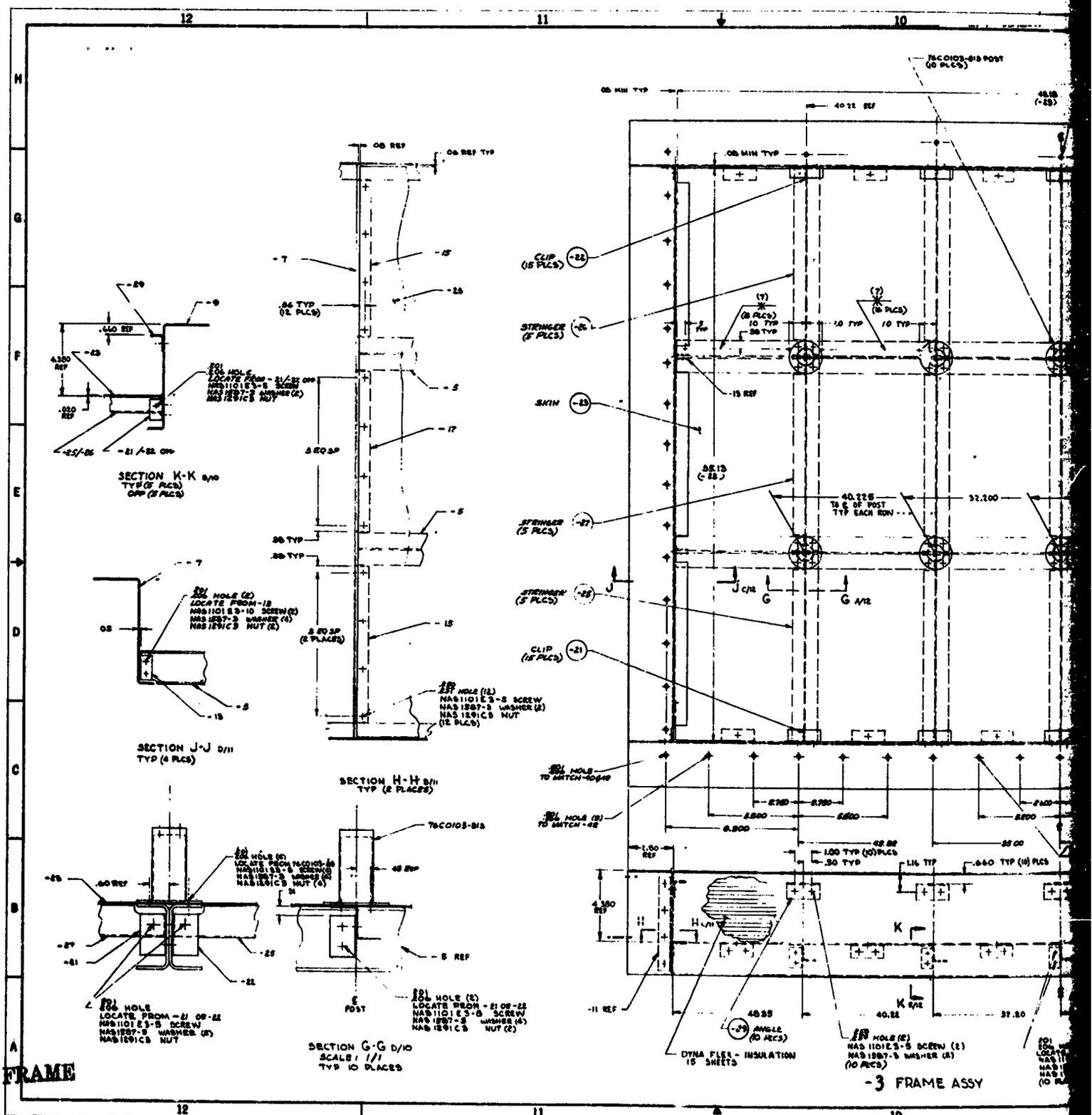

FOLDOUT FRAME

Figure 3-5. Nine-Panel TPS Assembly - Sheet 1 of 2

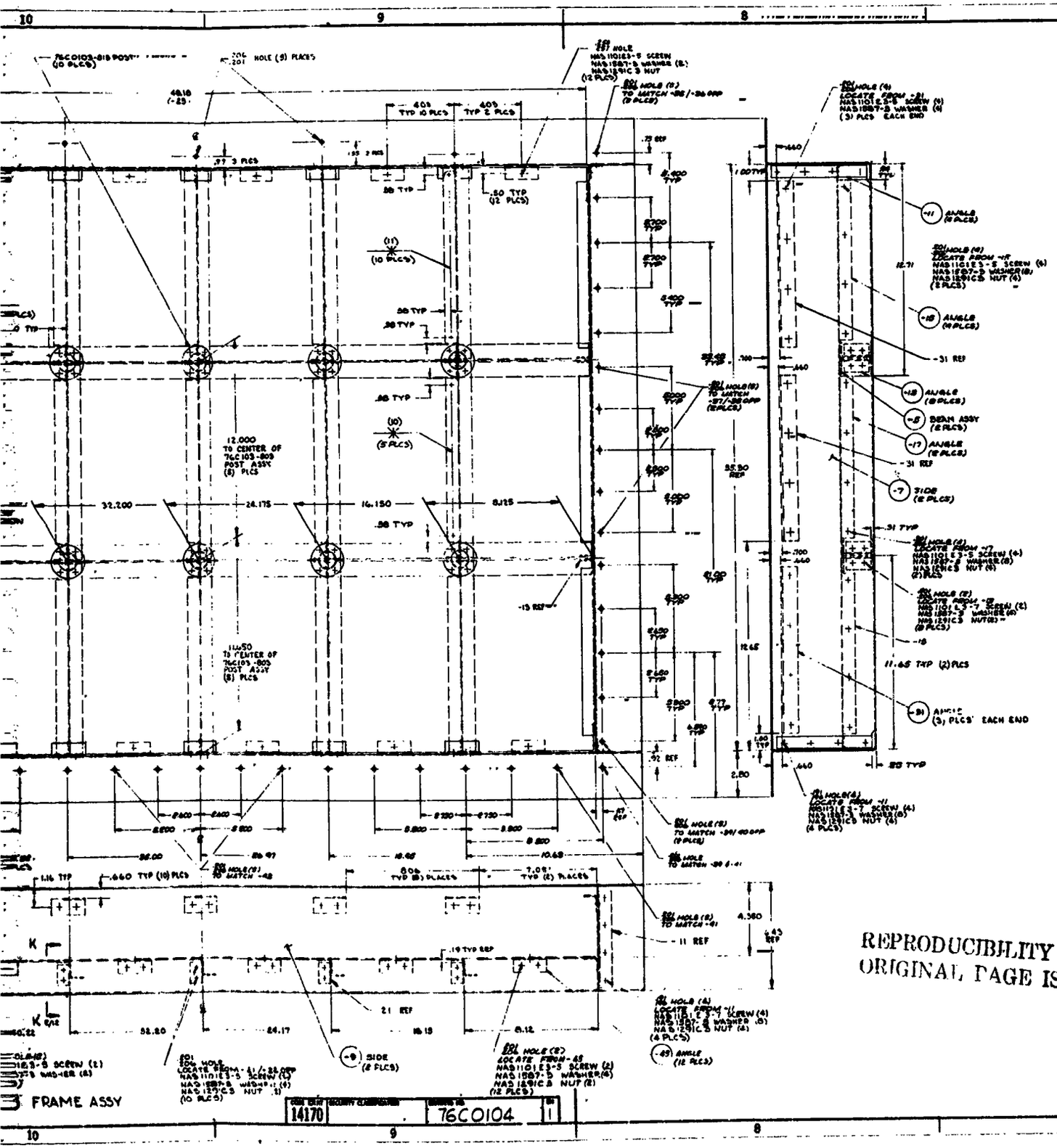

REPRODUCIBILITY OF THE ORIGINAL PAGE IS POOR

FOLDOUT FRAME 1

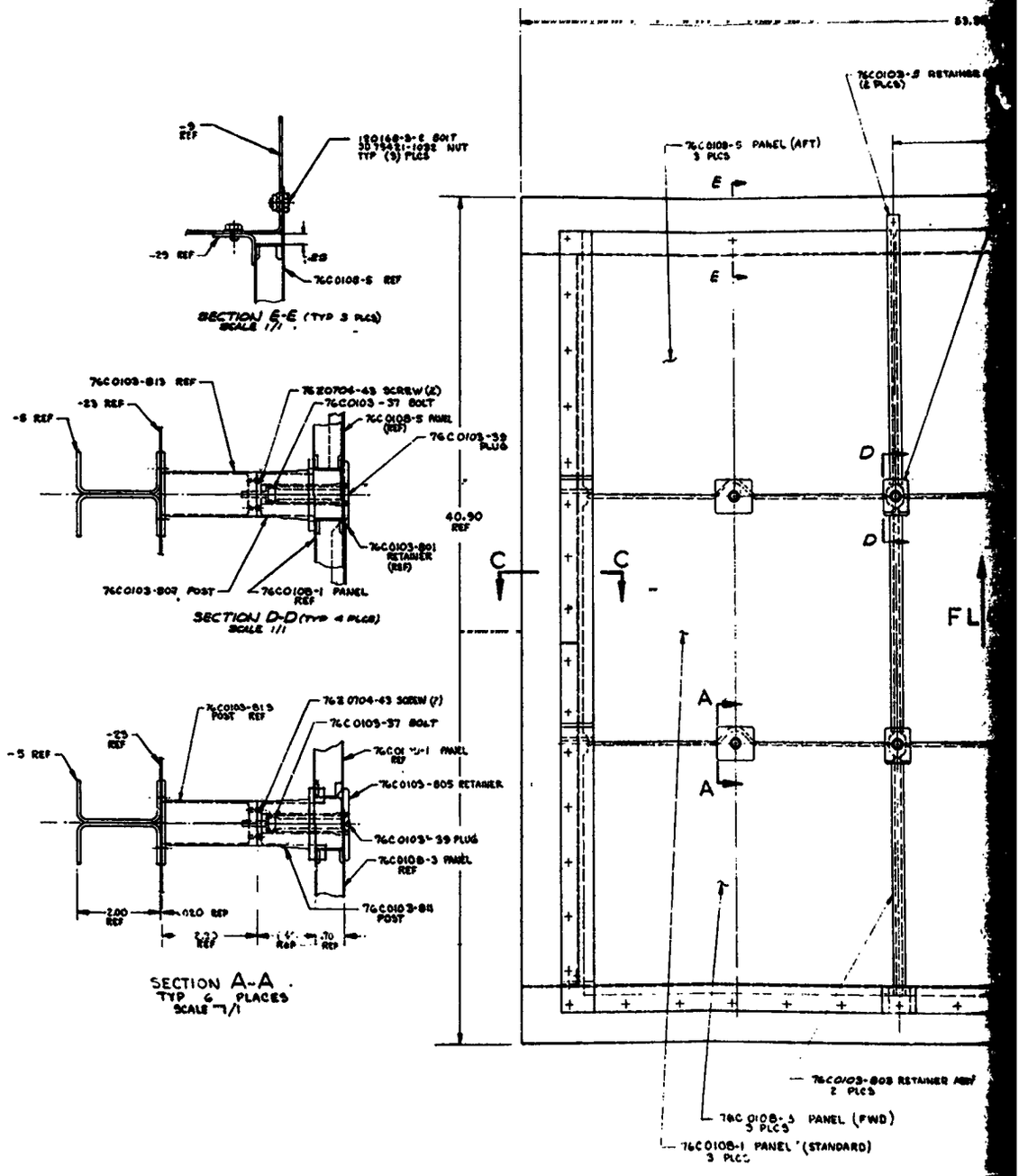

REPRODUCIBILITY OF THE ORIGINAL PAGE IS POOR

14170		76C0104	1

FOLDOUT FRAME

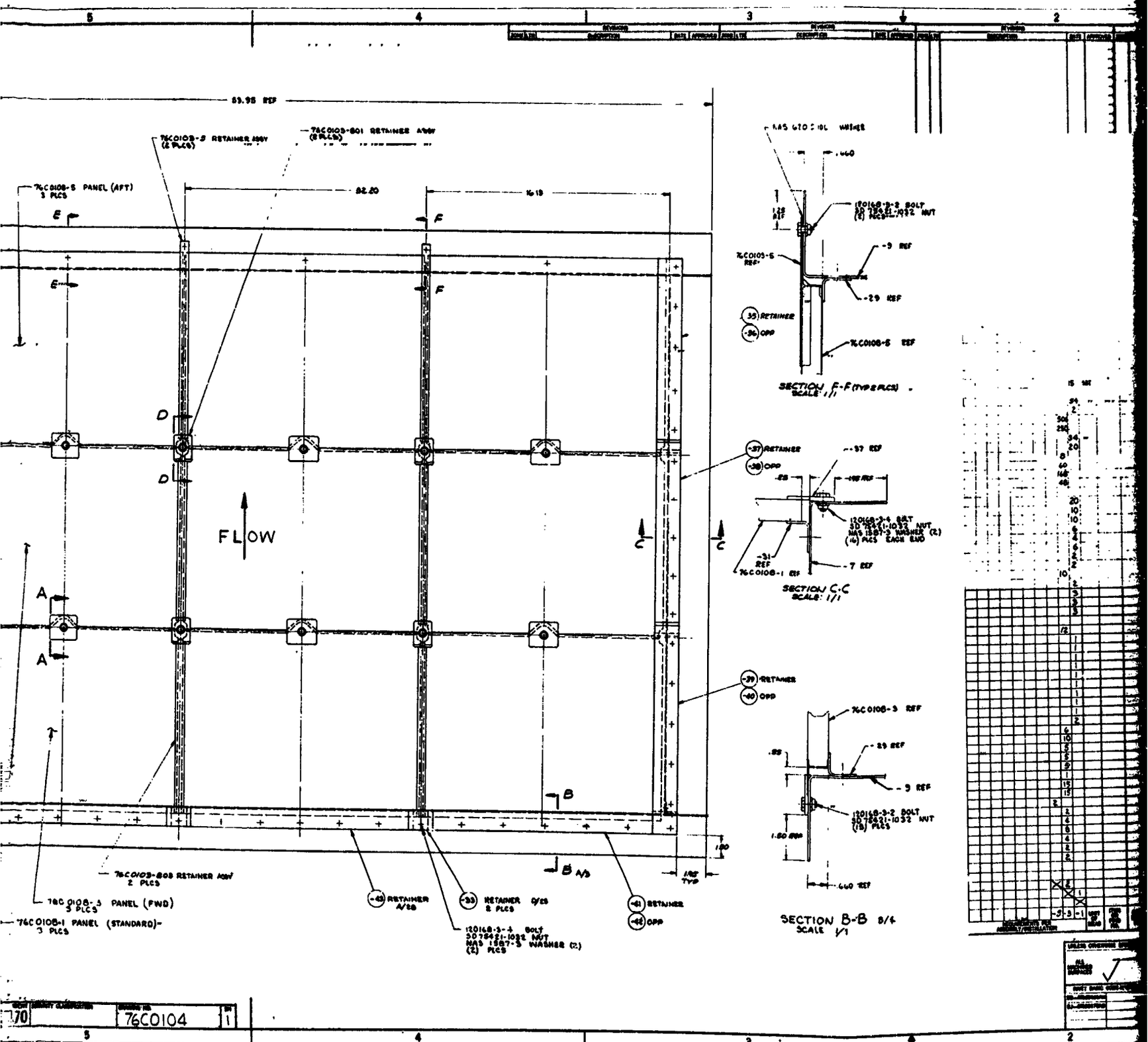

QUANTITY	DRAWING NO.	SH
70	76C0104	1

Figure 3-5. Nin

FOLDOUT FRAME

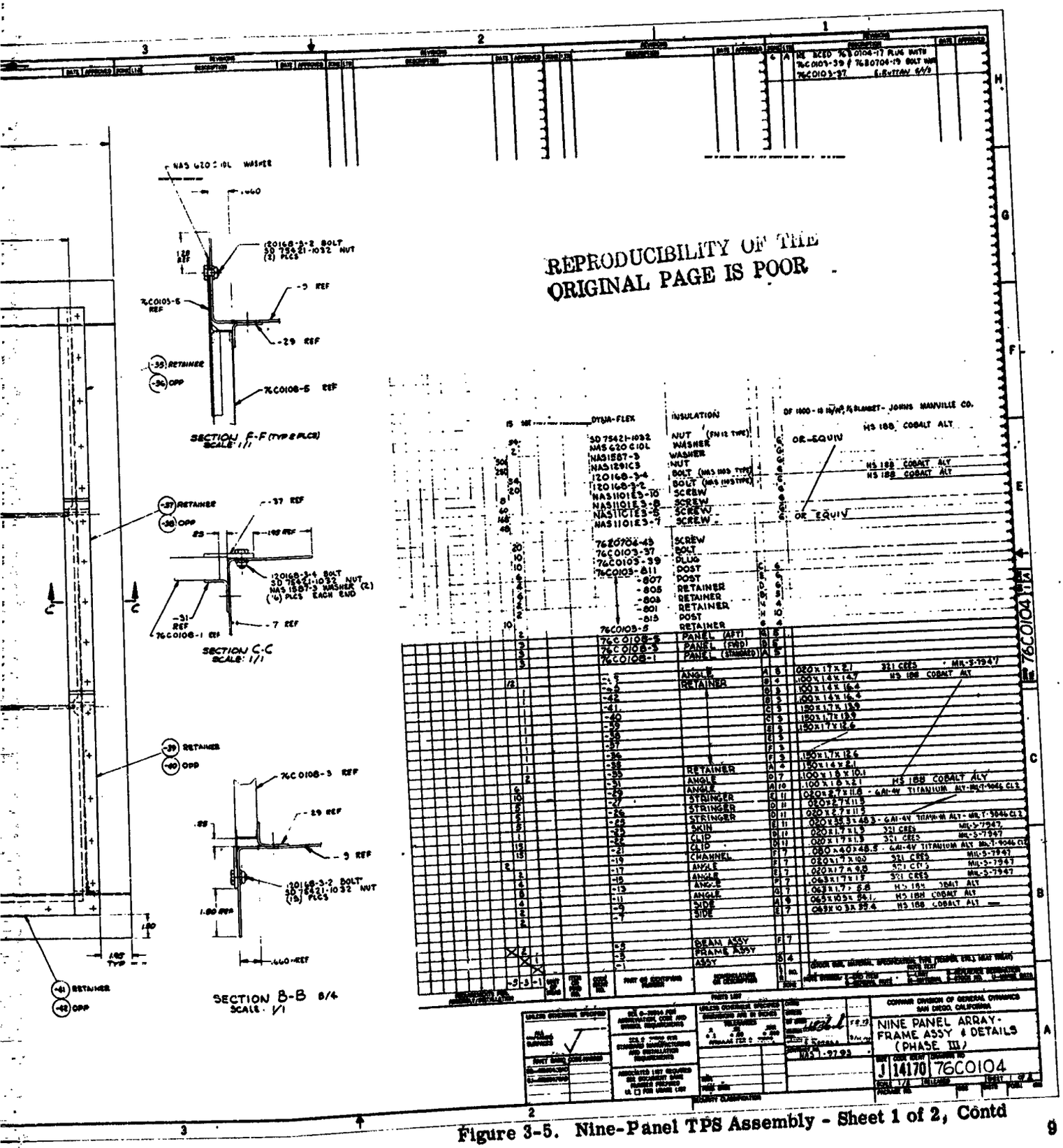

Figure 3-5. Nine-Panel TPS Assembly - Sheet 1 of 2, Contd

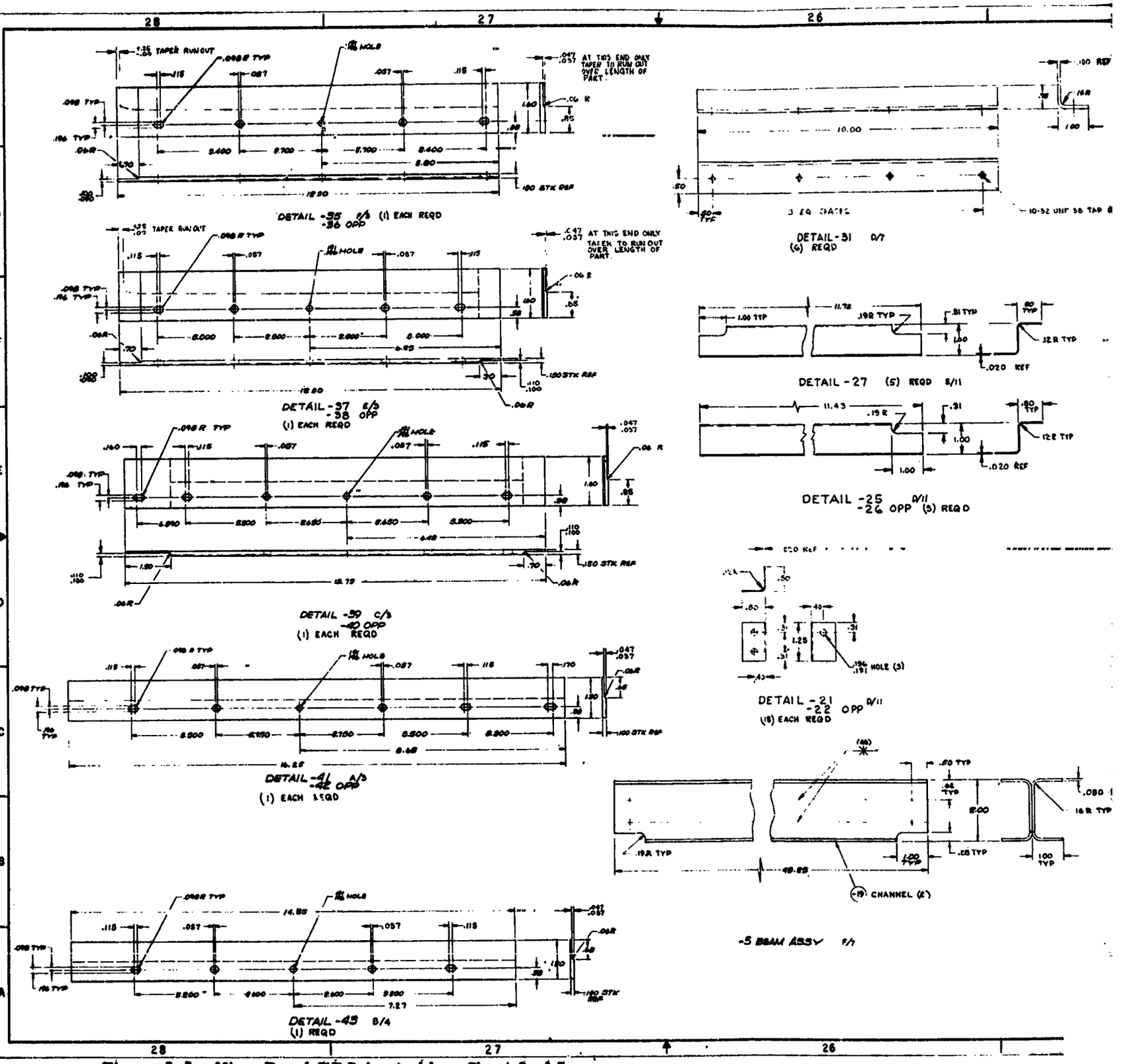

Figure 3-5. Nine-Panel TPS Assembly - Sheet 2 of 2

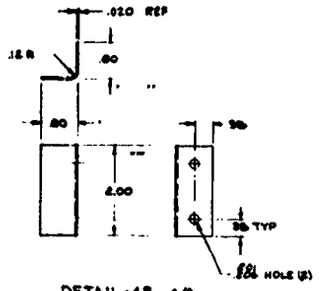

DETAIL -45 A/8
(12) REQD

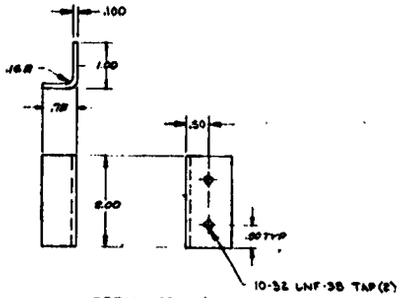

DETAIL -29 A/10
(10) REQD

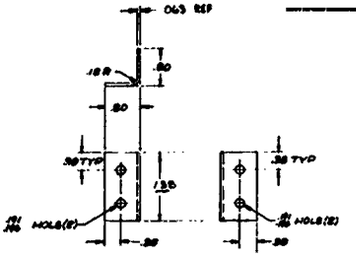

DETAIL -13 F/7
(2) REQD

REPRODUCIBILITY OF THE
ORIGINAL PAGE IS POOR

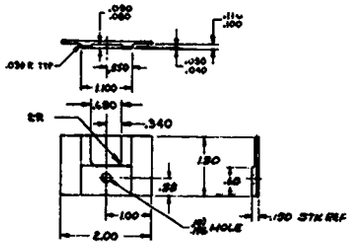

DETAIL -33 B/4
(2) REQD

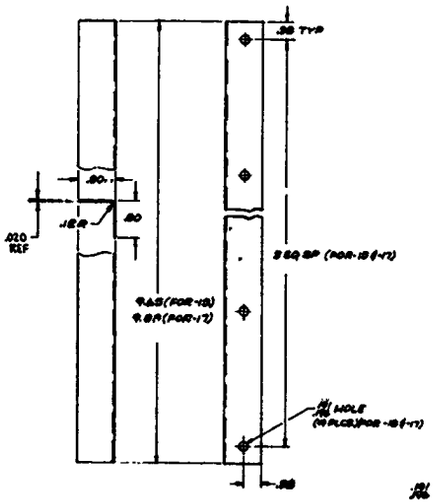

DETAIL -15 (4) REQD E/7
DETAIL -17 (SAME AS -15 EXCEPT AS NOTED) G/7
(2) REQD

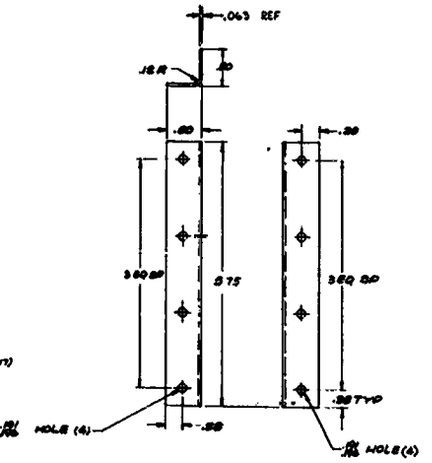

DETAIL -11 G/7
(4) REQD

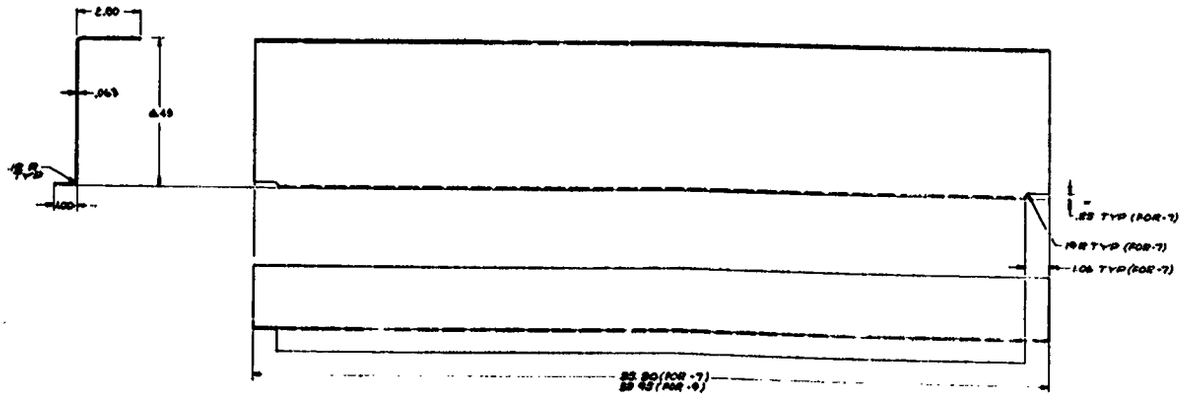

DETAIL -7 E/7
DETAIL -9 (SAME AS -7 EXCEPT AS NOTED) A/9
(2) EACH REQD
SCALE 1/2

FOLDOUT FRAME

14170		76C0104	2

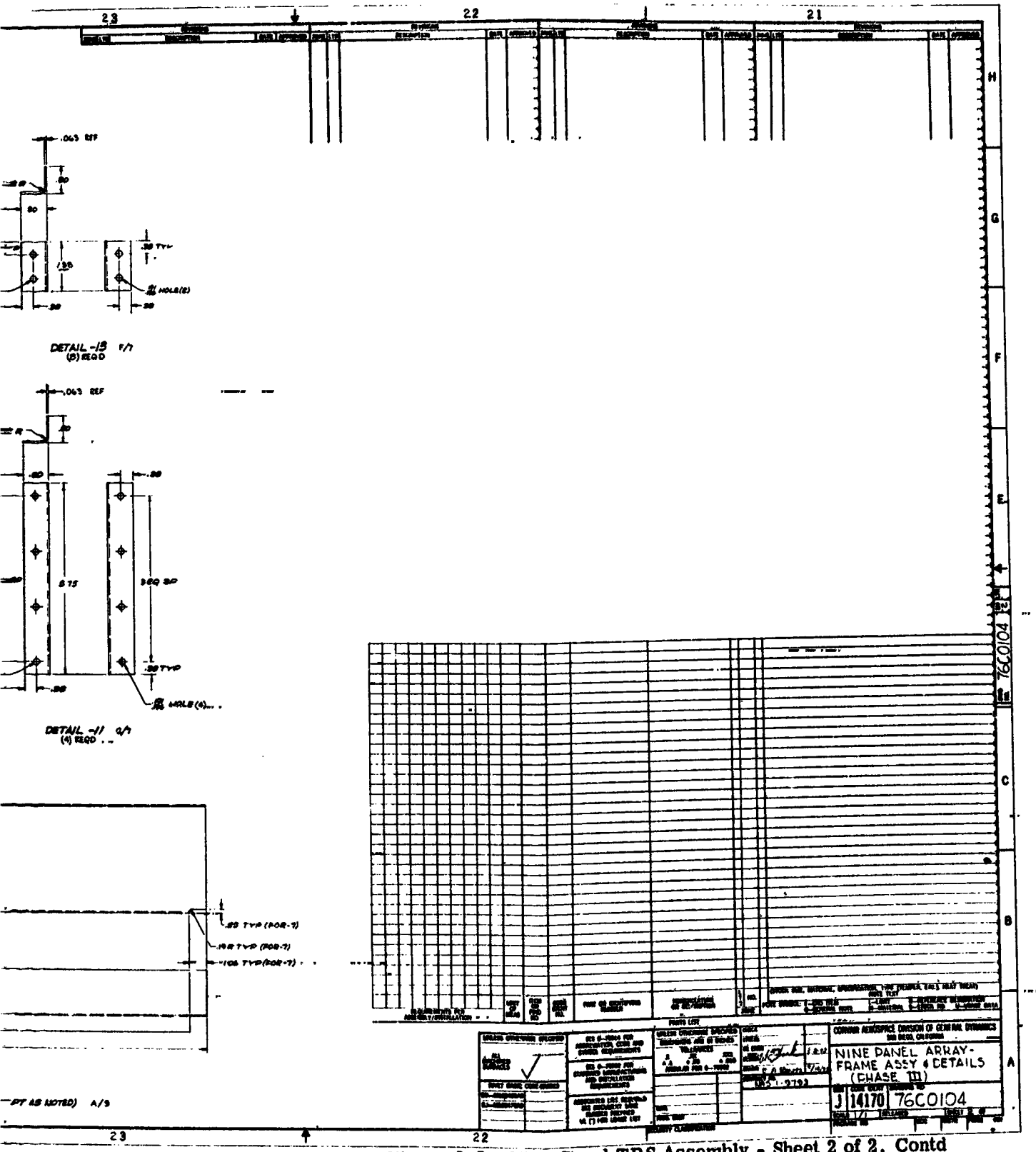

Figure 3-5. Nine-Panel TPS Assembly - Sheet 2 of 2, Contd

FOLDOUT FRAME

2

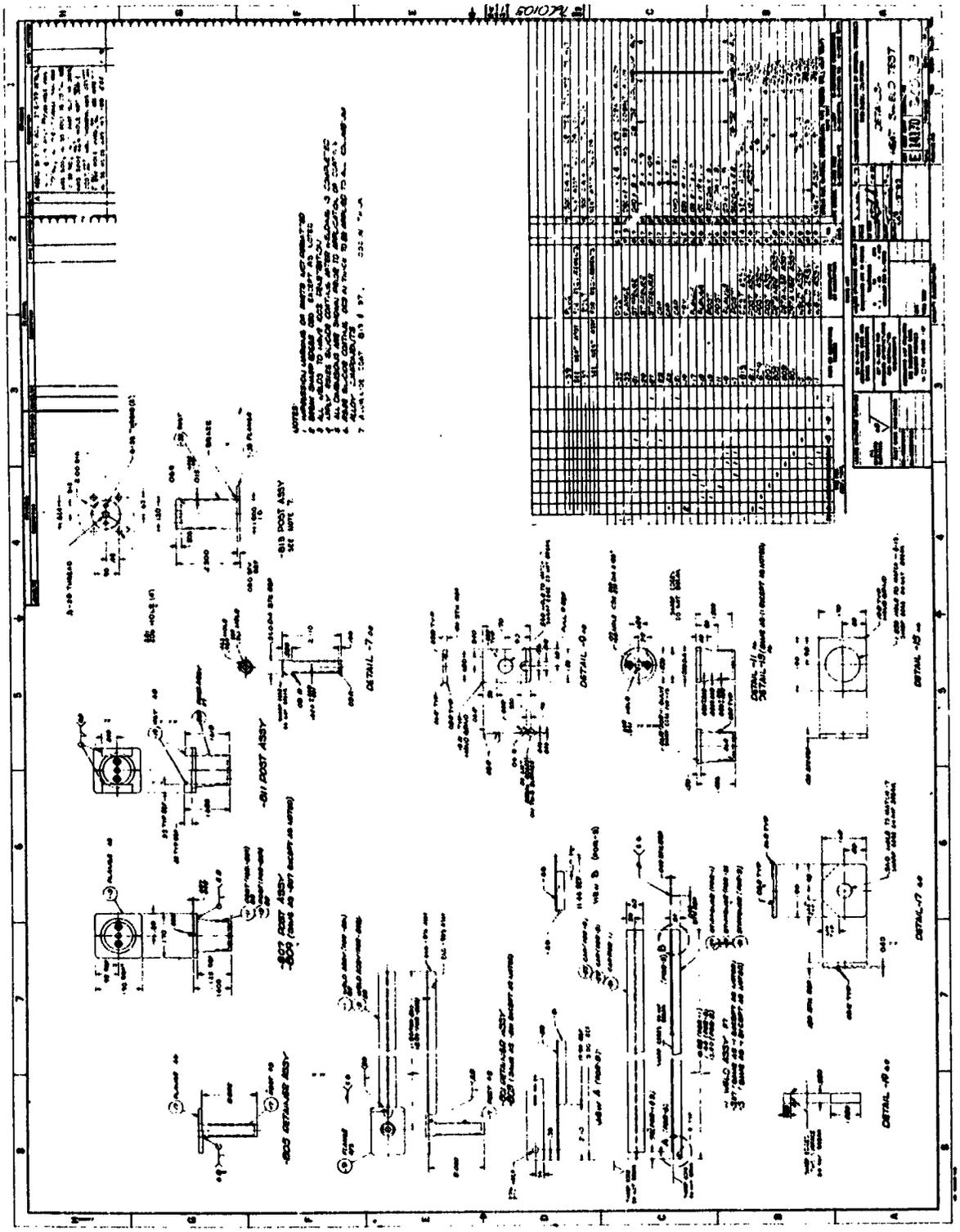

Figure 3-6. TPS Component Details – Sheet 1 of 2

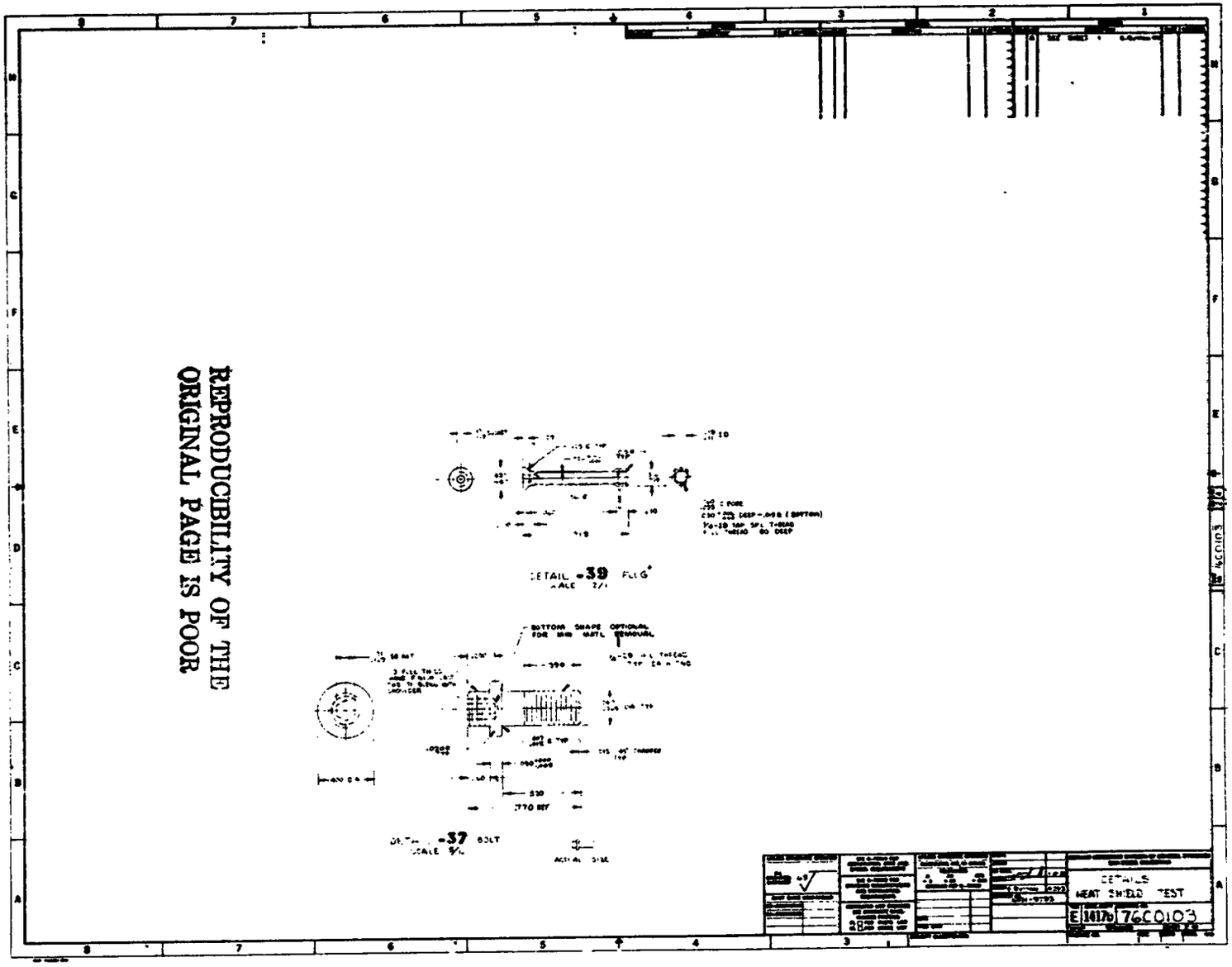

REPRODUCIBILITY OF THE
ORIGINAL PAGE IS POOR

Figure 3-6. TPS Component Details – Sheet 2 of 2

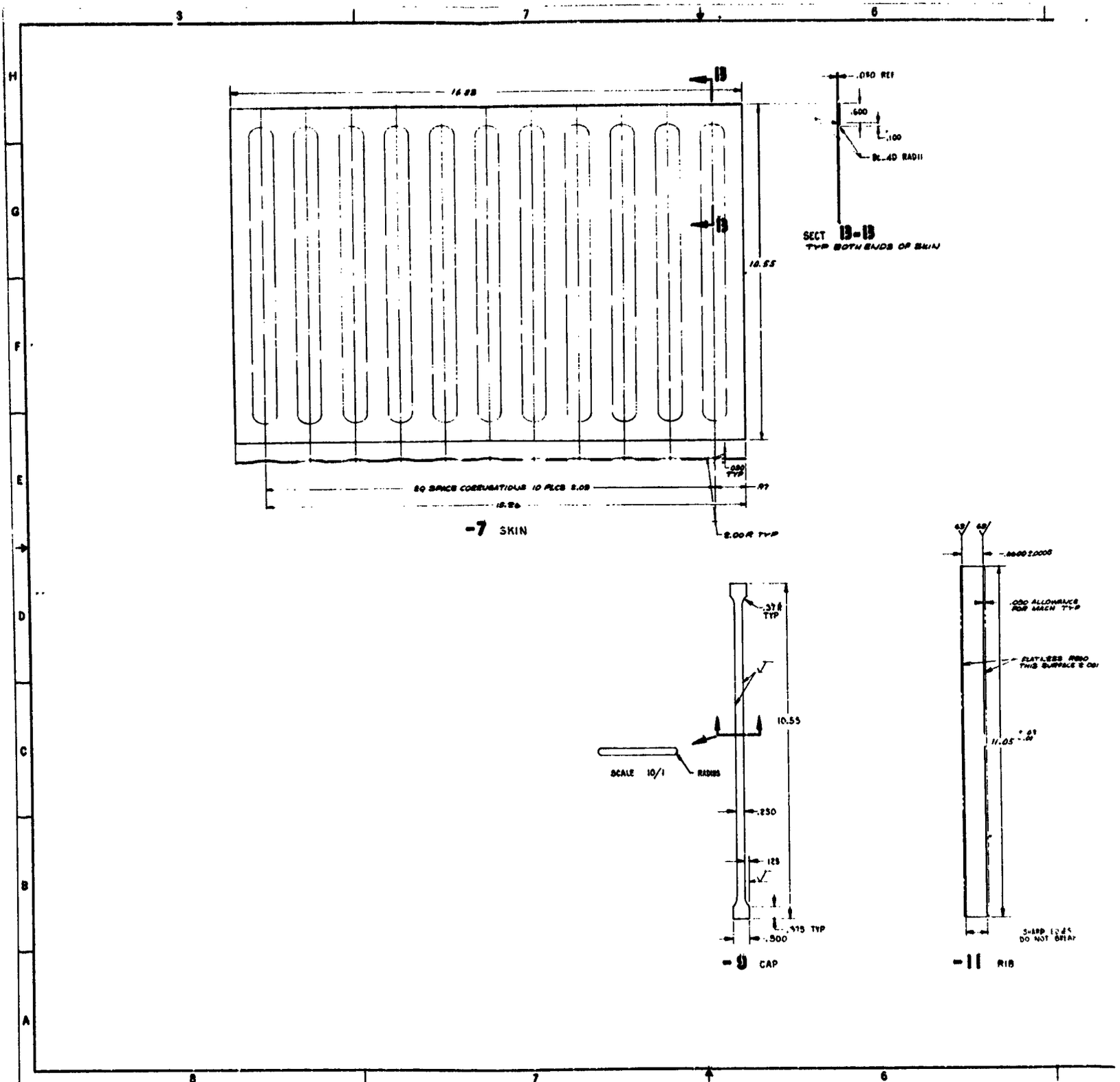

Figure 3-7. Heat Shield Panel - Sheet Metal

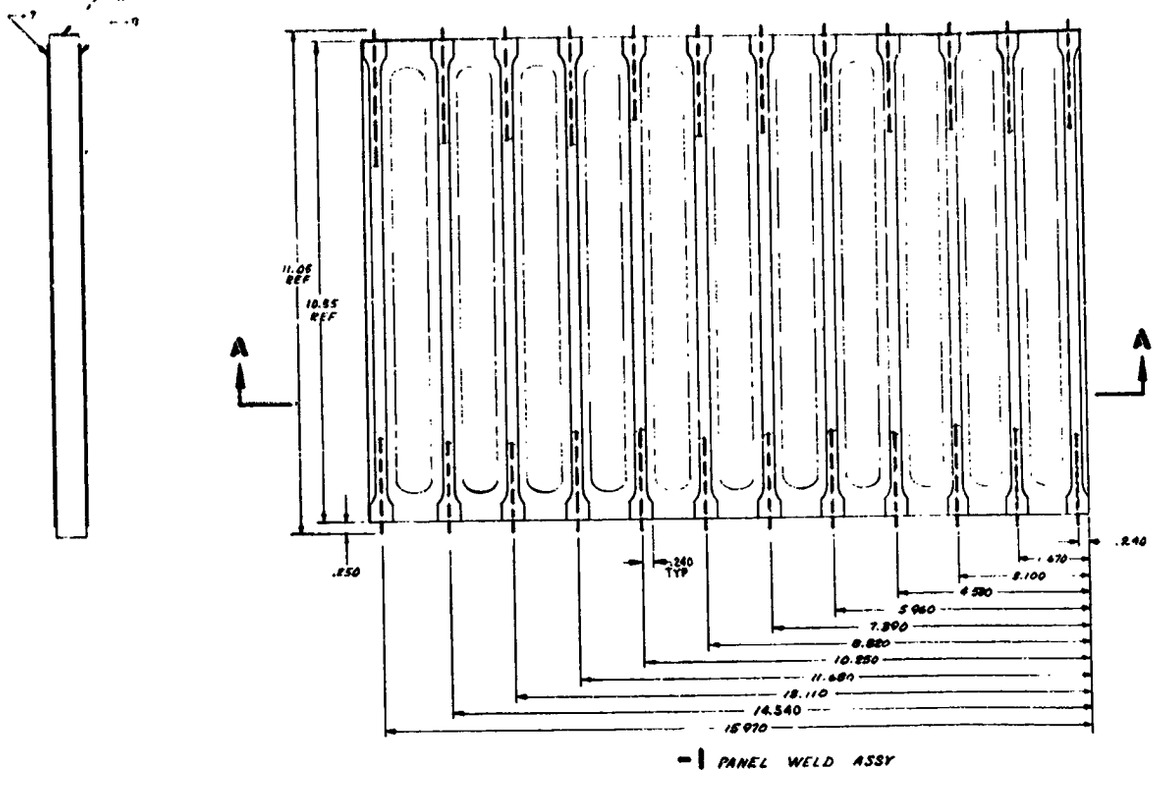

-1 PANEL WELD ASSY

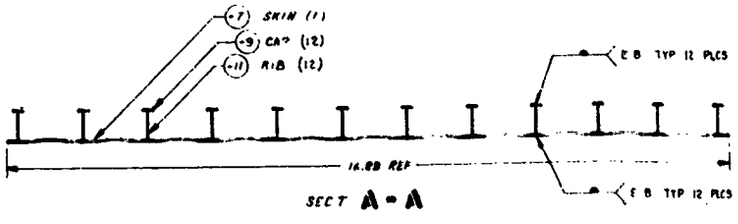

SECT A-A

CONT IDENT	SECURITY CLASSIFICATION	DRAWING NO	SH
14170		76C0105	1

FOLDOUT FRAME

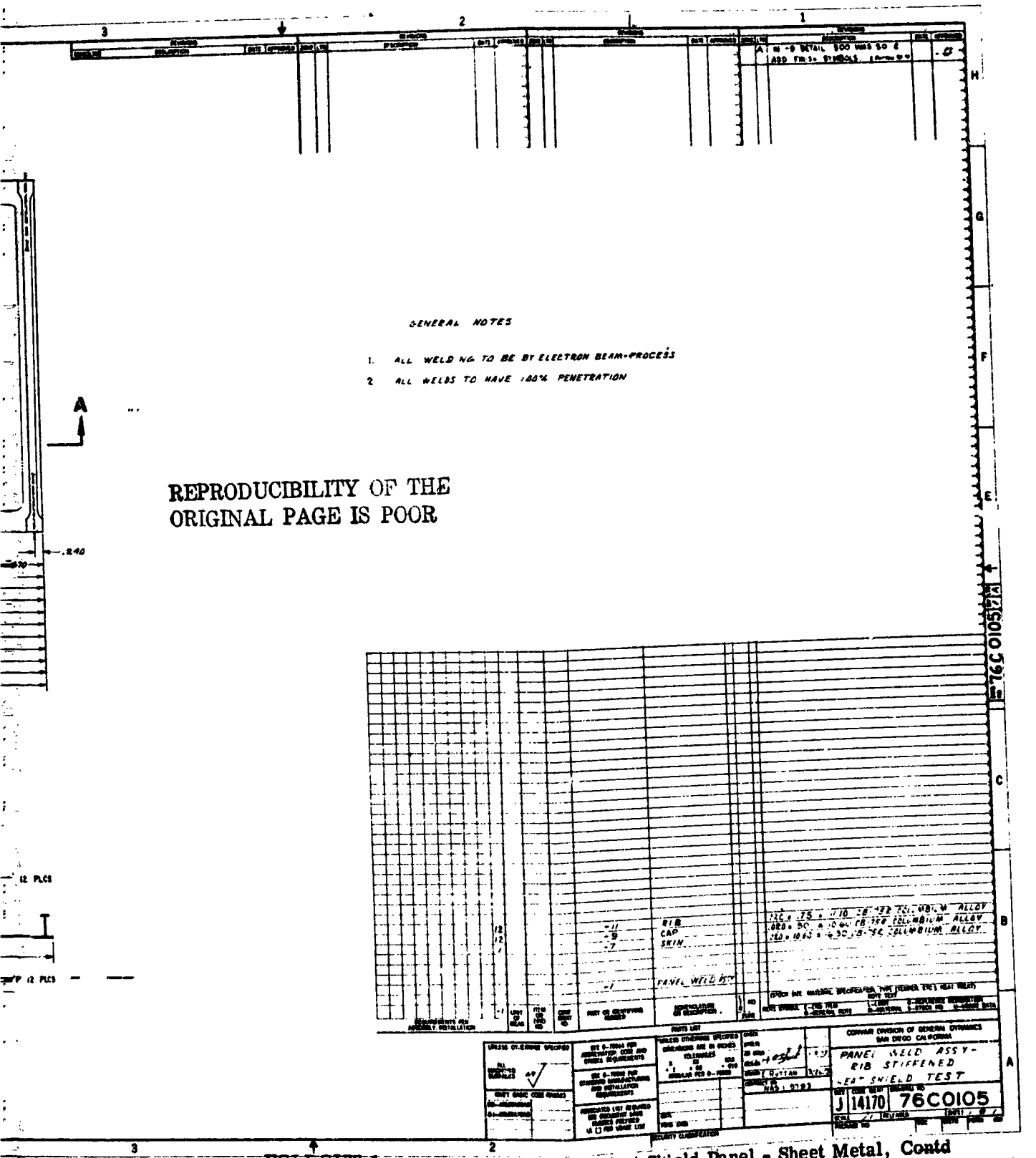

Figure 3-7. Heat Shield Panel - Sheet Metal, Contd

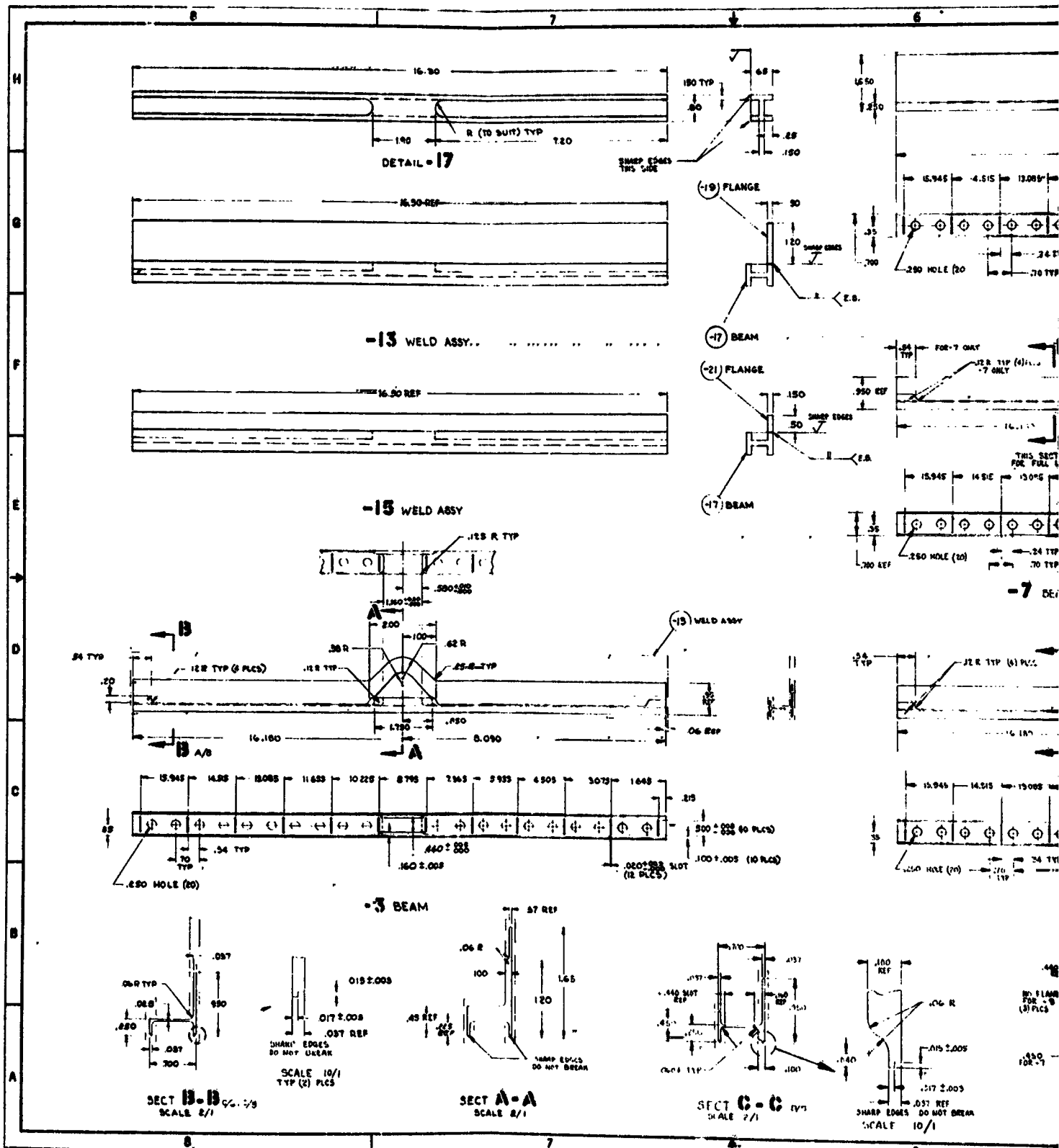

Figure 3-8. Heat Shield Panel - Subassemblies

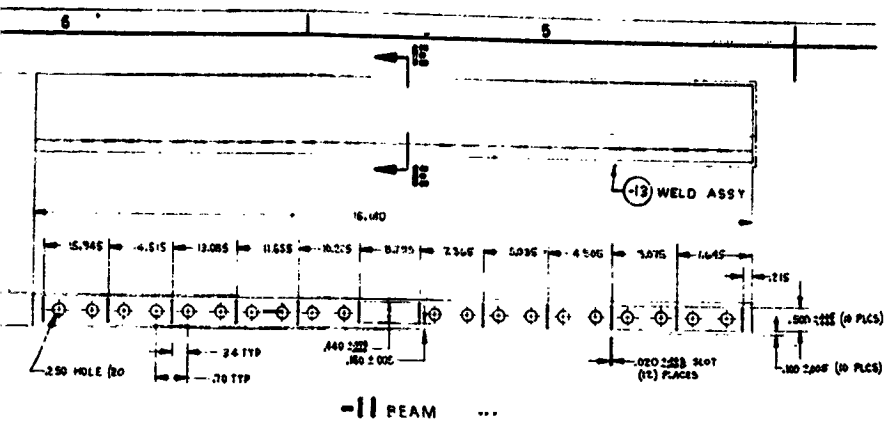

-11 BEAM ...

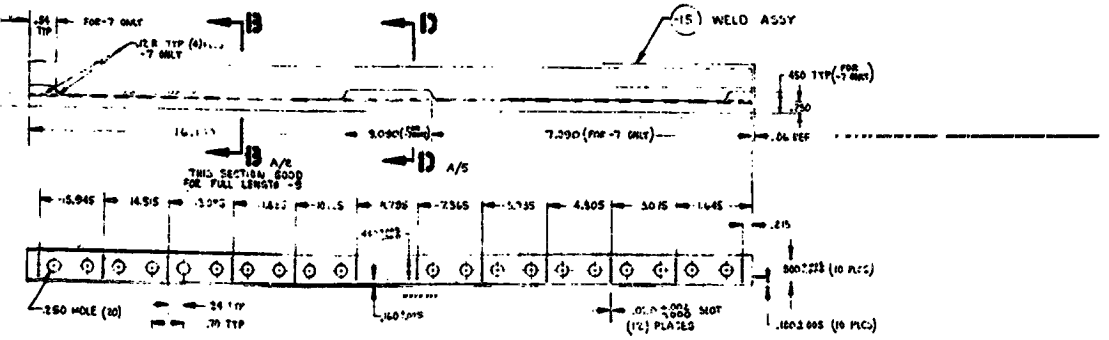

-7 BEAM, -9 BEAM SAME AS -7 EXCEPT AS NOTED

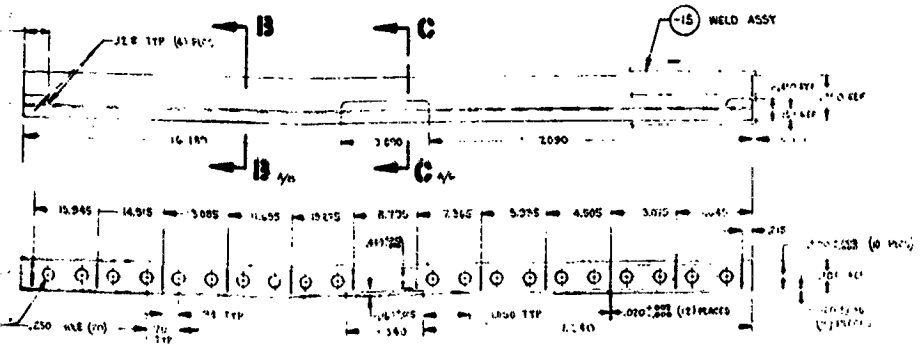

-5 BEAM

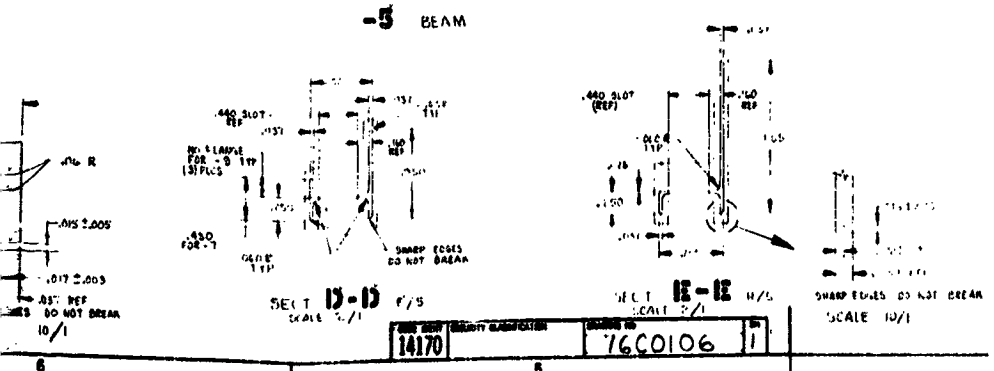

14170		76C0106

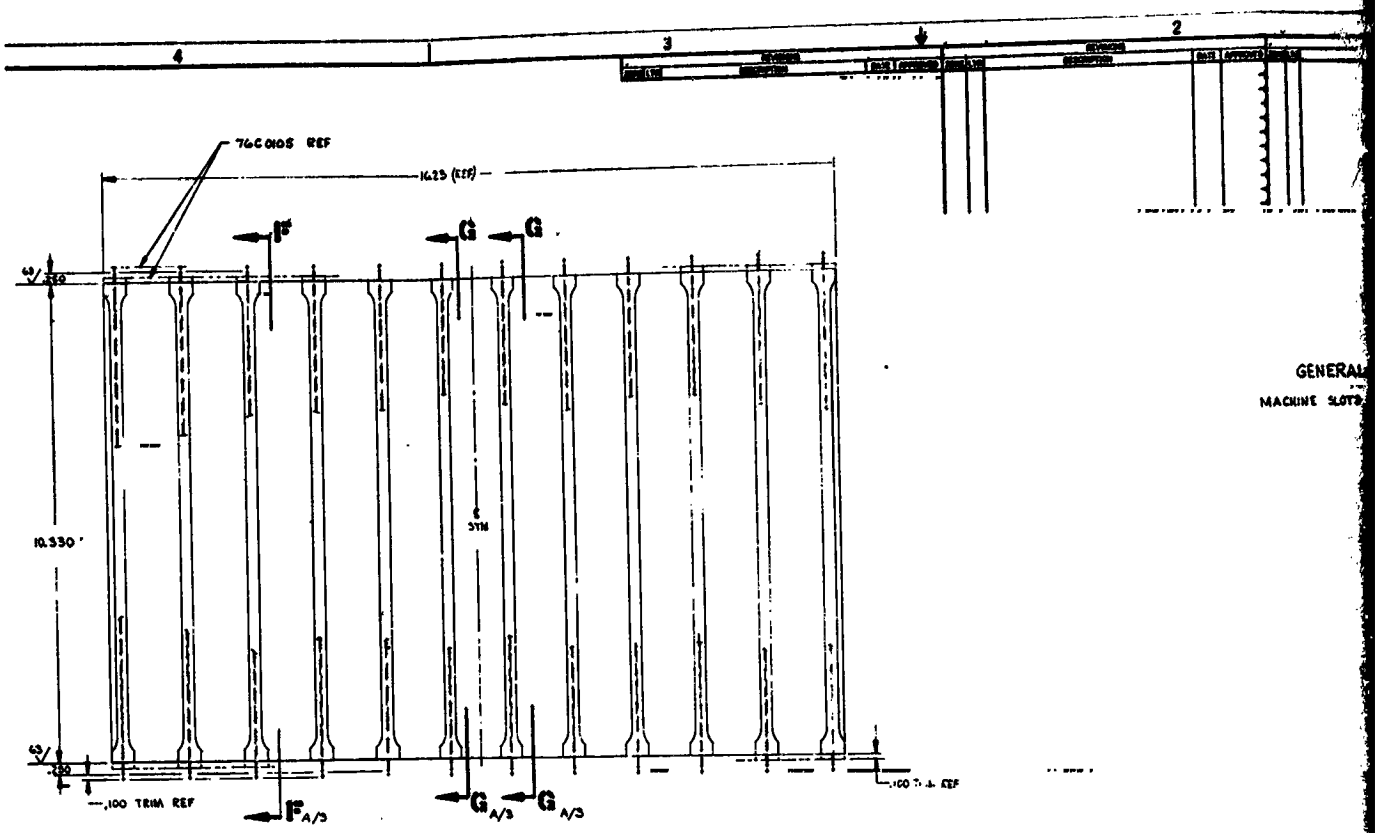

-1 PANEL

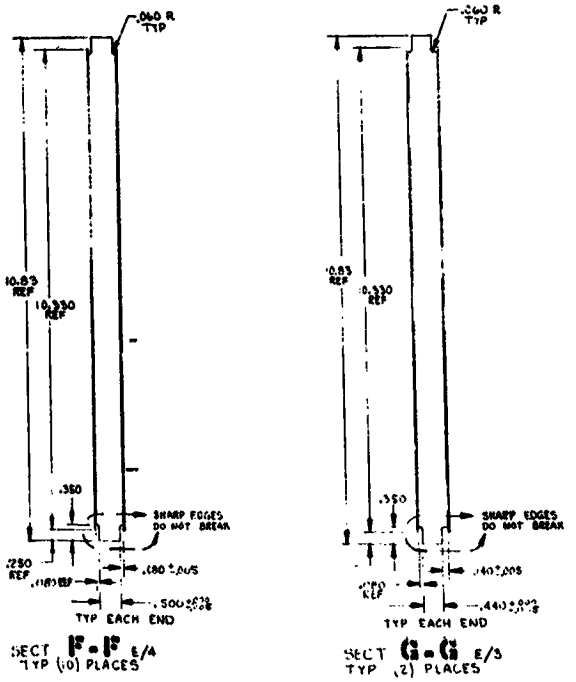

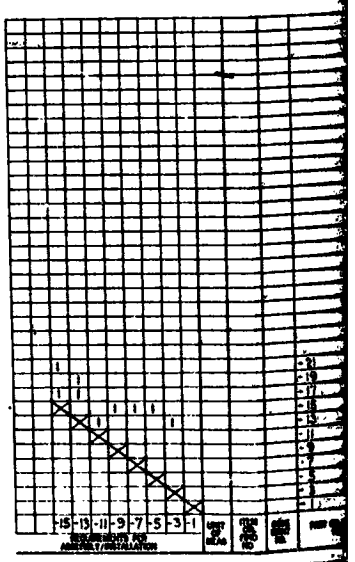

Figure 3-8.

FOLDOUT FRAME

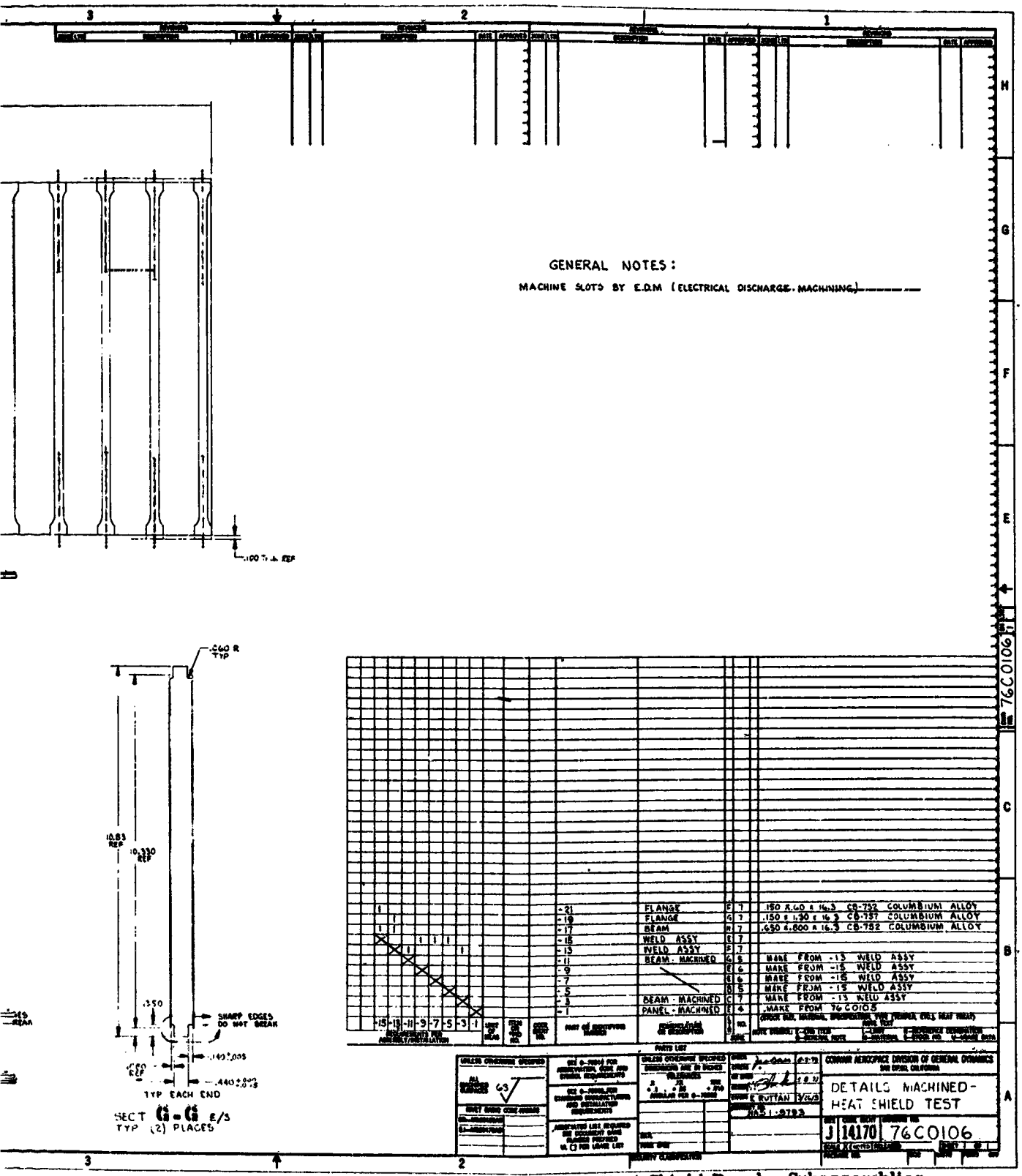

Figure 3-8. Heat Shield Panel - Subassemblies

FOLDOUT FRAME

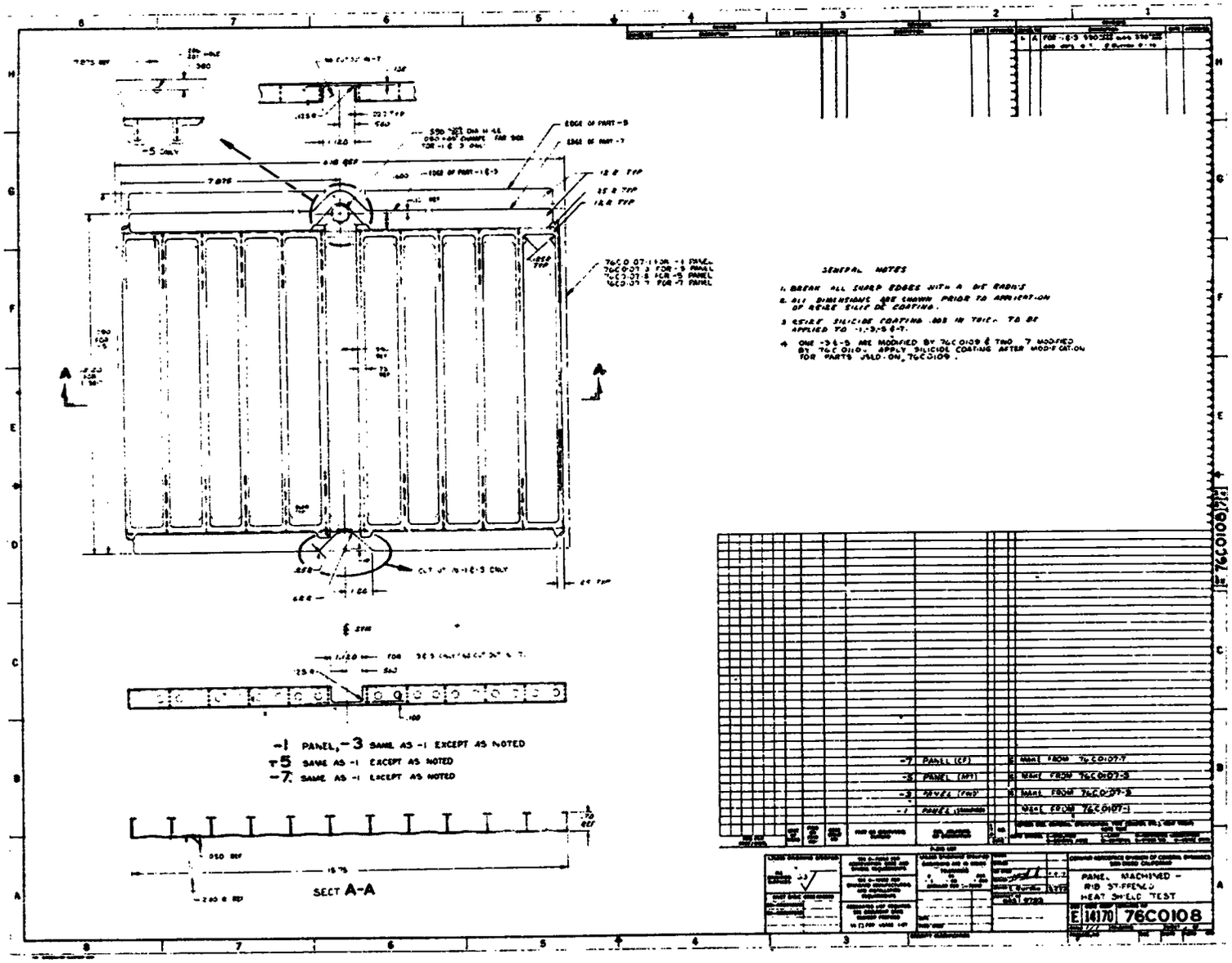

Figure 3-9. Heat Shield Panel – Final Machined

3.2 TPSTF Specimen

A specimen employing the same basic TPS structure was designed to investigate the effects of hypersonic flow in the NASA LaRC Thermal Protection System Test Facility. The overall specimen size is 24 by 36 by 6.6 inches (61 by 91 by 17 cm). The holding fixture was fabricated from HS-188 sheet. The simulated vehicle primary structure consisting of skin, frames, and stringers was fabricated from titanium. Two views of this structure are shown in Figures 3-10 and 3-11. Figure 3-10 shows the structure with the lower TPS support posts (HS-25) installed and ready for insulation installation. The specimen consists of three heat shields, one of which is completely isolated as the central test panel as shown in Figure 3-12 (76C0109). Adjacent to the heat shields in the transverse direction are auxiliary panels (76C0110) to separate the main heat shields from the holding fixture. The details of these edge panels are shown in Figure 3-13. The completely assembled TPSTF test specimen is shown in Figure 3-14.

3.3 Design Changes - Phase II to Phase III

Modifications were made in full-scale hardware designs from those tested in Phase II to improve fabrication efficiency and to reduce material costs. Extensive use was made of electron beam welding to reduce weight and material costs and to minimize machining operations. Both the total system cost and unit weight were reduced in the final full-size design, resulting in a net cost/weight saving of approximately 4-percent, with material costs reduced 70-percent and fabrication costs 21-percent. Material changes were made in the lower temperature regime, with the bottom portion of the two-section support posts being changed to HS-25 (L-605), a cobalt base alloy suitable for service to 2000° F (1366° K). The aluminum silicate plus chromia fiberous insulation (Dyna-Flex) was replaced with Fiberfrax H insulation with a density of only 6.0 pcf (96 Kg/m^3). This material is composed of aluminum silicate fibers and does not require a bakeout to remove undesirable binders.

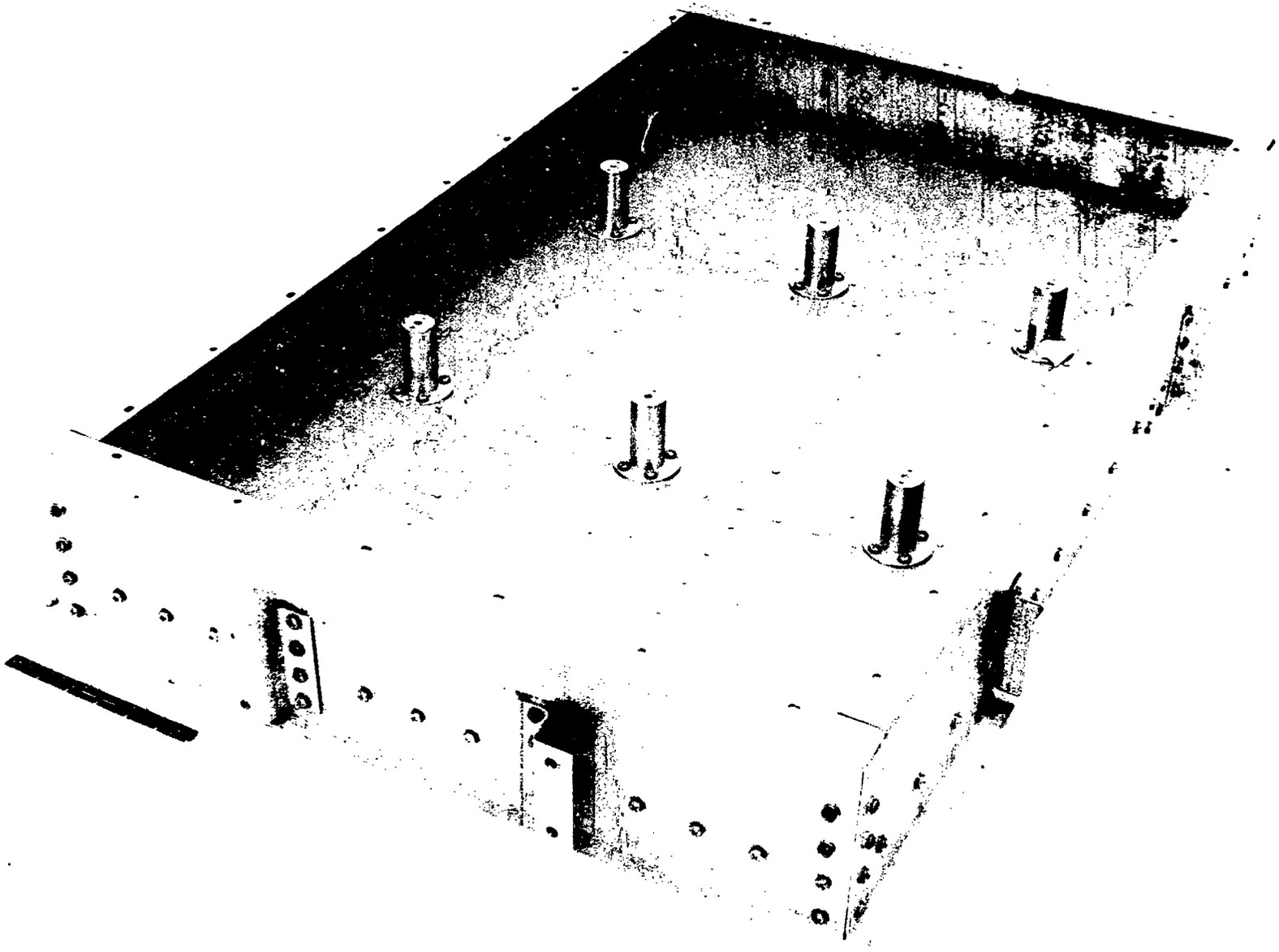

Figure 3-10. View of TPSTF Array Holding Fixture (137104)

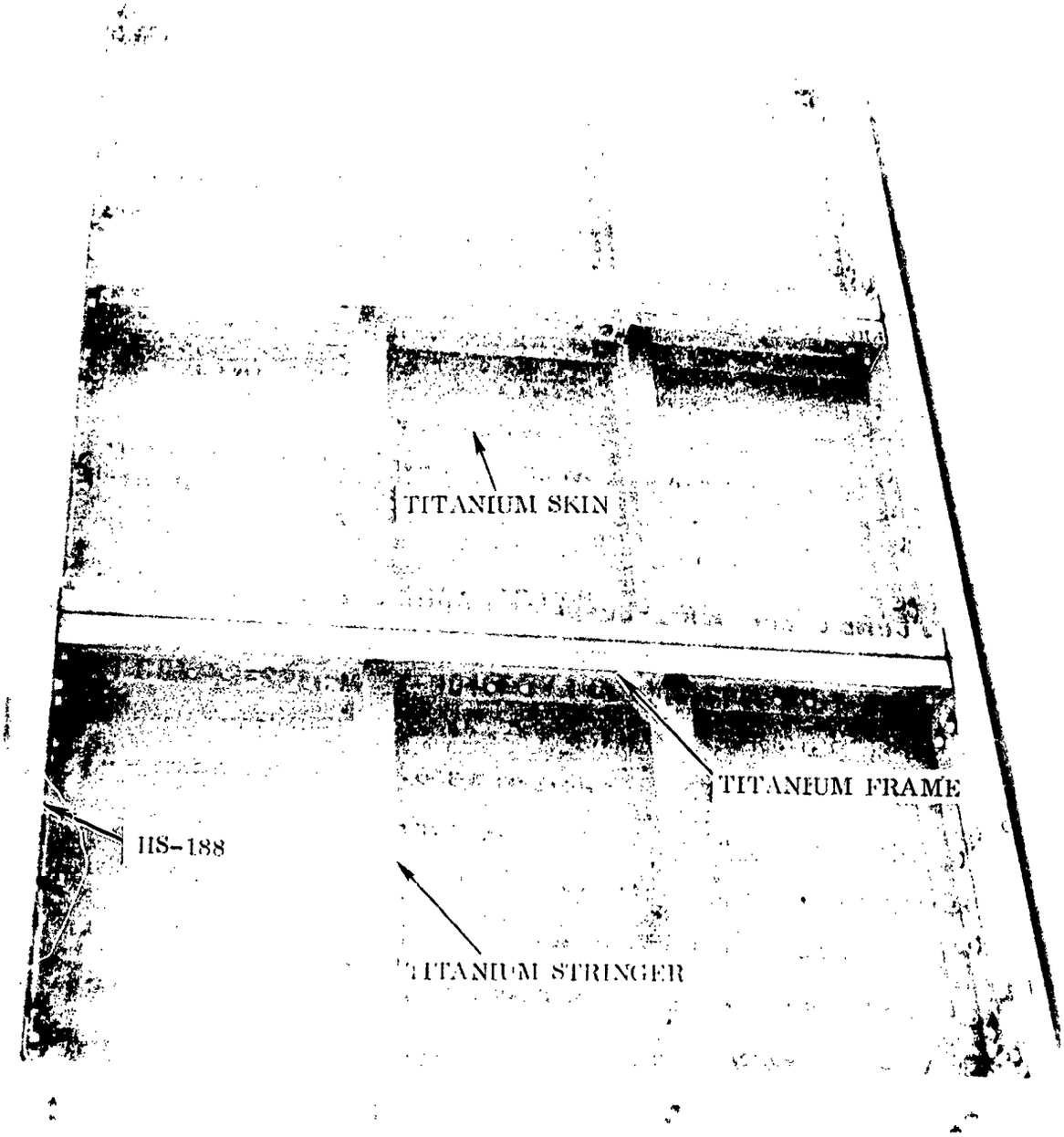

Figure 3-11. Bottom View of TPSTF Array Holding Fixture (134036B)

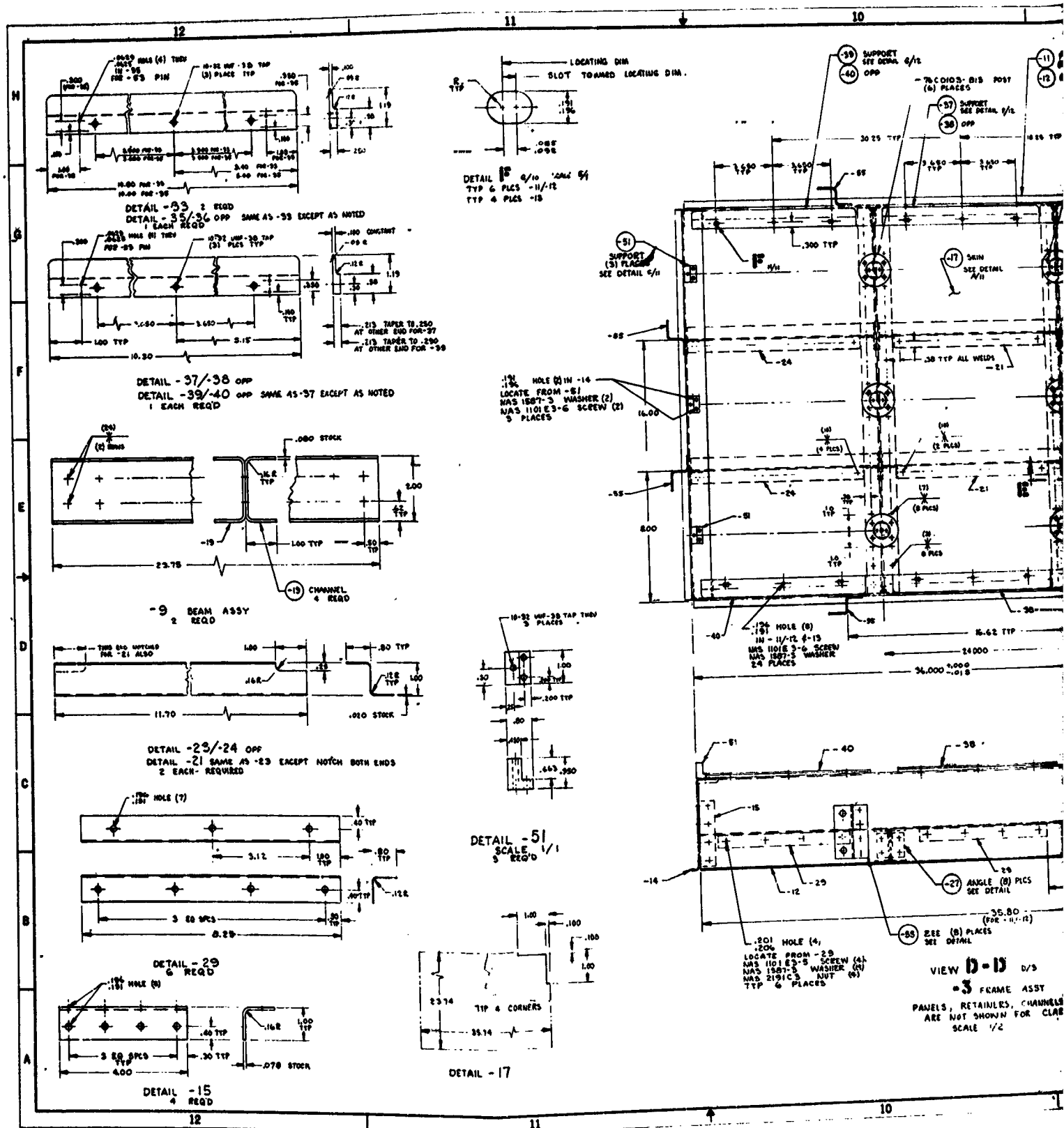

Figure 3-12. TPSTF Test Specimen Assembly and Details

FOLDOUT FRAME

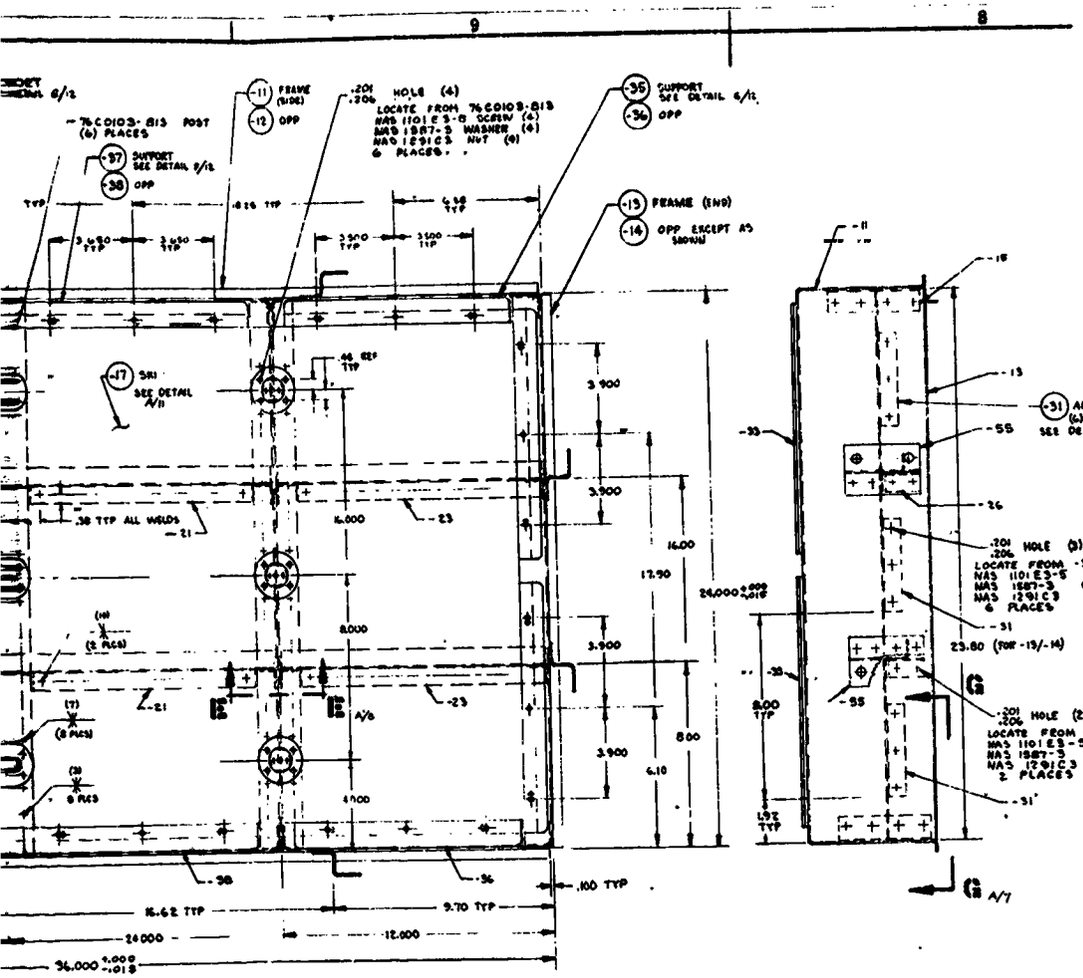

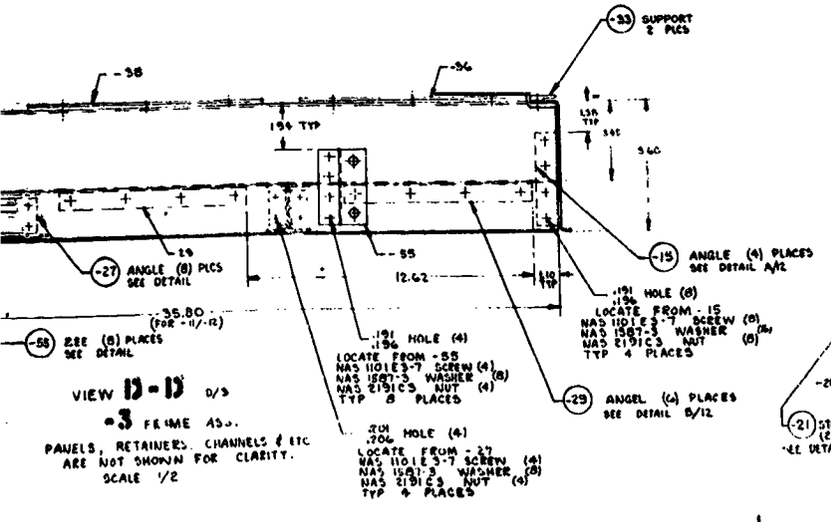

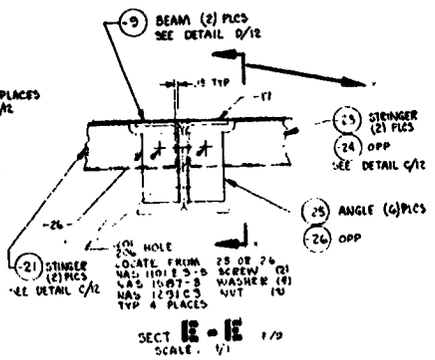

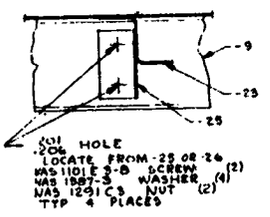

CODE IDENT	SECURITY CLASSIFICATION	DRAWING NO.	SH
14170		76C0109	1

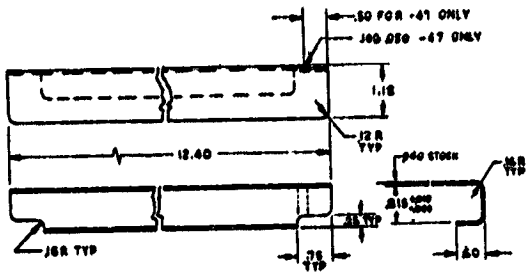

DETAIL -45
SCALE 1/1
2 REQ'D

DETAIL -47/48 OPP SAME AS -45
EXCEPT AS NOTED
1 EACH REQ'D

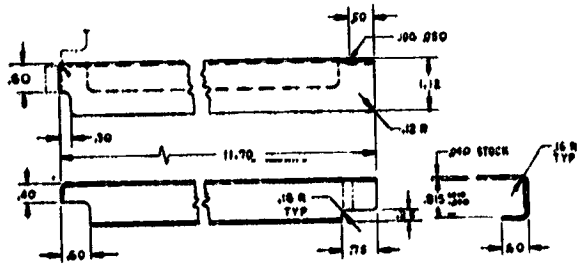

DETAIL -49/-50 OPP
SCALE 1/1
1 EACH REQ'D

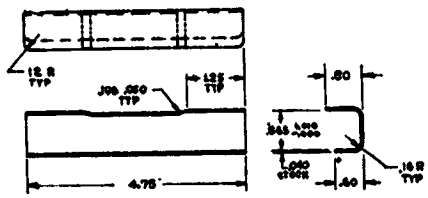

DETAIL -43
SCALE 1/1
2 REQ'D

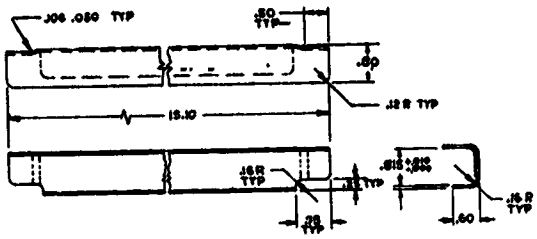

DETAIL -41
SCALE 1/1
1 REQ'D

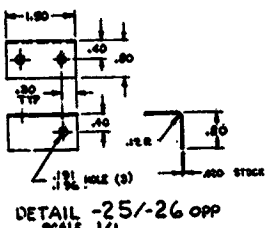

DETAIL -25/-26 OPP
SCALE 1/1
6 REQ'D EACH

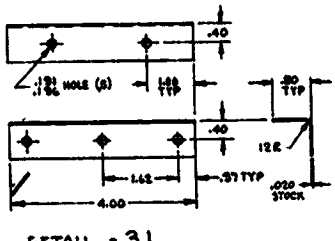

DETAIL -31
SCALE 1/1
6 REQ'D

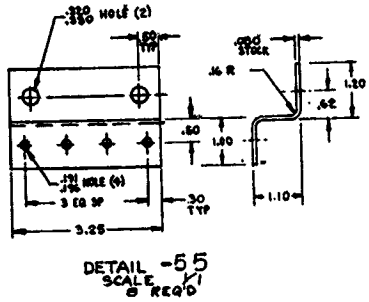

DETAIL -55
SCALE 1/1
8 REQ'D

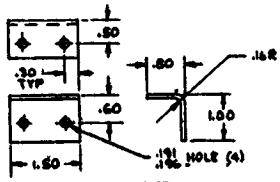

DETAIL -27
SCALE 1/1
8 REQ'D

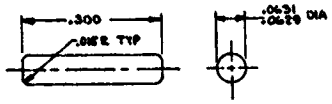

DETAIL -53
SCALE 10/1
24 REQ'D

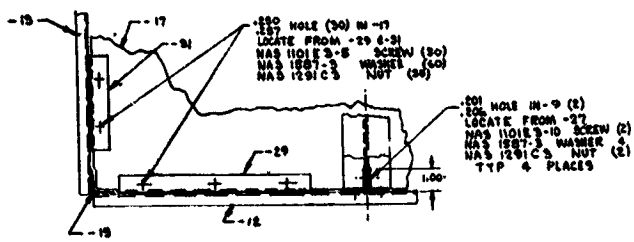

VIEW C3 = C3 R/S
SCALE 1/2

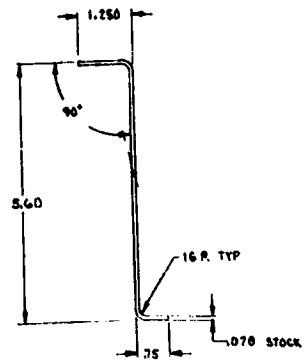

SECT TYP FOR -11/12 & -13/-14

14170

7 6 5

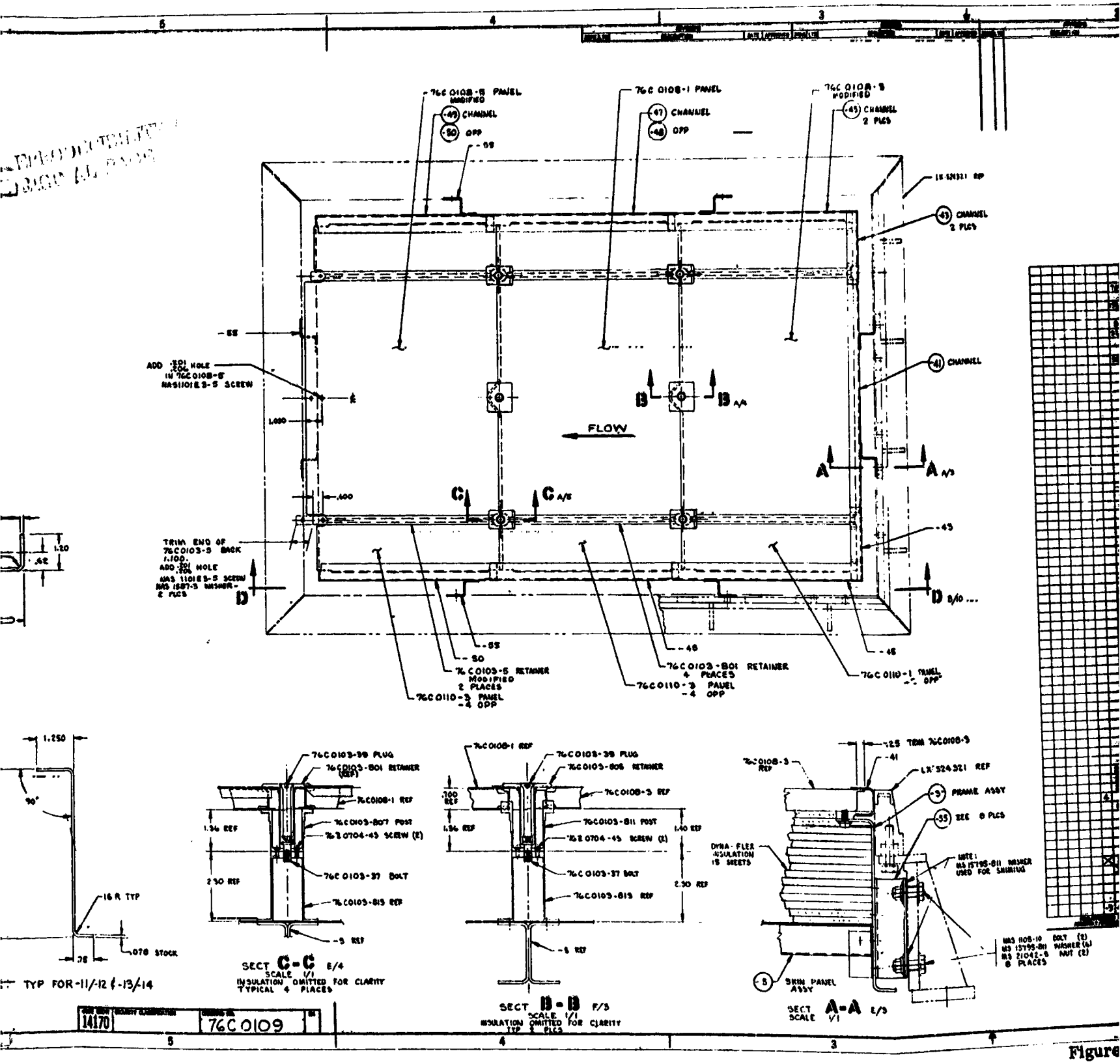

14170 | 76C0109

Figure

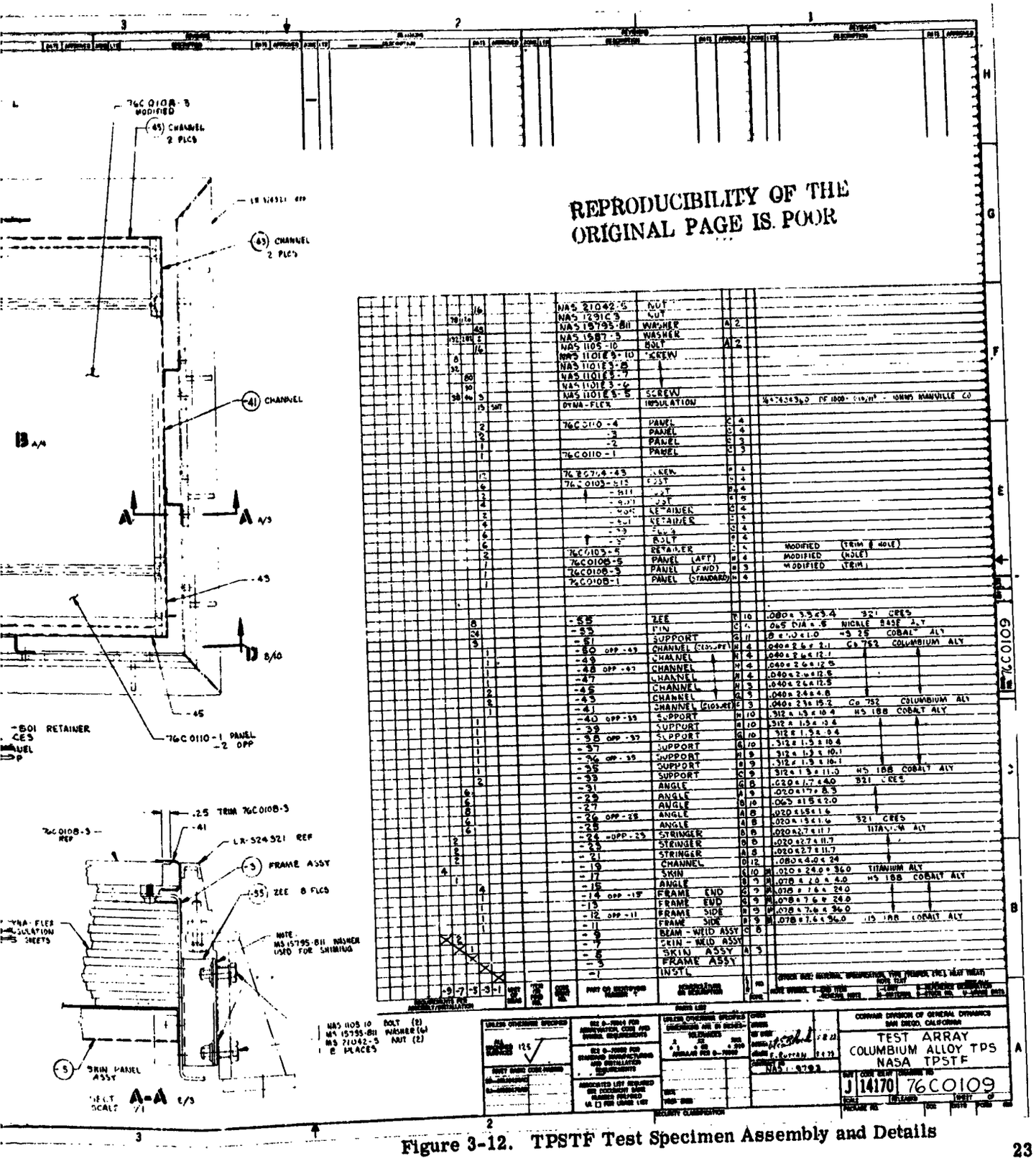

Figure 3-12. TPSTF Test Specimen Assembly and Details

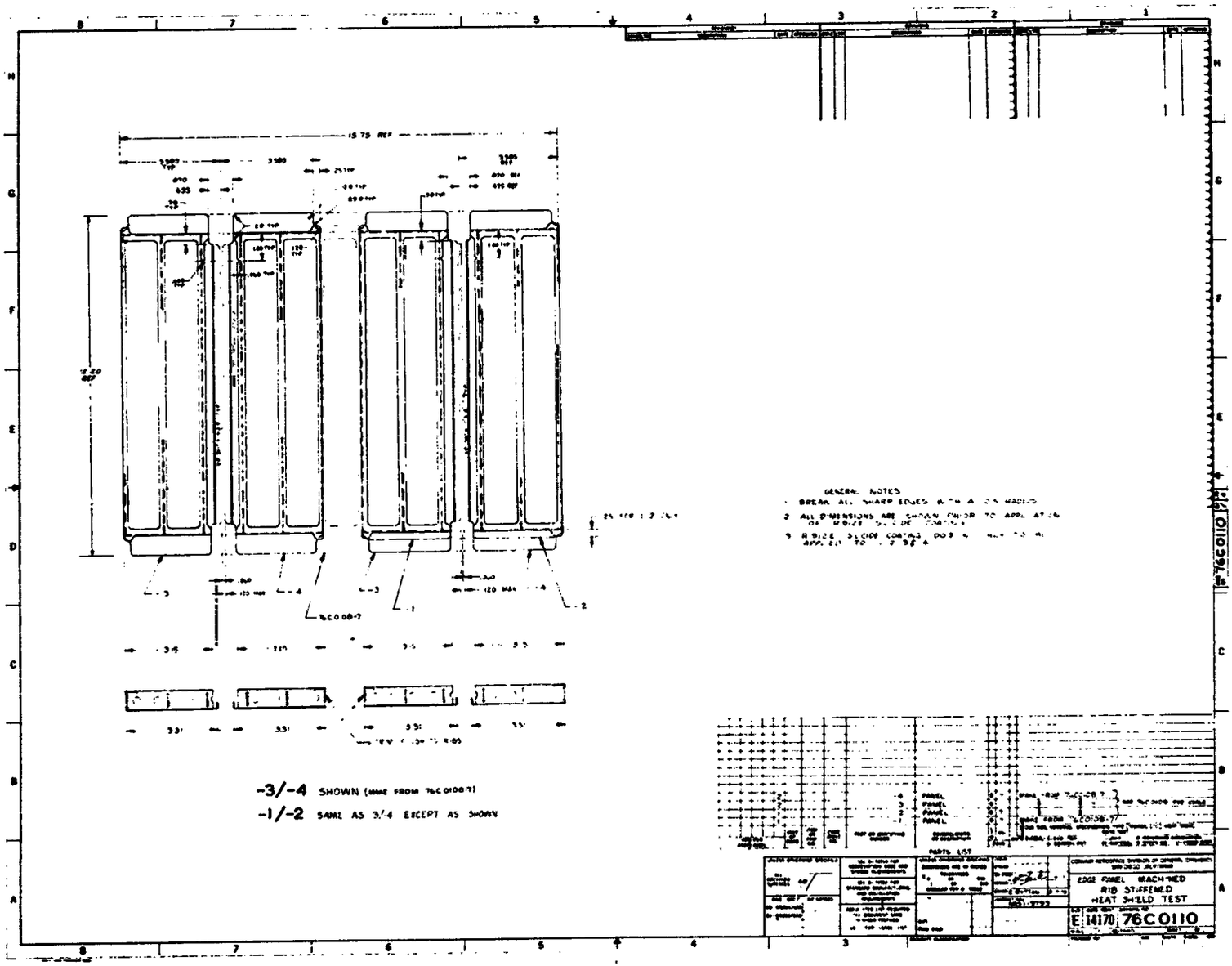

Figure 3-13. TPSTF Edge Heat Shield Panels

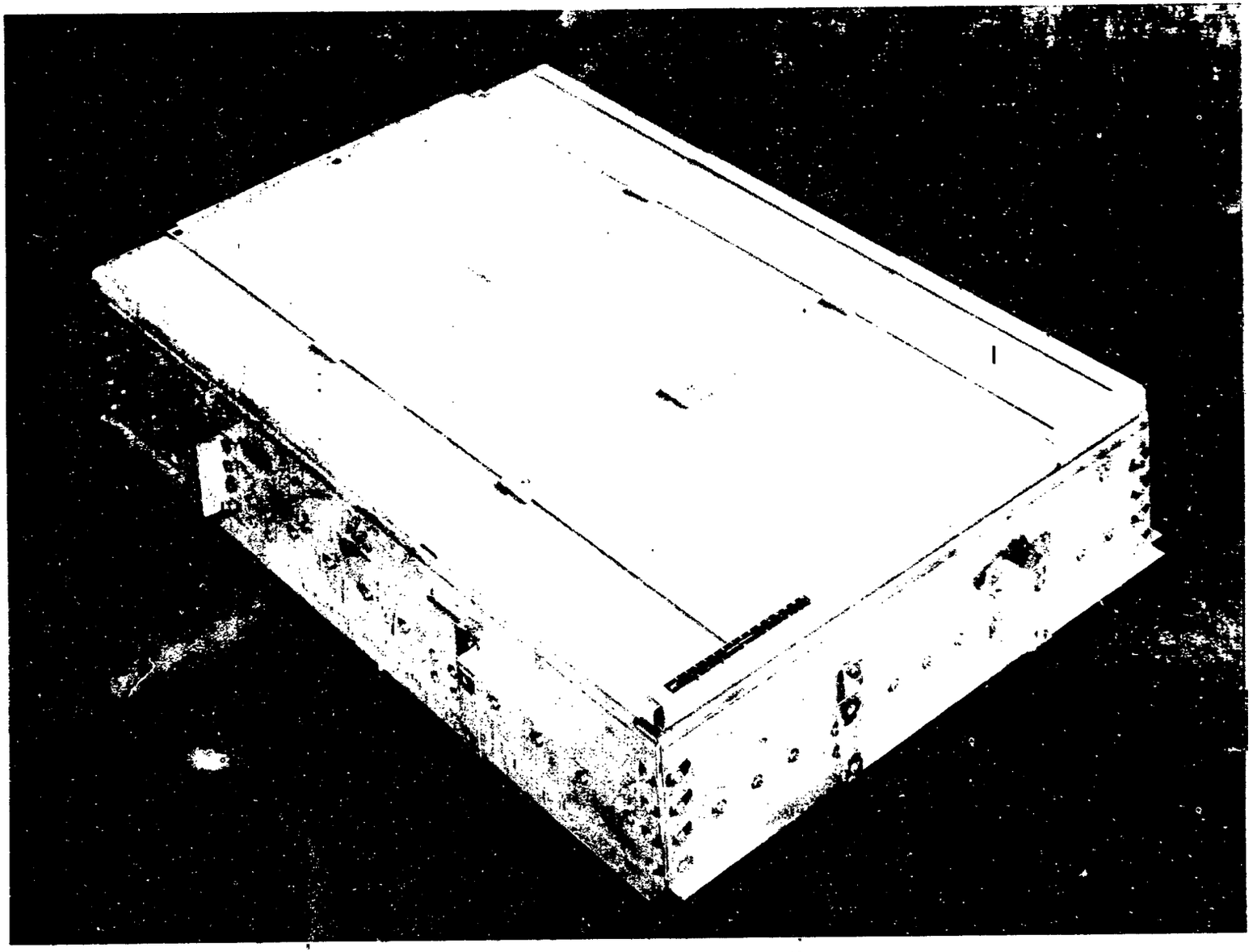

Figure 3-14. TPSTF Test Specimen and Holding Fixture

Tables 3-1 and 3-2 define the most significant changes made to standard thermal protection system hardware as a result of Phase II testing and post test evaluations. The majority of the changes were made to improve manufacturing and material efficiencies. These are discussed in Section 4, Fabrication. A number of changes were made to expedite and to reduce the costs of Phase III, some for Phase III economy and expediency but with engineering implications, and others were for improved structural or functional design.

Typical of design changes made to expedite and to reduce the costs of Phase III, was the standardization of material thickness for the flanges on center and panel edge retainers and on the upper support posts, and for the cap and stiffener of the tee retainers. All tapering of edges of protruding surface hardware was eliminated for Phase III as unnecessary for test hardware. Rectangular, similarly-sized flanges were used for economy throughout Phase III. It is recognized that with flight hardware and quantity production, weights, air flow and geometry can become critical and designs would be modified as required.

Changes having engineering implications but made primarily for Phase III economy and expediency are exemplified by the material changes to lower support post parts. For Phase III, the TD NiCr bar material used for Phase II was unavailable and a substitute was required. HS-188 was selected but its availability and cost directed the change to a two-piece, brazed assembly with a HS-188 flange and a HS-25 (L605) post.

Another example was the redesign of the upper center support posts using non-integral keying lugs on the top surface. Heretofore fillet welding for coated columbium hardware was not considered because of problems with weld quality, entrapped air, consequences of failure. For the upper center post of Phase III, it was judged satisfactory to fillet weld with the electron beam process which produces the highest quality weld and without entrapped air. The probability of weld or coating failure or of the part failing as the result of fillet welding during the life of the tests were considered to be extremely remote.

Certain other changes to Phase II designs were made for Phase III hardware; changes required to improve the thermal-structural design, to rectify engineering oversights, or to improve the functional aspects of the hardware. Changes to the post retainer bolt, the retainer post and the post filler plug are examples.

The thread size of the retainer bolt was increased to 1/4-28 in order to reduce the fastener stresses and to improve the reliability of these fasteners when carrying primary loads. The integral washer was increased in diameter to improve the bearing of the fastener on the retainer post and to reduce the bending stress in the fastener.

Table 3-1 . New and Redesigned Standard TPS Hardware - Phase II to Phase III

Part Name	Part Number	Changes Made To:* Mat'l	Const'n	Size	Th'kn's	Shape	Changes from Phase II and Notes
Panel Edge Retainer	76C0103 -801	No	Yes	No	Yes	No	• Modified joint from tee to post assembly • E.B. weld post assembly • Flange and tee cap thicker
Tee Retainer Subassembly	-1	No	Yes	No	Yes	No	• E.B. weld - 2 piece construction • Cap thicker
Tee Retainer Cap	-21	No	(New)	No	Yes	No	• Thicker and same as stiffener rib • Finish edges for coating before welding
Tee Retainer Stiffener	-27	No	(New)	No	No	No	• Thickness same as cap • Finish edges for coating before machining
Post Assembly	None	No	Yes	No	No	No	• E.B. weld - 2 piece construction • Modified tee retainer weld joint
Retainer Post	-7	No	(New)	Yes	Yes	Yes	• Turned and ground rod • Diameter increased • Shoulder added • Finish machined before weld assembly • Wall thickness decreased
Retainer Flange	-9	No	(New)	Yes	No	Yes	• Shorter • Standard flange stock thickness • End contoured for 2 E.B. welds • Hand grind corners • Finish machined before weld assembly

Table 3-1. New and Redesigned Standard TPS Hardware – Phase II to Phase III (Cont'd).

Part Name	Part Number	Changes Made To: *					Changes from Phase II and Notes
		Mat'l	Const'n	Size	Th'kn's	Shape	
Center Retainer Assembly	76C0103 -805	No	Yes	No	No	Yes	• E.B. weld – 2 piece construction • Finish machine flange & post before welding • Flange thicker • Flange edge taper removed • Hand radius flange corners
Retainer Post	-7	No	(New)	Yes	Yes	Yes	• Turned and ground rod • Diameter increased • Shoulder added • Finish machined before weld assembly • Wall thickness decreased
Center Retainer Flange	-17	No	(New)	No	Yes	Yes	• Standard flange stock thickness • Same dim. as upper post retainer flange • Hand grind corners • Finish machined before weld assembly • Peripheral taper removed
Upper Support Post Assembly	76C0103 -807	No	Yes	No	Yes	Yes	• E.B. weld – 2 piece construction • Finish machined before weld assembly • Flange rectangular and thicker
Upper Support Post	-11	No	(New)	No	No	No	• Turned and ground rod • Finish machined before weld assembly
Upper Support Flange	-15	No	(New)	Yes	Yes	Yes	• Flange thicker and rectangular • Standard flange stock thickness • Hand grind corners • Finish machined before weld assembly

Table 3-1. New and Redesigned Standard TPS Hardware - Phase II to Phase III (Cont'd).

Part Name	Part Number	Changes Made To:*					Changes from Phase II and Notes
		Mat'l	Const'n	Size	Th'kn's	Shape	
Upper Cntr. Sup't Post Assembly	76C0103 -811	No	Yes	No	Yes	Yes	• E.B. weld - 4 piece construction • Non-integral keys • Keys E.B. fillet welded to flange • Flange thicker
Upper Support Post Assembly	-807	No	Yes	No	Yes	Yes	• E.B. weld - 2 piece construction • Finish machined before weld assembly • Flange rectangular and thicker
Upper Support Post	-11	No	(New)	No	No	No	• Turned and ground rod • Finish machined before weld assembly
Upper Support Flange	-15	No	(New)	Yes	Yes	Yes	• Flange thicker and rectangular • Standard flange stock thickness • Hand grind corners • Finish machined before weld assembly
Key	-19	No	(New)	Yes	Yes	Yes	• Rectangular bar • Circumferential E.B. fillet weld to machined flange • Finish machined before weld assembly

Table 3-1 . New and Redesigned Standard TPS Hardware - Phase II to Phase III (Cont'd)

Part Name	Part Number	Changes Made To:*					Changes from Phase II and N tes
		Mat'l	Const'n	Size	Th'kn's	Shape	
Lower Support Post Assembly	76C0103 -813	Yes	Yes	Yes	No	No	• Material changed for flange & post • Brazed -2 piece construction • Flange & post finish machined
Lower Support Flange	-33	Yes	(New)	No	No	No	• Material changed to HS-188 • Finish machined before braze assembly
Lower Support Post	-35	Yes	(New)	No	No	No	• Material changed to HS-25 (L605) • Finish machined before braze assembly
Post Retainer Bolt	76C0103 -37	No	No	Yes	No	Yes	• Diameter and thread increased • Drive socket depth increased • Washer diameter increased • Washer thickness increased
Post Filler Plug	76C0103 -39	No	No	Yes	Yes	Yes	• Turned and ground rod • Head diameter increased • Socket depth increased • Wall thickness decreased

*Materials, construction, size, thickness, and shape

Table 3-2 . New and Redesigned Standard Heat Shield Panels - Phase II to Phase III

Part Name	Part Number	Changes Made To:* Mat'l	Const'n	Size	Th'kn's	Shape	Changes from Phase II and Notes
Finished Heat Shield Panel	76C0108	No	No	No	No	No	• Retainer post hole enlarged • Finish machine & edge prep rib cap ends
Final Assembly Welding	76C0107	No	No	No	No	No	• Weld ends of rib caps to beams - 22 places • Fuse unwelded, step-machined beam edges for coating - 20 places.
Panel Welding 1st Stage	76C0105 -1	No	Yes	No	No	No	• E.B. weld - 25 piece construction
Panel Skin	-7	No change from Phase II					
Panel Cap	-9	No	(New)	Yes	No	Yes	• Multiple caps • Edge prep for coating before welding • Machined contour
Panel Rib	-11	No change from Phase II					
Panel Beam Assembly	76C0106 -3, -5	No	Yes	No	No	Yes	• Load pads modified (-3 only) • Flange center contour changed (-3 only) • Web center pocket removed (-3 only) • E.B. welded - 2 piece construction
Beam	-17	No	(New)	No	No	Yes	• Interchangeable for all beam assemblies • Rough machine before E.B. weld assembly
Beam Flange	-19, -21	No	(New)	No	No	No	• Interchangeable for narrow or wide flange beams • Edge machine for E.B. weld assembly

*Materials, construction, size, thickness, and shape

its thickness was increased to reinforce the bottom of the hexagon drive socket and to permit it to act as a hoop stiffener for the socket. To minimize the problem of the fastener splitting when being removed, the depth of the hexagonal socket was increased for Phase III retainer bolts.

The increase in diameter of the washer on the retainer bolt required an increase in diameter of the retainer post. At the same time the wall thickness was reduced by 0.003 inch (0.076 mm) and a reinforcing shoulder was added at the top for increased strength. The latter changes were made to reduce the thermal path through the retainer post and to rectify a drafting error of Phase II.

Similarly the diameter of the head of the post filler plug was increased to accommodate the larger hole in the retainer post and the wall thickness was reduced 0.015-inch (0.38 mm) to reduce the thermal path. The depth of the hexagonal drive socket was increased to afford a better grip for the removal tool during disassembly.

The outlined changes in the panels in Table 3-2 were all made for economies in manufacturing and in materials and had no significant engineering implications.

The change made in insulating material from Phase II to Phase III had little impact on cost or fabricability, but did have engineering implications in that it effected the performance and weight of the TPS. Fiberfrax H blanket insulation (a product of the Carborundum Co.) replaced Dyna-Flex (a product of Johns-Manville). This change was made in an effort to increase the system thermal efficiency, reduce the unit weight, increase the ease of handling after exposure, and to evaluate an insulation material without a binder.

It had been noted previously when conducting thermal tests in a chamber heated by quartz lamps that a specimen containing an insulation with a binder required outgassing prior to insertion into the chamber. The consequences of not outgassing were excessive smoke and deposits on the quartz heating lamps or tubes.

The initial selection of Fiberfrax H was based on the work of T. A. Hughes (Reference 2) who determined that the material provided "excellent performance" under a simulated space shuttle environment. Subsequent investigations at Convair confirmed that the insulation had an acceptable dimensional stability and retained its flexibility after 100 hours at 2400° F (1589° K). The samples evaluated indicated that Fiberfrax H was approximately 33-percent more thermally efficient at 2400° F (1589° K) than Dyna-Flex on the basis of the conductivity-density product ($k\rho$). Finally, the use of Fiberfrax H at a nominal density of 6 lb/ft^3 (96 kg/m^3) would enable a significant reduction in system weight.

4 FABRICATION OF TPS HARDWARE

4.1 General

The fabrication of test hardware for the metallic thermal protection system employed standard manufacturing processes and techniques and included machining, electrical discharge metal removal, electron beam welding, brazing, vacuum heat treating and creep flattening, and standard sheet metal processing. Only the use of columbium alloys and the oxidation resistant coatings might be considered as unconventional.

When considering the design of hardware for Phase III of this program, it became evident from a review of Phase II fabrication that substantial savings could be effected through better material use and improved fabrication processing. The efficiency and effectiveness of electron beam welding for heat shield hardware had been clearly demonstrated during Phase II. This process had permitted the joining of finished machined parts without the usual problems of distortion normally associated with fusion welding.

Therefore, each detail, element, subassembly, and assembly for the Phase III hardware was evaluated. As a result, each item of hardware for the Phase III TPS was redesigned for improved material costs or availability, or to reduce the manufacturing costs. Material costs were considerably reduced by employing built-up welded sections for post or tube to flange assemblies, and for long, thin tee members which previously were machined from solid bar.

Examples of this are shown in Figure 4-1 with arrows denoting electron beam welds. This figure shows a center retainer and two styles of upper support posts, all of which were previously machined from solid bar, and a longitudinal edge retainer assembly previously made of two parts machined from solid bar and joined by welding. Each post or tube shown is a completely machined item joined by electron beam welding to a partially or completely machined flange. One support post has two rectangular keys which were circumferentially welded by electron beam after all machining was completed. The panel edge retainer shown is fabricated of two subassemblies. The tube and flange assembly consisting of completely machined details welded by the electron beam and a tee member made of a cap and a stiffener, both of which were completely edge-finished or edge radiused and joined by a linear, burn-through electron beam weld. The two subassemblies are joined with a short linear, burn-through tee weld between the flange and the stiffener and a transverse butt weld between the cap and the flange.

Extensive material cost reductions resulted from the redesign of the panel edge beam. These beams were originally machined from a single size of solid bar. As redesigned to a built-up member, it consisted of a rough-machined I-section, interchangeable for all panel beams, and a thin flange, tailored to the desired width before electron beam welding to the I-section. This construction is detailed in Figure 3-8.

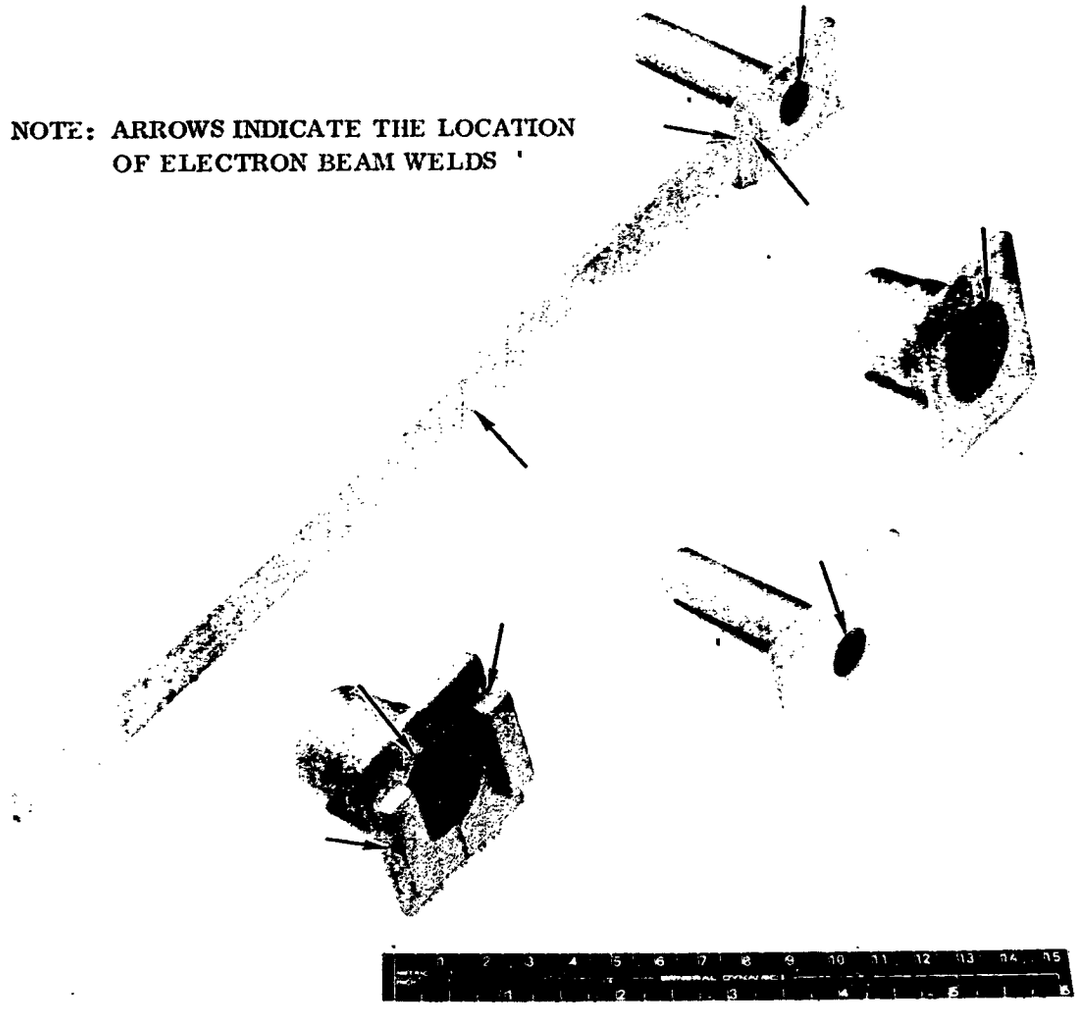

Figure 4-1. Welded Columbium Panel Retainers and Upper Support Posts (136947)

Another high cost area examined involved the edge finishing or radiusing of corners and edges of all columbium alloy hardware to permit efficient silicide coating. Whenever possible, the radiusing operation was done during detail machining, or by vibratory mechanical finishing equipment rather than by hand radiusing in assembly as in Phase II. In this way, parts are welded into final assemblies requiring little or no hand radiusing. On the heat shields, the edges of all twelve rib cap members were finish machined and mechanically radiused before welding.

One other reduction in hand radiusing on the panels was accomplished on the inboard edges of the closeout beams which had been step-machined to receive the rib caps for welding. The removal of this machined step and the radiusing of the edge after welding was required on the beam edges between each beam to cap weld. For Phase III panels, the step removal and radiusing was accomplished by utilizing the versatile electron beam to melt-down the step and to bulb and radius the edge.

4.2 Materials

The materials used in the fabrication of the TPS test hardware were: (1) columbium alloy Cb-752 for the heat shield and guard panels, panel retainers, the upper support posts, and plugs; (2) the dispersion strengthened nickel alloy, TD NiCr, for the threaded fasteners; (3) cobalt base alloys HS-25 (L-605) and HS-188 for the lower half of the support posts; (4) oxidation resistant coatings for columbium and for TD NiCr; (5) high temperature fibrous insulation blankets.

4.2.1 Metals. - The columbium alloy used was Cb-752 (Cb-10W-2.5 Zr) produced by Wah Chang Albany Corporation, Albany, Oregon and furnished in the fully recrystallized condition. Typical chemical compositions taken from supplier certifications are presented in Table 4-1.

TD NiCr was supplied from NASA Contract NAS1-11654 from material produced by Fansteel under NASA Contract NAS3-13490. The chemical analysis of this material is given in Table 4-2.

Both HS-25 (L-605) and HS-188 are commercially available cobalt base alloys produced by the Stellite Division of Cabot Corporation, Kokomo, Indiana. Typical chemistries of these alloys are given in Table 4-3.

4.2.2 Coatings - Coatings used were a silicide coating for the Cb-752 and an aluminide coating for the TD NiCr. The columbium coating was R-512E, a Si-20% Cr-20% Fe fused silicide coating applied by HiTemCo. This coating was applied to columbium hardware following chemical or mechanical cleaning. Chemical cleaning was accomplished in a

Table 4-1. Chemical Analysis of Phase III TPS Columbium Alloy Cb-752
Heat Treat Condition: Fully Recrystallized
Form: Sheet, Bar, and Rod

Element	Ingot Analysis - Percent by Weight		
	Heat 77043	Heat 77049	Heat 77059
W	10.2/10.2	9.5/9.4	9.3/9.5
Zr	2.5/2.6	2.5/2.5	2.4/2.5
Cb	Balance	Balance	Balance
Al	< 20 ppm		
C	60/< 40	40/50 ppm	40/30 ppm
Co	< 10		
Cr	< 20		
Cu	< 40		
Fe	< 50		
H	< 5	< 5	< 5
Hf	790/770	< 500	< 500
Mg	< 20		
Mn	< 20		
Mo	300/300		
N	45/27	70/60	60/60
Ni	< 20		
O	70/< 50	80/100	140/100
Si	< 50		
Sn	< 10		
Ta	4000/3800	4000/4000 ppm	4100/4600 ppm
Y	160/100 ppm		

Table 4-2. Typical Chemical Analysis of TD NiCr for Phase II Fasteners

Alloy:	Ni-20Cr-2ThO_2
Heat Treat Condition:	Partial Stress Relief (see note)
Form:	Rod
Heat Number:	3844

Source: Fansteel Inc., Metals Division
NASA-Lewis Contract NAS3-13490
NASA-Langley Contract NAS1-11654

Chemical Analysis - Percent by Weight

Carbon:	0.010
Sulphur:	0.0061
Chromium:	19.79
Thoria (ThO_2):	1.42
Nickel:	Balance

Note: Additonal Stress Relief accomplished during coating @ 2000° F (1366°K) for 1 hour.

Table 4-3. Typical Chemical Composition
Cobalt Base Alloys for Phase III.

Heat Treat Condition: Annealed
Form: Sheet and Bar

Element	Chemical Composition - Percent by Weight		
	HS-25 Heat 1860-2-1218	HS-188 Heat 1880-2-1611	HS-188 Heat 1880-2-1617
Cr	19.70	22.50	22.40
W	14.55	14.50	13.94
Fe	2.15	1.90	1.53
C	0.09	0.09	0.09
Si	0.10	0.35	0.31
Co	Balance	Balance	Balance
Ni	10.30	21.40	22.40
Mn	1.40	0.76	0.73
P	0.019	0.010	0.011
S	0.007	0.008	0.007
La	-	0.071	0.058

HNO_3-HF acid solution, and mechanical cleaning was by grit blasting with iron particles. The coating slurry was applied by dipping and spraying with all edges overcoated or beaded using a miniature striping roller. Spray overcoating was employed on edges when the geometry of a part prevented using the striping roller. After coating application, the parts were air dried at room temperature, followed by insertion into a high temperature vacuum furnace where they were baked at a low temperature, 400 to 600° F (478 to 589° K) to remove the coating binder and other volatiles. The furnace temperature was then increased to 2600° F (1700° K) where the coating fused and flowed evenly over all surfaces of the parts. This temperature was held for 60 minutes under a vacuum of less than one micron (133 mN/m^2) and the parts were then furnace cooled to room temperature. The thickness of the unfired or "green" coating was specified to be 20 to 25 mg/cm^2, which resulted in a fused coating thickness of 0.003 (0.076 mm) to 0.004 inch (0.102 mm).

All TD NiCr fasteners were coated with an aluminide to increase oxidation resistance and as a protective measure to avoid any incompatibility between the TD NiCr and the silicide coatings on the columbium. This coating is a Vac Hyd proprietary aluminide, VH-28 (Cr-Co-Al-Y).

4.2.3 Insulation - The high temperature insulating blanket material selected for use between the metallic heat shields and the primary load-carrying structure was Fiberfrax H. This material is a product of the Carborundum Company of Niagara Falls, New York. It is composed of alumina silicate (62% Al_2O_3 - 38% SiO_2) fibers having a fiber diameter range of 2 to 4 microns (2 to 4 μm), a fiber length up to 0.5 inch (12.7 mm), and a melting temperature above 3500° F (2200° K). The material was ordered in an nominal thickness of 0.25 inch (0.64 cm) and a nominal density of 6 lb/ft^3 (96 kg/m^3). The material received had an average thickness of 0.33 inch (0.84 cm) and a calculated density of 5.71 lb/ft^3 (91.4 kg/m^3). This was compressed during installation to a density of 7.1 lb/ft^3 (113.7 kg/m^3).

4.3 Test Hardware

The test hardware for Phase III involved tee-stiffened heat shields, edge retainers and hold-downs, insulation, and supports for one nine-panel test array and for the TPSTF array. Each panel was approximately 12 inches (30.5 cm) wide by 16 inches (40.6 cm) long. The depth of the complete TPS including the high temperature fibrous insulation and panel support posts was 4.4 inches (11.2 cm).

Figures 4-2 and 4-3 show one of the completed tee-stiffened heat shields ready for test. These panels were completely assembled by electron beam welding, each panel containing over 33 feet (10.1 m) of weld applied without straightening or intermediate heat treating of the panel.

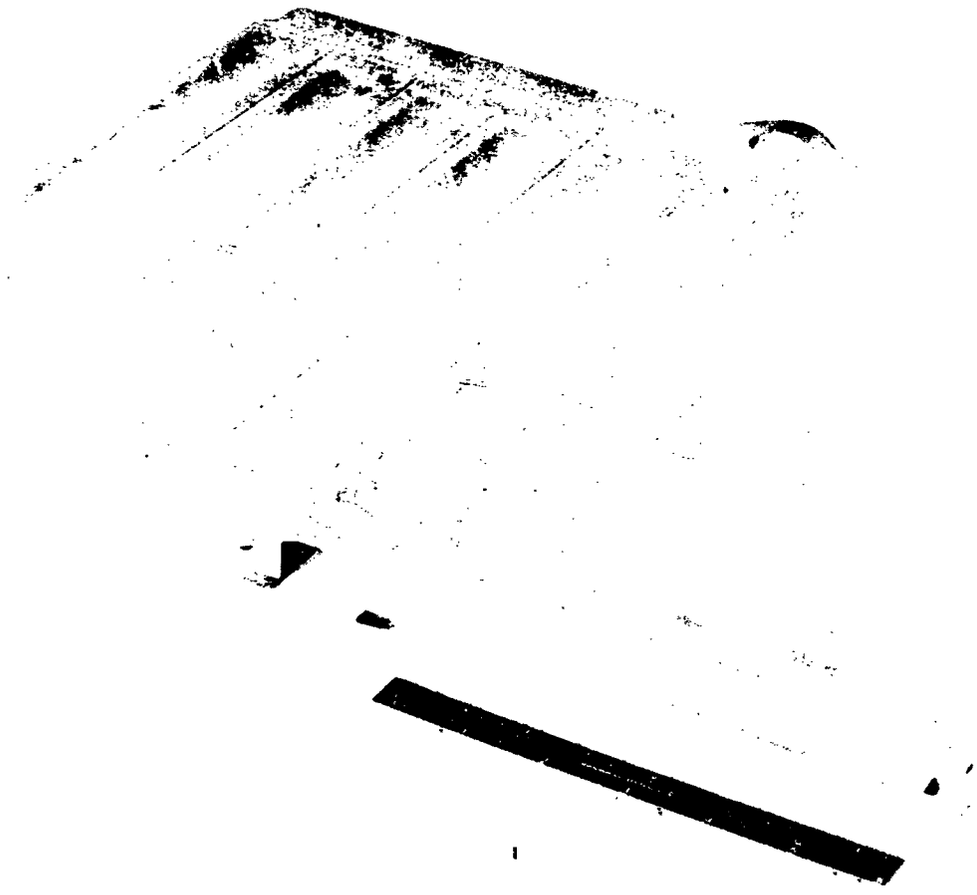

Figure 4-2. Coated Tee-Stiffened Heat Shield Panel – Skin Side (136945)

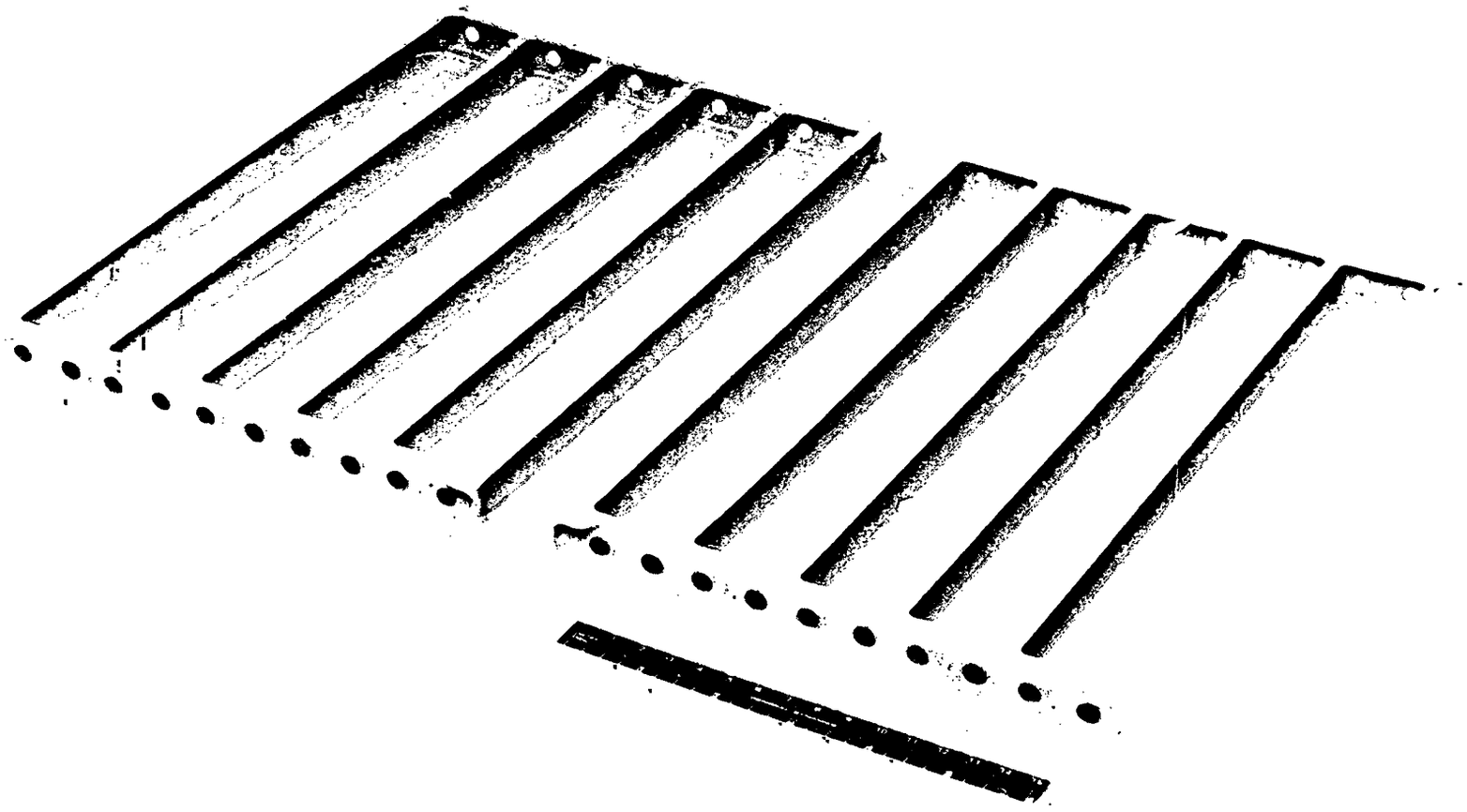

Figure 4-3. Coated Tee-Stiffened Heat Shield Panel – Interior Side (136946)

The panel skin, ribs and rib cap strips were first cleaned and then assembled into weld tooling for electron beam welding. The hard-chrome plated copper tooling shown in Figures 4-4 and 4-5 was designed to permit the completion of all the burn-through longitudinal tee welds on both panel faces without removing the assembly from the tooling. The maximum distortion resulting from this welding was 0.050 inch (0.127 cm) in the panel long dimension. Transverse distortion was negligible. The panel subassemblies composed of the skin, rib caps, and ribs were subsequently machined to receive the end closure beams for welding.

Closeout electron beam welding joined the machined panel subassembly to the completely machined closure beams. This consisted of an additional 4 feet (1.2 m) of step-butt weld joining the panel skin and the rib caps to the beams and 24 burn-down tee slot welds interconnecting the ribs and the beam webs. For the welding of the panel skin and rib caps to the closure beams, the assembly was placed in weld tooling which held the skin and caps in contact with the machined step of the beam flange during the electron beam welding on each side and on the ends of the panel. No interior tooling was necessary and no weld tooling was needed for the tee slot welds.

Following the completion of structural welding, the panel was positioned approximately 45° to the axis of the welding beam and the unwelded, machined step on the inboard edges of the closure beams were fused round and smooth, removing the machined surfaces and eliminating the need for edge radiusing for coating.

Details of the step-butt welds and the tee slot welds for joining the panel skin, rib caps and rib to the closure beam can be seen in Figure 4-6. The same joint, closed for welding, can be seen in Figure 4-7.

This approach to panel welding with the electron beam process was possible since: (1) the parts and subassemblies were designed to be self-locating, (2) the welding equipment could be precisely regulated, (3) the operator was able to observe, manipulate, and control the welding beam during all welding.

The post-to-flange and tube-to-flange weldments shown in Figure 4-1 were joined with the aid of simple positioning tools. In these cases, the weld joints were square butt joints with the cylindrical part penetrating through the flange. The welds were made from the flange side to approximately 90% penetration, and the weld completed with the parts rotated while in the inverted position.

The tee member of the longitudinal edge retainer was made with a burn-through weld joining the cap to the stiffener. The part was then annealed and straightened and its end machined for the square butt weld and the short burn-through weld joining the cap and stiffener to the flange of the tube and flange weldment.

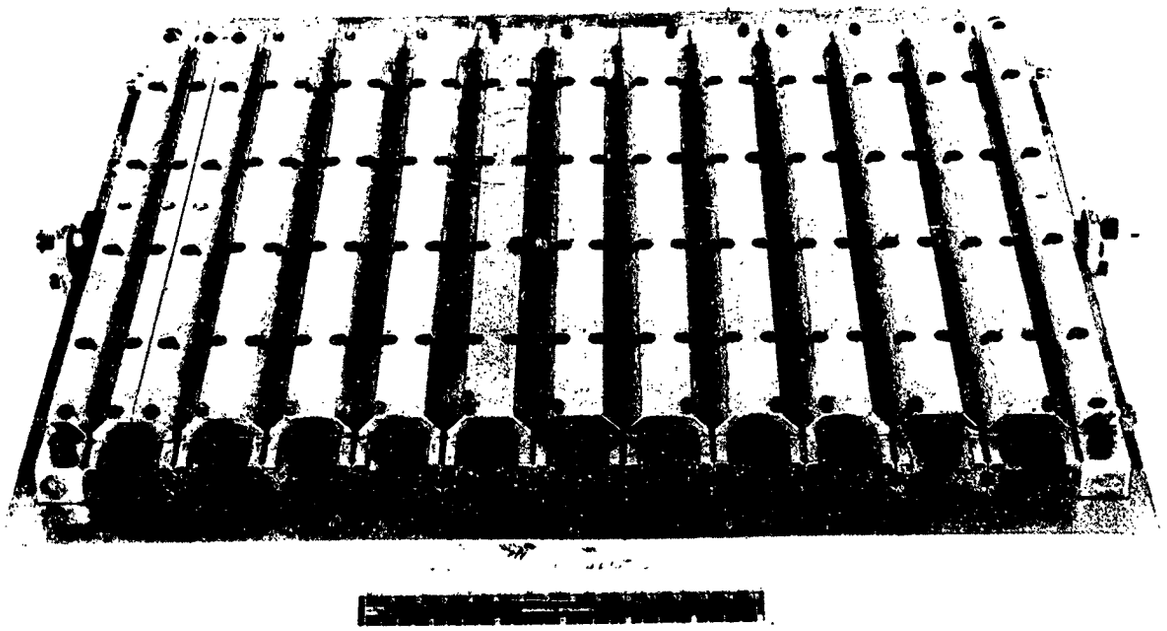

Figure 4-4. Welding Fixture for Tee-Stiffened Heat Shield Panel – Cap to Rib Weld (137277)

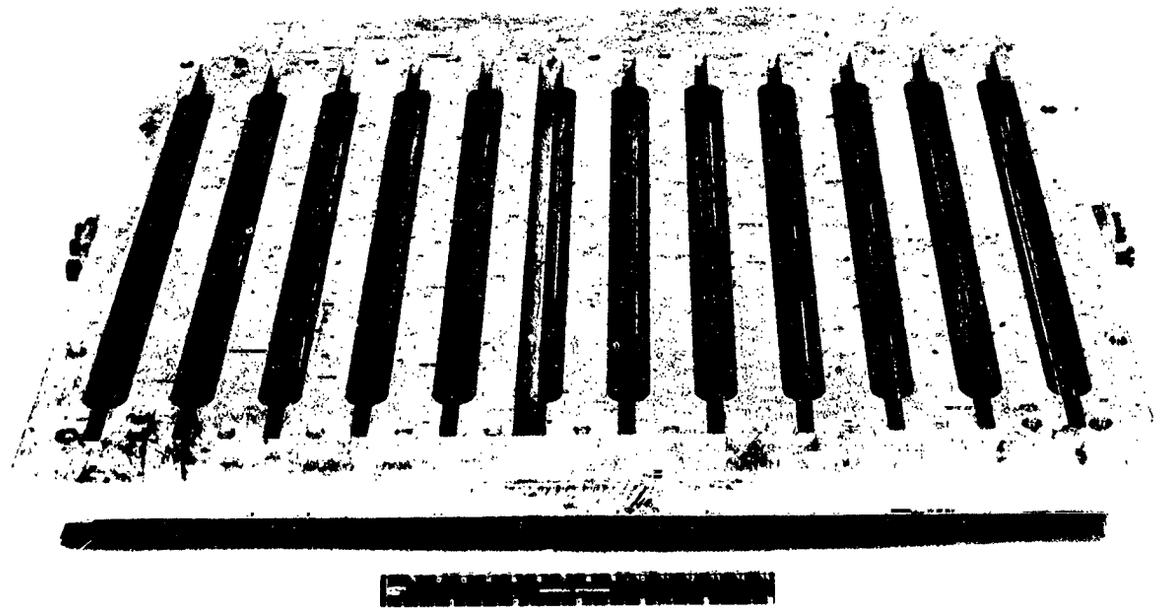

Figure 4-5. Welding Fixture for Tee-Stiffened Heat Shield Panel – Skin to Rib Weld (137278)

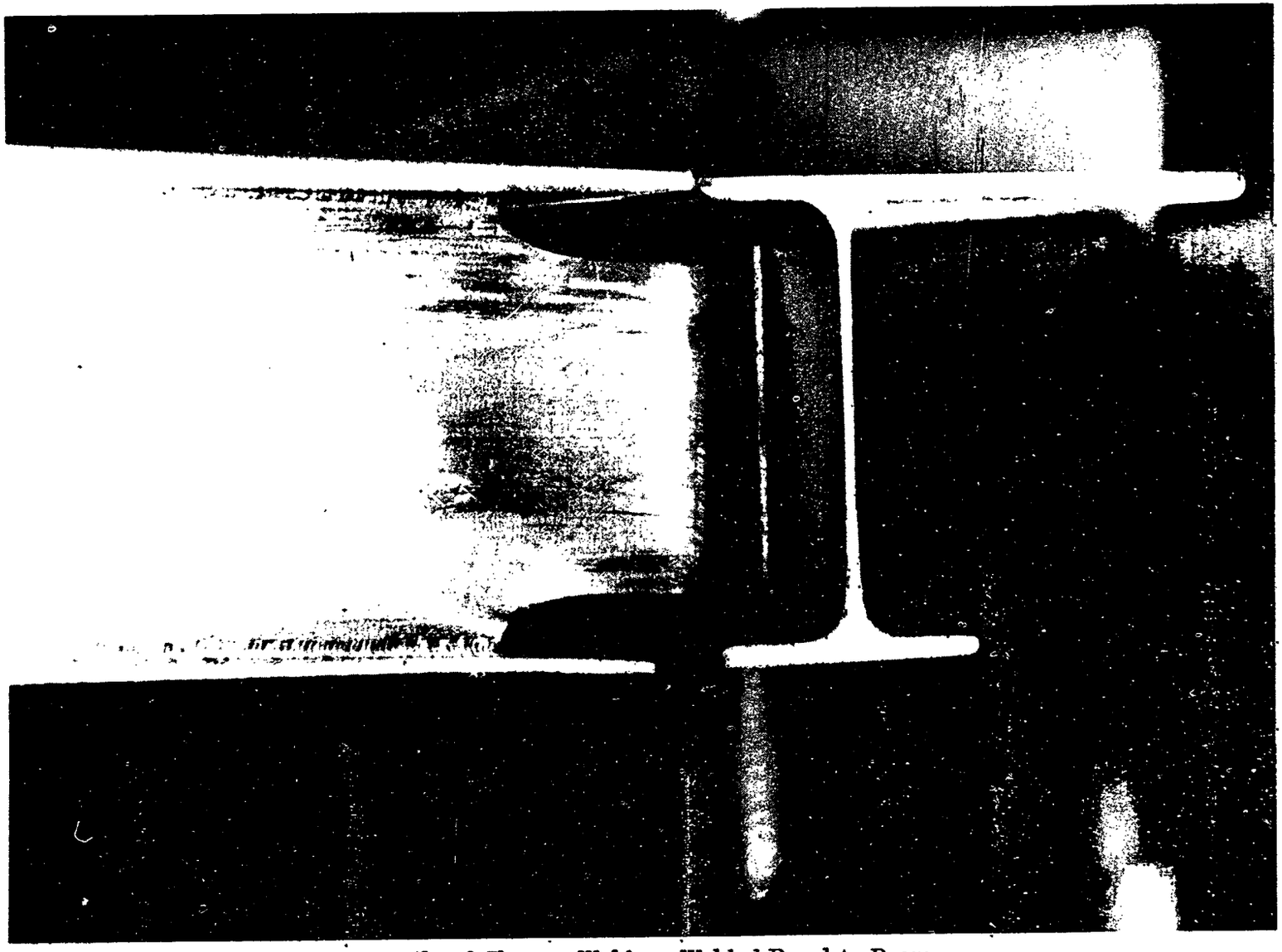

Figure 4-6. Details of Closure Welds – Welded Panel to Beam – Tee-Stiffened Cb-752 Heat Shield Panel (128069B)

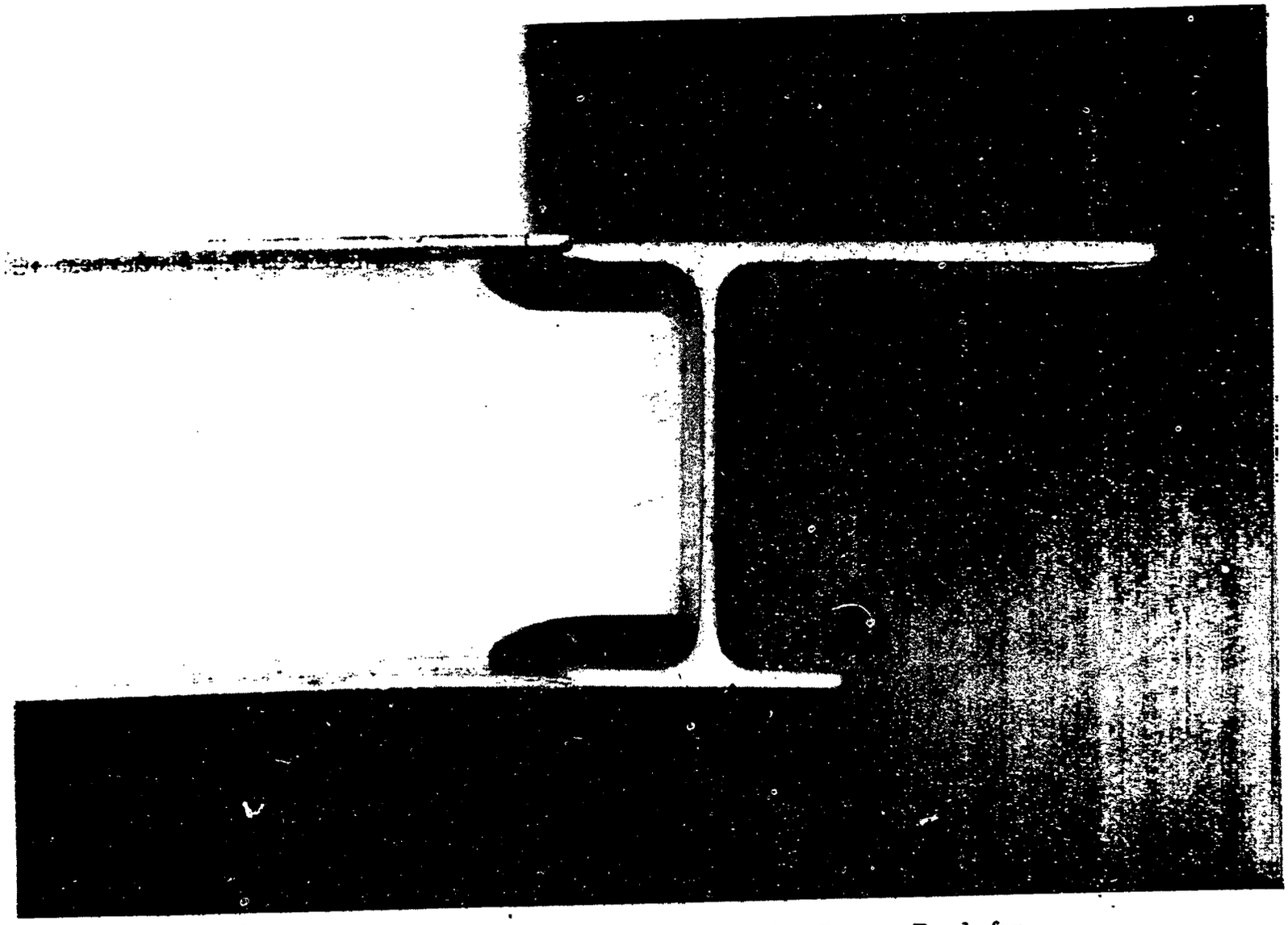

Figure 4-7. Detail of Closure Welds – Welded Panel to Beam – Ready for Welding, Tee-Stiffened Cb-752 Heat Shield Panel (128068B)

4.4 Fabrication Sequence

Typical fabrication flow charts for each of the major elements of the TPS are shown in Figures 4-8 through 4-12. Each item of illustrated hardware except for the lower post was made of welded columbium alloy. The lower post assembly had an HS-25 (L-605) body and an HS-188 flange joined by brazing. In all cases, the hardware fabrication utilized standard aerospace fabrication processes. The preparation for coating of the refractory metal consisted of rounding or radiusing edges and corners either manually or by vibratory finishing. This prepared the edges and corners with the best condition for the application of the silicide coating. In general, a radius of 0.015 inches (0.038 cm) was specified for all columbium alloy components. This task was generally performed before the weld assembly where the task could be accomplished during machining operations, or performed in the vibratory finisher. Edge preparation after weld assembly and/or machining was done either manually or by a combination of manual and mechanical means.

One coated panel with associated coated columbium retainers and support posts and TD NiCr fasteners is shown in Figure 4-13.

4.4.1 Welding. Electron beam welding was used extensively for the fabrication of Phase III hardware. The decision to use this process was based upon its demonstrated reliability and the experience and confidence developed during the Phase II fabrication and testing.

Electron beam welding involved several types of welds: (1) burn-through tee welds between the panel skin and rib caps attaching the ribs, and between the edge retainer tee caps and stiffeners, (2) step-butt welds between the panel skin and rib caps attaching the closure beams, (3) burn-down, tee slot welds between the ribs and beam webs, (4) square-butt welds used on all tube or post to flange joints, on all closure beam subassemblies joining a rough machined beam section to either a wide or a narrow flange, and the final assembly weld for the tee edge retainers, and (5) fillet welds joining the two panel locator keys to the flange of the center retainer posts.

Abutting edges of all weld joints were prepared by machining for the close fit required by electron beam welding. No filler material was applied except as provided by the base material in the joint design. Prior to welding, parts were alkaline cleaned and chemically etched using standard columbium cleaning procedures.

All welds required 100% joint fusion with full penetration and fillet formation and conformance with specification MIL-W-46132. Welds were made using chrome-plated copper and aluminum hard tooling. Chromium was applied to copper tooling to prevent contamination of the columbium during welding and assembly operations. As further insurance against contamination, all welded parts were acid etched to remove residual copper prior to each heating or welding operation.

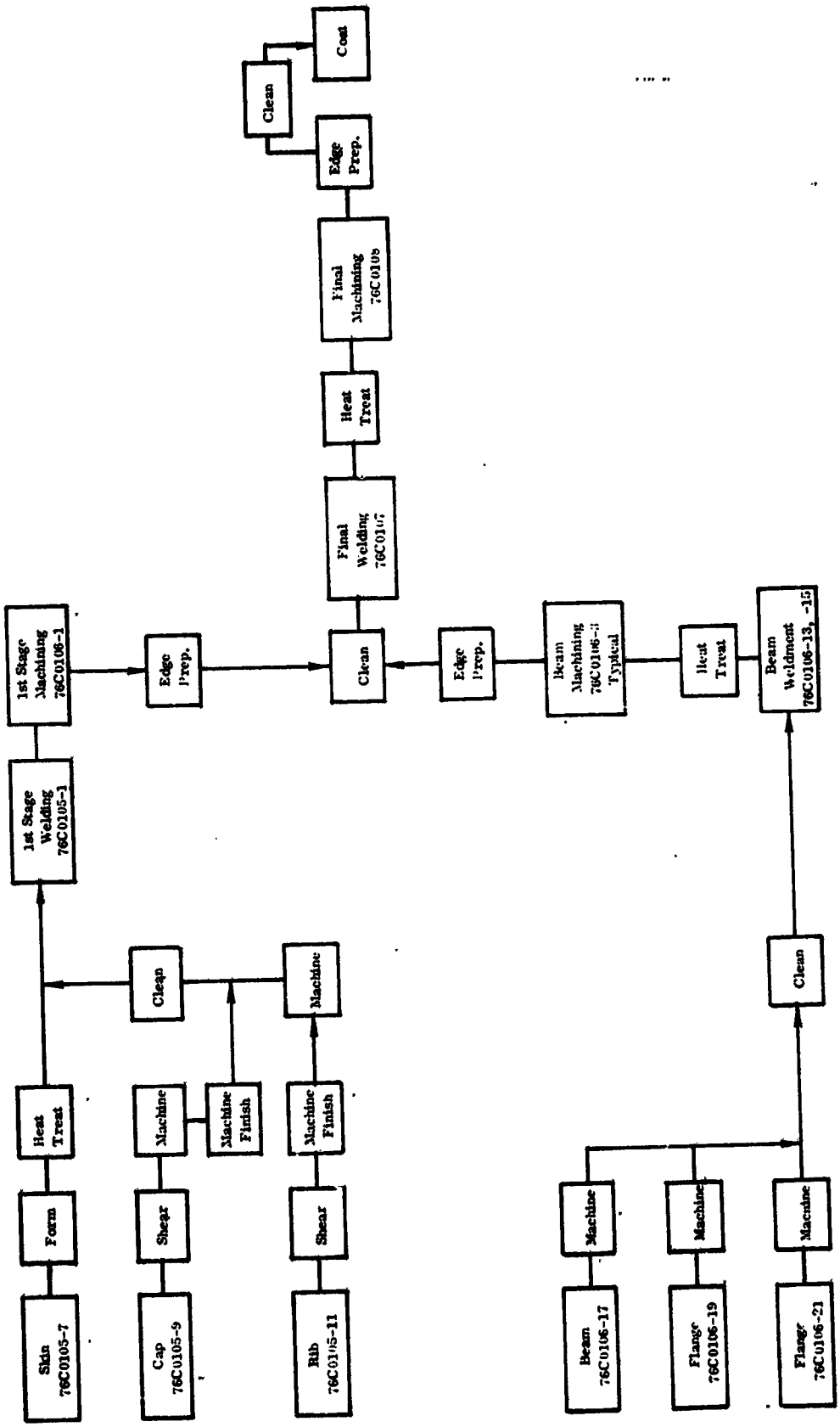

Figure 4-8. Fabrication Sequence for TPS Heat Shield Panels. 76C0108

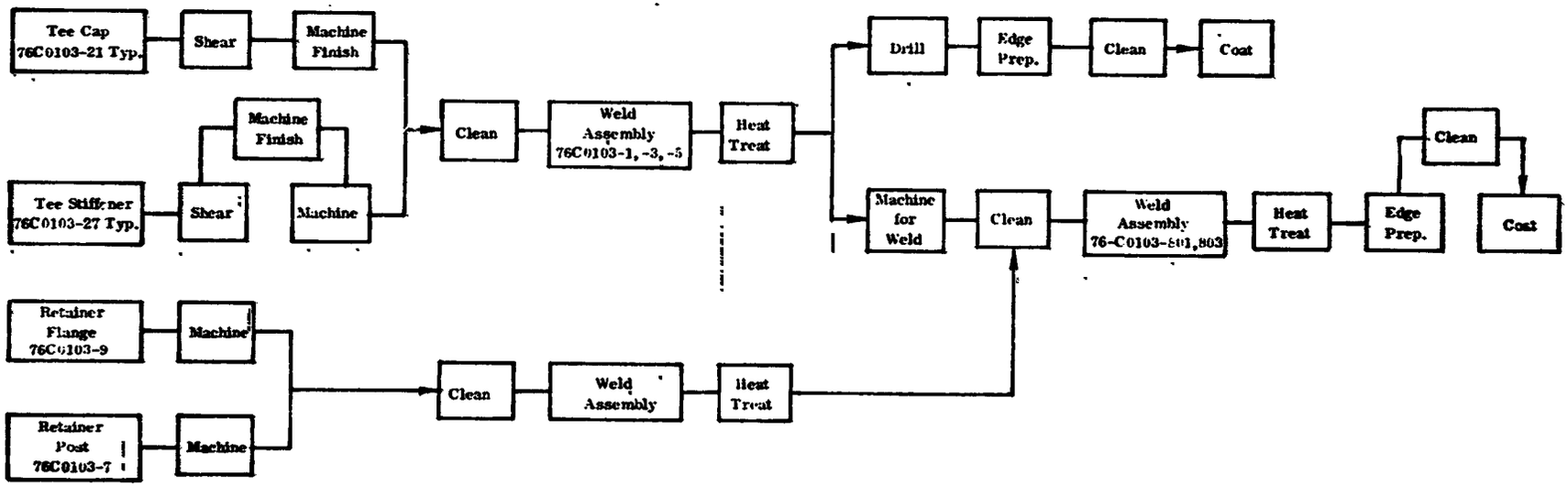

Figure 4-9. Fabrication Sequence for Edge Retainers. 76C0103-5, -801, -803

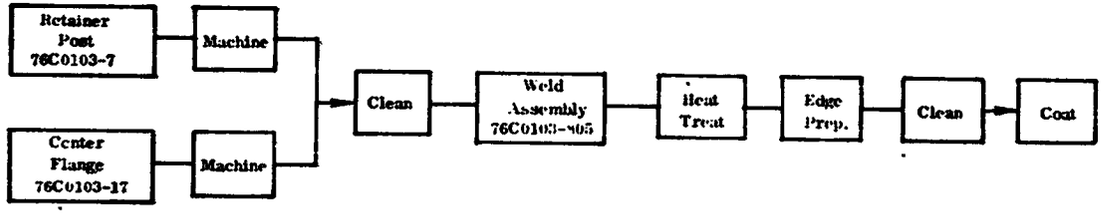

Figure 4-10. Fabrication Sequence for Center Retainers. 76C0103-805

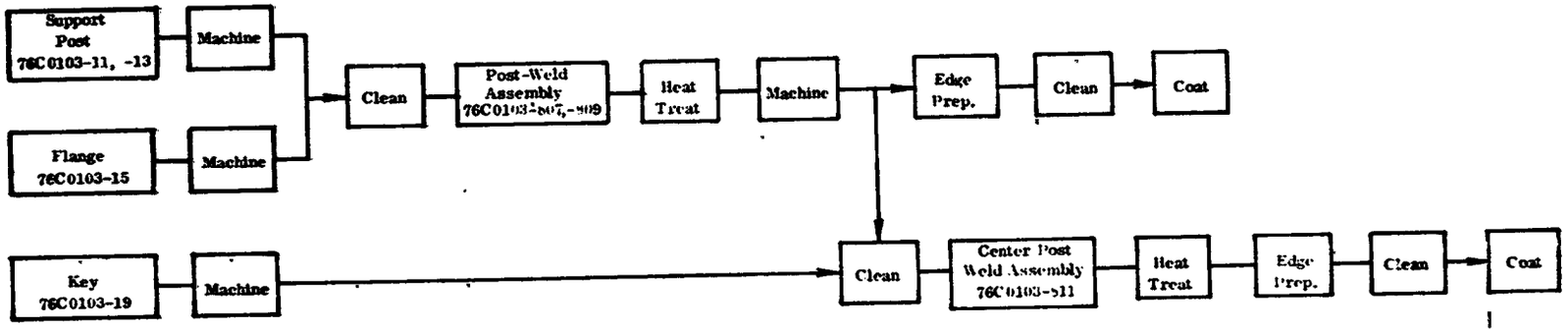

Figure 4-11. Fabrication Sequence for Upper Support Posts. 76C0103-807, -811

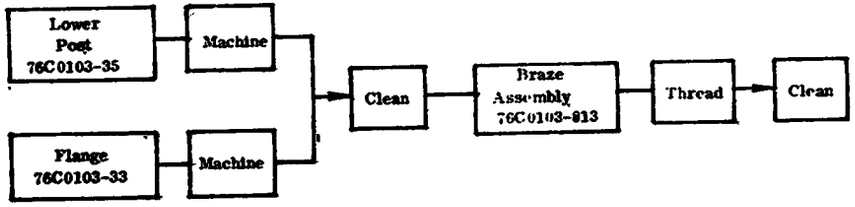

Figure 4-12. Fabrication Sequence for Lower Support Posts. 76C0103-813

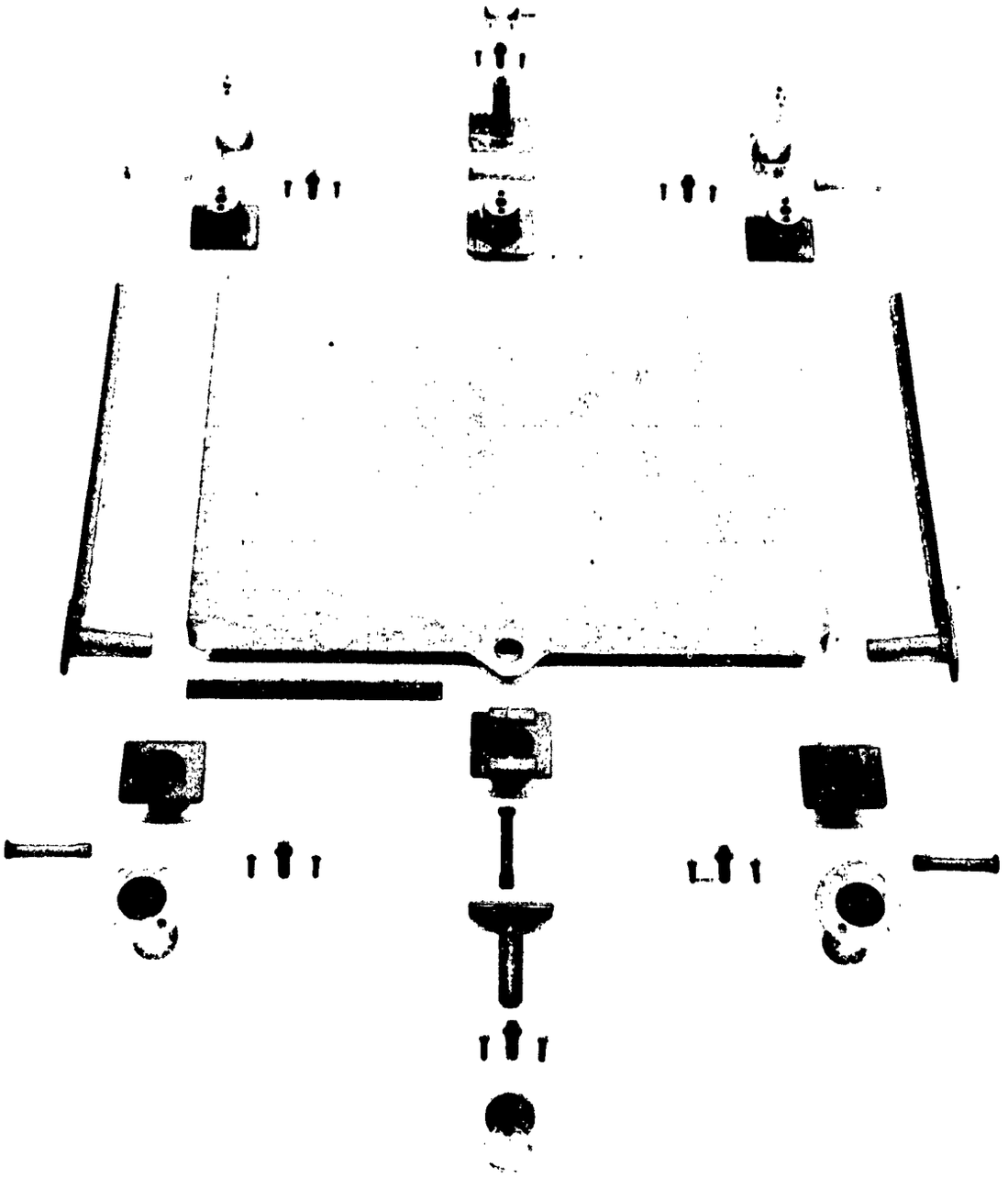

Figure 4-13. Tee-Stiffened TPS Components Prior to Testing (137103)

4.4.2 Heat Treatment. - Formed and welded parts were simultaneously annealed and creep straightened or flattened to assure stress-free and properly fitting parts. This operation was performed at 2500° F (1644° K) for one hour in a vacuum of at least 2.5 x 10^{-5} torr (3.33 mN/m^2). Intermediate annealing and flattening of rough beam weldments were done at 2600° F (1700° K). Parts were loaded with refractory metal weights during annealing to effect the creep straightening. All welded parts were vacuum annealed at the completion of all operations to assure stable parts during coating.

4.4.3 Brazing. - The only brazing performed in Phase III was in the fabrication of the cobalt base alloy lower support posts. Here the flange of HS-188 was brazed to a HS-25 cylindrical post using General Electric alloy J8100 (10Si-19Cr-3Fe-0.5 Mn-0.5 Co-0.15C-Bal Ni). Brazing was accomplished at 2150° F (1450° K) in a vacuum of 1 x 10^{-4} torr (1.33 mN/m^2) using white Nicrobraze stop-off material. The parts were cooled in the furnace to 1800° F (1155° K) followed by an argon back-fill and cooling to room temperature.

5. SYSTEM WEIGHTS AND COST

5.1. System Weights

A breakdown of the TPS component weights before and after coating, is presented in Table 5-1. In computing the unit weight the system is designated to be shared between adjacent components fore and aft, at the sides, and at the corners. Therefore, a unit is comprised of one each of a heat shield, side retainer, support post set, center retainer, two plugs, and two bolts plus four TD NiCr screws. The resulting unit weight of the metallic components before coating was 2.47 lb/ft^2 (0.105 kg/m^2). After coating the unit weight increased to 2.66 lb/ft^2 (0.113 kg/m^2). Using 7.1 pcf (113.7 kg/m^3) density Fiberfrax H, the insulation unit weight was 2.22 lb/ft^2 (0.093 kg/m^2). This resulted in a total system unit weight of 4.88 lb/ft^2 (0.206 kg/m^2) in the as-coated condition. This compares to 5.75 lb/ft^2 (0.243 kg/m^2) for the system fabricated during Phase II and represents a unit weight reduction of 15-percent (Reference 1b). See Section 6.7.2 for additional comments.

Although some efforts were made to reduce individual component weights as a result of the Phase II fabrication and testing, an extensive optimization sizing was not undertaken. The major reduction in weight was achieved by selecting a lower density fibrous insulation, i.e., 6 pcf (96 kg/m^3) compressed to 7.1 pcf (113.7 kg/m^3) Fiberfrax H instead of 10 pcf (160 kg/m^3) Dyna-Flex (see Section 4.3.3).

5.2 System Cost

The cost data presented herein is based on the actual fabrication costs for constructing components for the nine-panel array and the NASA TPSTF specimen. The data base, therefore, consisted of a total of sixteen heat shields including spares. This represents an area of approximately 21.3 ft^2 (2 m^2) or approximately two-thirds of the estimated applicable area of the baseline vehicle. The costs include raw material, machining, forming, finishing, joining, and coating.

The cost of the components (including heat shield, support system, and insulation) was $500.02/lb ($1101.36/kg). This compares with the $518.21/lb ($1141.43/kg) cost for the tee-stiffened TPS components fabricated during Phase II. Both the total system cost and unit weight were reduced during Phase III resulting in a net cost/weight saving of approximately 4 percent.

These reductions were made possible by attacking the highest cost and uncontrollable item encountered during Phase II, that is, the raw material. As shown in Table 5-2 the percent of material cost was reduced by 70 percent. This was accomplished by increasing the man-related functions such as machining and welding. It should be noted that while the table indicates significant percentage increases in fabrication process items the overall cost in terms of dollars per square foot was reduced by 21 percent.

Table 5-1. TPS Components Weight Breakdown

Component	Alloy	Weight, Grams	
		Before Coating	After Coating
Heat Shield	Cb-752	1086.5	1190.7
Retainer, Side	Cb-752	96.8	100.4
Post, Center, Upper	Cb-752	103.6	106.8
Post, Corner, Upper	Cb-752	72.3	74.6
Retainer, Center	Cb-752	54.5	56.7
Plug	Cb-752	6.0	6.9
Post, Lower	HS-25(L-605)	64.5	64.5*
Bolt	TD NiCr	4.6	4.7
Screw	TD NiCr	0.9	1.0

* No coating required.

Table 5-2. Fabrication Process Percentage Cost Breakdown

	Percent of Total Cost	
	Phase III	Phase II
Material	10.3	34.2
Machining	41.2	31.1
Forming/Finishing	7.8	5.8
Welding	15.1	11.3
Coating	25.4	17.4
Brazing	0.2	0.2

In accordance with the procedure established during Phase II, the individual components cost data has been compiled into an nth unit format and the costs projected for five orbiter vehicles plus spares. This information is shown in Table 5-3.

The assumptions were: that 24 heat shield units would be required per vehicle; the current actual costs were baseline; there would be no reduction in per pound material cost; and there would be approximately an 89-percent composite learning factor applied to all fabrication parameters. The composite was based on the assumptions that learning factors were 100-percent for material; 90-percent for machining, joining, and coating; and 85-percent for forming and finishing. The cumulative average cost for n units is shown in Figure 5-1. In addition to the Phase III components cost projections, those generated during Phase II (Reference 1b) are also shown for comparison. The variation in the curves is due to the initial cost since the same learning curve factors at an 89-percent slope were applied.

In interpreting the data in Table 5-3 and Figure 5-1 it can be seen that for one ship set of 24 heat shields, components and insulation covering an area of 32 ft^2 (3 m^2) the cumulative cost would be \$49,870. This relates to approximately \$342/lb (\$753/kg). Similarly, for five ship sets of 120 heat shields and components the cumulative cost would be \$193,520 or \$265/lb (\$584/kg).

Table 5-3. Columbium Alloy TPS Cost Projection

Tee Stiffened TPS Configuration (Composite Rate = 89%; Reference 3)

	Quantity Produced[2]							
	1	10	24	50	100	120	150	200
nth unit cost	0.302	0.205	0.177	0.156	0.139	0.135	0.130	0.124
cumulative cost (n units)	0.302	2.359	4.987	9.271	16.610	18.352	23.330	29.656
cumulative average cost (n units)	0.302	0.236	0.208	0.185	0.166	0.161	0.156	0.148

1. Cost in thousand of 1973 dollars exclusive of TPS assembly effort.

2. Estimated 24 heat shield sets per orbiter vehicle [32 ft^2 (3 m^2)]; 5 production orbiter vehicles.

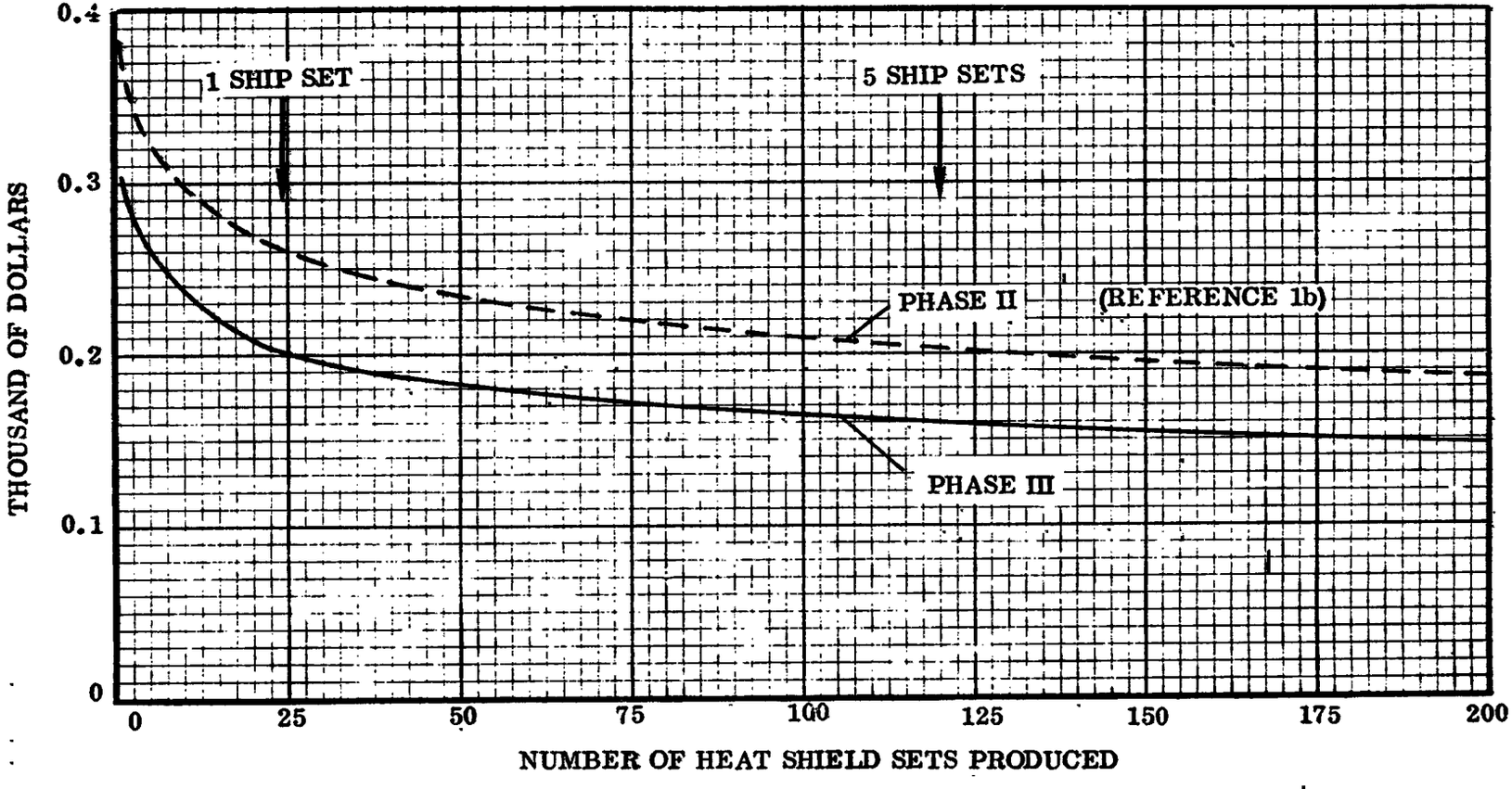

Figure 5-1. Tee-Stiffened TPS Cumulative Average Cost

6 TESTING

The objective of the Phase III testing program was to functionally test full-scale, vehicle-sized, thermal protection system test specimens consisting of heat shield panels, panel retainers and supports, close-outs, and insulation, and to evaluate the effects on the system of simulated shuttle orbiter missions. Two test specimens and two test facilities were planned for use. A three-panel test specimen was prepared for testing in the NASA Langley Research Center Thermal Protection System Test Facility (TPSTF), and a nine-panel test specimen for testing by Convair. The TPSTF specimen would be used to investigate the effects of hypersonic hot gas flow on heat shield panels and on parallel and transverse heat shield joints, and on the complete TPS. Recommended test conditions for the TPSTF are given in Appendix C.

The test conditions for the nine-panel array were 50 cycles of simulated flight environment with boost and reentry times, temperatures, pressure loads, oxygen partial pressures and 100 cycles of acoustics pressure. Since the maximum acoustic excitation and associated potential damage occur during boost and without temperature considerations, testing was planned to be accomplished in three steps. First the specimen was to be acoustically tested at room temperature through 50 simulated boost cycles of noise, followed by 50 simulated flight cycles of temperature and load. Finally, the specimen was to be exposed to 50 simulated boost cycles of noise at room temperature. This represents a conservative approach with the specimen repeatedly acoustically loaded to maximum levels, after having sustained the full term effects (50 cycles) of thermal cycles).

6.1 Test Specimens

Two full-size thermal protection systems representing a portion of the shuttle orbiter underbody heat shield were designed for testing based upon the evaluation of the results of Phase II. The designs satisfied vehicle requirements for location, loading and frame spacing.

One specimen, to be tested at Convair, consisted of a rectangular array of nine tee-stiffened heat shield panels (three panels long by three panels wide) with ten panel support posts, six fixed-point panel center retainers, six panel edge retainers and high temperature insulation, all mounted on a simulated vehicle load structure with titanium skin, frames and stringers. A water-cooled test specimen support frame enclosed the nine panels and supported the load structure. The nine-panel arrangement permitted the complete isolation of the center panel, affording freedom from the test frame edge effects. It also allowed the inclusion and testing of a variety of panel edge restraints which are normal to flight hardware. The nine-panel test specimen, shown in Figure 6-1 was fabricated to Convair Drawing 76C0104, Figure 3-5.

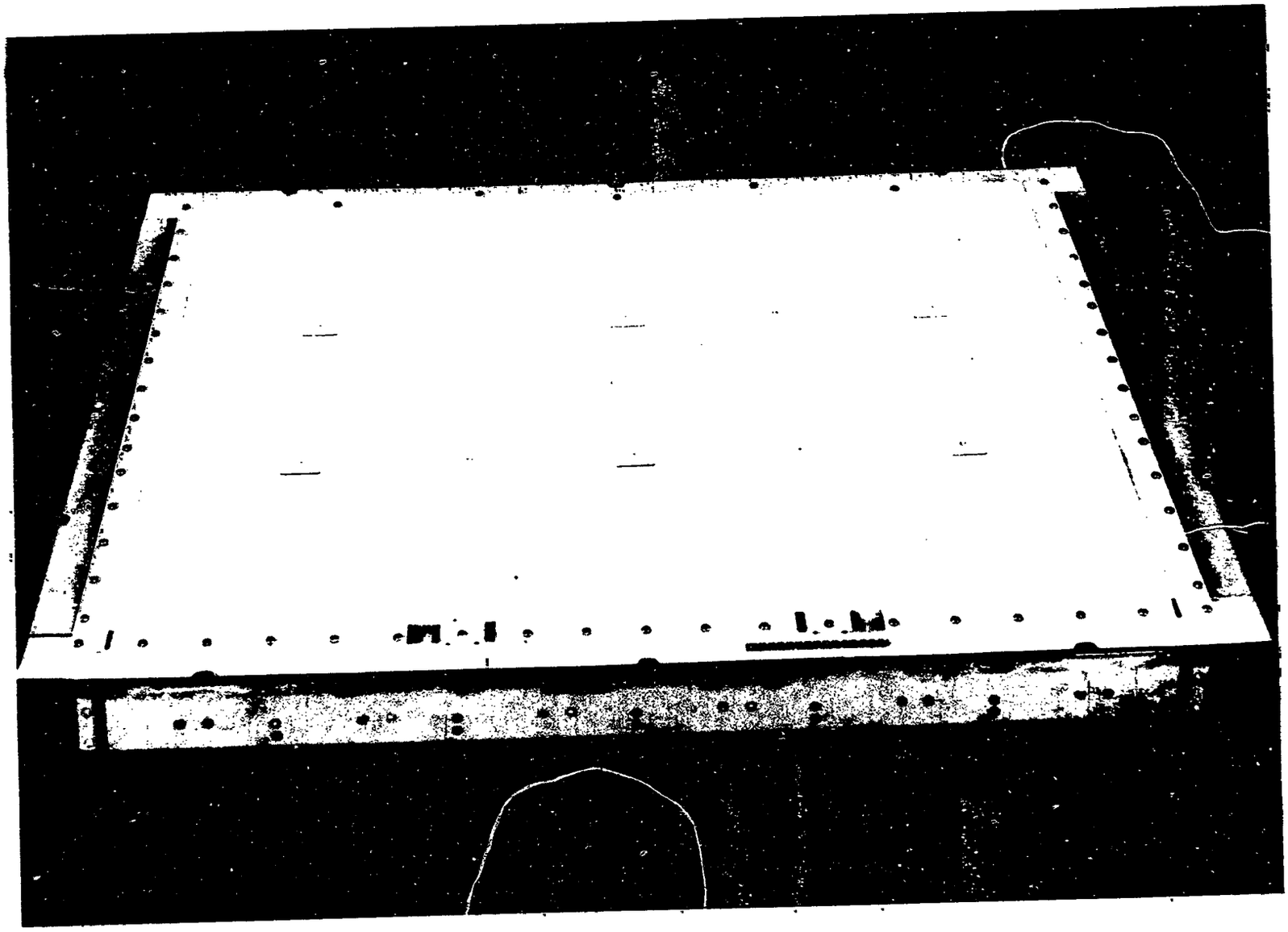

Figure 6-1. Nine-Panel TPS Test Specimen Ready for Test (137400)

A second test specimen was fabricated for testing in hypersonic hot gas flow in the NASA Langley TPSTF. This specimen possessed three, full-size, tee-stiffened heat shield panels mounted in line with the hot gas flow, and six adjacent narrow side panels with six panel support posts, two fixed-point panel center retainers, six panel edge retainers and high temperature insulation. These were all mounted on a simulated load structure with titanium skin, frames, and stringers. A HS-188 high temperature alloy test fixture supported the test hardware and the simulated load structure. This test specimen, with its isolated center panel, permits investigation of hypersonic hot gas flow on the TPS, panels, panel joints and panel retainers. The TPSTF test specimen shown assembled in Figure 6-2 was fabricated to Convair Drawing 76C0109, Figure 3-12.

6.2 Test Facilities and Procedures

The Phase III thermal protection system nine-panel test specimen was tested in facilities at Convair developed to subject the system to a series of repeated orbiter missions of simulated flight conditions and environment. The TPSTF test specimen will be tested at NASA.

6.2.1 Acoustics. — Acoustic testing of the nine-panel test specimen was performed in a 128 cubic foot (3.62 m^3) reverberation chamber with the test array mounted vertically in the wall, with apparent air flow going from the top of the specimen toward the bottom. The specimen was supported from the rear and was vibration-isolated from the acoustic chamber structure. It was mounted so that only the external surface of the columbium alloy heat shields were subjected to direct acoustic excitation. The center of the array was instrumented with nine miniature accelerometers to record the response of the panel and panel retainers to the acoustic flight environment. Figure 6-3 shows the acoustic test facility with the test specimen mounted in place. Note the horn projecting from the chamber on the side opposite to the test specimen. In Figure 6-4 is seen the complete nine panel test specimen mounted in the wall of the acoustic chamber with accelerometers and monitoring microphone positioned for test.

Prior to installation of the test specimen in the reverberation chamber, the center of the test array was instrumented with nine miniature accelerometers, Endevco Model 2222B, bonded to aluminized Mylar tape and mounted to the face of the panel and retainers with Eastman 910 adhesive. Figure 6-5 shows the locating dimensions for instrumentation. Accelerometer number 5A was moved to position 5B after Cycle 50. During the modal survey, a tenth accelerometer was located for reference on the center line of the frame of the fixture and normal to the heat shield surfaces. This accelerometer was located as shown in Figure 6-5 for acoustic Cycle 51 through Cycle 100. The microphone for measuring the acoustic environment was located 18-inches (45.7 cm) in front of the center of the test specimen.

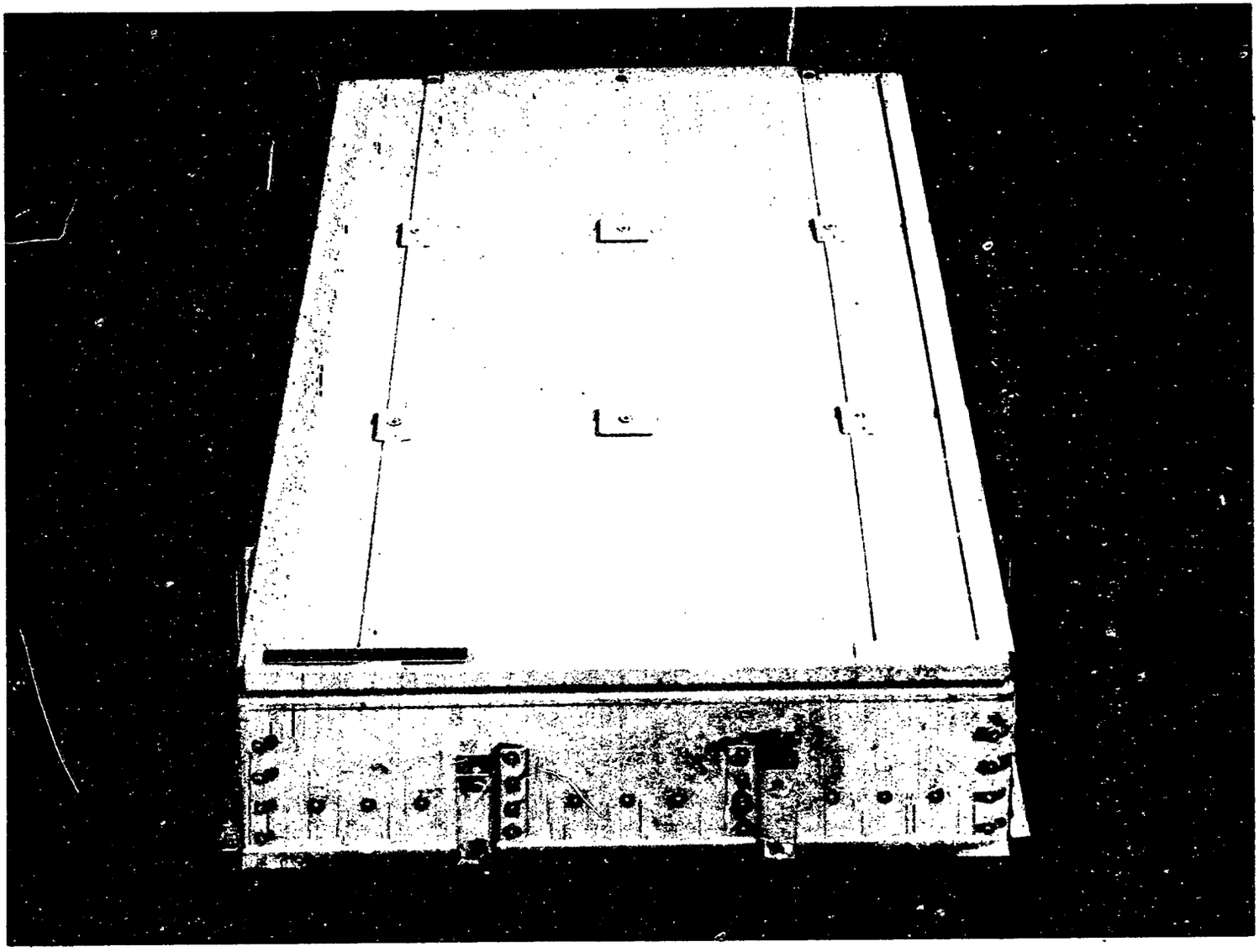

Figure 6-2. TPSTF Test Specimen Ready for Test

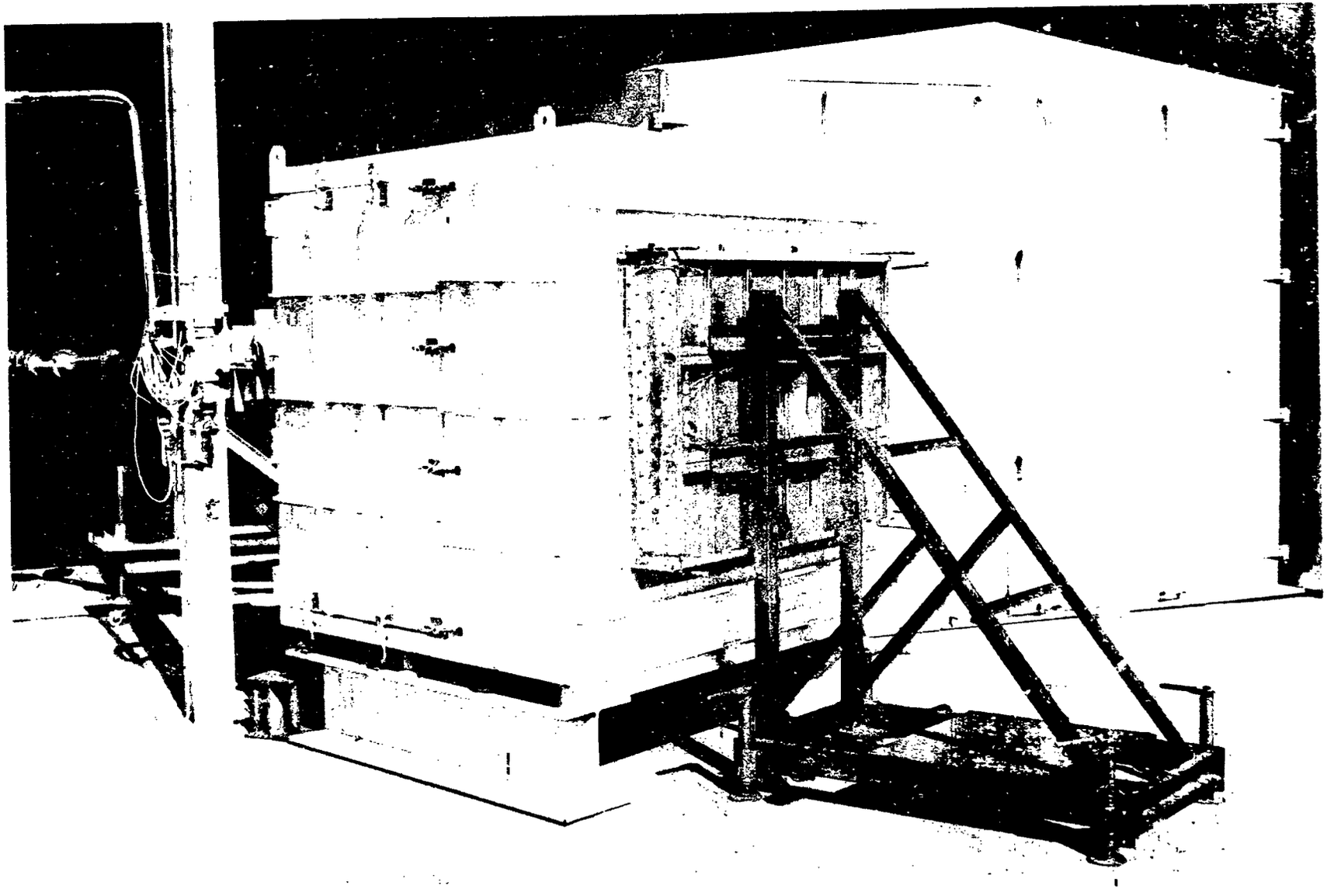

Figure 6-3. Acoustic Test Facility with Nine-Panel TPS - Test Specimen Mounted in Side Wall (137475)

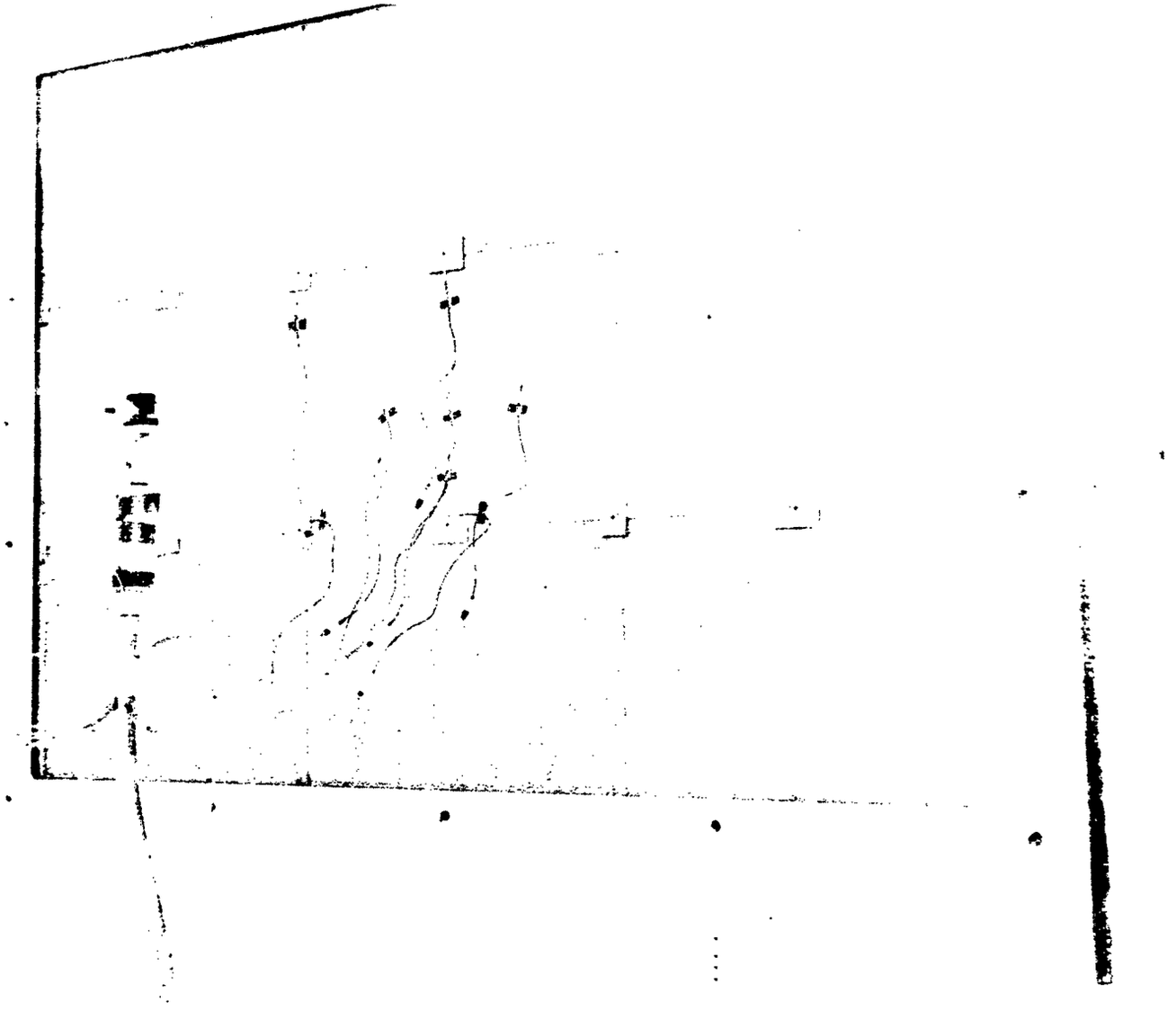

Figure 6-4. Nine-Panel TPS Test Specimen Mounted in Acoustic Test Chamber (137477)

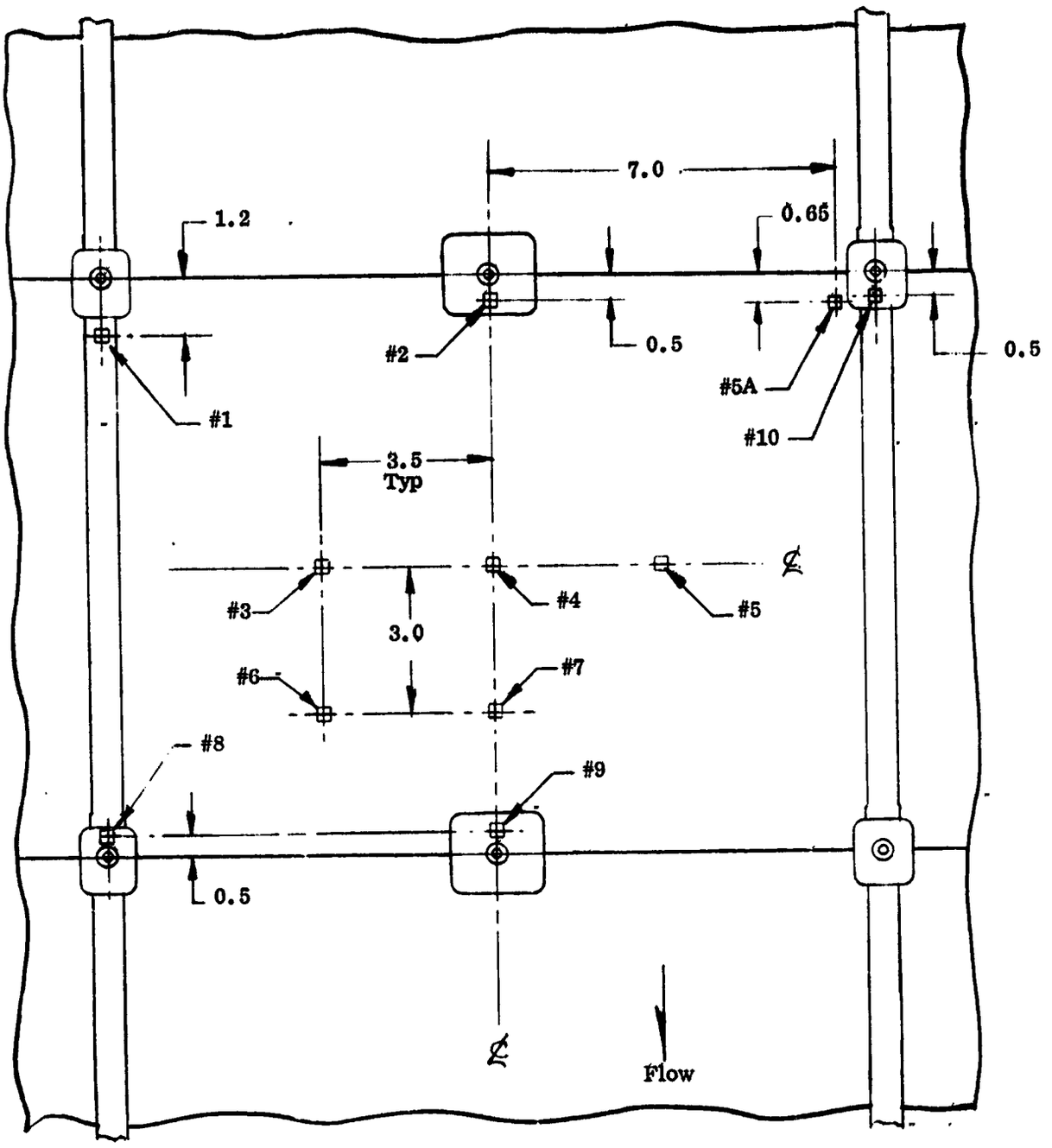

Figure 6-5. Accelerometer Locations

Before boost simulation testing was started, the specimen was subjected to a low level sinusoidal sweep from 50 to 1000 Hz to determine the resonant frequencies of each accelerometer position and the phase relationship referenced to No. 10 accelerometer mounted on the test fixture frame (Table 6-1). The specimen was then subjected to 50 cycles of boost simulation, each cycle composed of 10 seconds at an overall sound pressure level of 158 dB followed by 40 seconds at 155 dB OASPL. Visual inspection of the specimen was performed at least once each 10 cycles during Cycles 1 to 50 and at least once every five cycles thereafter. Figure 6-6 details the noise environment expected during shuttle boost and Figure 6-7 shows the boost vibration spectrum.

The response of all accelerometers and of the microphone was recorded for each test cycle on magnetic tape. The tape recorder and test control console are shown in Figure 6-8. Microphone data from Cycles 1, 25, 50, 51, 75, and 100 were reduced for preparation of plots of octave band width versus sound pressure levels, and accelerometer data for these same test cycles were reduced for plots of power acceleration spectral density versus frequency (see Appendix B).

Acoustic testing during Phase II was performed at a maximum OASPL of 155 dB and at 152 dB OASPL for the lower level. It was desired during Phase II to test to the same levels as used during Phase III acoustic testing, 158 dB OASPL and 155 dB OASPL. However, facilities were not then available for this testing. For Phase III acoustic testing, facilities were available and were used for the higher desired levels of acoustic pressures.

6.2.2 Thermal-Mechanical. — Thermal-mechanical testing was performed in Convair's high-temperature, flight simulation test facility for multi-panel thermal protection systems. This facility was designed to apply a controlled, simulated, orbiter flight environment of temperature, pressure, and oxygen partial pressure to the nine-panel test specimen.

After completion of 50 cycles of acoustic testing, the nine-panel test specimen was mounted in the high temperature testing facility seen in Figures 6-9 and 6-10 and schematically in Figure 6-11. The specimen is shown mounted horizontally, facing upward in the test facility in Figure 6-12, prior to testing.

This facility consists of two box-like, stainless steel enclosures: the bottom enclosure which mounted the test specimen and temperature sensing instruments, and the top enclosure which mounted the power distribution system, the heat lamps, the cooling air distribution system, the pressurization gas and oxygen partial pressure manifolding, and the hot air plenum and exhaust ducting. The top enclosure is insulated with approximately two inches (5 cm) of fused silica foam insulation (Glasrock) which is mechanically mounted. An oxygen partial pressure sensor line was also mounted in the top enclosure. The two enclosures are hinged to open in a clam-shell fashion exposing the skin surfaces of the test specimen. Opening was facilitated by two hydraulic

Table 6-1. Modal Survey and Resonant Frequencies

Freq. (Hz)	Accelerometer Location								
	1	2	3	4	5	6	7	8	9
185	-	+	-	0		-	0	-	-
260	-	-	+	+		+	+	0	-
365	0	-	+	+		+	+	+	+
408	0	+	+	+		+	+	0	+
445	0	0	0	-		0	-	0	0
530	0	-	-	0	NO DATA	0	0	0	0
570	0	0	0	-		0	+	0	-
620	0	0	-	-		-	-	0	-
718	+	-	+	-		0	0	+	+
850	0	-	+	+		+	+	-	-
980	0	-	-	-		0	+	0	0

NOTES: (1) Accelerometer Locations are as Shown in Figure 6-5.

(2) (+) Indicates In-Phase With Reference Signal.
(-) Indicates Out-of-Phase With Reference Signal.
(0) Indicates Phase Relation Undefined.

(3) All Accelerometers Referenced to Accelerometer No. 10 Located on Frame.

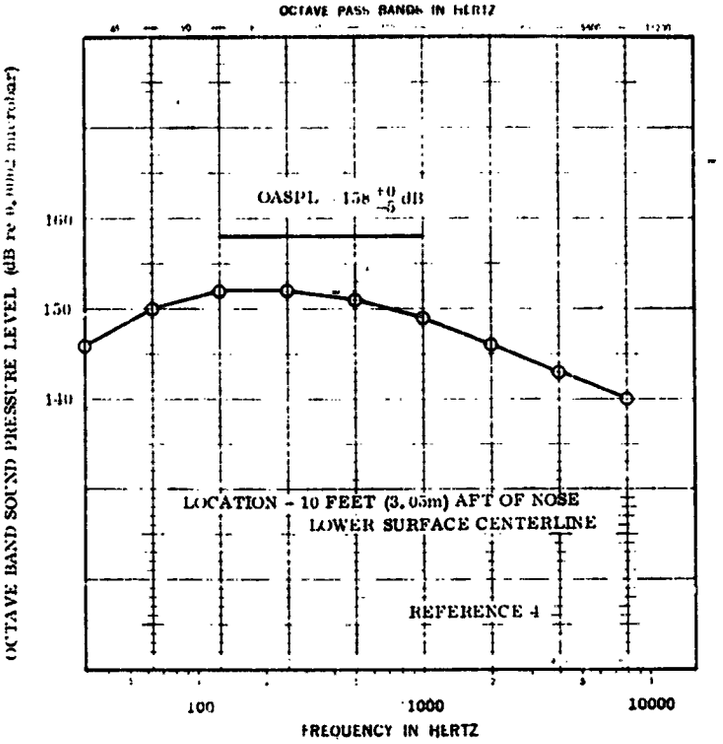

Figure 6-6. Boost Acoustic Environment

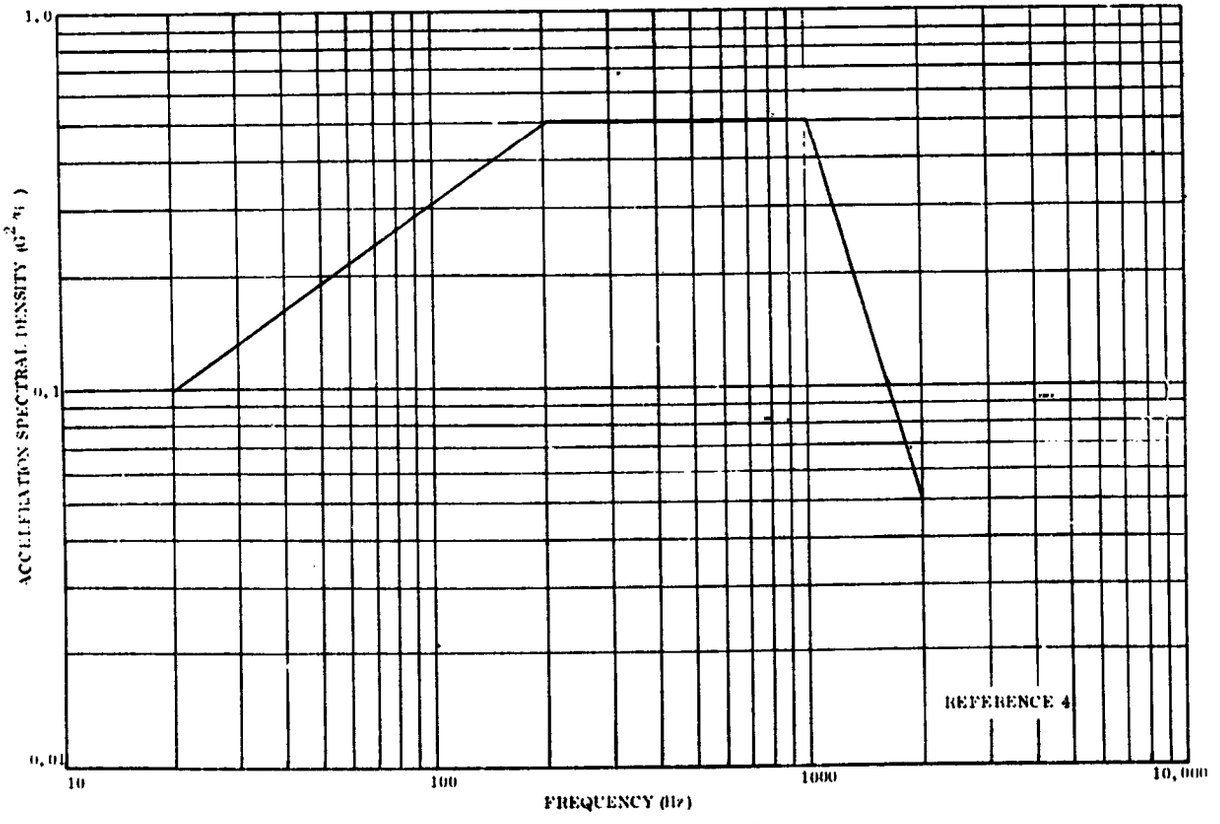

Figure 6-7. Boost Vibration Spectrum

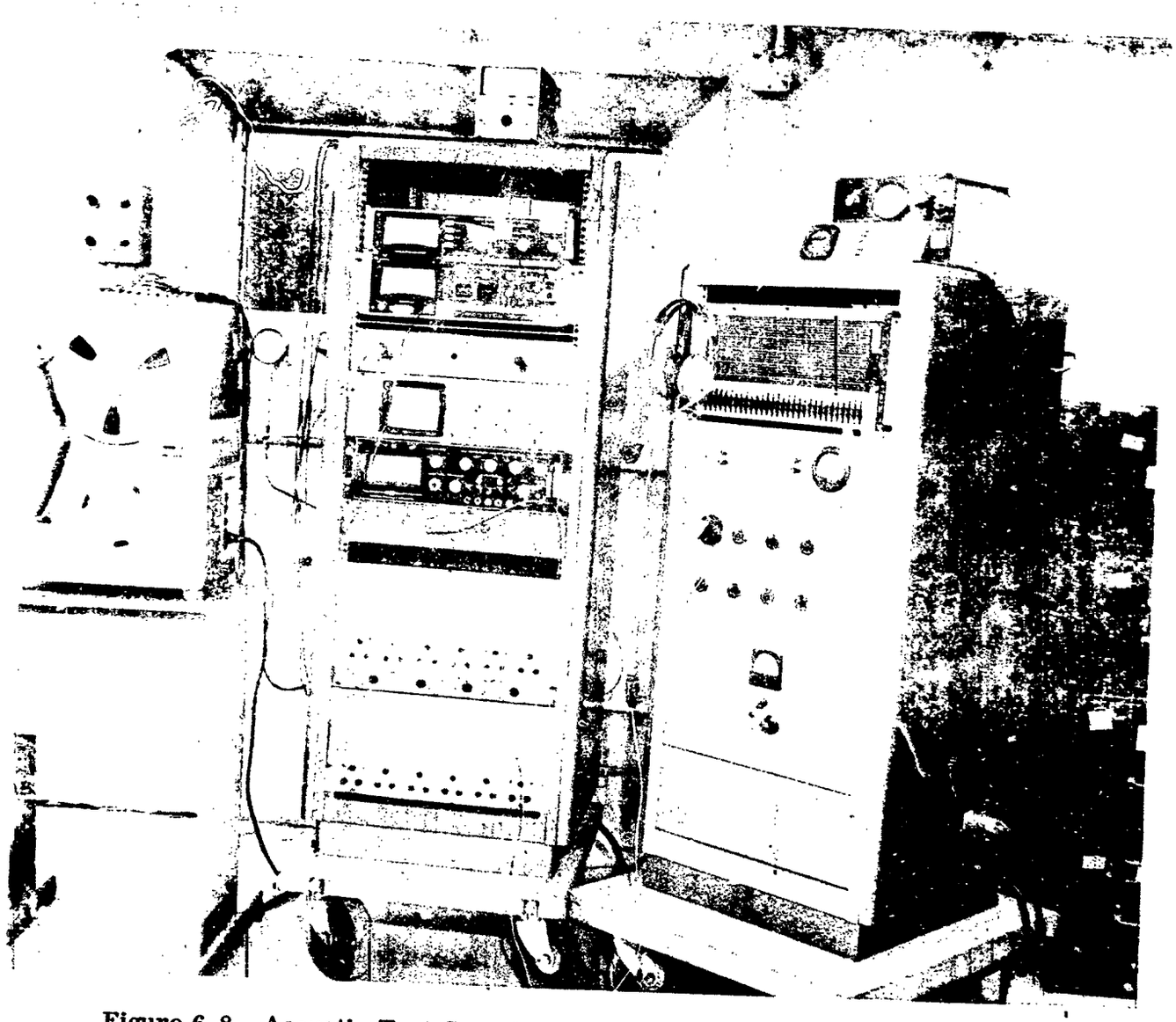

Figure 6-8. Acoustic Test Console and Recording Equipment (130940B)

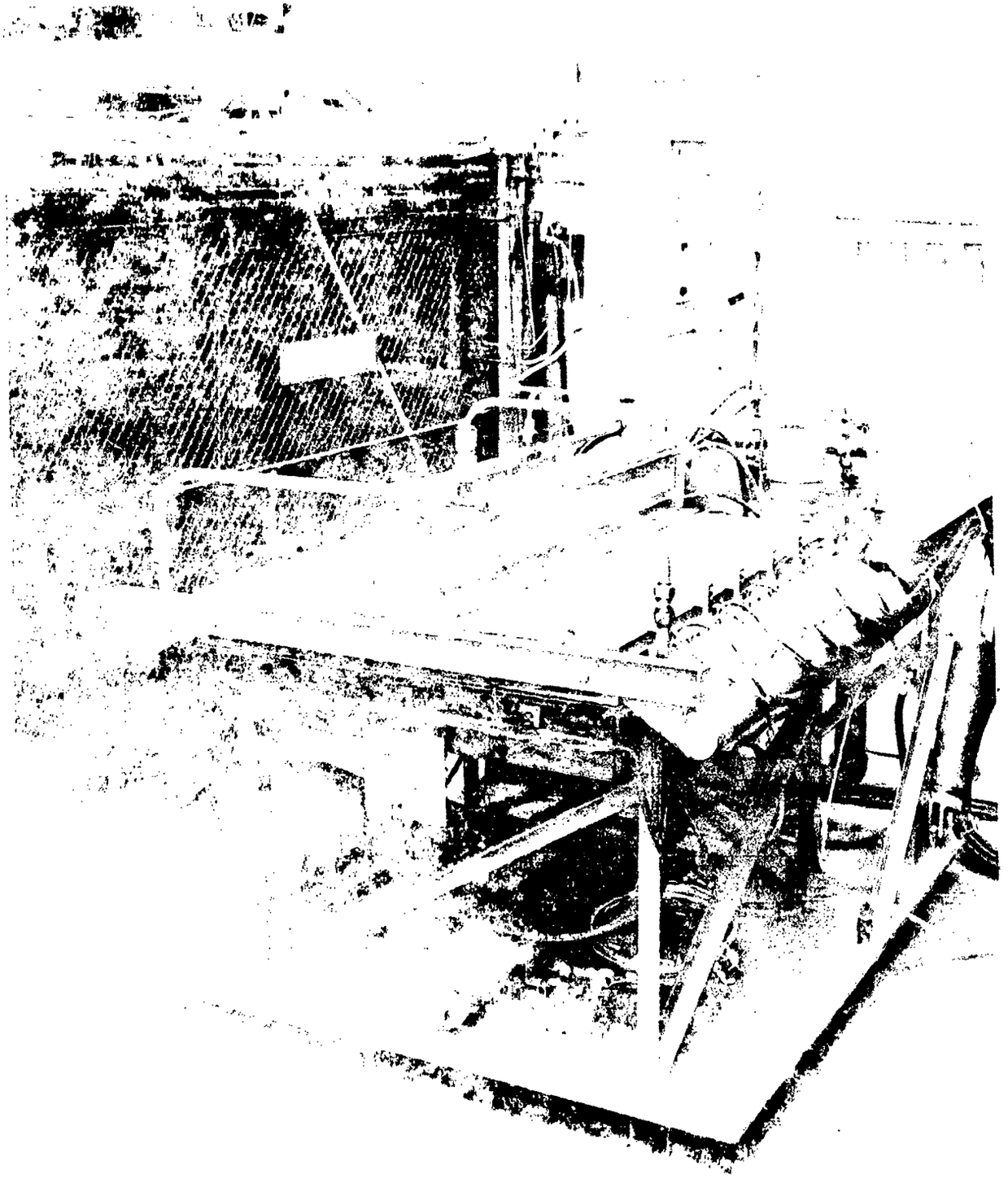

Figure 6-9. Facility for Thermal, Load, and Environmental Testing of Multi-Panel TPS (135431)

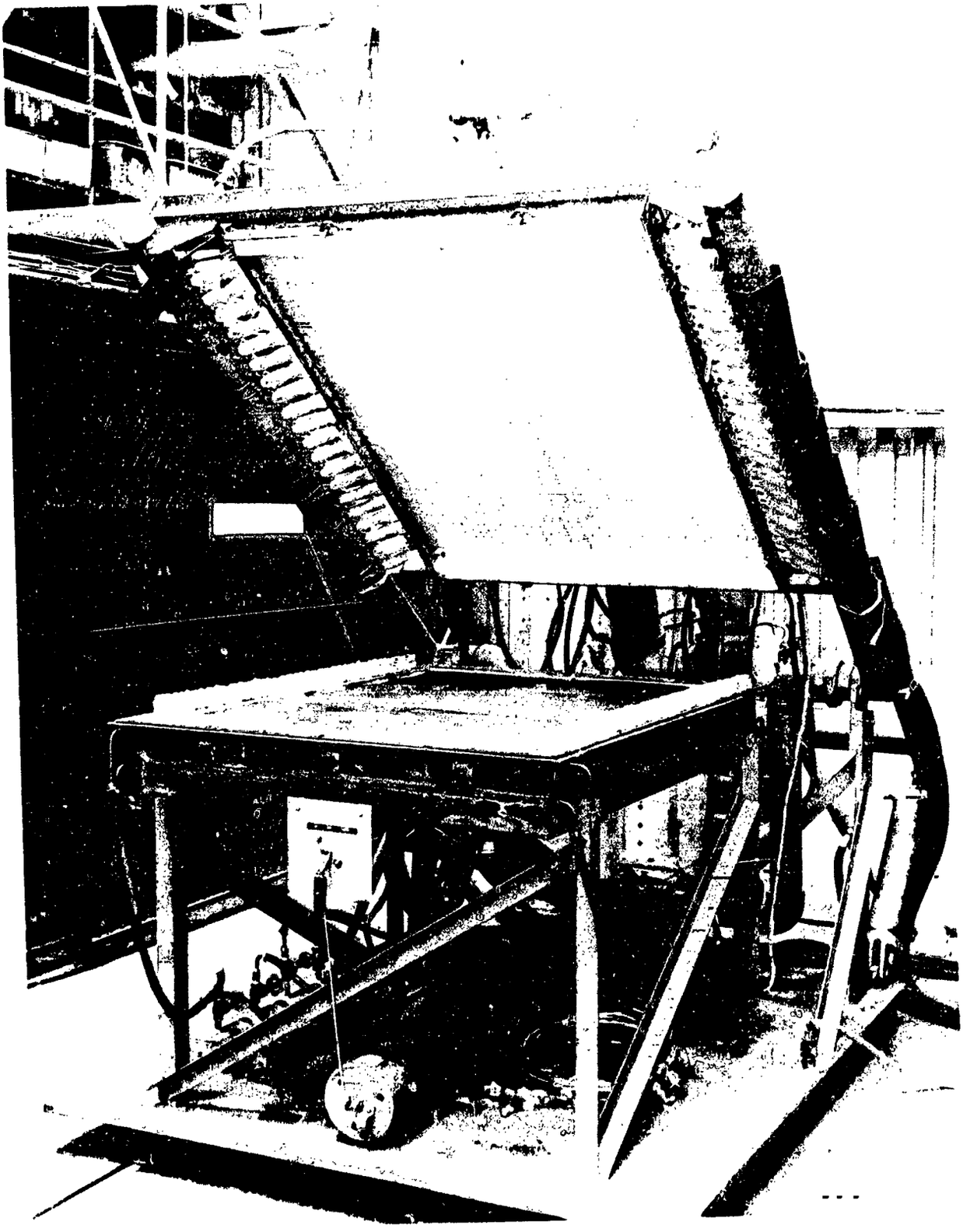

Figure 6-10. Facility for Thermal,Load, and Environmental Testing of Multi-Panel TPS (135429)

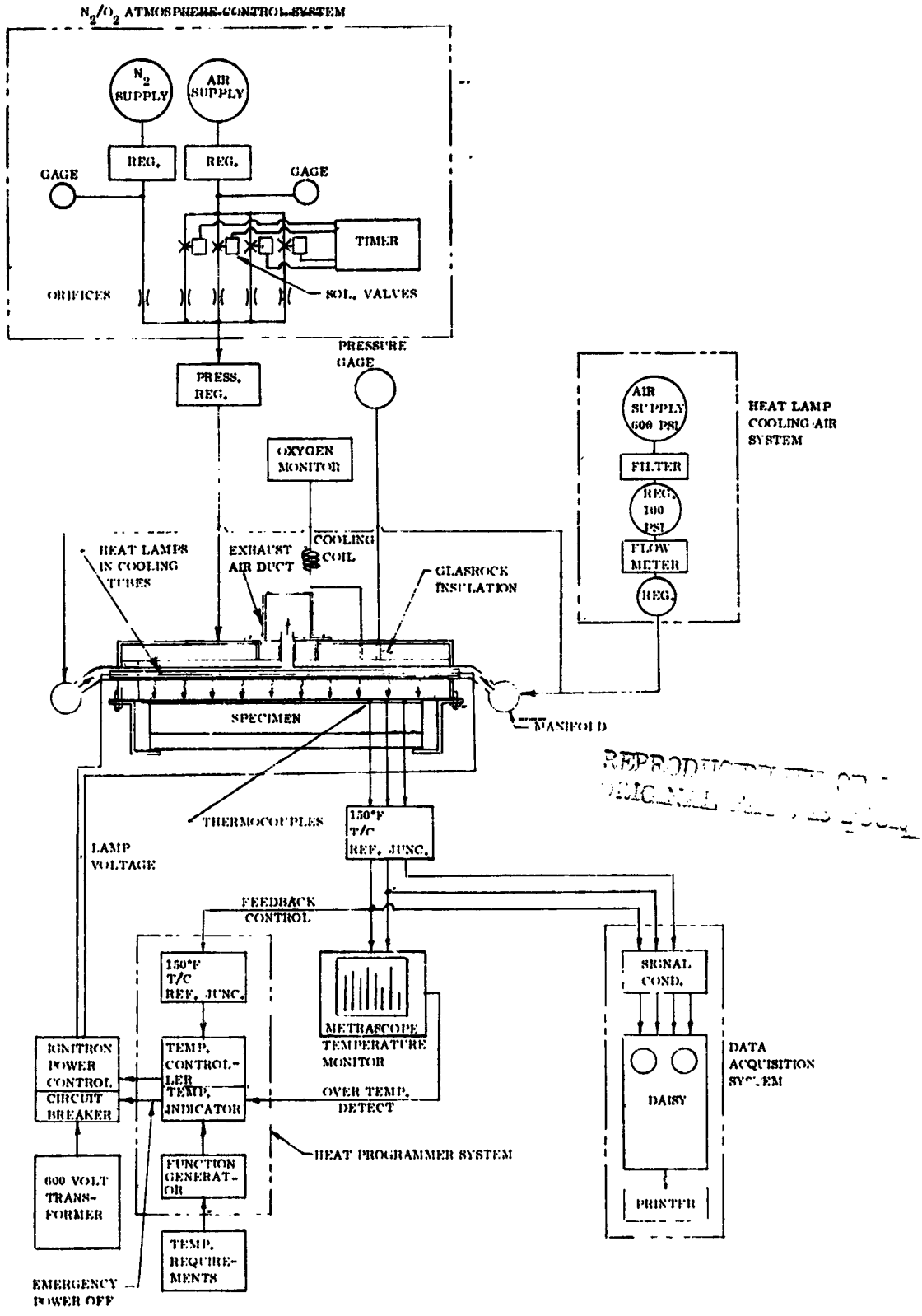

Figure 6-11. Schematic for Multi-Panel TPS Test Facility

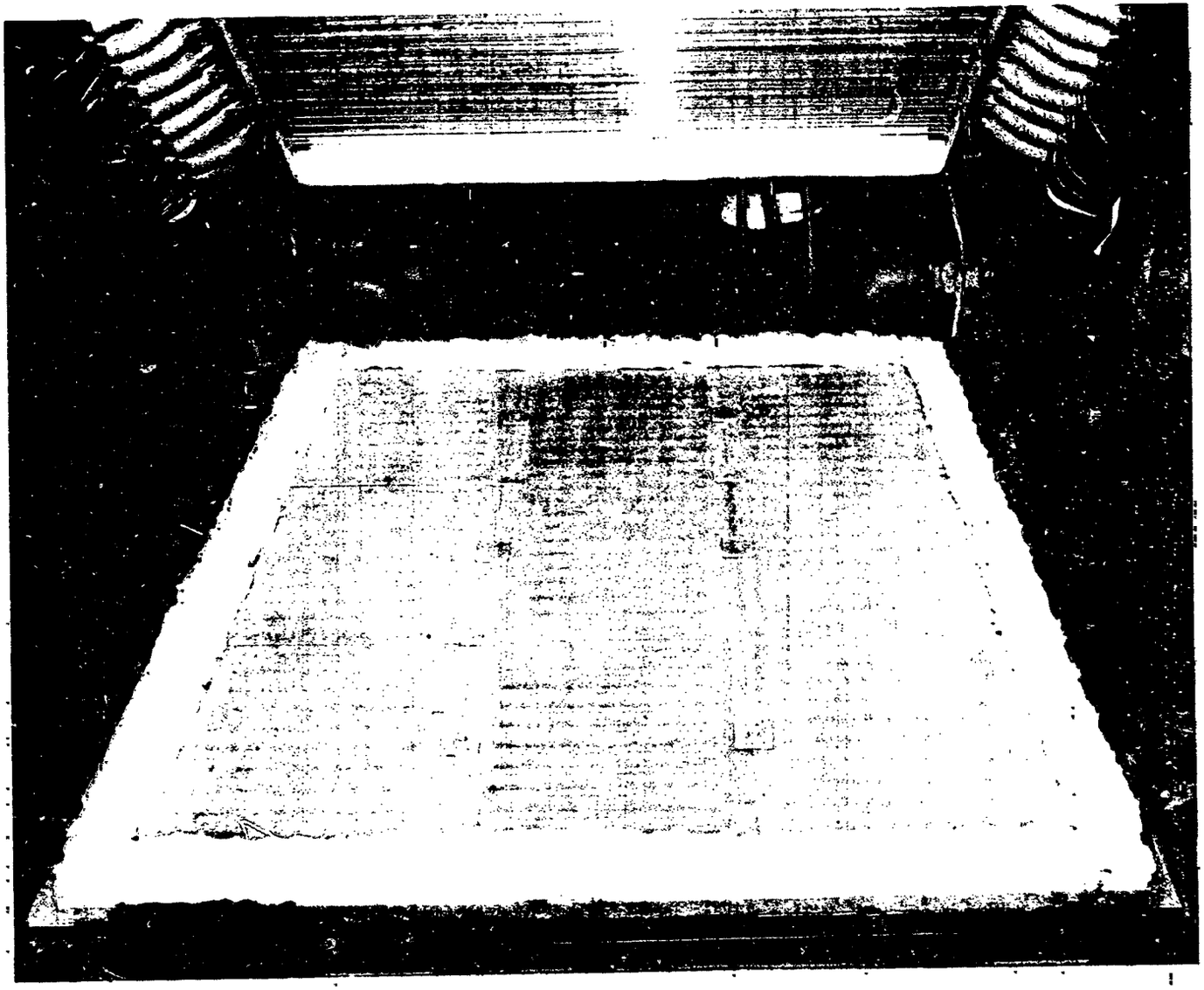

Figure 6-12. Nine-Panel TPS Test Specimen Mounted for Thermal, Load and Environmental Testing (137621)

cylinders operated from an air-hydraulic accumulator using shop air. The two enclosures closed and sealed against a silicone rubber gasket, permitting pressurization of the cavity over the test specimen. Water cooling was provided to both enclosures as required to maintain reasonable operating temperatures and to prevent damage to temperature sensitive materials.

In this facility, the specimen was heated by 78 clear quartz infrared heat lamps, No. 3800 T3/CL, rated 3800 watts at 570 volts (100 watts per inch), which were mounted in pairs in 38 clear quartz tubes, 28 mm diameter by 1.5 mm thick. The average spacing of the heating lamps was 0.6-inch (1.5 cm) which provided 24 kW per square foot at rated voltage, supplied from a 600 volt, 3000 kVA system controlled by ignitron power controllers. The temperature of the test specimen was controlled in three zones by a programmed power system using temperature feedback in a closed loop from three sensing control thermocouples which were spring loaded against the underside of the specimen's hot face. The temperature program was provided by a servo-controlled Research Incorporated heat programmer with a drum mounted function generator.

The cooling tubes, installed in the top enclosure as seen in Figure 6-10, were fabricated with a central tee outlet. Cooling air for the lamps was supplied into both ends of each tube and exhausted through the central outlet into the exhaust plenum mounted on the center of the top enclosure. Exhaust air provided efficient cooling of the quartz lamps during facility operation and was exhausted at approximately 750 °F (673 °K). The cooling tubes were on 1.2-inch (3.05 cm) centers and were 0.75-inch (4.45 cm) above the test specimen. Filtered cooling air was supplied from a 600 psi (4137 kN/m^2) supply and during testing was used at the rate of 50 pounds (23 kg) per minute.

Before the start of the reentry portion of the test cycle, the cavity over the surface of the test specimen was flooded with nitrogen gas until the oxygen content approached zero. During reentry, the amount of oxygen in the nitrogen atmosphere was increased with time, controlled by metering air through solenoid operated orifices, thus providing in a stepped function, the desired oxygen content and oxygen partial pressure over the test specimen. The automatic four-step metering of oxygen into the mixture provided a good approximation of the desired oxygen content during reentry. The air-nitrogen mixture for simulation of oxygen partial pressure was evenly distributed and supplied to the top enclosure at the four corners, through four one-inch (2.5 cm) tubes from a central supply point. The oxygen content of the gas mixture was monitored by sampling through a tube entering the cavity of the top enclosure and analyzed by a Westinghouse Model 209 Oxygen Analyzer. The analyzer and facility control console are shown in Figure 6-13.

The design and test profile for the TPS, showing temperature, pressure differential loading and local surface pressures versus vehicle flight time, are shown in

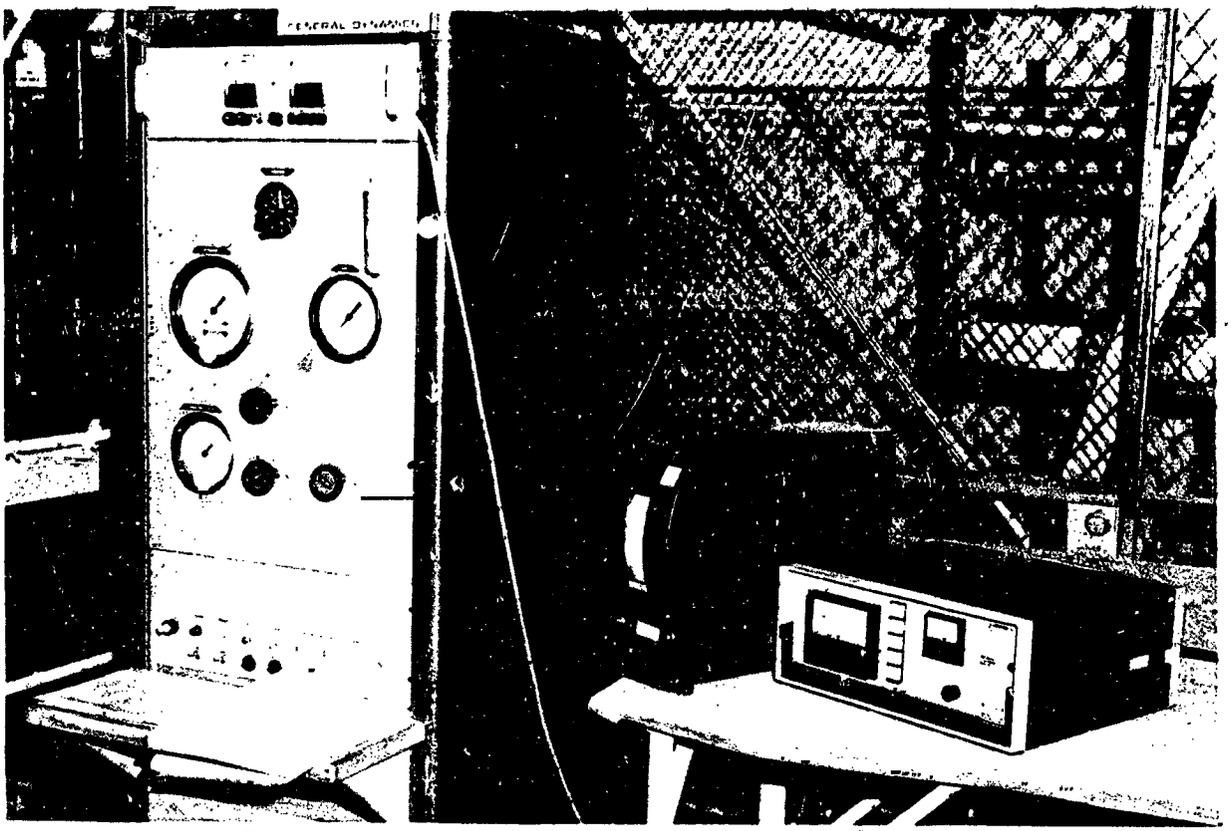

Figure 6-13. Test Console and Oxygen Analyzer for Multi-Panel TPS Test Facility (138486)

Figure 6-14. The local surface pressure is a function of the oxygen partial pressure and the volume percent of oxygen present. Reentry differential pressure loading starts at 0.06 psi (0.4 kN/m^2), rises to 0.15 psi (1.04 kN/m^2) when the temperature is 2400 °F (1589° K) and holds until the temperature drops to 2150 ° F (1440 ° K). The other reentry differential steps are 0.4 psi (2.7 kN/m^2) and 0.85 psi (5.9 kN/m^2).

Fifty thermocouples were installed in the test specimen to acquire thermal profile data during test cycles. Of these, 14 were tungsten-rhenium (W-5 Re/W-26 Re) sheathed thermocouples which were spring-loaded against the back of the hot face of all nine test panels. Thirty-six were chromel-alumel thermocouples installed to measure temperatures of the support posts, the titanium skin cold face, and the insulation. The locations of all thermocouples are shown in Figure 6-15. Thermocouples 5, 7, and 10 were control thermocouples for each heating zone and thermocouples 31, 33, and 36 monitored the cold face beneath the control thermocouples. Readout temperatures for these were continuously displayed in bar graph form on a Metrascope. During thermal cycles 1, 2, 3, 5, 11, 26, 47, and 50, data from all 50 thermocouples were sampled every 32 seconds by a high speed data acquisition system and stored on magnetic tape for processing and print out upon command. During all other thermal cycles, all tungsten-rhenium thermocouples excepting No. 5, 7, and 10 were removed from the

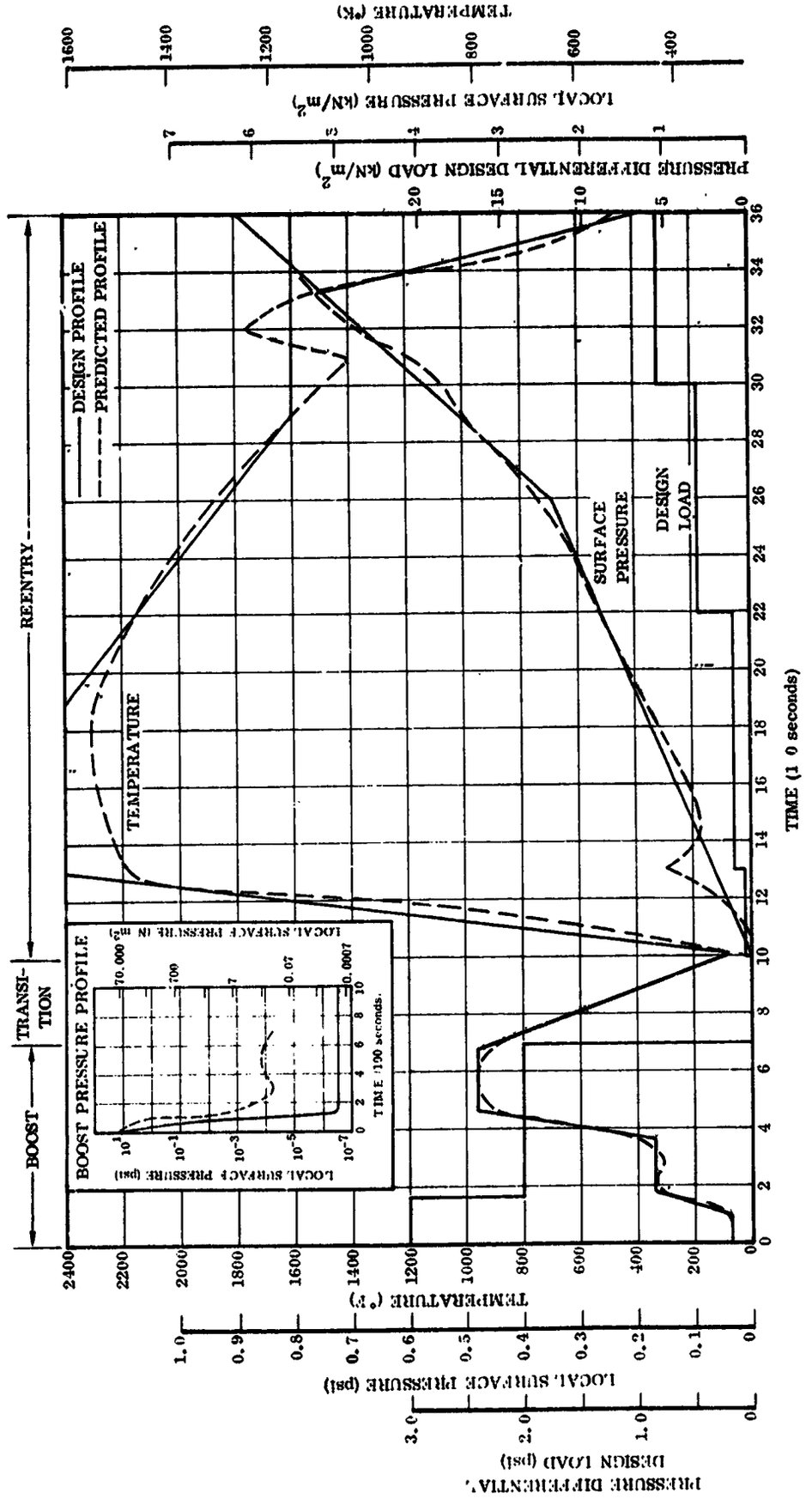

Figure 6-14. Design and Test Profile

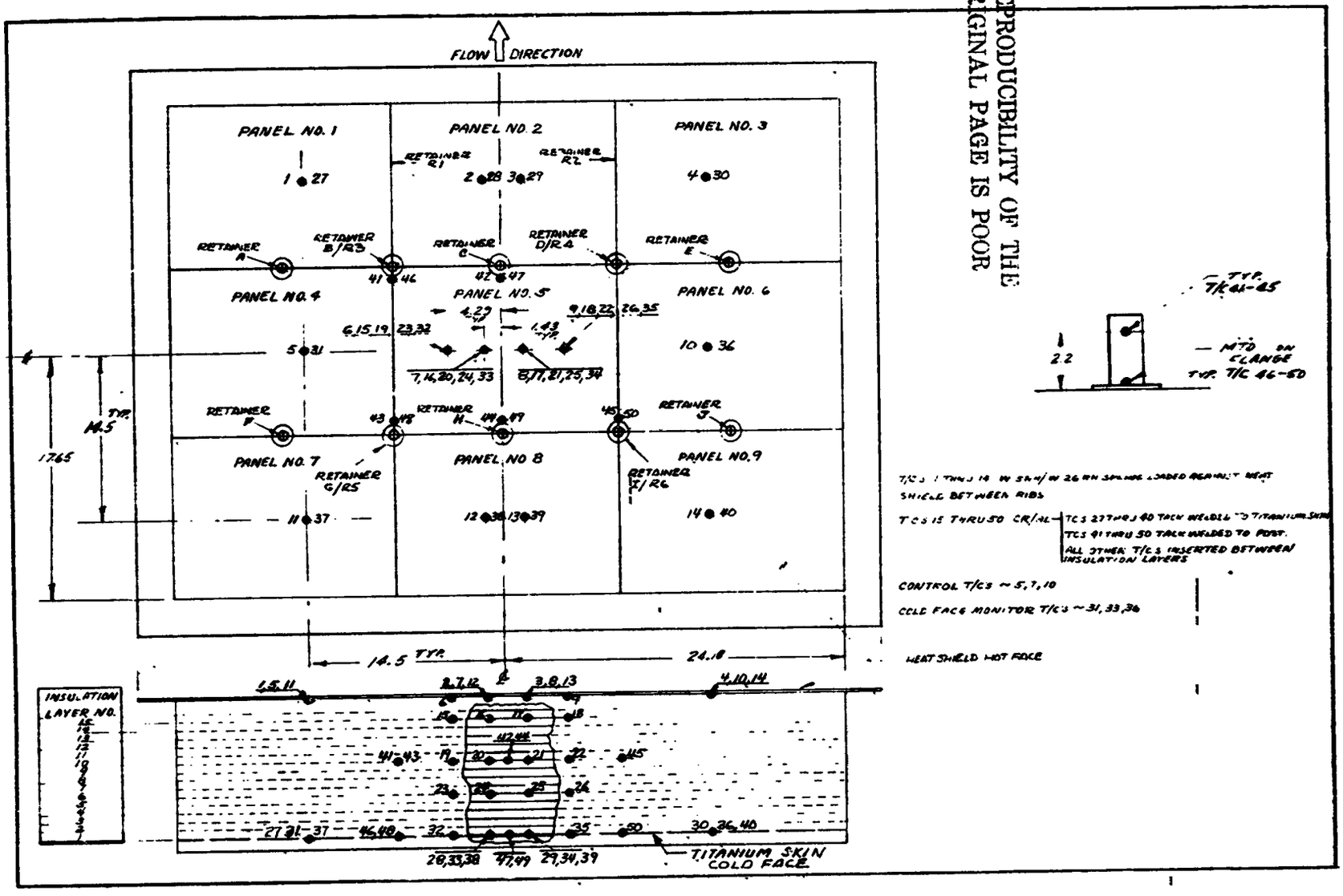

Figure 6-15. Thermocouple Location in Nine-Panel Test Specimen

test specimen. Cold face temperatures and insulation cool-down rates were monitored on the Metrascope.

When the nine-panel test specimen became available and was installed in the high temperature simulation flight test facility, pressurization tests were run to determine the pressure loading capability of the test system. Earlier investigations by Cross and Black, Reference 5 , had indicated that the maximum desirable leak rate through the TPS specimen was 15 cfm (0.007 m^3/sec) calculated on the basis of an average leakage area of 0.0075 in^2 per inch (0.019 cm^2/cm) of heat shield edge length. From Figure 6-14 it can be seen that the maximum required test pressure during boost was 3.0 psi (20.7 kN/m^2), and 0.15 psi (1.04 kN/m^2) during high temperature reentry. Pressurization tests indicated that for a pressure of 1.08 psi (7.45 kN/m^2), 220 cfm (0.104 m^3/sec) of air was required. Thus for 3.0 psi (20.7 kN/m^2) an intolerably high flow rate was indicated. Pressure testing was performed which isolated the specimen and the facility and which showed that 56-percent of the apparent leaks were around the specimen holding fixture and through the test specimen. The balance of the losses were through the top enclosure around the quartz cooling tube penetrations and the quartz tube penetrations into the hot gas plenum where temperatures of 1200° F (922°K) were anticipated.

Continued testing at decreasing pressures, indicated that to attain the desired reentry pressure of 0.15 psi (1.04 kN/m^2), a gas flow of 55 cfm (0.026 m^3/sec) was needed. Assuming that all other losses could be arrested, then 56-percent of the flow or 30.8 cfm (0.015 m^3/sec) would be around and through the test specimen when at the desired pressure of 0.15 psi (1.04 kN/m^2). Flow rates of this magnitude would have unrealistically heated the insulation, the support system, and the simulated vehicle structure and would have invalidated the test results.

Based on the considerations of high flow rate, the probability of success in sealing facility leaks, and the unpredictability of modification costs and schedule impact, a decision was made to discontinue the boost phase portion of the test cycle and all pressure loading of the test specimen during reentry. All other test parameters of time, temperature, and oxygen partial pressure were maintained (Figure 6-16).

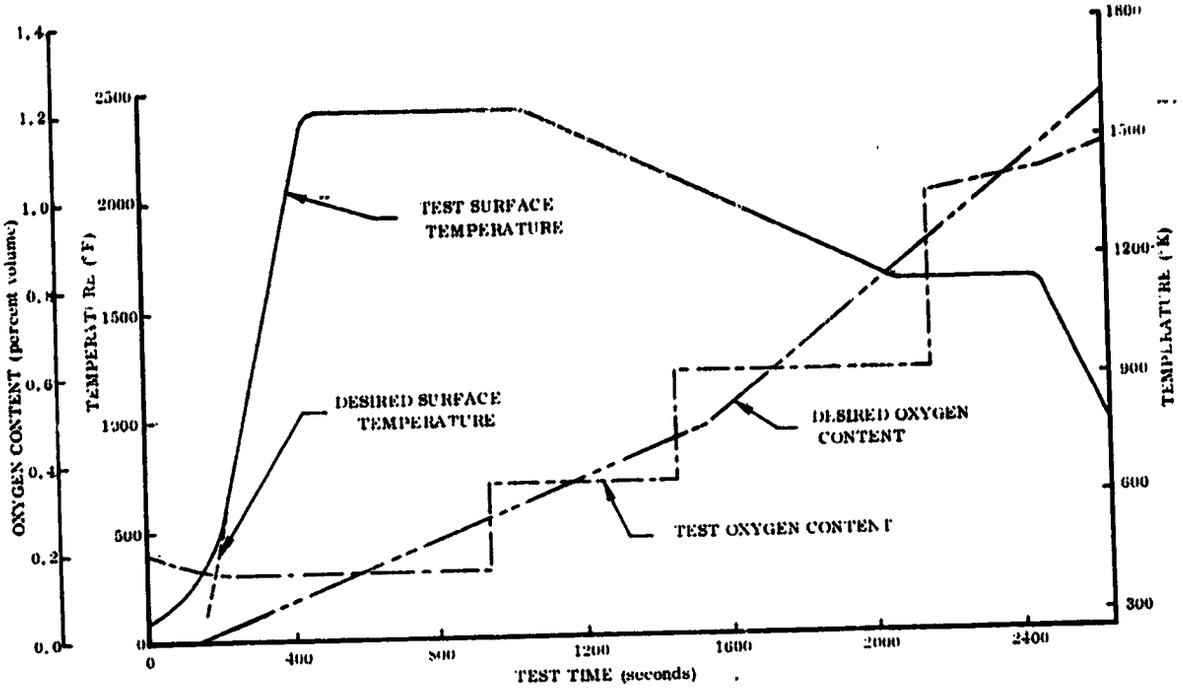

Figure 6-16. Thermal Test Parameters in Nine-Panel Test Specimen

6.3 Test Results

The nine-panel test specimen survived 50 thermal and 100 acoustic cycles of flight simulated reentry, verifying the thermal/structural design and demonstrating significant tolerance to oxidation damage. The isolated center test panel of the array remained flat and undamaged by thermal stresses, justifying the nine-panel test arrangement. The center test panel was readily disassembled for inspection and reinstalled after repair.

Three types of damage repair were attempted and verified: on-site, in-place, and in-shop. The on-site and in-place repairs were very successful. Disassembly and reassembly of individual heat shields and retainers for inspection, refurbishment and repair, or replacement were demonstrated at the end of Cycle 21 and Cycle 50. These removals simulate post-flight, external panel removal from a flight vehicle.

Damage sites in noncritical parts or areas were allowed to grow without repair to verify the design capability of removal when severely damaged. Both repaired and unrepaired hardware were thermally exposed through 50 simulated missions and acoustically excited to investigate their susceptibility to damage growth and/or propagation.

Following the completion of the tests, the complete nine-panel TPS test specimen was disassembled for post-test evaluation of performance. Further information was gathered on types of damage to test hardware, insulation performance, and problem areas of disassembly and inspection.

6.3.1 Acoustic Testing. — At no time during and after the first 50 acoustic test cycles was there any evidence of damage, excessive movement, or physical change in the components of the test specimen. Data were accumulated and recorded on acoustic cycles 1, 25, and 50. For these cycles, data plots were prepared of the microphone sound pressures at both the high and the low sound level and of the acceleration spectral density for each accelerometer at both sound levels. Typical data plots are found in Appendix B. All post fasteners and plugs required retorquing after acoustic testing to the 15-inch pounds (1.7 Nm) torque level established for this test.

At the completion of thermal cycling, acoustic testing was resumed with Cycles 51 through 100. In anticipation of possible structural failure resulting from thermal damage to the post of the side retainer G/R5, accelerometer 5 was relocated to position 5B at the corner of the test panel held by retainer G/R5. There was no structural damage nor excessive movement of the components identified during test. Two post filler plugs, which are non-structural, failed during acoustic test and as a result of retorquing between test cycles. Post test inspection also showed no structural damage identifiable to acoustic excitation, no propagation of defects, and no unusual coating rubbing or scrubbing on mated surfaces. Inspection of the test specimen was performed

initially every cycle and each fifth cycle after Cycle 5. This inspection revealed that acoustic excitation was loosening the post retainer bolts which are buried at the bottom of the retainer posts. Repeated retorquing to the established test level of 15 inch-pounds (1.7 Nm) did not solve the problem. After test cycle 66, all ten post retainer bolts were tightened to a minimum of 25 to 30 inch-pounds (2.8 to 3.4 Nm) torque, solving the loosening problem during acoustic test. However during final disassembly of the test specimen, removal torques were found to be as low as five inch-pounds (0.6 Nm), showing that the problem of fastener torquing or locking had not been resolved.

Data from acoustic test cycles 51, 75 and 100 was accumulated and recorded and data plots of microphone sound pressure levels and accelerometer power spectral densities were prepared as before. These data plots are found in Appendix B. Figure 6-17 shows the test specimen at the completion of testing.

6.3.2 Thermal Testing — After completing the 50 thermal cycles simulating orbiter reentry flight, the nine-panel test specimen was in excellent condition as seen in Figure 6-18. All heat shield panels were flat and free of local warpage or buckling. Panel edge retainers remained in contact with heat shields and there was no evidence of problems related to thermal/structural design. Oxidation damage sites arising from several causes — the majority being test peculiar — were evident and had been documented from first sightings. Oxidation damage had been arrested by repair coating or permitted to grow to allow observation of problems associated with oxidation damage during continued thermal exposure and the dynamics of acoustic excitation. Oxidation sites which had been satisfactorily repair-coated continued to protect the metallic substrate.

The test specimen was acoustically tested for an additional 50 simulated boost cycles and disassembled for detailed evaluation of the structural integrity, reusability, damage tolerance, and for insulation performance, studies of refurbishment and repair of problems associated with disassembly and inspection.

6.3.3 Disassembly — Disassembly started with the removal of the center heat shield panel, simulating the removal of an external panel from a vehicle, see Figure 6-19. The center panel was disassembled from the array by removing the post filler plugs, unbolting the retainers, and sliding the panel from under the adjacent panel. Plugs which had been damaged by oxidation or torqued to failure, did not delay removal of the submerged post retainer bolts. The balance of disassembly was normal, excepting the removal of one post filler plug which had been permitted to oxidize, Figure 6-34, so that no drive socket remained. This plug was drilled through and removed with an "Easyout" hand tool, a possibility which had been considered in design. During disassembly of the test specimen, one of the plugs was torqued to failure. Since the body of the plugs are cylindrical, access to the retainer bolt at the bottom of the posts was still possible and the bolt was removed. All post retainer bolts were removed without difficulty, although the design would accommodate removal by "Easyout" tools if necessary.

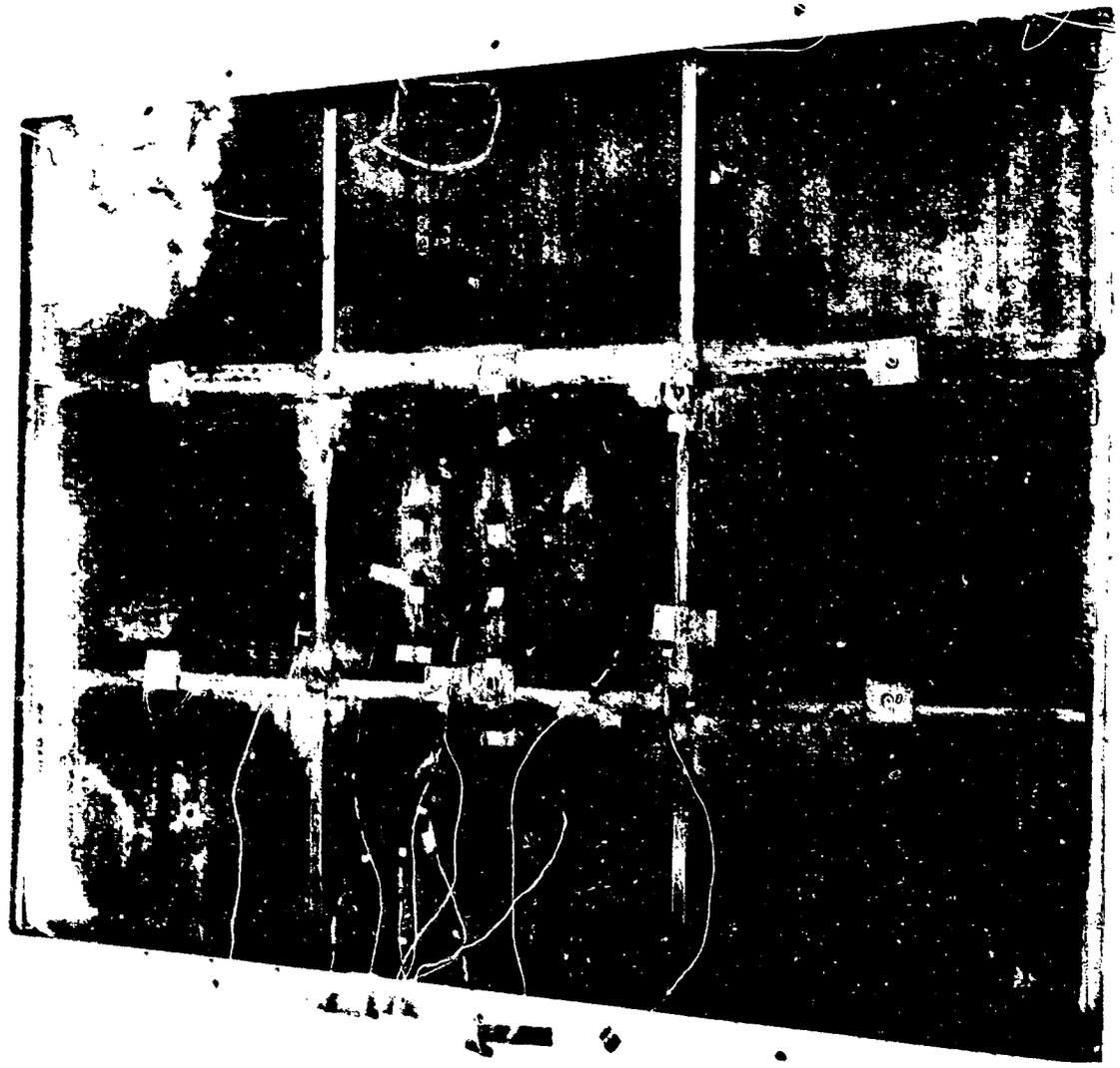

Figure 6-17. Nine-Panel TPS Test Specimen after 100 Cycles of Acoustic and 50 Cycles of Thermal Flight Simulation (138625)

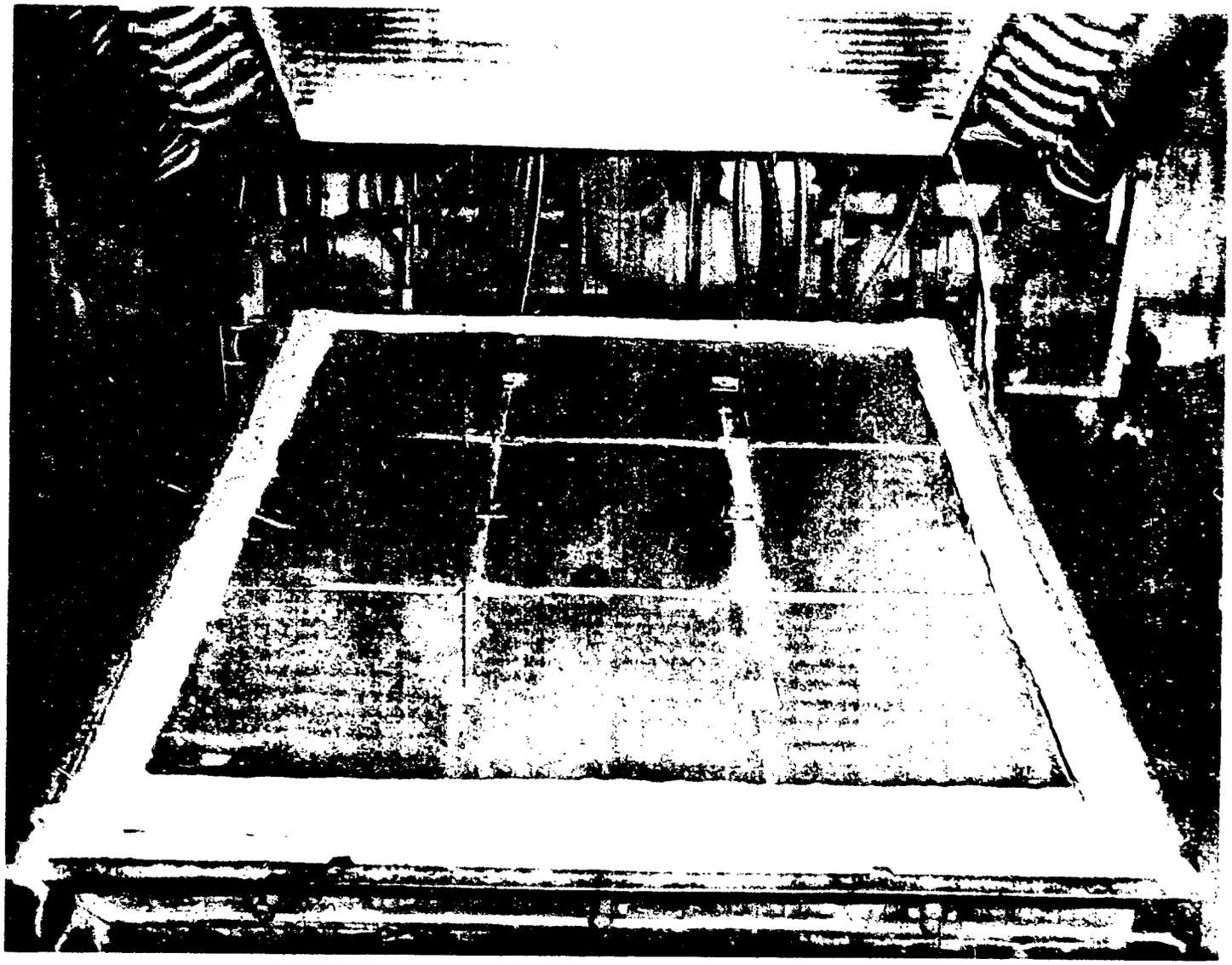

Figure 6-18. Nine-Panel TPS Test Specimen after 50 Cycles of Thermal Flight Simulation (138414)

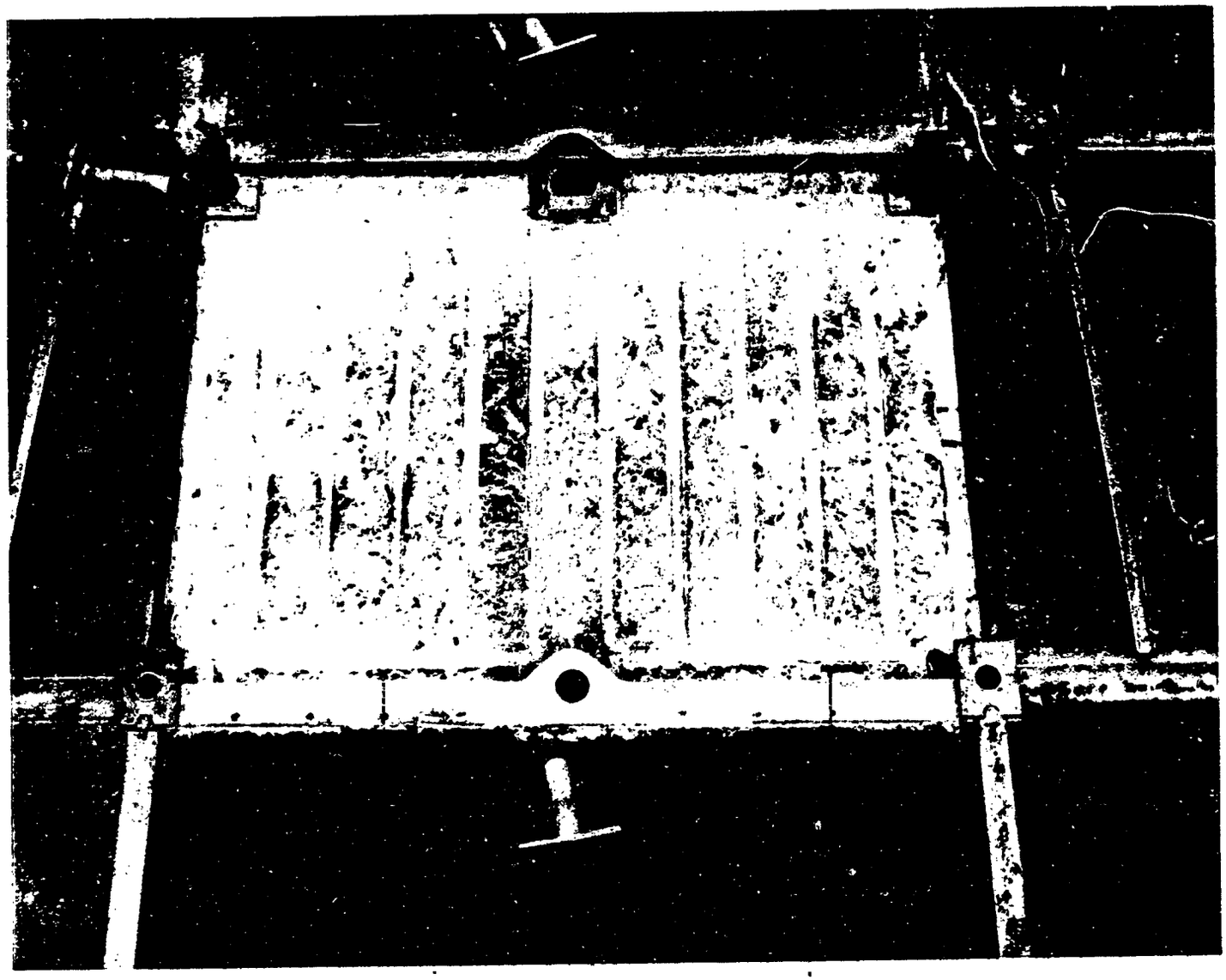

Figure 6-19. Center Heat Shield Removed from Nine-Panel Test Specimen (135624)

6.3.3.1 Condition of panels: The center heat shield panel of the test specimen which had experienced thermal and mechanical edge conditions during test which were representative of those imposed on a typical flight heat shield, remained flat and free of local distortion and warpage after completion of tests. This is seen in Figure 6-20. The balance of the heat shields seen disassembled in Figures 6-21 and 6-22 display the same absence from local distortion and warpage as the center panel, though the edge effects of the 2000° F (1366° K) thermal gradient from the panels to the water-cooled fixture, are evident in overall warpage of these peripheral guard panels. This warpage did not interfere with the guard panels remaining flat with the normal edge restraint afforded by panel retainers and by the test fixture.

6.3.3.2 Condition of insulation: The fibrous insulation selected for the Phase III thermal protection system performed satisfactorily under the test conditions. There was no evidence of incompatibility with the test hardware nor with the test environment, it remained dimensionally stable and did not densify due to sintering, and it did not disintegrate nor compact during test. Figure 6-23 shows the top surface of the insulation mass with all surface hardware removed. Figure 6-24 is looking into one insulation hole where an upper post has been removed. The condition of the insulation and the lack of compacting is clearly evident.

6.4 Damage Assessment

Major areas of concern in Phase III were the tolerance of the TPS to oxidation damage caused by coating breakdown, and the ability of the hardware to retain its integrity while damaged and subjected to repeated reentry flight cycles. Evaluations in these areas were made continuously throughout all testing, followed by a detailed, piece-by-piece assessment of the damage to the test hardware at the completion of all acoustic and thermal testing. These inspections revealed that the majority of the damages were of a minor nature or were unrelated to flight hardware, and that such damage did not compromise the ability of hardware to properly perform its design functions throughout the complete planned spectrum of acoustic and thermal testing.

All damage to the nine-panel thermal protection system test hardware during Phase III thermal testing was by oxidation of the columbium substrate, resulting from coating breakdown. Causes for the majority (80%) of coating damage have been identified and characterized. A detailed assessment was made of the damage and the location for each item of coated columbium, and a probable cause was assigned for each case of coating damage. The data in Tables 6-2 to 6-5 display all of the identified damage to each item of test hardware, grouped as to heat shield panels, panel retainers, upper support posts and the nonstructural, post filler plugs. The probable causes or sources of damage are as follows:

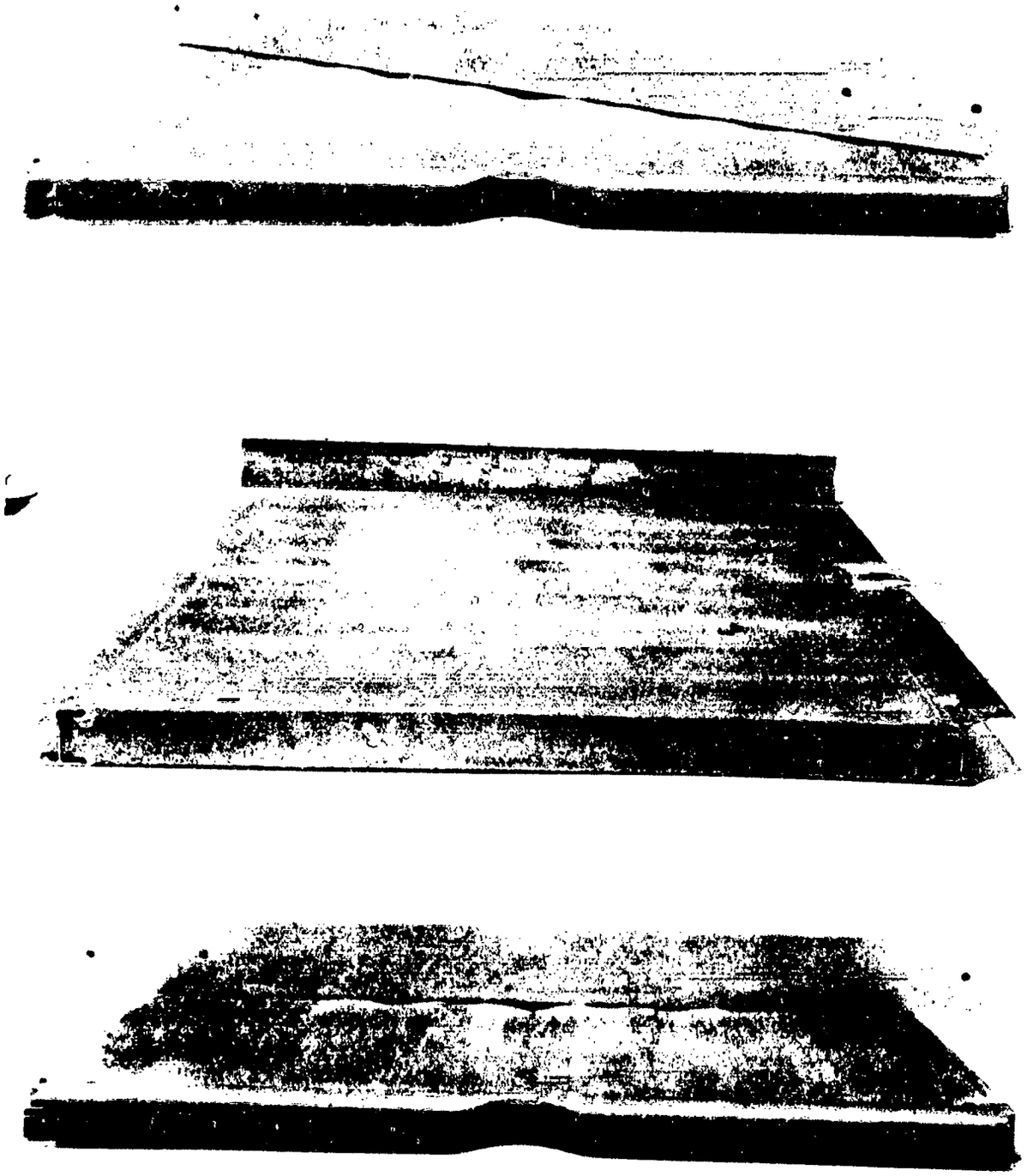

Figure 6-20. Center Test Panel from Nine-Panel Test Specimen after 50 Thermal and 100 Acoustic Life Cycle Tests (138714, 138719, 138725)

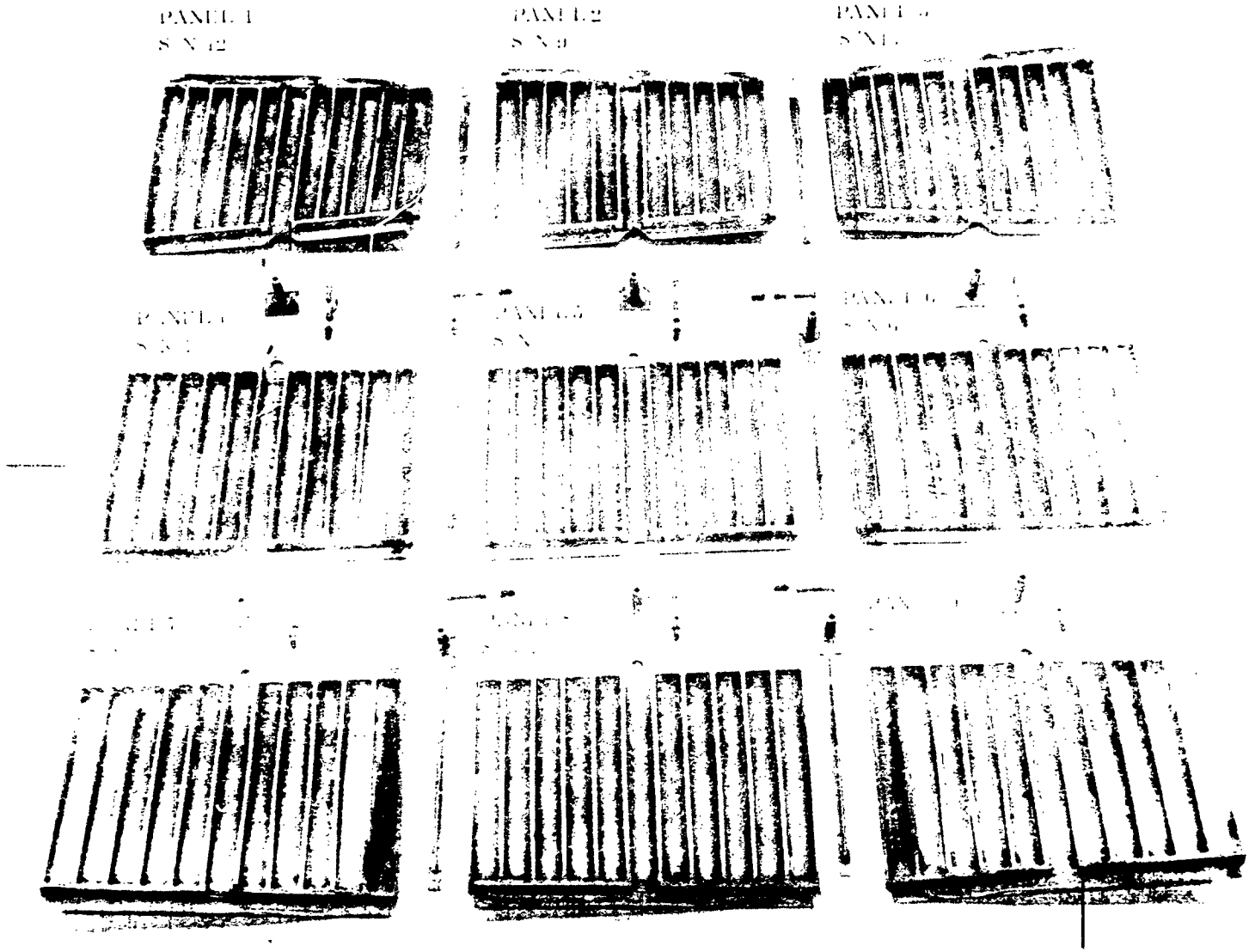

Figure 6-21. Disassembled Nine-Panel Test Specimen after 50 Thermal and 100 Acoustic Life Cycle Tests (138756)

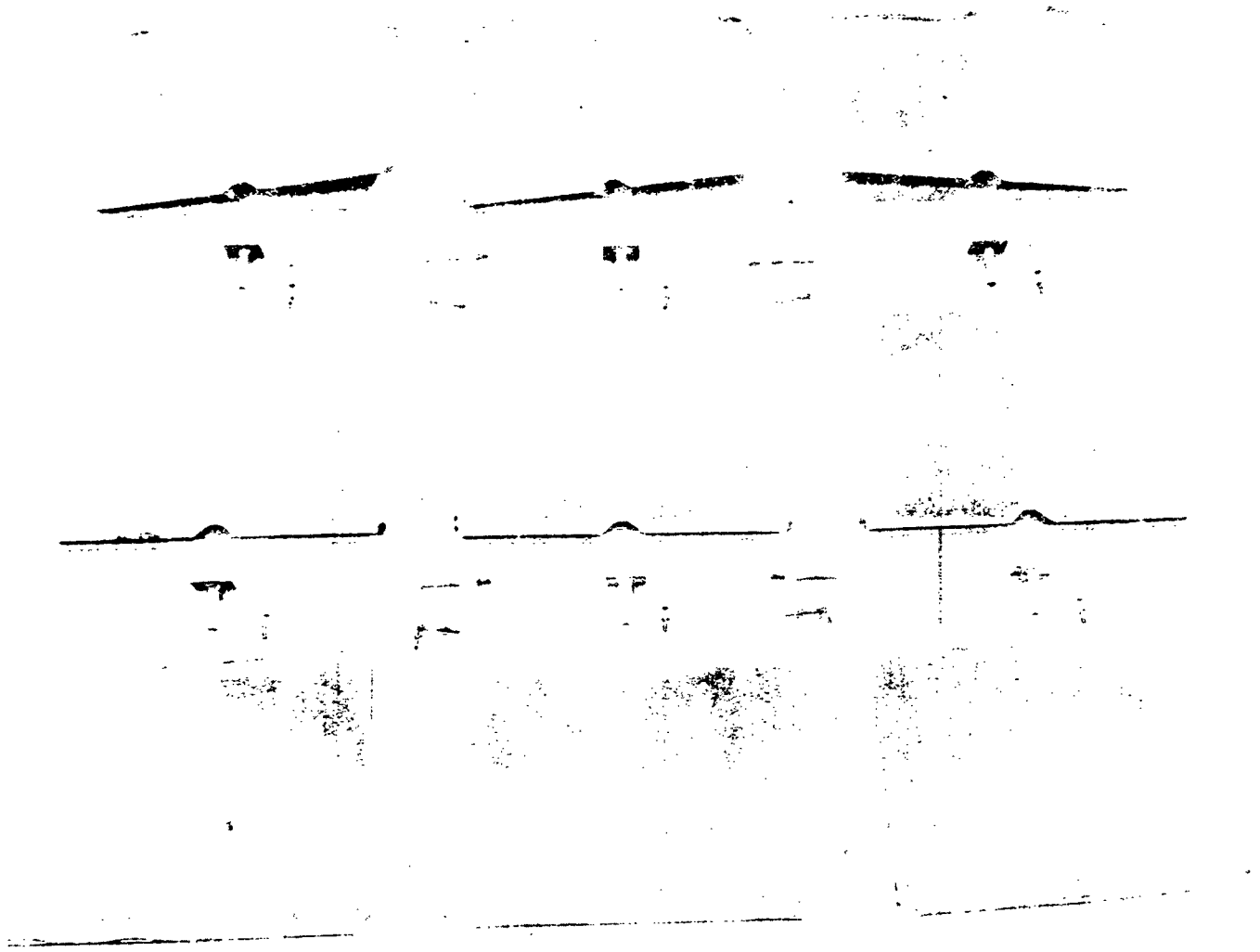

Figure 6-22. Disassembled Nine-Panel Test Specimen after 50 Thermal and 100 Acoustic Life Cycle Tests (138755)

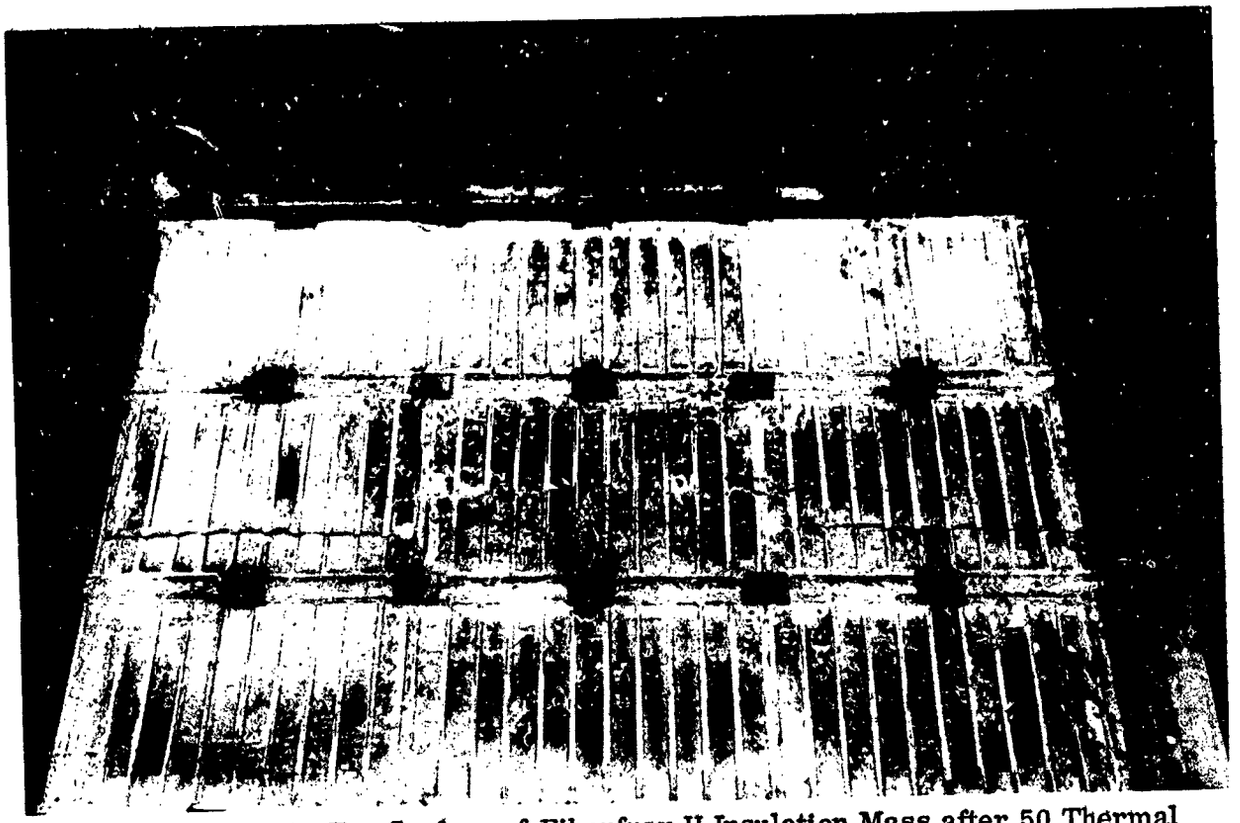

Figure 6-23. Top Surface of Fiberfrax H Insulation Mass after 50 Thermal Cycles to 2400°F and 100 Acoustic Cycles – Heat Shields and Panel Retainers Removed (138754)

Figure 6-24. Hole in Insulation with Upper Support Post Removed Showing Condition of Insulation after 50 Thermal and 100 Acoustic Life Cycle Tests (138749)

1. Design - Damage caused by an error in design which provided inadequate clearance between parts and allowed impacting during acoustic excitation, damaging the coating on one or both parts. An example of this is shown in Figures 6-25 and 6-26 where the panel corner impacted the shoulder of the retainer post B/R3 during acoustic testing and eventually resulted in the hole in the post. The retainer post had been increased in diameter and the shoulder thickened after Phase II without complete clearance checks with adjacent panels.

2. Manufacturing - Damage resulting from inadequate manufacturing quality control which allowed discrepant parts to go into assembly. Discrepancies consisted of dimensional errors, improper finishing, or undetected flaws. In Figure 6-27, the dimensionally incorrect load pads on the longitudinal beams of the panel allowed the pad to impact the retainer post, damaging both the pad and the body of the post. This pad, during acoustic vibration, impacted the body of a retainer (replaced after Cycle 21) creating an oxidized hole similar to those seen in retainer G/R5 of Figure 6-26.

An example of improper finishing is illustrated in Figure 6-28. (This panel also displays corner damage due to design discrepancies.) The weld bead extended under the retainer and was not ground flush permitting high local loading and impacting during acoustic excitation, creating coating damage and eventual failure.

The large oxidized area to the left in Figure 6-29 is thought to have been the result of an undetected crack or flaw in the beam material. (No components were inspected by NDT prior to testing.) An attempt was made to repair this site, which was unsuccessful due to its inaccessibility and an unsatisfactory furnace atmosphere during fusing of the repair coating. Other similar cases are the damage sites of I/R6 and R1 in Figure 6-26.

3. Coating - Damage identified to have resulted from inadequate quality control of the silicide coating process. This includes the quality of the materials, the distribution of constituents before and after fusing, and the thickness of coating on all surfaces, particularly on interior cylindrical surfaces, edges and corners. Evidence of inadequate coating protection on interior surfaces is seen in Figure 6-26 on the plugs and the post inside diameter of retainer D/R4. Examples of local coating lack of protection are seen in Figure 6-30 which has two damage sites, one hole through a rib and the other an area on the beam web. Figure 6-31 illustrates two cases of edge damage caused by unsatisfactory coating. In Figure 6-32 are seen two other typical damage sites caused by poor quality coating.

Figure 6-25. Panel Corner Damage Caused by Design Deficiency – 50 Cycles (138746)

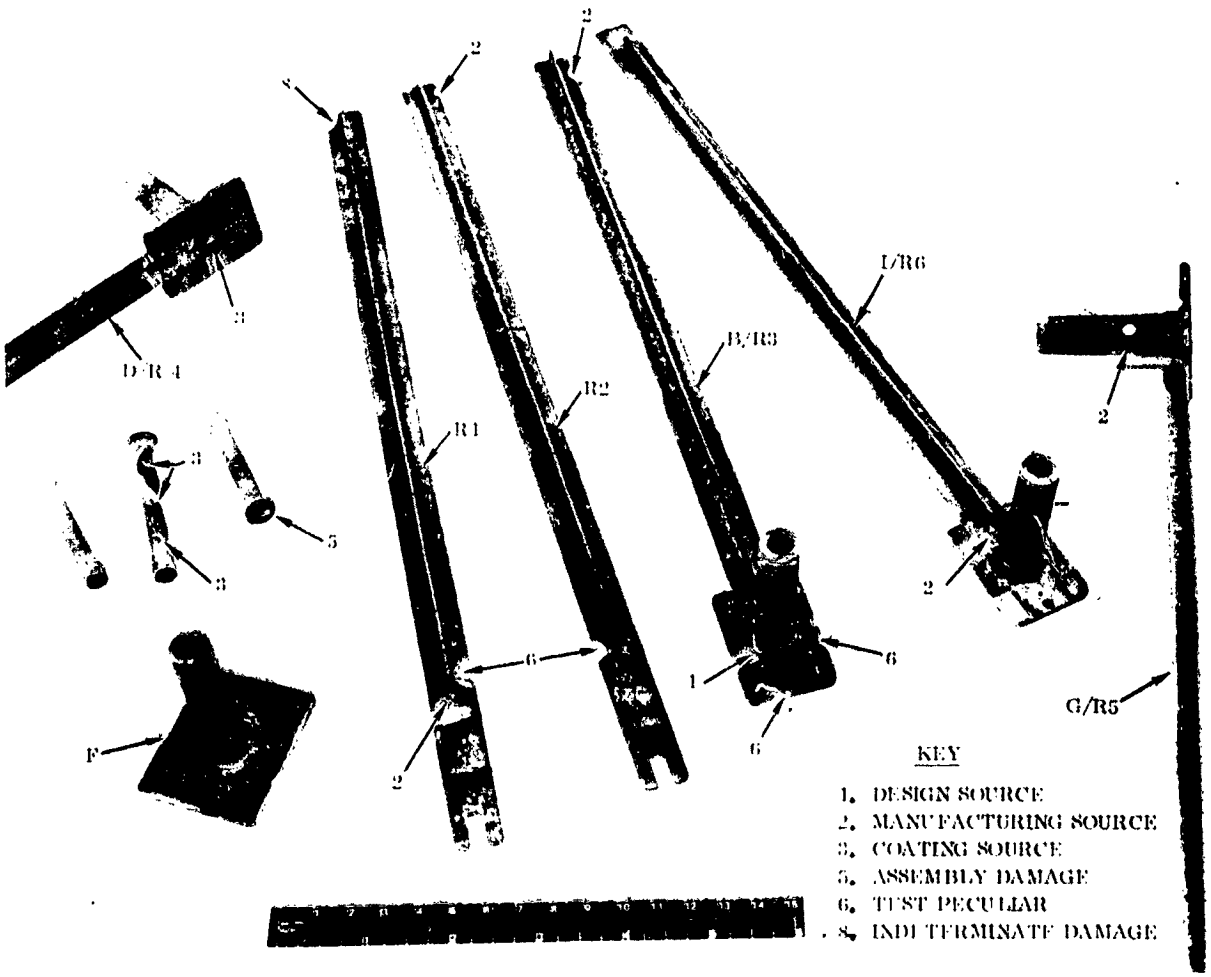

Figure 6-26. Panel Retainers and Plugs with Damage from Several Causes – 50 Cycles (138726)

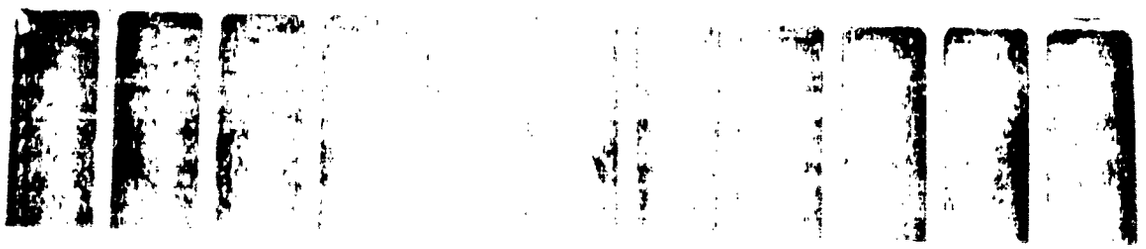

Figure 6-27. [illegible] to Load Path Caused by Manufacturing Discrepancy of Part Inspection = 50 Cycles (138742).

Figure 6-28. Skin Damage to Panel Caused by Improper Weld Finishing = 50 Cycles (138731).

Figure 6-29. Part with Oxidized Crack Site Not Detected During Manufacturing = 50 Cycles (138724)

Figure 6-30. Panel with Oxidation Damage and Hole Caused by Coating Deficiencies - 50 Cycles (138710)

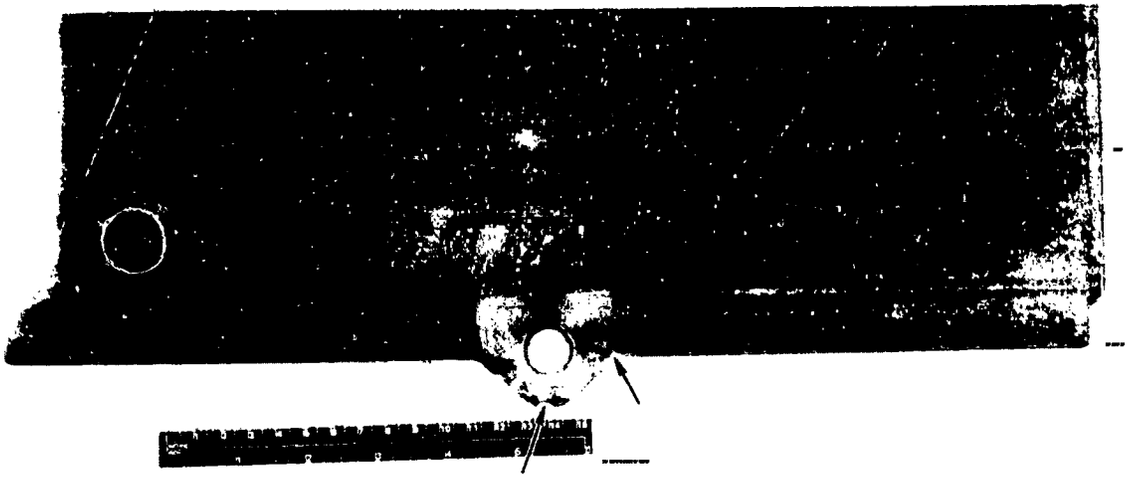

Figure 6-31. Edge Oxidation to Panel Caused by Coating Deficiencies - 50 Cycles (138732)

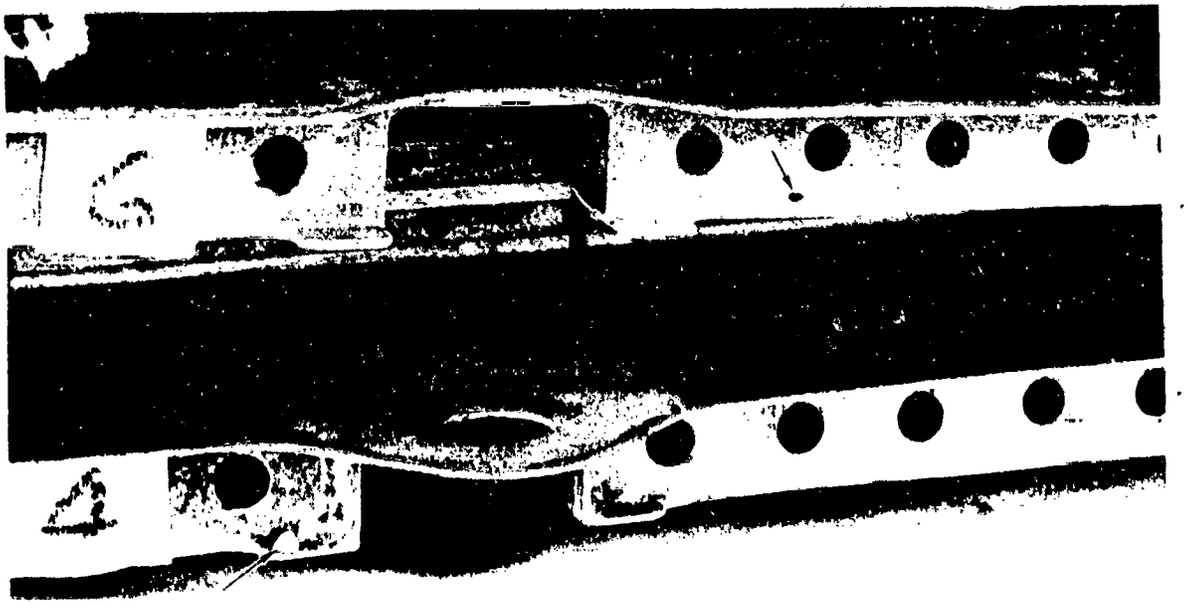

Figure 6-32. Panels with Local Damage Sites Caused by Coating Deficiencies - 50 Cycles (138728)

4. Materials - Damage caused by the use of unsatisfactory or incompatible materials which reacted adversely when exposed to the flight or test conditions of temperature, local atmosphere, time and pressure, or loads. One case of apparent incompatibility of materials was revealed. The situation was a test peculiar condition unrelated to flight hardware and involved the spring-loaded metal sheathed, tungsten-rhenium thermocouple probes, which reacted with the silicide coated hot skin during thermal cycling. Though 14 such probes were in use under similar conditions, only four caused coating damage, three of which became through holes in the skin. Figure 6-33 shows two views on the skin surface of such a site before a through-hole developed. This damage is discussed further in Section 6.5.

5. Assembly - Coating damage resulting from normal assembly and disassembly operations encountered during turn-around inspection. The damage sites in the hexagonal drive socket of the post filler plugs shown in Figures 6-34 and 6-26 are of this type. This damage developed during wrenching operations and is expected of coated fasteners. (The situation may have been worsened by improper edge preparation for coating). The plug is a nonstructural, throw-away item and the socket oxidation did not impair its removal.

6. Test Peculiar - Damage to coating which resulted from conditions [illegible] exclusively to the particular test and which were not realistic of flight conditions. Several examples of this were available from the nine-panel test specimen due to the steep thermal gradients experienced by the guard panels which surrounded and isolated the center test panel from edge effects created by the tests. The cracking and oxidation sites in the guard panels of Figure 6-35 were test peculiar. Other damage sites resulted from the distortion of guard panels - a product of the severe thermal gradients. These panels flexed rather vigorously with an over-center action during disassembly for inspection and repair, causing coating damage to themselves and adjacent parts. This damage was test peculiar since such distortion resulted from the test thermal gradients and not from normal assembly and disassembly operations. Examples of this test peculiar damage are seen in the guard panel in Figure 6-36 and on the retainers R1, R2, and B/R3 in Figure 6-26.

7. Flight Normal - Damage to coating which was considered to be a normal condition and realistic to vehicle hardware. Examples of this were the damage caused by parts in contact responding to the thermal, mechanical, and physical aspects of the repeated flight environment. An example is the damage site at the base of the panel locating key on the upper support post in Figure 6-37. Two other cases after 50 thermal cycles are seen in Figure 6-38, both serious enough to require a design improvement in this panel area.

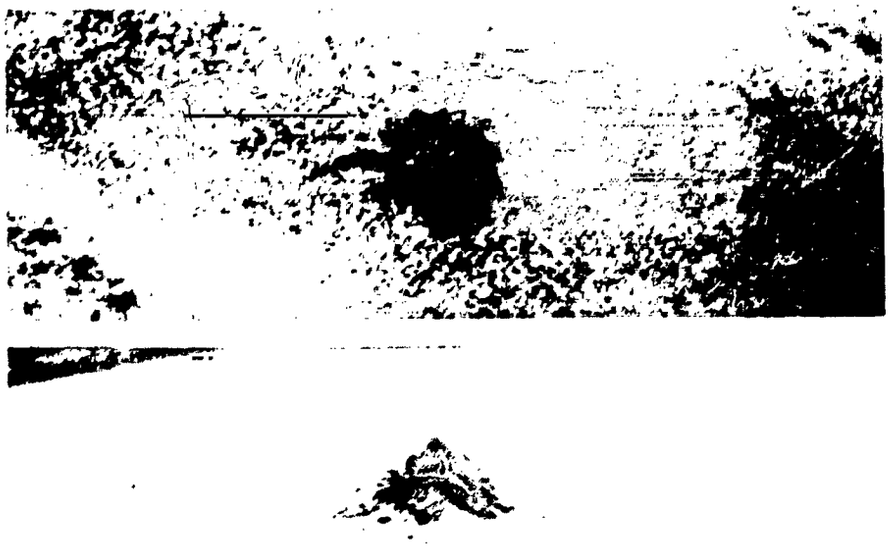

Figure 6-33. Damage Site on Panel Located Over Thermocouple Probe – Both Sides Shown – Cycle 8 (138747, 138748).

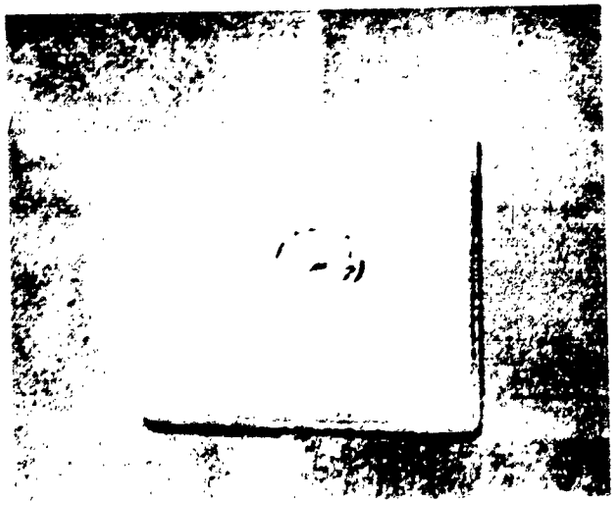

Figure 6-34. Oxidation of Hexagonal Drive Socket of Post Filler Plug – Assembly Damage – 50 Cycles (138488)

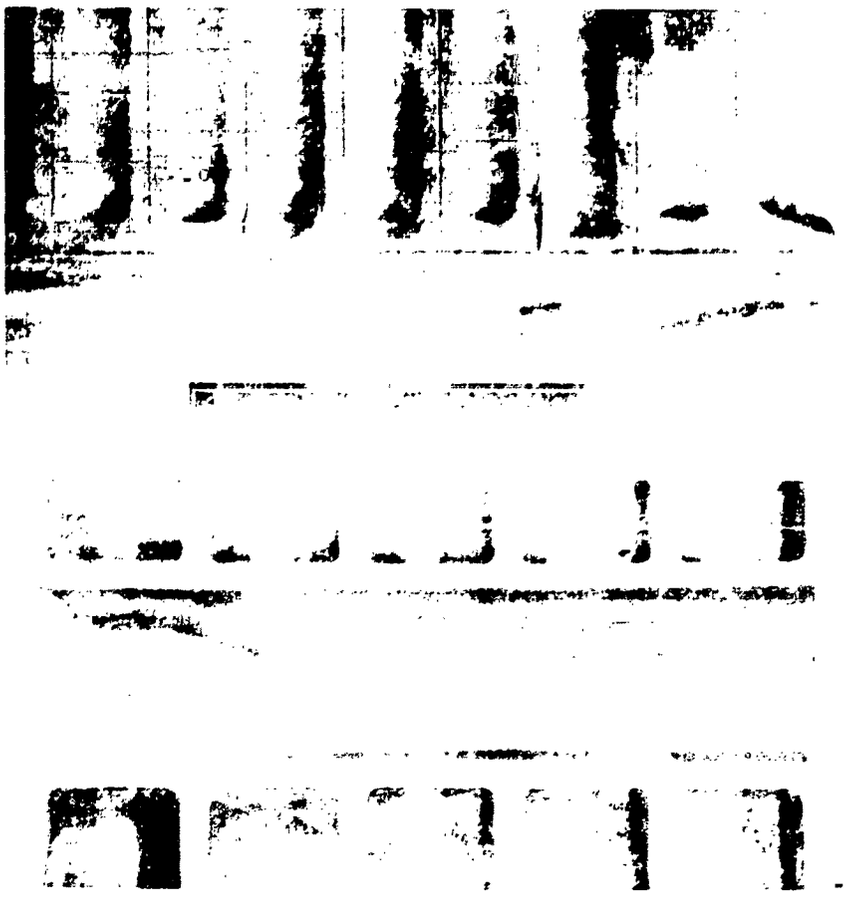

Figure 6-35. Oxidized Cracks in Corner Guard Panels Caused by Steep Thermal Gradients – Test Peculiar – 50 Cycles (138711, 138712)

Figure 6-36. Guard Panel Damage Caused by Flexing of Transverse Beam – Test Peculiar – 50 Cycles (138737)

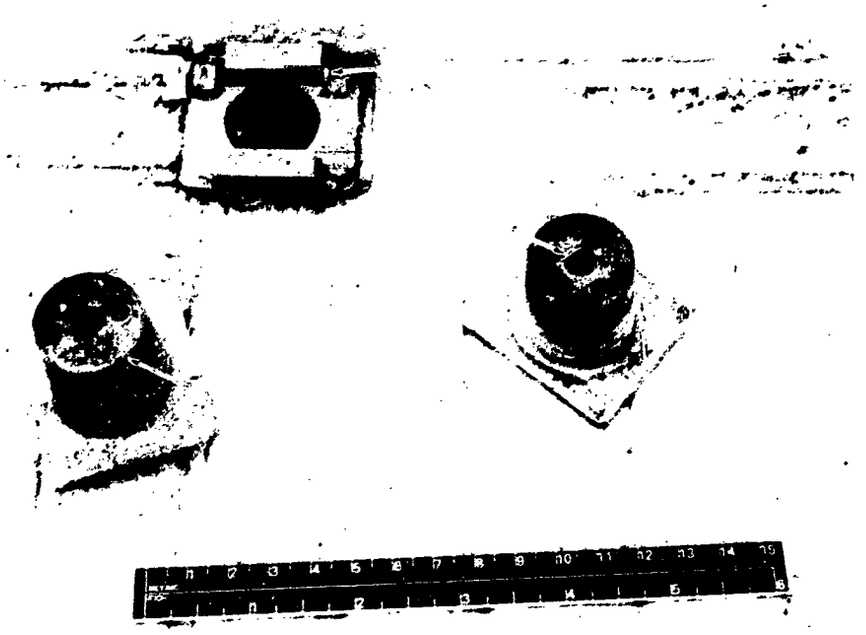

Figure 6-37. Upper Post Damage Due to Flight Normal Causes - Top, Indeterminate Causes - Bottom, 50 Cycles (138729)

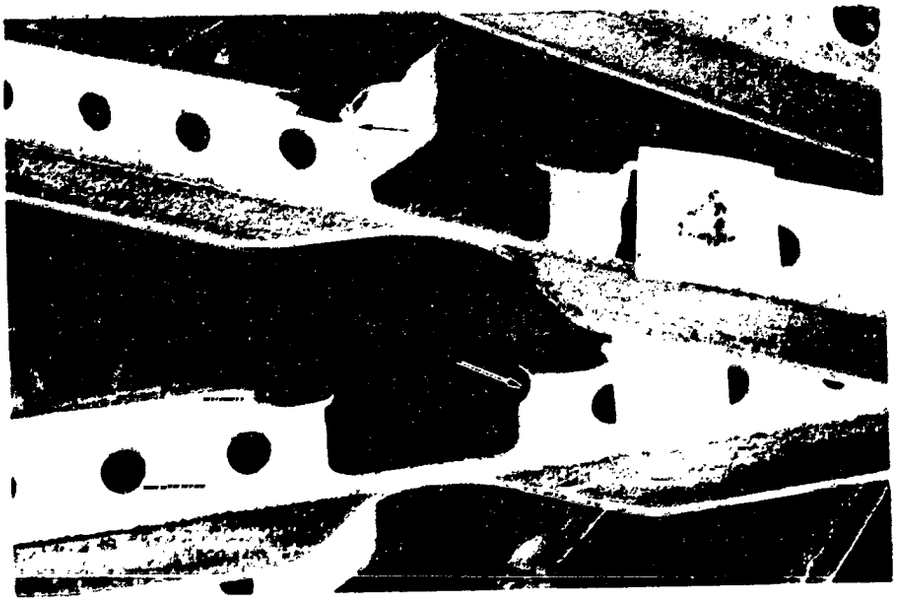

Figure 6-38. Flight Normal Panel Damage Requiring Redesign - 50 Cycles (138727)

8. Indeterminate - Cases of damage where there was no clear-cut cause or source of coating damage. In most cases, a combination of causes undoubtedly contributed to the damage. The ends of the heat-shield panels contained numerous examples of indeterminate damage. Here were found built-in problems of manual edge preparation of thin sheet for coating, for application and evaluation of edge coatings, coupled with manufacturing variances and a design not conducive to good end producibility. The result is damage sites such as shown in Figure 6-39. A simple design change permitting the skin and rib cap to overhang the rib rather than trimmed flush, might eliminate most of the panel end defects. Another example is the retainer end damage to Retainer R1, Figure 6-26, where the cause could be attributed to one of several discussed classifications.

From the data compiled in Tables 6-2 through 6-5, it is possible with each type of hardware to identify the principal location of coating damage and the principal causes or sources of such damage.

6.4.1 Heat Shield Panel Flight Hardware. - On the heat shield panels, the main damage (see Table 6-2) was found to be to the skins (33.3%), dominated by test peculiar causes, and to the panel ends (23.4%) mostly from indeterminate causes. This is in agreement with the principal causes of damage to all panels where 35.6 percent were test peculiar and 25.5 percent were for indeterminate reasons.

For flight heat shields, where improvement efforts have been focused on potential damage causes, the reliability can be improved 40 times to an average of only 2.5 defects per panel per 50 flights. The remaining defects would be localized principally at panel ends and at noncritical ends and edges resulting in a low possibility of flight failure in 50 cycles. This would be accomplished by review of the Phase III panel designs to remove design interferences and to improve the producibility and coatability of the panel, to minimize the potential for normal flight damage, and by improved quality control during manufacturing and coating operations. The test peculiar and material compatibility problems encountered by Phase III test hardware would not be present for flight hardware. In actual flight operations, any panel which is found to be critically defected during routine turnaround inspections would be repaired or replaced.

6.4.2 Panel Retainer Flight Hardware. - From Table 6-3, it is seen that the principal damage to the retainers was to the posts (35.3%) with the principal cause of damage in design and coating deficiencies. Next principal damage was to the tee retainer cap (29.4%) followed by the flange (23.5%), with all but two cases attributed to test peculiar conditions.

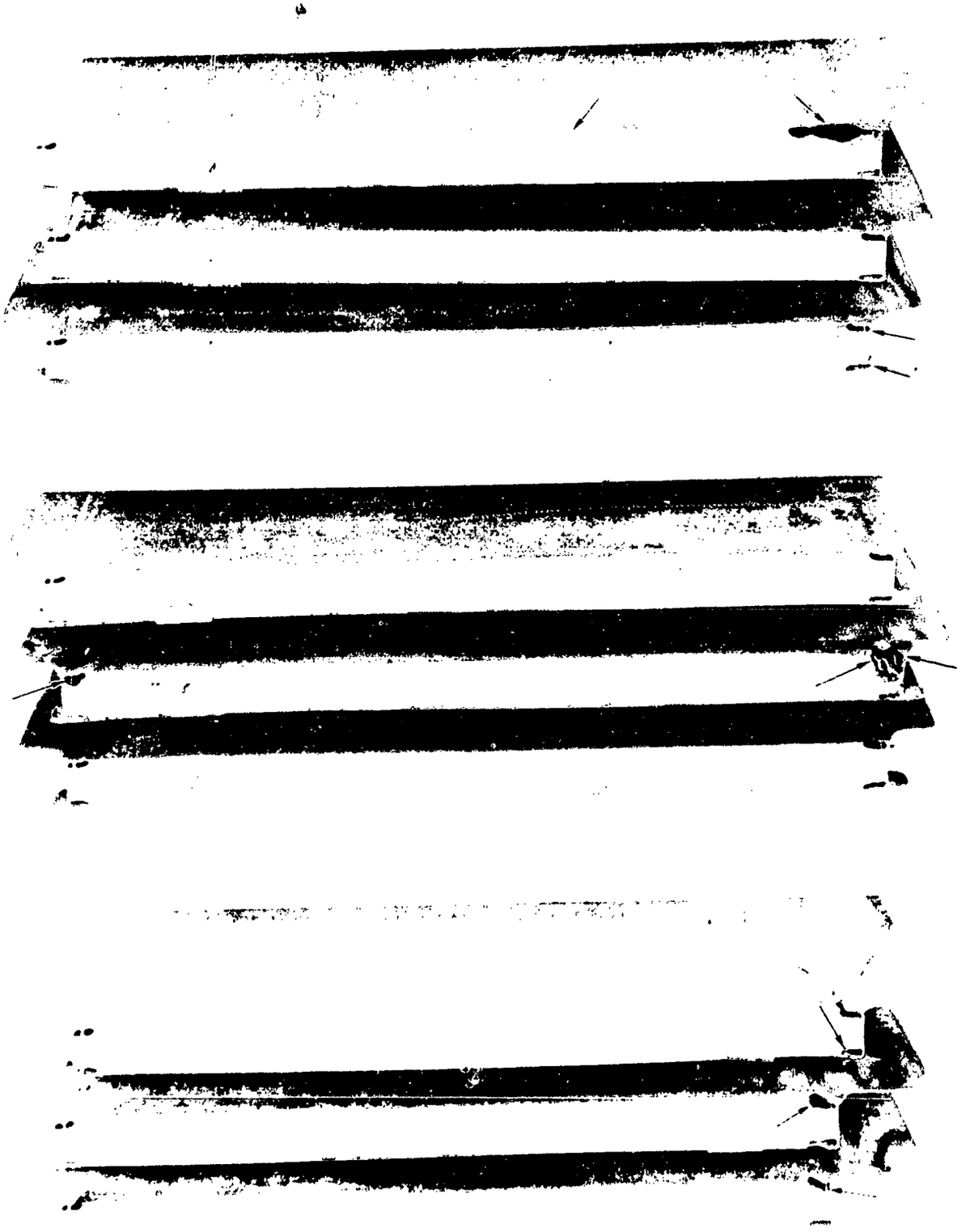

Figure 6-39. Oxidation Site at Ends of Panels - Indeterminate Causes - 50 Cycles (138715, 138720, 138722)

Table 6-2. Heat Shield Panels - Damage Assessment
9 Parts - 100% Inspection

Location or Type	Probable Defect Source or Cause								Total	Percent
	Design	Mfg.	Coating	Mat'l.	Ass'y.	Test Peculiar	Flight Normal	Indeter-minate		
Panel Ends						4		17	21	23.4
Skin		9		4		17			30	33.3
Beam Edges	4		3						7	7.8
Beam Web		1	1						2	2.2
Rib Cap Edges						4	1	5	10	11.1
Load Pads		1	2				1		4	4.4
Ctr Web Cutout						5	1	1	7	7.8
Rib/Cutout									0	0
Rib Cap Weld		1	1						2	2.2
Holes, Misc.			5						5	5.6
Flange Crack						2			2	2.2
TOTAL	4	12	12	4	0	32	3	23	90	
Percent of Total	4.5	13.3	13.3	4.5	0	35.6	3.3	25.5		100.0

Table 6-3. Panel Retainers - Damage Assessment
10 Parts - 100% Inspection

Location or Type	Probable Defect Source or Cause								Total	Percent
	Design	Mfg.	Coating	Mat'l.	Ass'y.	Test Peculiar	Flight Normal	Indeter-minate		
Posts	2		4						6	35.3
Flange			1			3			4	23.5
Tee Cap						4		1	5	29.4
Tee Web		1				1			2	11.8
TOTALS	2	1	5	0	0	8	0	1	17	100.0
Percent of Total	11.8	5.9	29.4	0	0	47.0	0	5.9		

Table 6-4. Post Filler Plugs - Damage Assessment
10 Parts - 100% Inspection

Location or Type	Probable Defect Source or Cause								Total	Percent
	Design	Mfg.	Coating	Mat'l.	Ass'y.	Test Peculiar	Flight Normal	Indeter-minate		
Socket		4			4				8	25.8
Body O.D.			6						6	19.4
Body I.D.			16						16	51.6
End								1	1	3.2
Edges									0	
TOTALS	0	4	22	0	4	0	0	1	31	100.0
Percent of Total	0	12.9	71.0	0	12.9	0	0	3.2		

Nearly half (47%) of all retainer damage were found to be test peculiar followed by coating causes (29.4%) and by design (11.8%). By a review of the Phase III design, clearance of the retainer posts and heat shield panels and by improving quality control efforts during manufacturing and coating operations, the retainer defect rate can be reduced to one defect in 2.5 panels per 50 flights. Except for the end of the tee member, this part is structurally critical and would require frequent turnaround inspection to remove damaged parts. This is readily accomplished by in-place inspection and by easy removal.

6.4.3 Post-Filler Plugs Flight Hardware. - The dominant damage to post filler plugs as seen in Table 6-4 was caused by oxidation sites on the inside diameter of the body (51.6%) and on the outside of the body (19.4%), accounting for 71 percent of all damage. Socket damage of 25.8 percent arose from assembly operations and possibly from improper edge preparation. The main thrust for improved filler plug reliability must be to improve the coating of the body, particularly on the inside diameter. The most optimistic improvements could not reduce the damage rate to less than one per part per 50 flight cycles. However, the filler plug is nonstructural and functions only to shield and protect the submerged superalloy panel fastener. Excessive oxidation damage or loss of a plug does not impact flight safety nor impair disassembly operations as shown during disassembly of the nine-panel test specimen after 50 simulated flight cycles. Here one plug was "lost" during final acoustic testing, one was torqued to failure during test, and one was so seriously damaged by oxidation as to require removal with an "Easy-out" tool. In all cases further disassembly was unaffected.

6.4.4 Upper Post Flight Hardware. - Very little damage was evident on the upper posts (see Table 6-5) which were examined. Four posts were completely removed and inspected and six were inspected in place with the top flange, locator keys and the post inside diameter visible to inspection. The absence of damage indicates good design for coated columbium hardware. The total damage was limited to two cases of flight normal damage to the welds which affix the keys to the flange on two parts and some unassigned damage to a bottom edge and to a clearance hole. None of these damages could have reasonably caused ultimate failure of the part in 50 to 100 flight cycles. The damage rate of the parts tested and inspected was 0.5 per part in 50 flights and this probably could not be improved for flight hardware.

6.4.5 Damage Assessment Summary. - The total number of damage sites (see Table 6-6) can be substantially reduced for flight hardware by efforts to improve coating and manufacturing quality control and by design review and improvement to remove interferences and to increase producibility. Conservatively, the damage could be reduced to 6.8 site per TPS unit consisting of seven parts of coated columbium (see Section 5.1), or less than one damage site per part per 50 flight cycles. Most of these sites would have been discovered during turnaround inspections of the vehicle thermal protection system and the damaged parts repaired or replaced.

Table 6-5. Upper Post - Damage Assessment
10 Parts - 4 Inspected 100%, 6 Partial Inspection

Location or Type	Probable Defect Source or Cause								Total	Percent
	Design	Mfg.	Coating	Mat'l.	Ass'y.	Test Peculiar	Flight Normal	Indeter-minate		
Edges								2	2	40.0
Welds							2		2	40.0
Holes								1	1	20.0
TOTAL	0	0	0	0	0	0	2	3	5	100.0
Percent of Total	0	0	0	0	0	0	40	60		

Table 6-6. Summary of all Damage to Nine-Panel TPS
Total 39 Parts

	Design	Mfg.	Coating	Mat'l.	Ass'y.	Test Peculiar	Flight Normal	Indeter-minate	Total
Total TPS Damage Sites	6	17	39	4	4	40	5	28	143
Percent of Total	4.2	11.9	27.3	2.8	2.8	27.9	3.5	19.6	100

As had been anticipated during design, the coated columbium parts did suffer oxidation damage from the repeated simulated reentry flights. Most of the damage was of a minor nature and did not structurally degrade the hardware. Panels, panel fasteners, plugs, and retainers were removed when desired for inspection and assessment of oxidation damage, and severely damaged plugs and fasteners were removed for replacement without damaging adjacent parts. The damage tolerance and the ability of the TPS to perform its design functions, though damaged, were most evident from the post test review of the TPS hardware.

6.5 Materials Problems

Two problems arose during Phase III fabrication and testing which were traceable to the materials. The first involved the Cb-752 columbium alloy supplied by Wah Chang Albany Corporation. The other involved the material selected as sheathing for the high temperature, tungsten-rhenium thermocouple.

During fabrication, several cracks were encountered in or near electron beam welds and during cold straightening operations. Cracking of this nature had not been experienced during Phase II fabrication of identical hardware using the same processes. It was discovered that the columbium sheet and plate furnished by Wah Chang for Phase II differed from that furnished for Phase III. Phase II material had included a Wah Chang proprietary additive which enhanced weldability and minimized cracking probabilities. This additive was present in only one heat of material furnished for Phase III fabrication and this only for use on a minor part. The procuring purchase order, as recommended by Wah Chang, had specified that the material be furnished "..... fully recrystallized and best weldable quality." It is believed that the absence of this additive influenced the cracking experienced during PhaseIII fabrication. If such a crack were present and undetected prior to silicide coating, a major oxidization site such as that seen in Figure 6-29 could have resulted.

The second problem encountered during Phase II involved the sheathing material for the high temperature thermocouples. For Phase II an iridium sheath had been used. However, the sheath was very brittle, thereby creating problems during fabrication and installation. In addition, the iridium was procured from a non-domestic source which resulted in an extensive lead-time and a total cost beyond the budgetary restrictions of this program. After an in-house evaluation, Inconel 600 [72 Ni-15 Cr-8Fe-1Mn (plus Si, Cu, C, S)] was selected for the sheathing. The evaluation consisted of thermal exposure from 2000 to 2400°F (1366 to 1589°K) at one atmosphere in air with thermocouples in contact with R-512E/Cb-752 coupons, under pressure loads ranging from approximately 400 to 650 psi (2.76 to 4.48 MN/m^2). The duration of the exposure was 62 to 66 hours. No macroscopic reaction was observed on either the coupons or the sheathing material.

Fourteen thermocouples sheathed with Inconel 600 were installed in the test specimen and spring-loaded against the skin hot face. After one cycle at 2250°F (1505°K), a small eruption of slag-like material was evident on the top face of the skin opposite to one thermocouple. This was accompanied by a deformation of the skin due to excessive spring loading by the probe. The spring pressure on all probes was reduced to prevent further deformation damage to the skins. After thermal cycle 4 and later after cycle 31, similar surface eruptions were observed over thermocouple locations in adjacent panels. These three damage sites resulted in through holes in the skin.

After completion of testing and during disassembly, a similar damage site was found on a fourth panel. This site was only visible on the side of the panel contacted by the thermocouple probe. There was no indication of an eruption on the top skin surface. It is notable that there were ten other high temperature thermocouple positions where the Inconel 600 sheathing was in contact with the silicide coated columbium and there was no evidence of reaction between the sheathing and the silicide. A total of 27 sheathed tungsten-rhenium thermocouples were installed in the test specimen during Phase III testing.

It was evident that an incompatibility problem existed between the sheathing material and the coated columbium under the circumstances and conditions of thermal testing. It was not a predictable situation since but four thermocouple positions showed evidence of reactions. Subtle differences may have existed from position to position that would account for the differences in reaction. These might include: (1) temperature variances, (2) load on the probe, (3) the presence of oxide films on either contacting surface, or (4) remnants of insulation on the tip of the probe acquired during installation. It has been reported that under the proper conditions of temperature, time, pressure and atmosphere, nickle base alloys such as Inconel 600 react unfavorably with silicide coatings and with columbium (Reference 6). A thin barrier layer of insulation or of an oxidation resistant foil such as iridium can be used to prevent the occurence of problems such as those encountered during Phase III testing.

6.6 Acoustic Analysis

As described in Section 6.3.1, the tee-stiffened heat shield panel survived the acoustic test program without any structural-damage attributable to sonic fatigue. The purpose of the subject evaluation, therefore, was to compare analytical and test results in order to validate analytical sonic fatigue prediction procedures used during this program.

Test panel responses to acoustic excitation were measured by accelerometers located as shown in Figure 6-4. Response data were presented as plots of acceleration spectral density in G^2/Hz versus frequency in Hz. However, acoustic fatigue analyses were made by use of Convair Aerospace Computer Program P5454, which computed panel responses in terms of dynamic stresses. (Reference 1b, Appendix C.) It was necessary, therefore, to estimate the dynamic stresses corresponding to the measured accelerations in order to establish a compatible basis for comparing analytical and test results.

The test panel, being effectively supported only at two ends, was considered as a simply supported beam. A simply supported beam under a uniformly distributed load has its maximum bending deflection (y) and stress (f) at mid-span.

$$y_{max} = \left(\frac{5}{384}\right)\left(\frac{W\ell^3}{Ef}\right), \text{ and } f_{max} = \frac{Mc}{I} = \left(\frac{1}{8}\right)\left(\frac{W\ell c}{I}\right)$$

For a panel exposed to acoustic pressure, the acoustic pressure applied statically can be substituted for W. By ratioing the normalized stress to the normalized deflection, i. e., $(f_{max}/W)(y_{max}/W)$, the following expression is obtained,

$$f = \frac{48Ecy}{5\ell^2}$$

where c is the distance from the neutral axis of the beam to the extreme fiber.

From review of the panel modal survey data contained in Table 6-1, in conjunction with the acceleration spectral density plots obtained during acoustic fatigue tests, it was determined that the panel bending mode at a frequency of 295 Hz developed maximum bending stresses. It is noted that this is the same mode and frequency reported in Reference 1b. Stresses were calculated by the following procedure. First, rms accelerations were calculated by taking the square root of the product of acceleration spectral density times filter bandwidth and multiplying by the gravitational constant, 386 in/sec^2. The rms displacements were then obtained by dividing the rms accelerations in in/sec^2 by the square of the resonant frequency in radians per second. Considering the phase relationships among the several accelerometers, the maximum relative

rms displacement along the panel was then obtained. This displacement was then substituted in the expression

$$f = \frac{48Ecy}{5\ell^2}$$

to yield the dynamic rms stress in psi.

The measured responses of the panel include the effects of inherent damping (dynamic magnification), but do not include the effects of local stress raisers. Inspection of the half-power points on the acceleration spectral density plots indicates that the average panel damping coefficient in the 295 Hz mode, c/c_c, is 6 percent of critical; this corresponds to a dynamic magnification factor, Q, of 8.33. However, if the filter bandwidth is greater than the structural bandwidth, the damping estimate may be high.

The dynamic rms stress in the 295 Hz mode calculates to be 1218 rms psi for the high-level, 158 dB OASPL, input shown in Figure 6-40. If a local stress raiser of $K_T = 4.0$ is considered, the local dynamic stress is 4872 rms psi. The 4σ maximum local dynamic stress is then 18,488 psi and the critical stress (f_{cr}) for maximum partial damage is 9,244 psi. From Reference 1b, Page 269, the total required life of the TPS panel for 100 flights is 5,000 seconds under acoustic excitation during lift-off and ascent of the Space Shuttle vehicle. At a resonant frequency of 295 Hz, this corresponds to 1.475×10^6 stress reversals.

Fatigue life evaluation of the test panel was made in two ways, based on reversed bending (R = -1) stress-cycle (S-N) curves shown in Figure 6-63 of Reference 1b. First, using the local dynamic stress level of 4,872 rms psi in conjunction with the derived random S-N curve, it is seen that the fatigue life expectancy is about 10^8 stress reversals. Second, using the critical stress level of 9,244 psi, the fatigue life expectancy is in excess of 10^8 stress reversals, based on the sinusoidal S-N curve. Hence, by either procedure a large margin of safety is shown as predicted.

In summary, as predicted in Reference 1b for the columbium alloy TPS panels, margins of safety are large and fatigue life expectancy is indefinite with respect to acoustic exposure. As a matter of interest, dynamic stresses developed under acoustic exposure, reported in Reference 1b, when normalized by the incident acoustic pressures are the same as the normalized stresses obtained during the tests reported herein.

6.7 Thermal Analysis

6.7.1 Methods of Analysis. — The thermal analysis presented herein was conducted using a computer program designated GAWEB 9793, Transient, Two-Dimensional Heat Transfer Program. This program accommodates a variety of engineering thermal analysis requirements. The program includes provisions for radiation interchange between

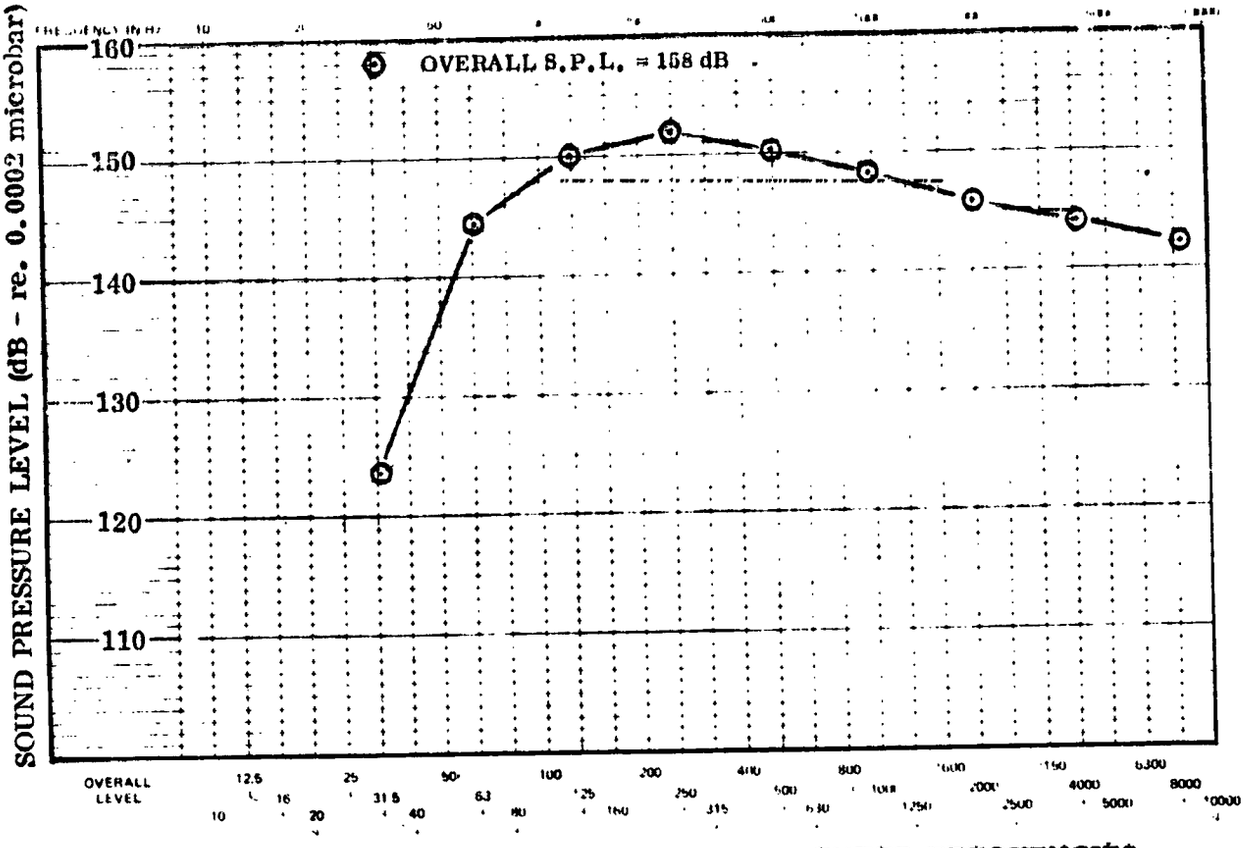

Figure 6-40. Acoustic Spectrum - High Level (pre-thermal tests)

elements of the test specimen model and the test chamber. [This program differs from the one used during Phase II, Convair Aerospace Computer Program 1272, which predicted thermal interactions between the TPS model and deep space.] Problems involving a multitude of materials with various conductivities, specific heats, and emittances as functions of temperatures, and with conductivity as a function of both temperature and pressure are analyzed.

Aerodynamic heating of the panel surface is simulated as a time-variable heat flux. The effect of wall temperature on heat flux was included. View factors between elements of the thermal model and between the model and the test chamber were obtained by using the computer programs of References 7 and 8 . The overall radiant interchange factors including multiple reflections for gray diffuse surfaces at constant emittances were obtained from the program of Reference 9 . Symmetry was used to yield a minimal of thermal elements within the model.

For the columbium alloy components the same metallurgical assumptions were used herein as those used during Phase II. That is, when coated, one-third of the coating thickness results from penetration of the base metal. Diffusion of the coating into the base metal continues as the material is cycled at high temperatures. A coating of 0.003 inch (0.008 cm) was applied to the panels manufactured under this program, and it was assumed that a diffusion of 0.00001 inch (0.00003 cm) per side would occur during each cycle. Thus, if the original panel thickness is 0.020 inch (0.051 cm), after coating the new base metal thickness is 0.018 (0.046 cm), and the total thickness is 0.024 inch (0.061 cm). After 100 cycles, the final base metal thickness is 0.016 inch (0.041 cm). Thermal properties of the coating material and diffusion zone are not known at present. In this study, panel temperatures and temperature gradients are based on (1) conduction using the base metal thickness after 100 cycles (0.016 inch (0.041 cm) in above example), and (2) thermal inertia using the total thickness (0.024 inch (0.061 cm) in above example) and the thermal conductivity and specific heat of Figures 6-41 and 6-42. The conduction heat transfer terms used for the coated columbium elements in the support post analysis, however, are based on the total thickness. These assumptions should yield the worst case panel gradients and the worst case with respect to heat transfer through the support post to the backup structure.

6.7.2 Thermal Sizing — The insulation sizing was based on a thermal model that includes effects of both temperature and pressure on insulation thermal conductivity. The local static surface pressure at X/L = 0.025 was employed. A 0.020 inch (0.051 cm) titanium adiabatic backup structure was used, and it was assumed that the insulation and backup structure were initially at +100°F (311°K) prior to entry.

Insulation sizing results based on the 7.2 lb/ft^3 (115.3 kg/m^3) Fiberfrax H data of Figures 6-43 and 6-44 from Reference 10 are presented in Figure 6-45. This indicates that an insulation thickness of approximately 3.4 inches (8.6 cm) would be required to limit the load carrying structure to 650°F (616°K). However, the post length had been sized to 3.7 inches (9.4 cm) on the basis of using Dyna-Flex and the analysis of Phase II (Reference 1b, Figure 6-33). With 3.7 inches (9.4 cm) of Fiberfrax H the predicted titanium structural temperature was 580°F (577°K).

It therefore follows that the unit weight of the insulation could have been reduced from 2.22 lb/ft^2 (0.093 kg/m^2) noted in Section 5.1 to 2.07 lb/ft^2 (0.087 kg/m^2). Together with the reduction in post height the theoretical TPS unit weight should have been 4.72 lb/ft^2 (0.199 kg/m^2).

No variations to the Phase II panel analysis (Reference 1b, Section 6.3.6) were employed and those predicted temperature distributions were assumed to be valid for the Phase III effort.

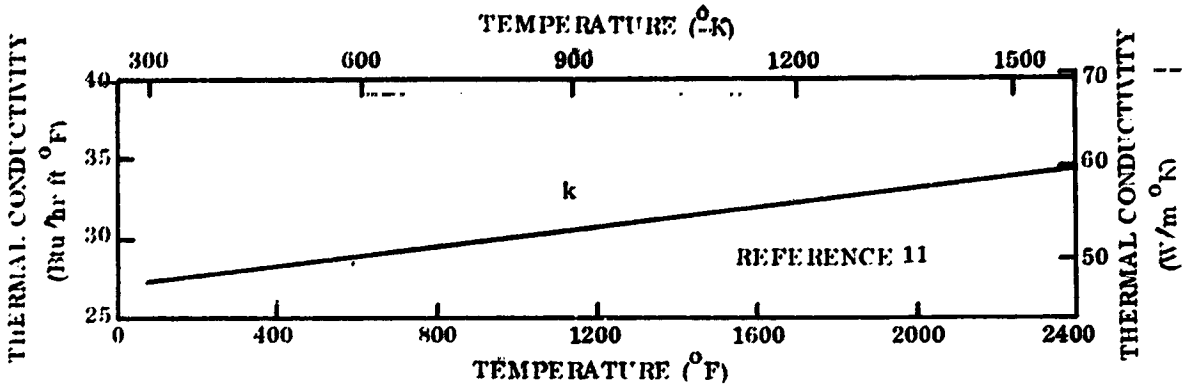

Figure 6-41. Thermal Conductivity of Cb-752

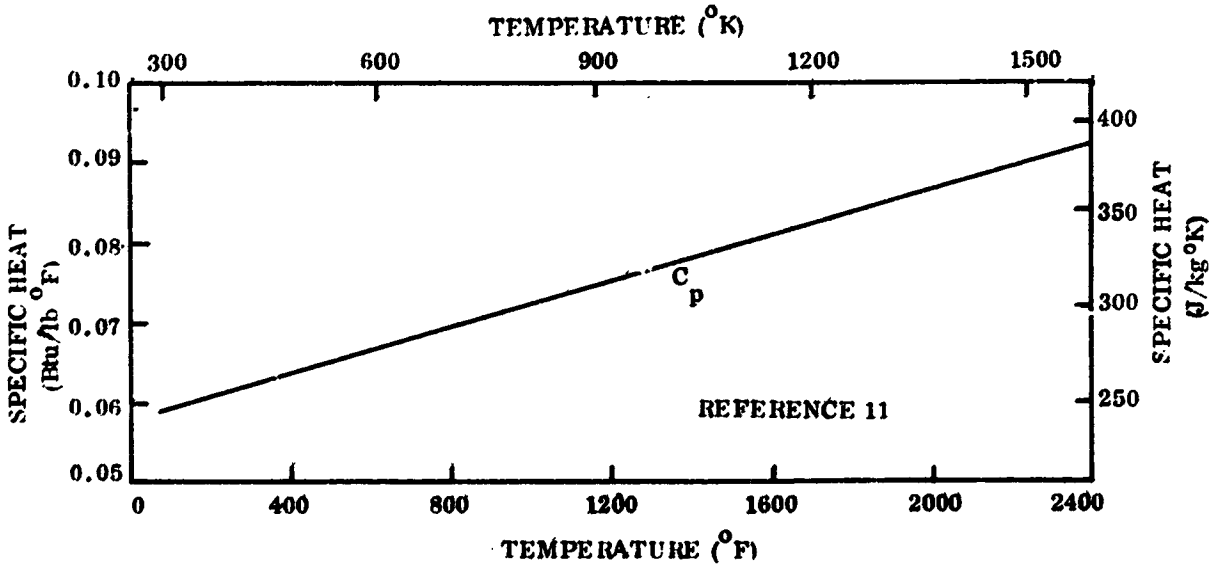

Figure 6-42. Specific Heat of Cb-752

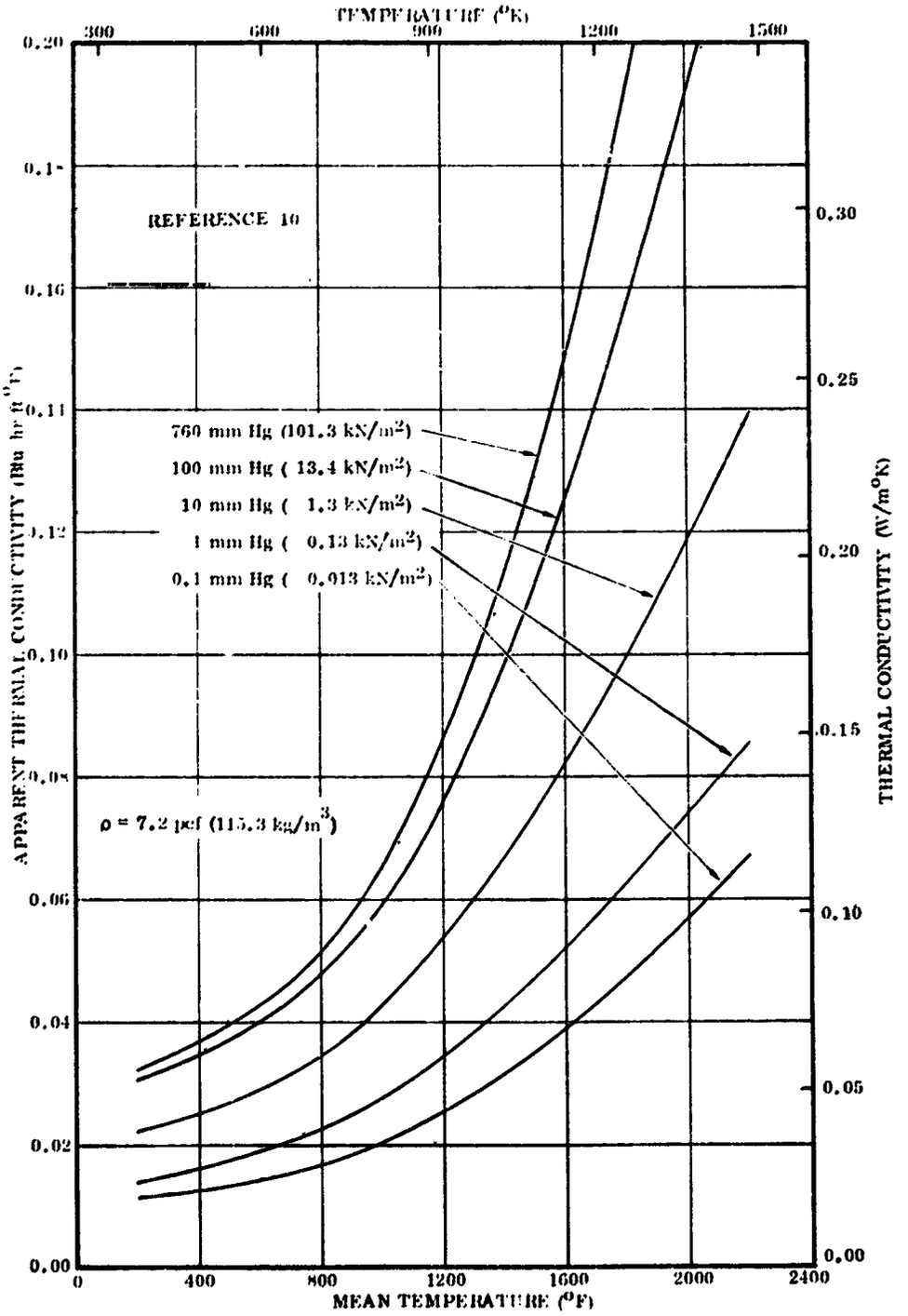

Figure 6-43. Thermal Conductivity of Fiberfrax H Insulation

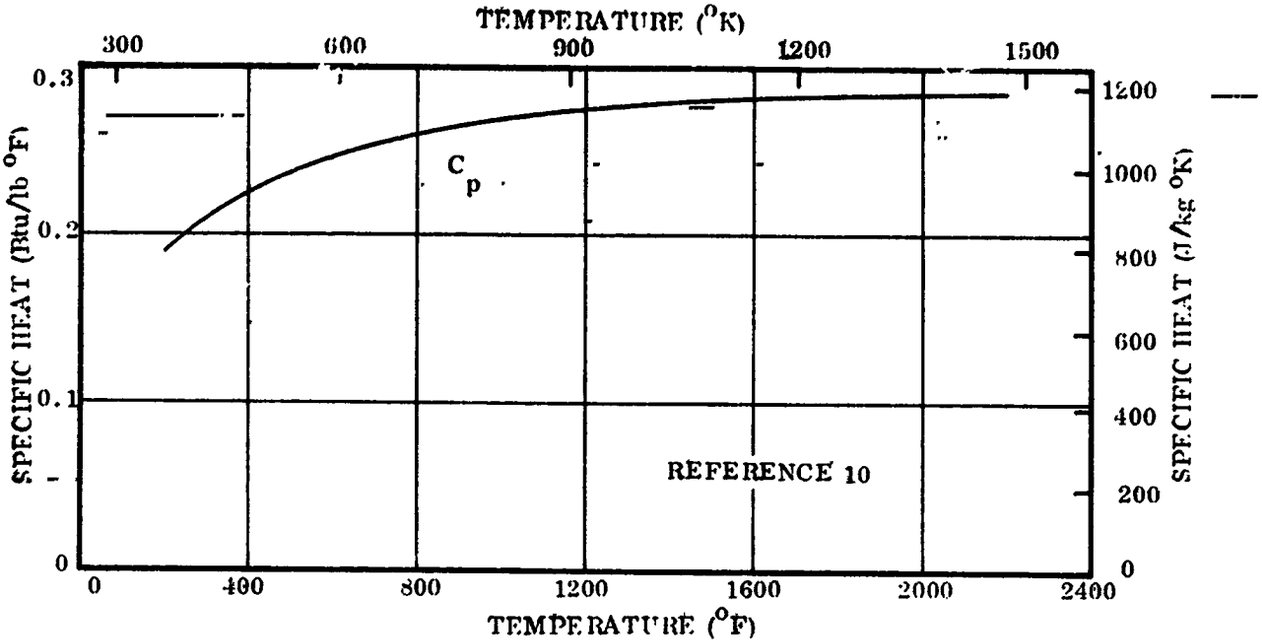

Figure 6-44. Specific Heat of Fiberfrax H Insulation

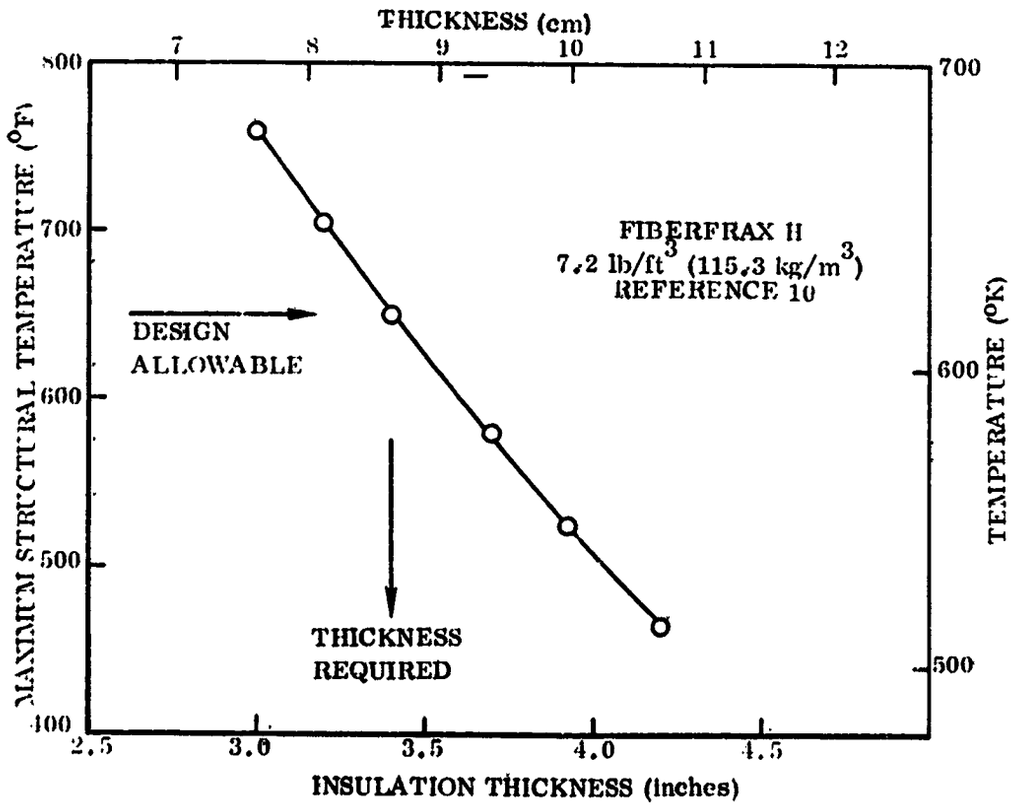

Figure 6-45. Insulation Thickness Determination

For the panel support structure, modifications were made to the bi-metal posts and to the titanium structure that altered the heat transfer from that of the Phase II tests. The primary modification to the Cb-752 upper post was the addition of more massive heat shield guides (keys); these provided a greater heat sink and contributed to a higher post interface temperature than desired [2100°F (1422°K) instead of 2000°F (1366°K)]. The primary change to the lower portion of the post was the change from TD NiCr to HS-25(L-605) with its lower thermal properties (Figures 6-46 and 6-47). The predicted temperature at the base of the post was 650°F (616°K).

The third modification in the analysis was the consideration of heat transfer to 0.020 inch (0.051 cm) titanium skin and the heat sink effects of supporting frames and stiffeners. These had a tendency to produce lower temperatures on the primary structure from those experienced in Phase II. The thermal properties of Ti-6Al-4V used in this analysis are shown in Figures 6-48 and 6-49.

6.7.3 Thermal Correlation. – The average temperature measurements for the test series showed acceptable uniformity [+8° F (4° K), -22° F (13° K) at peak temperature] over the surface of the specimen. The average maximum temperature over the heat shield surfaces was 2398° F (1587° K) with the maximum temperature recorded at the specimen center of 2408° F (1593° K). The maximum recorded temperature was 2440° F (1611° K) which occurred during Cycle 3.

Data plots of the average temperature history for four critical locations are shown in Figure 6-50. The data shown have been shifted to compensate for startup lag. The average maximum temperature at the center of the heat shield surface as recorded on the interior side was 2408° F (1593° K) compared to a programmed and predicted 2400° F (1589° K). The data closely follows the predicted curve until the final cool-down period after 2400 seconds from start of reentry. At this point the cool-down rate was slower than anticipated. This deviation was probably due to the heat stored in the Glasrock insulation above the lamps.

The bimetallic support post interface maximum temperature was 2095°F (1419°K) compared to a predicted level of 2100° F (1422° K). This data set exhibited excellent correlation over the entire recorded range with slight deviations occurring during the heat up and during the simulated reentry maneuver (2000 to 2400 seconds following start of reentry).

The average maximum temperature at the base of the support post was 625° F (602° K) compared to a prediction of 650° F (616° K). The test data followed the predictions but were consistently lower. This is attributed to a possible difference in the thermal properties of HS-25(L-605), greater lateral thermal conductivity of Fiberfrax H than anticipated, and/or convective cooling air below the fixture.

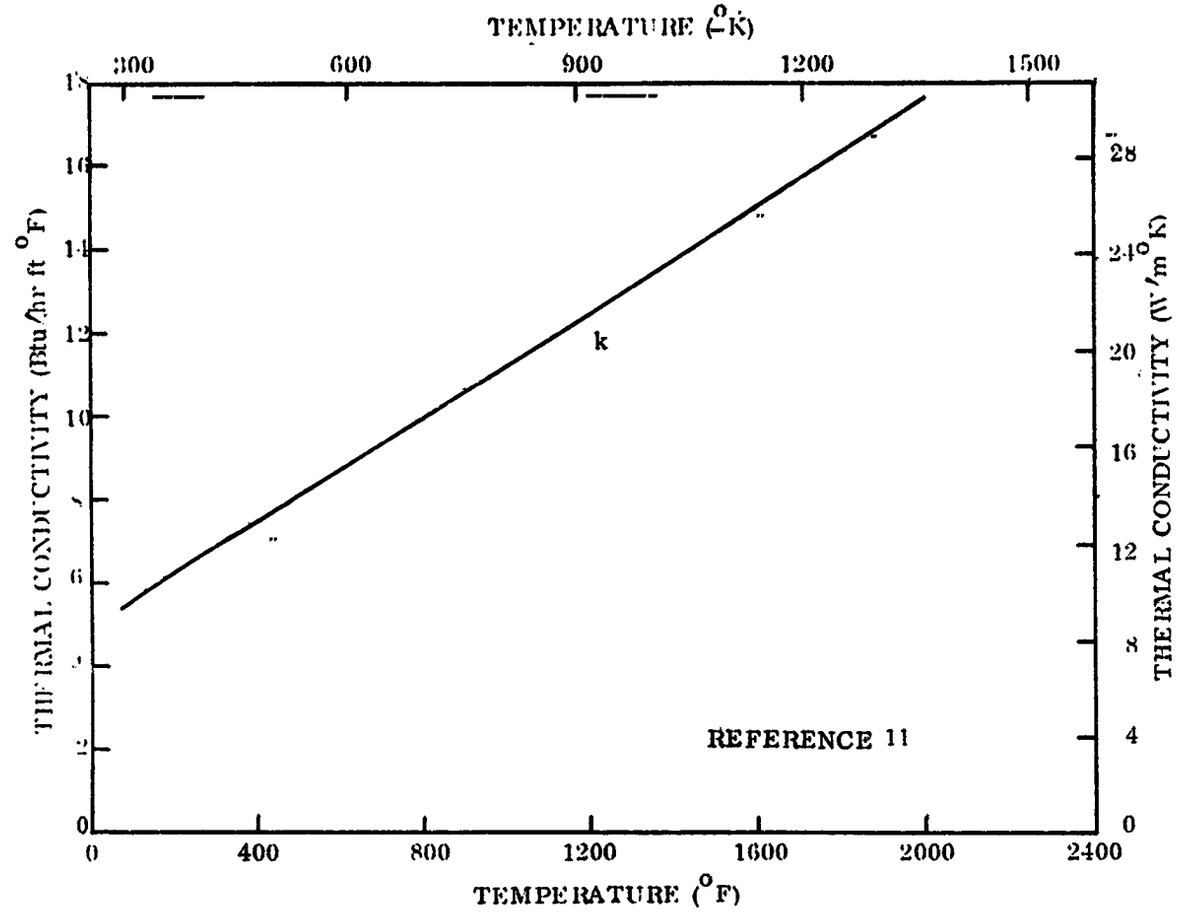

Figure 6-46. Thermal Conductivity of HS-25 (L-605)

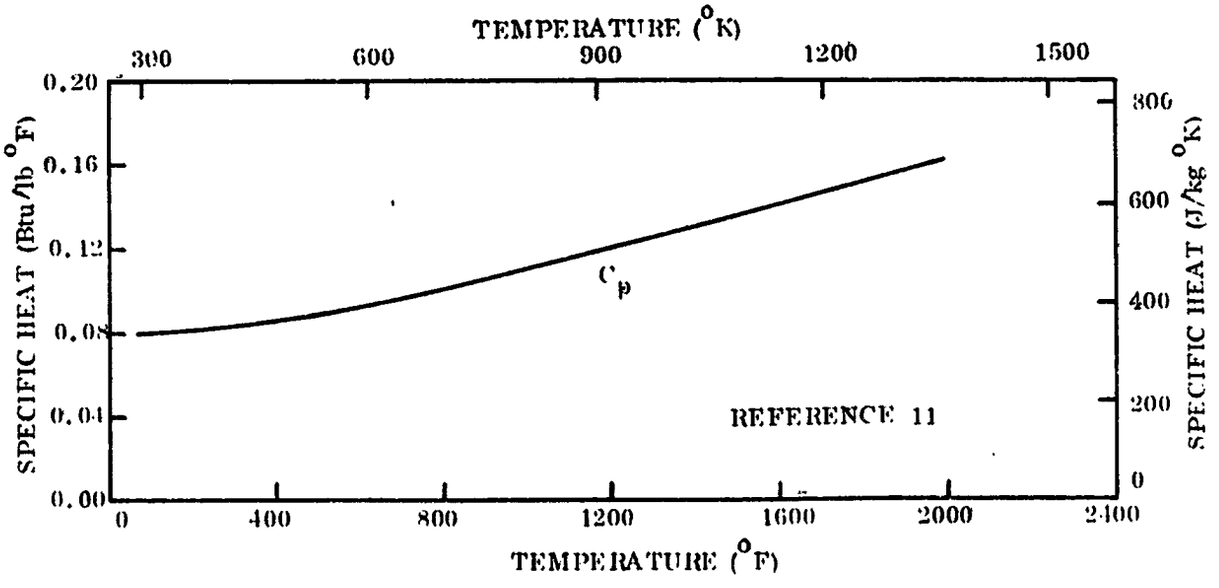

Figure 6-47. Specific Heat of HS-25 (L-605)

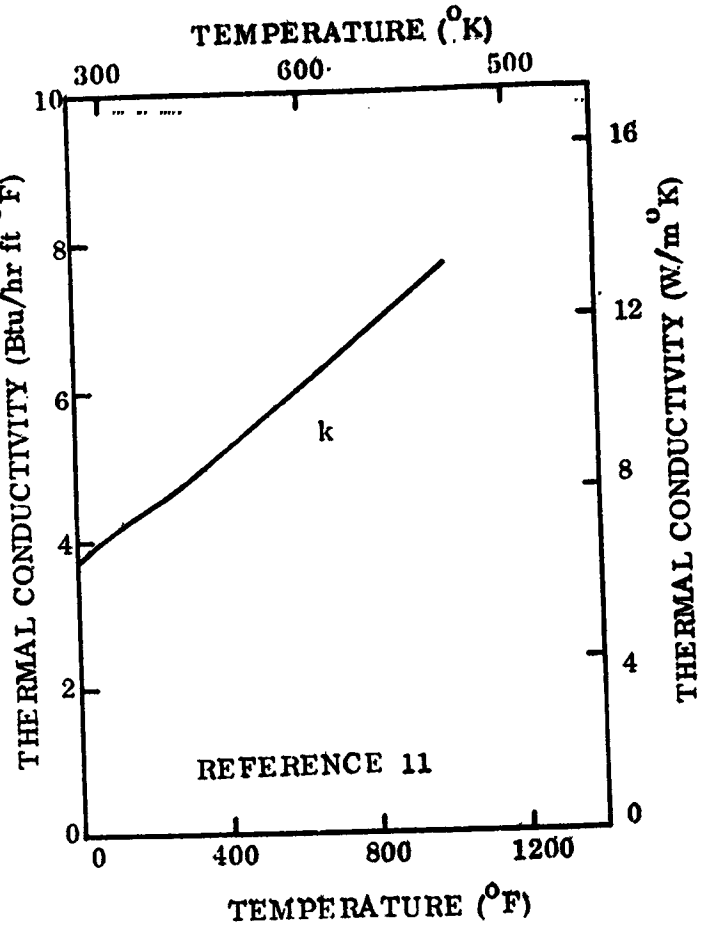

Figure 6-48. Thermal Conductivity of Ti-6Al-4V

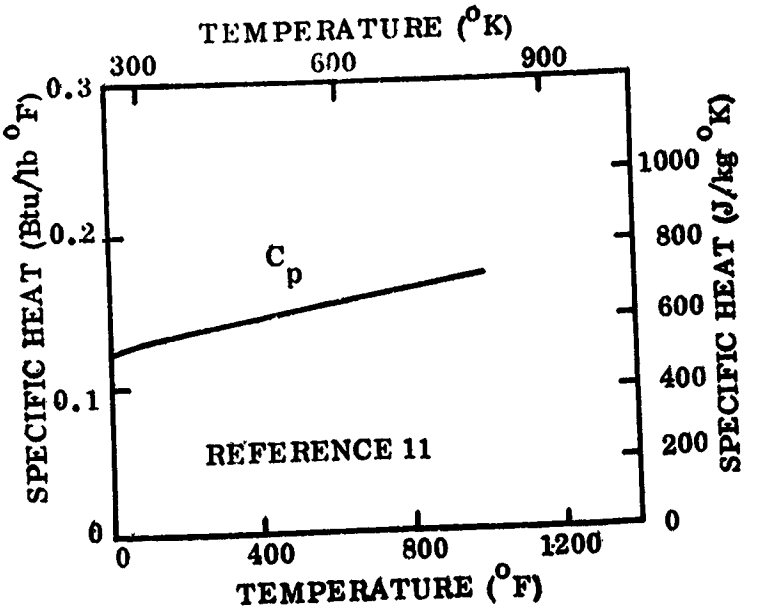

Figure 6-49. Specific Heat of Ti-6Al-4V

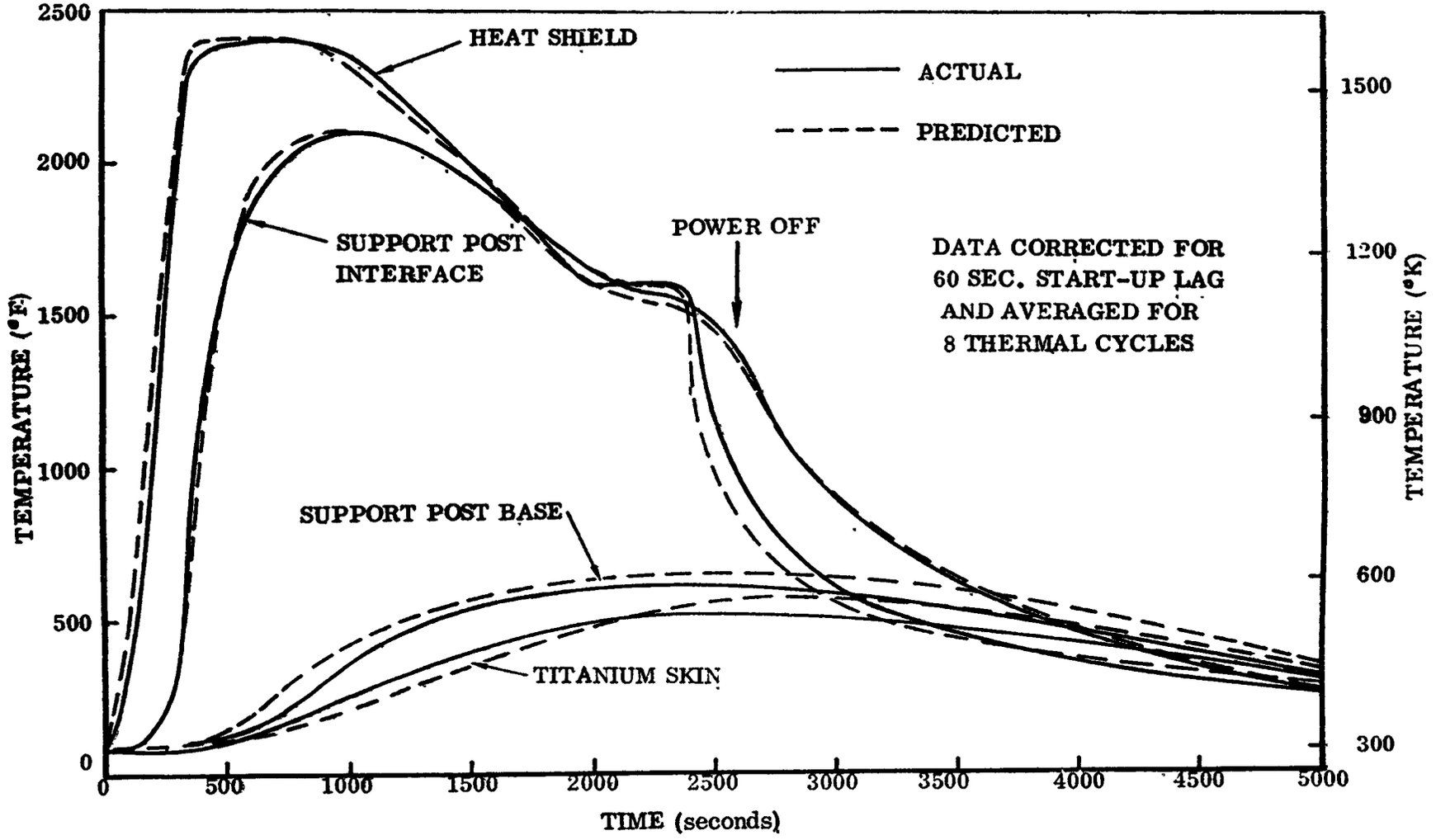

Figure 6-50. Radiant Heat Test Composite Temperature Distribution

Similarly, the titanium primary structure (consisting of skin, frames, and stiffeners) temperature data deviated considerably from the predictions. The average maximum temperature was 525°F (547°K) compared with a prediction of 580°F (577°K). This could be the result of a variance in the thermal properties of Fiberfrax H, an error in the assumption of the thermal mass of the titanium structure, and/or convective cooling air below the fixture.

Comparing the curve fits of the predicted and the actual temperature data of Phase II with those in Phase III show that the Phase III curves of predictions versus actuals do not fit as well. Since changes were made in the design of the support post (hence, the thermal model), lower support post material, insulation material, and primary structure thermal mass, plus exposure of the understructure to circulating ambient air, considerable work would be required to isolate the exact cause of the deviations. However, since the predictions were generally higher than the actual recorded data (varying from less than 1% to 9%) and are, therefore, conservative, the method of analysis was determined to be acceptable.

6.7.4 Thermal/Structural Performance. – Verification of the thermal design of the heat shield panels and justification for the selection of the nine-panel test array of heat shields were demonstrated by the results of the tests. The isolated center panel survived the full test spectrum with no thermal distortion or thermal stress failures. This panel experienced thermal and mechanical edge conditions that were representative of a typical heat shield on a flight vehicle. The flatness of the panel and the absence of distortion and thermal damage can be seen in Figure 6-20. As previously noted in Section 6.3.3.1 during discussion of the post test condition of heat shield panels and in Section 6.4, Paragraph 6, under test peculiar damage, considerable distortion occurred in the edge of guard panels making up the balance of the nine-panel test array. These panels experienced severe thermal gradients unlike any encountered by flight hardware. The thermal gradients were created by the contact of these panels with the water-cooled frame of the holding fixture and caused thermal differentials in the order of 2000°F (1366°K) during thermal cycling.

Prior to fabrication of the holding fixture, it was predicted that the top flange of the support frame would experience temperatures in the order of 2000°F (1366°K) and that the thermal gradients along the sides of the frame would not contribute to frame distortion since the frame was free to expand along its length. However, during the system checkout, the frame did distort excessively, necessitating the addition of frame side member water cooling tubes. However, design modifications were not made in the edge panels to accommodate the new thermal gradients existing between the heated panels and the water-cooled frame of the fixture. As a result, the edge panels all experienced warpage and thermal damage to some degree, and as expected, the four corner panels with two cool edges experienced more warpage and thermal stress damage than did the other four guard panels that had only one cool edge.

In retrospect, it would have been preferable to have more thoroughly analyzed the relationship between the water-cooled frame and the edge panels. This would have shown the necessity for isolating the edge panels from the frame by using guard panels such as were successfully employed in the Phase II test specimens. [The guard panels, although originally planned for the Phase III specimen, were eliminated in an effort to reduce the number of components and to ease the specimen assembly.]

An analysis has been made of the edge panels in an attempt to explain their thermal stress damages and the differences between the edge panels. Thermal stress damage to the two corner panels in Figure 6-21, Panel #1 and Panel #3, was limited to cracks in the skin to rib welds along the long, cool panel edge. These cracks, shown in Figure 6-35 (top picture), terminated at one end at the longitudinal weld joining the beam to the skin and at the other end at a location approximately in line with the ends of the stiffening beads in the panel skin. A crack was also evident in the skin running diagonally in the cool corners of the panels to the first tee rib. Panel #2, an edge center panel, has similar damage to that seen in Panels #1 and #3, but without the diagonal end crack. Panels #7 and #9 also had damage from the severe thermal gradients found along the cool edges of the panels. Damage to these two panels consisted of a highly local series of small, parallel, oxidized cracks in and near the outer cool edge of the flange of the long, narrow beam. These damage sites were equidistant from the cool corners of each panel as seen in Figure 6-35 (bottom picture).

The thermal stresses creating edge damage to the corner panels were essentially the same for all four corner panels. However, they displayed themselves differently in Panels #1 and #3 which had a cool, longitudinal beam with a wide flange which was twice as wide as the cool flange of the edge beams in Panels #7 and #9. TPS designs permitted Panels #1 and #3 to expand and move freely in the plane of the skin, constrained by one fixed point in the wide flange of the cool, longitudinal beam. Panels #7 and #9 had their fixed point on the opposite edge of the panels. All panel edges except the wide beam edges of Panels #1 and #3 were held and cooled by edge retainers which permitted in-plane panel movement during thermal cycling.

The apparent stress fields creating the damage to the corner panels were located: (1) in the unbeaded portion of the skin adjacent to the longitudinal beam at the cool edge and (2) at right angles to this in the skin and rib tee stiffeners adjacent to the shorter cool edge of the panels. These regions were partially constrained during heat-up by the cooler portions of the panels and consequently were thermally upset and became stress free due to creep at elevated temperatures. When the temperatures were reduced, the material went into tension introducing the two stress fields in the panels. One field was parallel to the long cool beam and placed the unbeaded portion of the skin in tension.

The other system, at right angles to the first, created tensile stresses in the skin and ribs at the cool, short edge of the panel. The narrow flanged beam of Panels #7 and #9 deformed plastically under the stresses, causing extensive local tensile cracking of the silicide coating at the outer regions of the cool, narrow flange and permitting oxidation of the columbium. The plastic deformation of the cool beam aided in the reduction of the tensile stresses along the cool longitudinal beam precluding additional sites of thermal stress damage to the panels. Another possibility is that the cooler edge of the narrow flanged beam did not permit as much creep deformation and thus lower stresses were present parallel to the beam during cool down.

The wide flanged beam of Panels #1 and #3 did not deform plastically or elastically sufficient to unload the two stress fields. The result was that the two tensile stress fields created combined tensile stresses in the cool corners which produced the diagonal corner crack. Tensile stresses along the long cool beam became sufficiently high to cause cracking at sites normal to the cool beam. Cracking initiated in the skin to rib welds due to a notch effect and a slightly reduced skin cross-section created by the weld. The cracking along the length of each weld was limited to that portion of the skin which was not beaded to accommodate thermal strains. Successive thermal cycling caused the cracks to open and to oxidize and new ones to form.

It is reiterated that the thermal conditions of the peripheral heat shields that existed during the Phase III test series were significantly different from those predicted for vehicle flight. All panels should perform similar to the central test panel, that is, free of thermal distortion and thermal stress failures. The history of this program, both Phases II and III, has shown that when properly isolated from the thermal abnormalties of the test frame, no thermal/structural failures will occur in the main heat shield.

7 REFURBISHMENT AND REPAIR

During thermal testing, opportunities arose which permitted investigation of refurbishment and repair of hardware for a typical thermal protection system. The earliest opportunity was presented at the end of thermal Cycle 2 followed by local damage to the hexagonal drive socket of the post filler plug after Cycle 5. The damage after Cycle 2 was determined to be test peculiar, arising from an apparent incompatibility of the thermocouple sheathing material, while under pressure in the test environment, with the silicide coating of the test hardware. The hexagonal socket damage was considered to be a normal condition for flight hardware resulting from mechanical coating damage during wrenching operations or improper edge preparation for coating. Both cases were allowed to grow unarrested. The thermocouple damage site was repaired after Cycle 21 when it had grown to 0.2-inch (0.5 cm) diameter hole. Wrenching damage was left unchecked for the complete test to assess the effect of uncontrolled oxidation on the removal of plugs.

At the conclusion of thermal Cycle 21, a damage site in the center test panel had progressed to a point requiring coating repair. Evidence of oxidation at this site was first noted at the end of Cycle 12. This site was at the end of a skin to beam longitudinal weld where the weld bead had not been ground flush. The retainer strap, during acoustic excitation, had impacted the weld bead causing coating damage to both the retainer and the weld. Subsequent thermal cycling caused oxidation, material loss, and a small hole at the weld.

The damaged center panel was disassembled from the heat shield array, as planned for flight hardware, by removing six post filler plugs, four post retainer bolts - two others were only loosened, two center retainers, and two panel edge retainers. It was moved approximately 0.25-inch (0.64 cm) aft or downstream to clear it from its overlaying forward panel, then lifted out. The forward panel and the three adjacent panels were not disturbed nor loosened to assist disassembly.

With the center panel removed, three types of coating damage repair were attempted. The center panel was repaired under the best conditions, in-shop. One downstream panel was removed for a field repair on-site and repairs were made to other damage sites without hardware removal from the array-field repairs in-place. In all cases the damage sites were prepared for repair coating by scraping and filing to remove the oxide layers and to expose base substrate. The repair techniques used were developed by McDonnell Douglas - East, under Contract NAS8-26121 (Reference 12). The in-shop damage sites to the center panel were further prepared by cleaning the areas adjoining the sites using a S.S. White Airbrasive Unit grit blaster and alumina powder. Other panels and damage sites received no preparation of surrounding surfaces. Following cleaning, a glass frit mixture of 60 w/o - 325 mesh Pyrex frit, 30 w/o - 270

mesh alumina (flame spray grade), 10 w/o -325 mesh amorphous boron, mixed with Nicrobraze clear cement, was applied generously to the damage site.

The repaired center panel was air-dried and fired in a vacuum furnace to 2150° F (1561° K) for 12 minutes and furnace cooled. After removal, the repaired areas appeared cracked and unfused. Investigation revealed that a vacuum atmosphere had been erroneously recommended and that an air or inert gas furnace atmosphere was the proper recommendation. It is suggested that the vapor pressure of one of the constituents or reactive products may have been too high at 2150° F (1561° K) for the vacuum atmosphere, and that this material was then lost from the mixture, raising the melting point of the resultant mixture, and forestalling fusing at temperature. It was decided to reinstall the panel into the test array since some oxidation protection may have been accomplished and to further repair if the need arose. After reinstallation the panel remained in place without further repairs for the balance of 29 thermal and 50 acoustic test cycles.

The panel downstream to the center panel had one through-hole in the skin due to thermocouple damage and several minor damage sites. These were all repaired by filing and scraping away the oxidation product to clean metal or clean coating and applying the same glass frit repair coating mixture as used on the center panel. With the panel removed from the array, site preparation and coating mixture could be applied to all sides of a damage site. A second panel with thermocouple damage was repaired in the same manner but without removing the panel from the array. Only the upward facing side of the skin damage site was available for repair preparation and coating. The repair mixture was air dried, fired, and fused with all test hardware reassembled in place for test, by using the heating of the next thermal cycle. In this case the repair material fused as anticipated forming a glassy repair in and around the damage sites.

The two panels which were field repaired (one on-site, one in-place) survived only ten additional thermal cycles when continued oxidation to the thermocouple damage sites indicated a need for a second repair. The same repair coating glass frit mixture was used but the method of repair site preparation was changed. A Weller Minishop high speed (24,000 rpm) grinder was employed to remove the oxidized and contaminated material without removing either panel from the test array. All visual traces of the oxide were removed using a 0.125-inch (0.31 cm) diameter abrasive wheel. The repair material was applied as before but from one side only, and the repair site air dried at 500° F (533° K) while installed in the test facility. Fusing was then accomplished during the next thermal cycle. The two repairs accomplished in this fashion protected the material from further oxidation throughout the balance of nineteen test cycles. Examination of these panels after 50 thermal cycles showed that the two in-place field repairs made at Cycle 31 protected the substrate, were well-fused and glassy appearing for a minimum distance of 0.1-inch (0.25 cm) concentric to the hole, on both sides of each panel.

8 CONCLUDING REMARKS

8.1 Conclusions

(1) The flight-size, full-scale metallic thermal protection system designed and tested in Phase III performed most capably and proved to be not only reusable for at least 50 simulated reentry flights and 100 simulated boost flight cycles, but also rugged and durable and possessed of a high degree of damage tolerance. The heat-shield surface hardware (i.e., heat shield panels and panel retainers) remained flat and free of undesirable distortion throughout testing, thereby validating thermal/structural design and analysis.

(2) Disassembly and reassembly of individual heat shield panels, simulating inter-flight removal from flight vehicles, was demonstrated between test cycles and at the end of simulated reentry flights. Refurbishment and repair of TPS hardware was accomplished, when needed, following disassembly from the system, and with the hardware in-place in the TPS array. Properly applied repair coatings displayed good life expectancy.

(3) Savings in weight and cost of the metallic TPS during Phase III resulted from design improvements to the components. Redesigning to reduce material costs by the extended use of electron beam welding to build up components, decreased materials costs by 70 percent, although welding and machining costs rose 50 percent. A net cost reduction of 21 percent under Phase II costs resulted from design and fabrication improvements introduced into the Phase III TPS.

(4) A major system weight improvement for Phase III over Phase II resulted from the change to Fiberfrax II insulation to replace Dyna-Flex. Improved thermal efficiency also resulted from this change and potential testing problems with outgassing were avoided.

(5) Design improvements to threaded parts were included in Phase III hardware. Redesigned coated columbium filler plugs and superalloy panel retainer bolts were readily removed by conventional means both between test cycles and at the completion of testing. As anticipated in design, the expendable retainer bolts and plugs were removable with "Easyout" tools when part damage precluded the use of conventional tools. Removals would be required for flight TPS hardware for inspection, refurbishment, repair, and replacement.

(6) The reliability of TPS columbium hardware was improved in Phase III by the use of extensive mechanical edge preparation and edge weld fusing of detail parts and subassemblies, replacing manual edge preparation of assemblies prior to coating. As a result, 108 rib cap edges representing 90 feet (27.5 m) of coated edges sustained no damage when repeatedly exposed to the full spectrum of simulated flight tests.

(7) The test facilities and procedures, and associated instrumentation and recording equipment employed during Phase III, functioned satisfactorily in imposing and indicating the simulated flight test environments on the test TPS. An exception to this was the inability of the multi-panel, thermal-mechanical test facilities to impose or sustain the desired differential pressure load on the test specimen during thermal testing.

8.2 Recommendations

(1) The number of coating damage sites, after flight simulation testing, at the ends of the heat shield panels indicates a need for minor panel design modifications to facilitate edge finishing and to improve producibility and coatability of the ends. Since mid-panel tee-members suffered no coating damage, consideration should be given to designing the panel end tee-members to a similar configuration.

(2) Effective locking methods are needed for threaded parts. Torquing requirements for the retainer bolts and filler plugs require re-evaluation and correction to higher torque preloads commensurate with the materials and the fastener operating conditions. The coating of the threads becomes part of this consideration due to the tendency of the coatings on mated thread surfaces to interdiffuse under repeated reentry heating. During Phase III, coated filler plugs became bonded to the aluminide coated retainer bolts. In some instances, when these were disassembled, the filler plugs were torqued to failure. Examination showed that the aluminide coating was not diffused properly upon application to the retainer bolts, and it tended to "shell" off, crumble, and to lock the mated threads. A review of other coatings and coating processes for fasteners is warranted.

(3) The number of hardware damage sites that were attributed to coating problems, indicates a need for continued work in the control of coating materials and formulations, and in the application and distribution of coating materials on TPS hardware. The coating of interior surfaces, especially small diameter interior surfaces, requires particular attention. Improvements are needed for predicting the life expectancy of coatings and for detecting those coating disparities which foreshortened the protective function of coatings. Coating non-destructive evaluation techniques should be pursued which would enable 100 percent inspection of all coated surfaces, edges, and ends for TPS hardware.

(4) All burn-through electron beam structural welds should be followed by a weld pass with added filler material to replace the weld material displaced to form the weld fillets. This will increase the cross-section of the welds, remove the potential notch, and increase the weld strength.

(5) Columbium alloys selected for coated TPS hardware should possess good weldability and formability in those material sections contemplated for fabrication and should retain these properties after repeated annealing and creep flattening operations.

(6) The design of the TPS test fixture and the edge conditions and edge panels of the test specimen should be reviewed and modified to isolate, as much as possible, the test specimen from fixture edge effects. During Phase III thermal testing, the edge effects and extreme thermal gradients existing between the test specimen and the test fixture created an unnecessary number of test-peculiar conditions, damage sites, and panel warpage. Attention should be directed to the inclusion of "boiler plate" edge members for isolating the test specimen, to a hot versus cold test fixture frame, and to thermal freedom for the fixture, such as employed during Phase II testing.

(7) The sheathing material for high temperature thermocouples which contacts silicide coated columbium during test should be compatible with the coating under all test conditions. The use of a buffer or barrier material for separation of the thermocouple and the coating should be considered.

(8) Thermocouples should be located throughout the test specimen so that they indicate true site temperatures, uninfluenced by artificial, test-peculiar heat shorts such as introduced by thermocouple probes.

(9) All removal and reassembly tools and handling devices should be coated with durable plastic to prevent damage to coated hardware.

(10) Removal of surface hardware for inspection of unexposed coated surfaces for damage should not be necessary before the end of the 20th flight cycle. The Phase III TPS hardware has shown good damage tolerance and durability, if damaged, and should experience no coating damage early in the system life.

APPENDIX A

CONVERSION OF U.S. CUSTOMARY UNITS TO SI UNITS

The International System of Units (designated SI) was adopted by the Eleventh General Conference on Weights and Measures in 1960. The units and conversion factors used in this report are taken from or based on NASA SP-7012, "The International System of Units, Physical Constants and Conversion Factors — Revised, 1969".

The following table expresses the definitions of miscellaneous units of measure as exact numerical multiples of coherent SI units, and provides multiplying factors for converting numbers and miscellaneous units to corresponding new numbers of SI units.

The first two digits of each numerical entry represent a power of 10. An asterisk follows each number that expresses an exact definition. For example, the entry "-02 2.54*" expresses the fact that 1 inch = 2.54×10^{-2} meter, exactly, by definition. Most of the definitions are extracted from National Bureau of Standards documents. Numbers not followed by an asterisk are only approximate representations of definitions, or are the results of physical measurements.

ALPHABETICAL LISTING

To convert from	to	multiply by	
atmosphere (atm)	newtons/meter^2 (N/m^2)	+05	1.0133*
British thermal unit, mean (Btu)	joule (J)	+03	1.056
Fahrenheit (F)	kelvin (K)	$t_k = (5/9)(t_f + 459.67)$	
foot (ft)	meter (m)	-01	3.048*
inch (in.)	meter (m)	-02	2.54*
mil	meter (m)	-05	2.54*
millimeter of mercury (mm Hg)	newton/meter^2 (N/m^2)	+02	1.333
nautical mile, U.S. (n.mi.)	meter (m)	+03	1.852*

To convert from	to	multiply by —	
pound force (lb_f)	newton (N)	+00	4.448*
pound mass (lb_m)	kilogram (kg)	-01	4.536*
torr	newton/meter^2 (N/m^2)	+02	1.333

PHYSICAL QUANTITY LISTING

Acceleration

foot/second^2 (ft/sec^2)	meter/second^2 (m/sec^2)	-01	3.048*

Area

foot^2 (ft^2)	meter^2 (m^2)	-02	9.290*
inch^2 (in^2)	meter^2 (m^2)	-04	6.452*
inch^2 (in^2)	centimeter^2 (cm^2)	+00	6.452

Density

pound mass/foot^3 (pcf, lb_m/ft^3)	kilogram/meter^3 (kg/m^3)	+01	1.602
pound mass/inch^3 (lb_m/in^3)	kilogram/meter^3 (kg/m^3)	+04	2.768
pound mass/inch^3 (lb_m/in^3)	gram/centimeter^3 (g/cm^3)	+01	2.768

Energy

British thermal unit, mean (Btu)	joule (J)	+03	1.056

Energy/Area Time

Btu/foot^2 second (Btu/ft^2 sec)	watt/meter^2 (W/m^2)	+04	1.135

Force

kilogram force (kg_f)	newton (N)	+00	9.807*
pound force (lb_f)	newton (N)	+00	4.448*

APPENDIX A — Continued

To convert from	to	multiply by	
	Length		
foot (ft)	meter (m)	-01	3.048*
inch (in.)	meter (m)	-02	2.54*
micron	meter (m)	-06	1.00*
mil	meter (m)	-05	2.54*
mile, U.S. nautical (n.mi.)	meter (m)	+03	1.852*
	Mass		
pound mass (lb_m)	kilogram (kg)	-01	4.536*
	Pressure		
atmosphere (atm)	newton/meter^2 (N/m^2)	+05	1.013*
millimeter of mercury (mm Hg)	newton/meter^2 (N/m^2)	+02	1.333
pound/foot^2 (psf, lb_f/ft^2)	newton/meter^2 (N/m^2)	+01	4.788
pound/inch^2 (psi, lb_f/in^2)	newton/meter^2 (N/m^2)	+03	6.895
	Temperature		
Fahrenheit (F)	Kelvin (K)	$t_K = (5/9)(t_f + 459.67)$	
	Volume		
foot^3 (ft^3)	meter^3 (m^3)	-02	2.832*
inch^3 (in^3)	meter^3 (m^3)	-05	1.639*
inch^3 (in^3)	centimeter^3 (cm^3, cc)	-01	1.639

APPENDIX A — Concluded

PREFIXES

The names of multiples and submultiples of SI units may be formed by application of the prefixes:

Multiple	Prefix
10^{-6}	micro (μ)
10^{-3}	milli (m)
10^{-2}	centi (c)
10^{-1}	deci (d)
10^{3}	kilo (k)
10^{6}	mega (M)
10^{9}	giga (G)

APPENDIX B

ACOUSTIC TEST DATA

The data presented herein are accelerometer power spectral density plots for nine locations in the center test region of the nine-panel test specimen (Figure 6-5). This data is for one test cycle at the high (158 dB) overall sound pressure level. All test data were reviewed and for purposes of calculations, the data from test cycle number 1 was used since these data displayed values which were generally close to the maximum. The accelerometer outputs were recorded on magnetic tape and reduced to the form of power spectral density plots. Acoustic levels were measured 18 inches (45.7 cm) from the test specimen face. Acoustic levels were also recorded on magnetic tape and reduced to octave band sound pressure levels (Figure 6-40). Since the data shows no significant shift in the recorded fundamental frequency, it was assumed that no structural degradation of the system had occurred. Post test disassembly and examination confirmed this assumption.

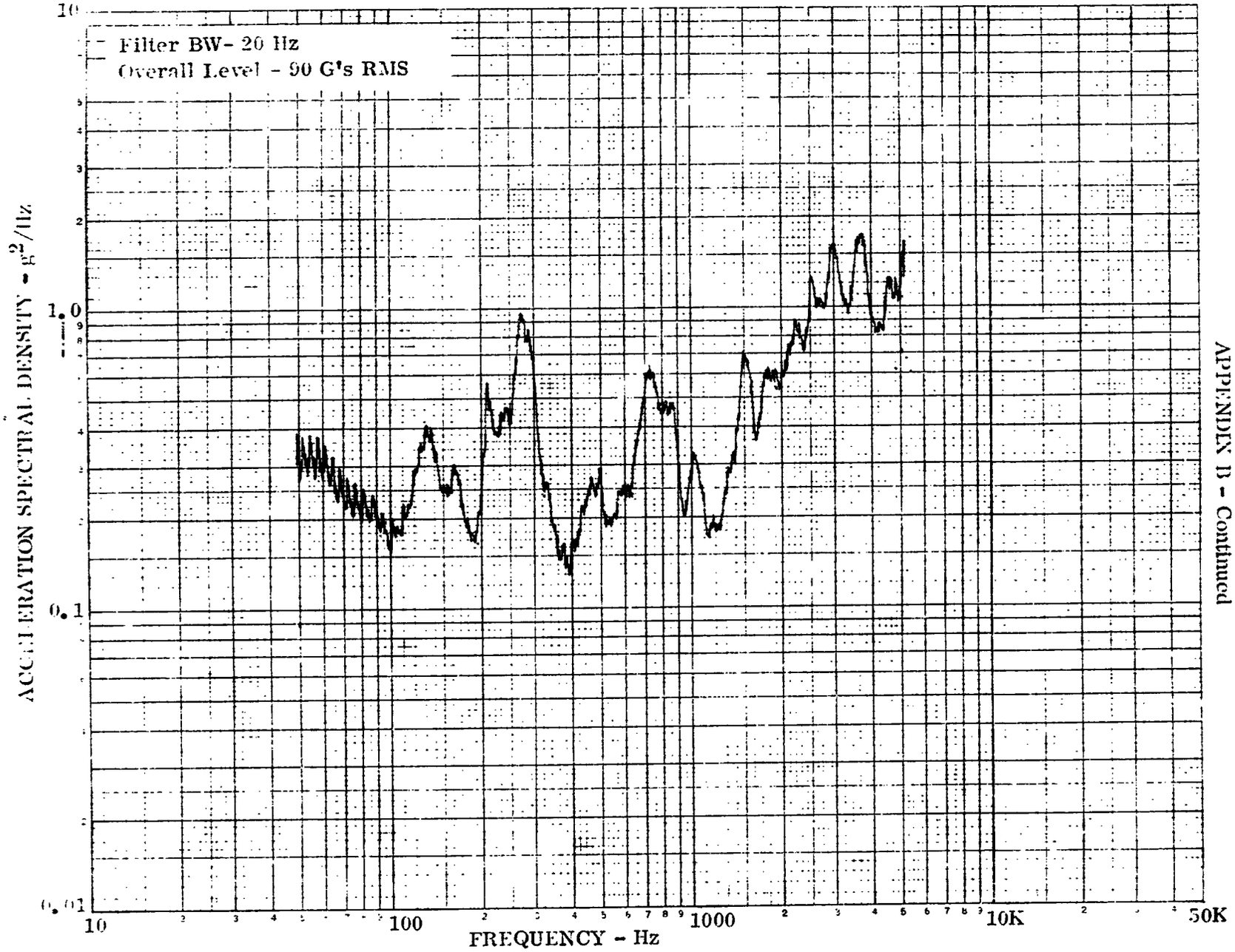

Figure B-1. Accelerometer No. 1, 158 dB OASPL, Cycle No. 1

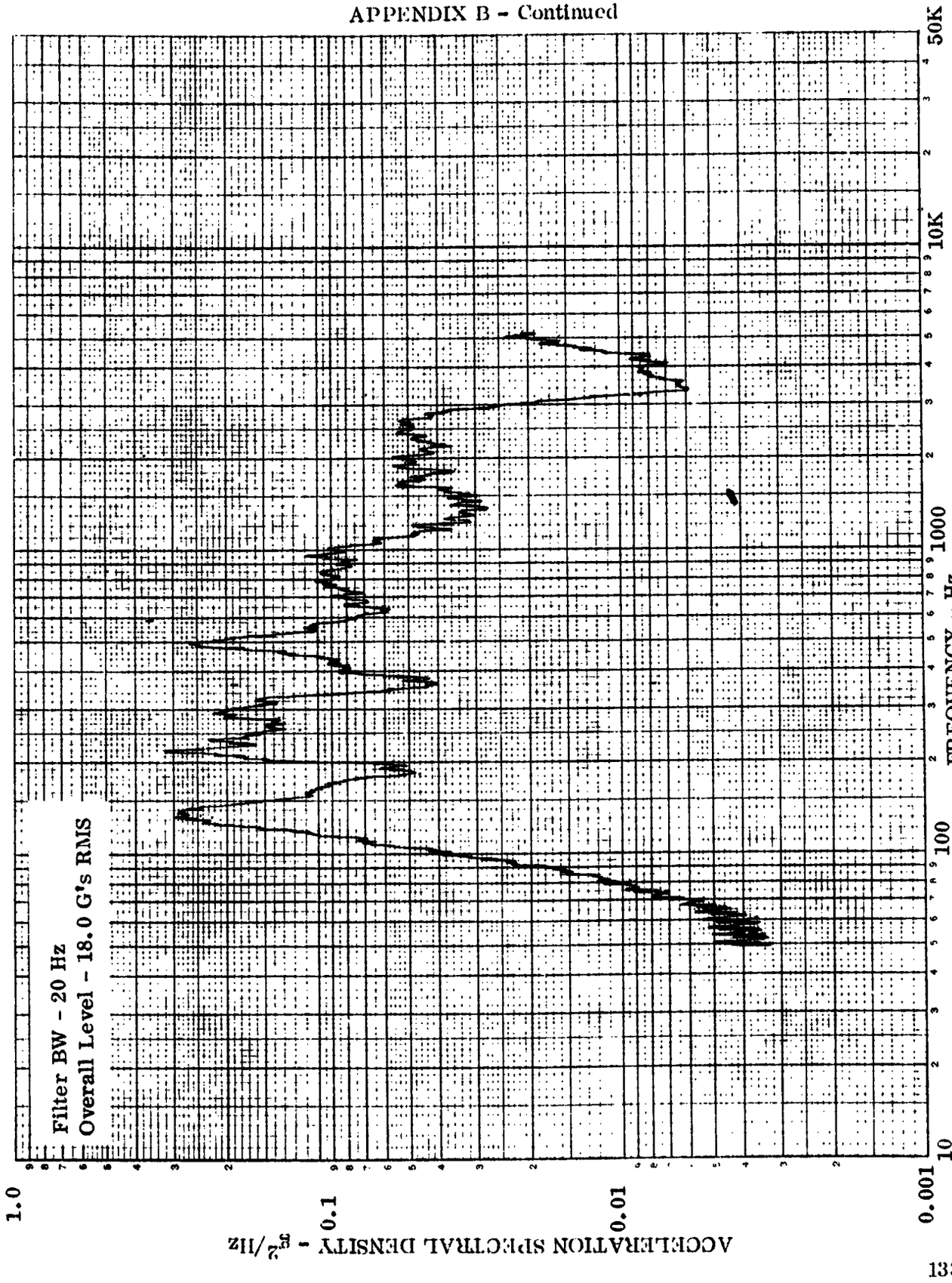

Figure B-2. Accelerometer No. 2, 158 dB OASPL, Cycle No. 1

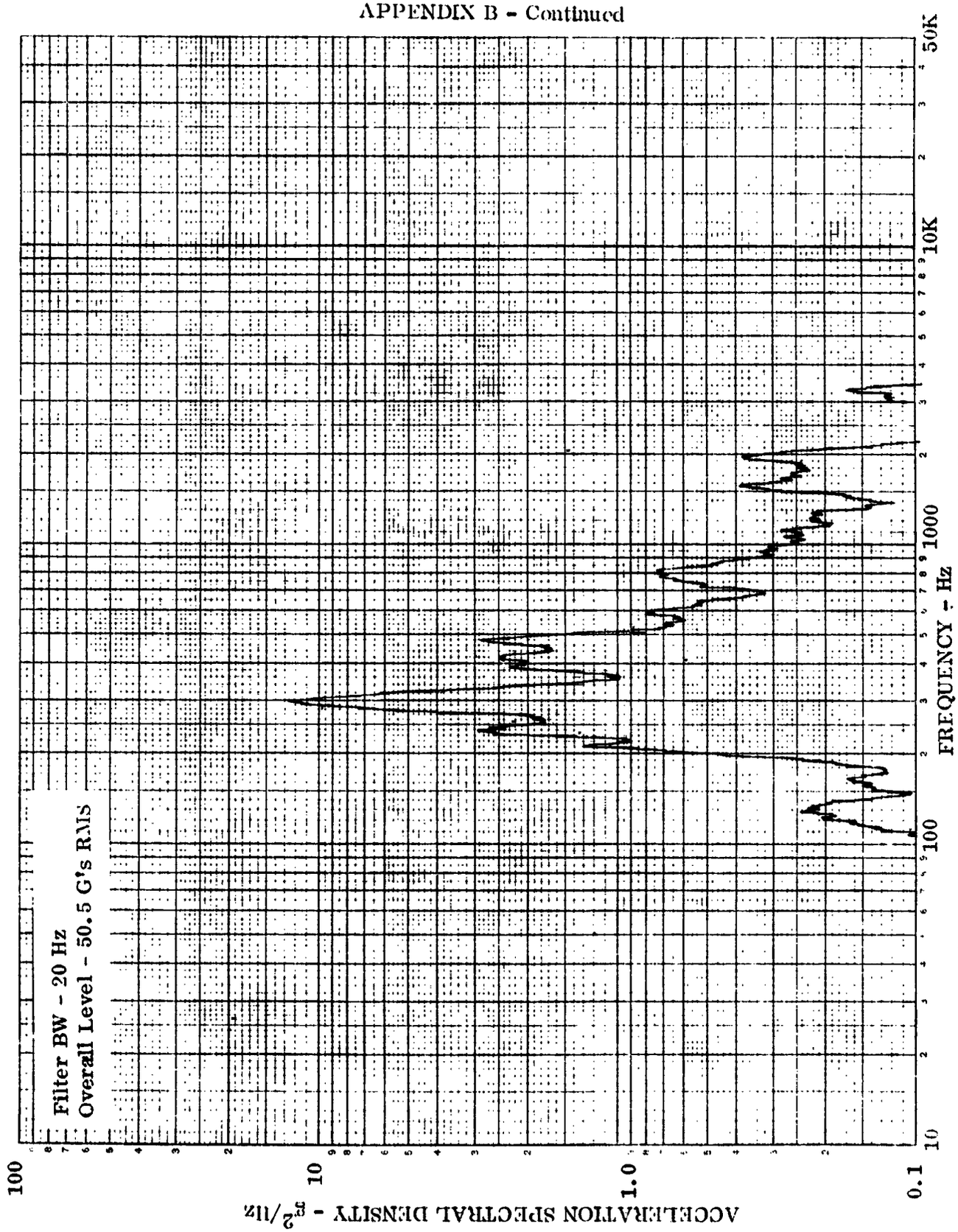

Figure B-3. Accelerometer No. 3, 158 dB OASPL, Cycle No. 1

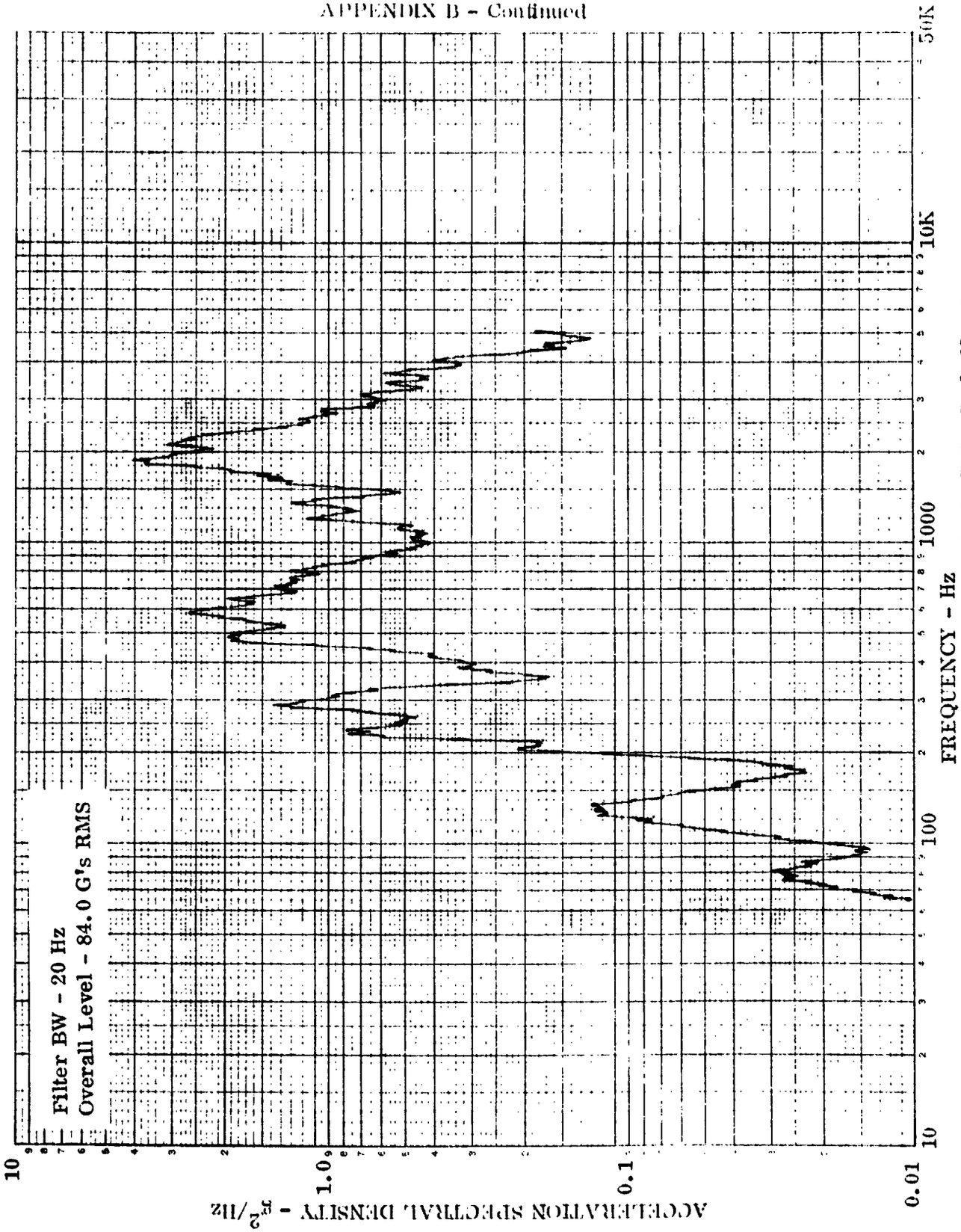

Figure B-4. Accelerometer No. 4, 158 dB OASPL, Cycle No. 1

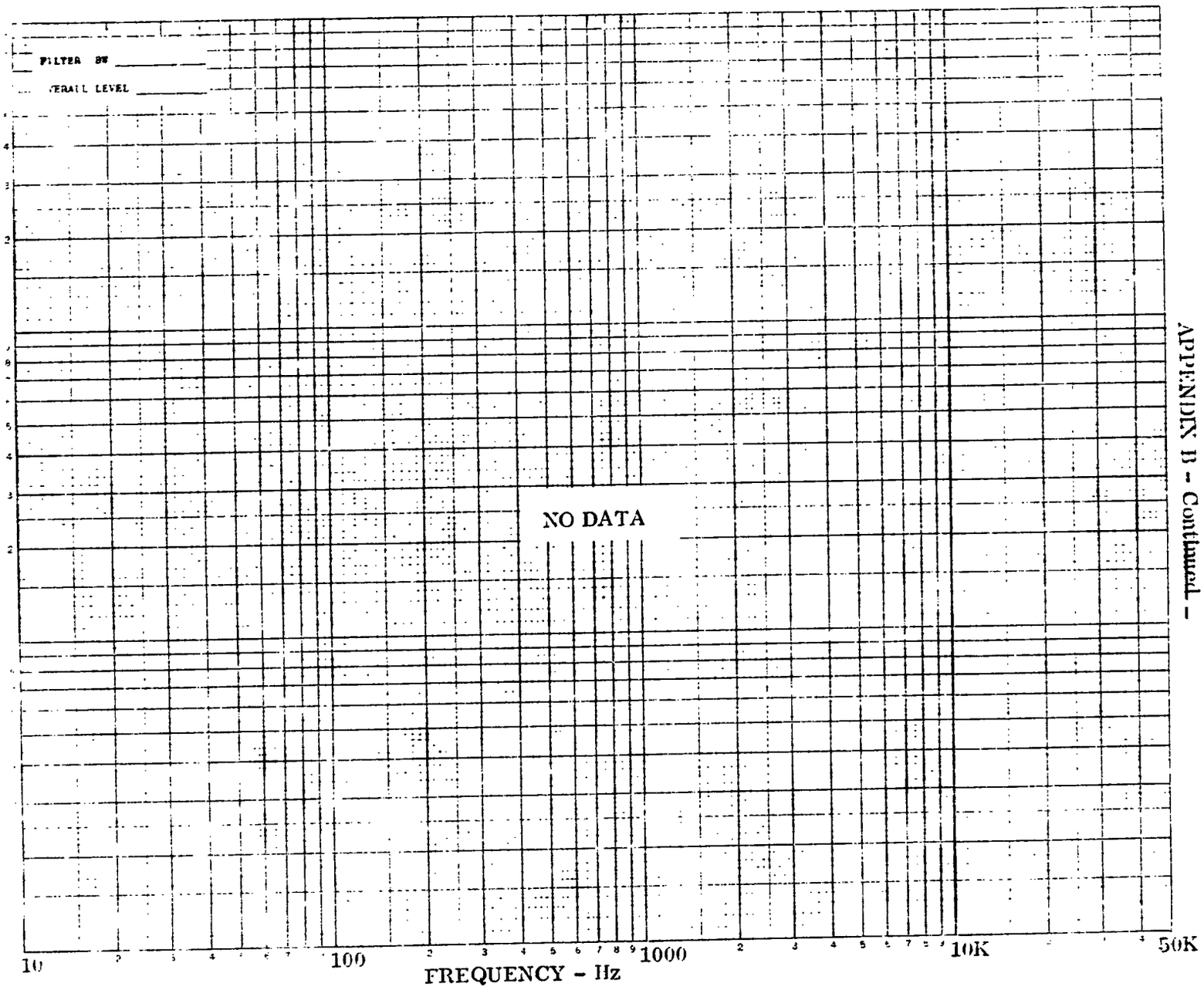

Figure B-5. Accelerometer No. 5, 158 dB OASPL, Cycle No. 1

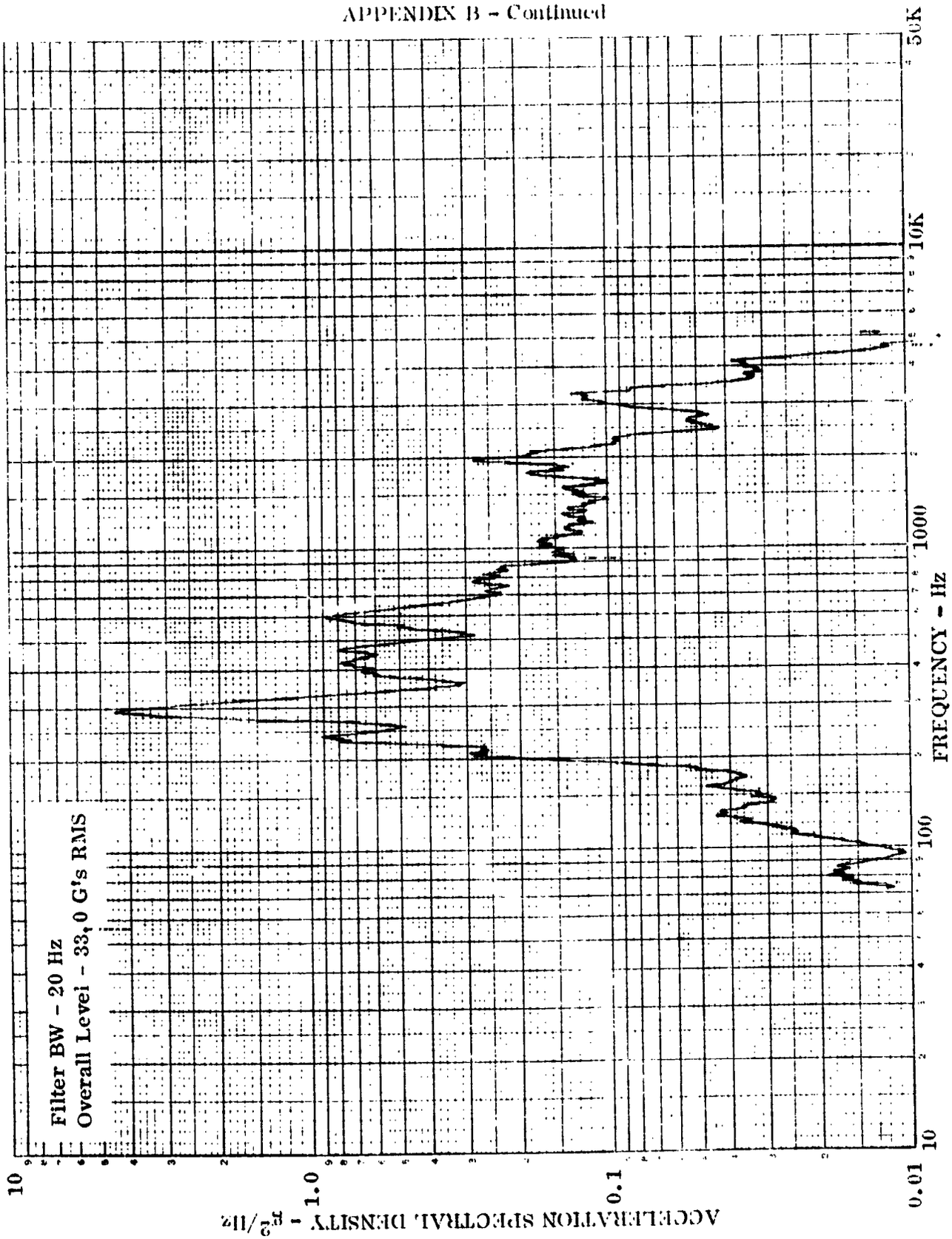

Figure B-6. Accelerometer No. 6, 158 dB OASPL, Cycle No. 1

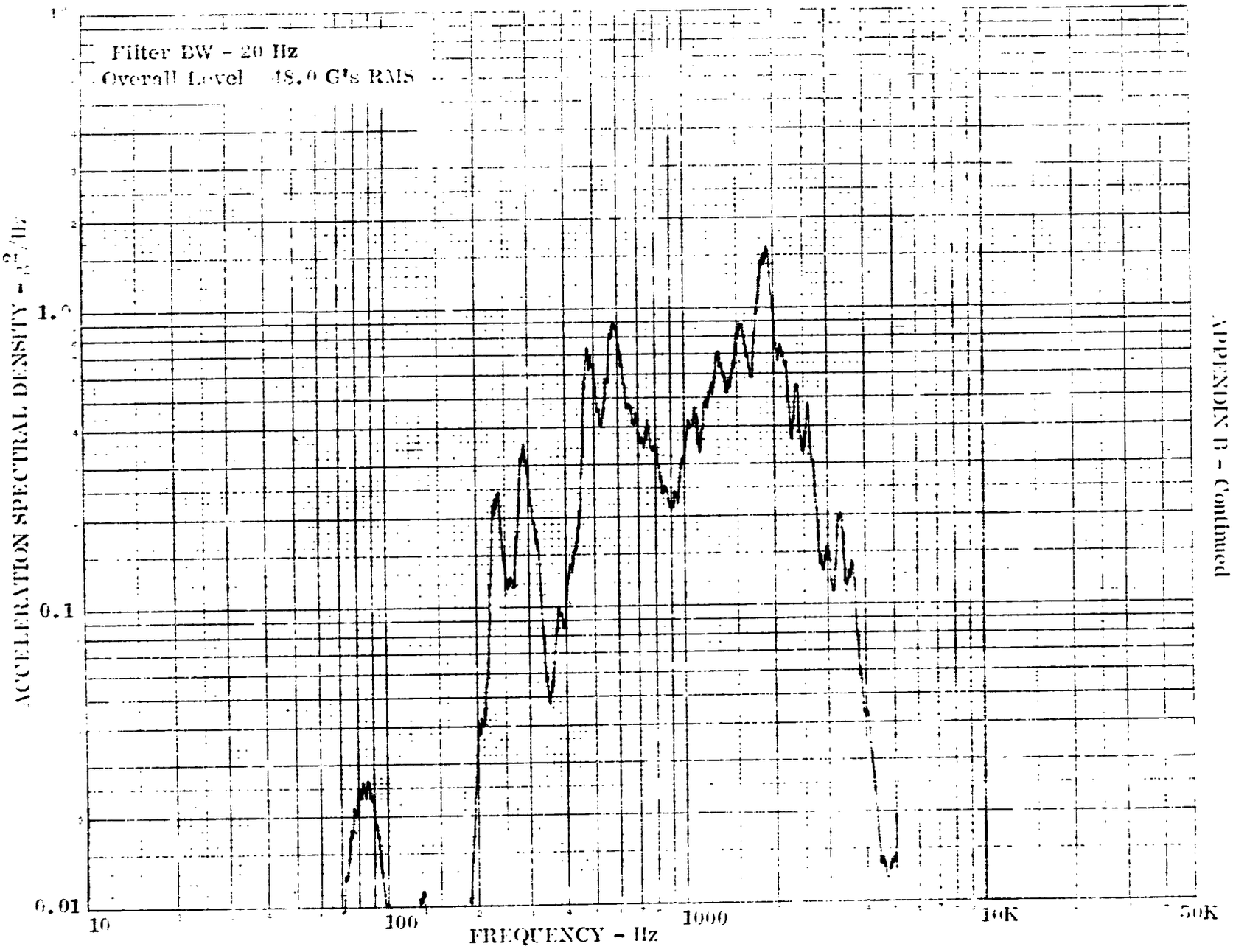

Figure B-7. Accelerometer No. 7, 15° dB OASPL, Cycle No. 1

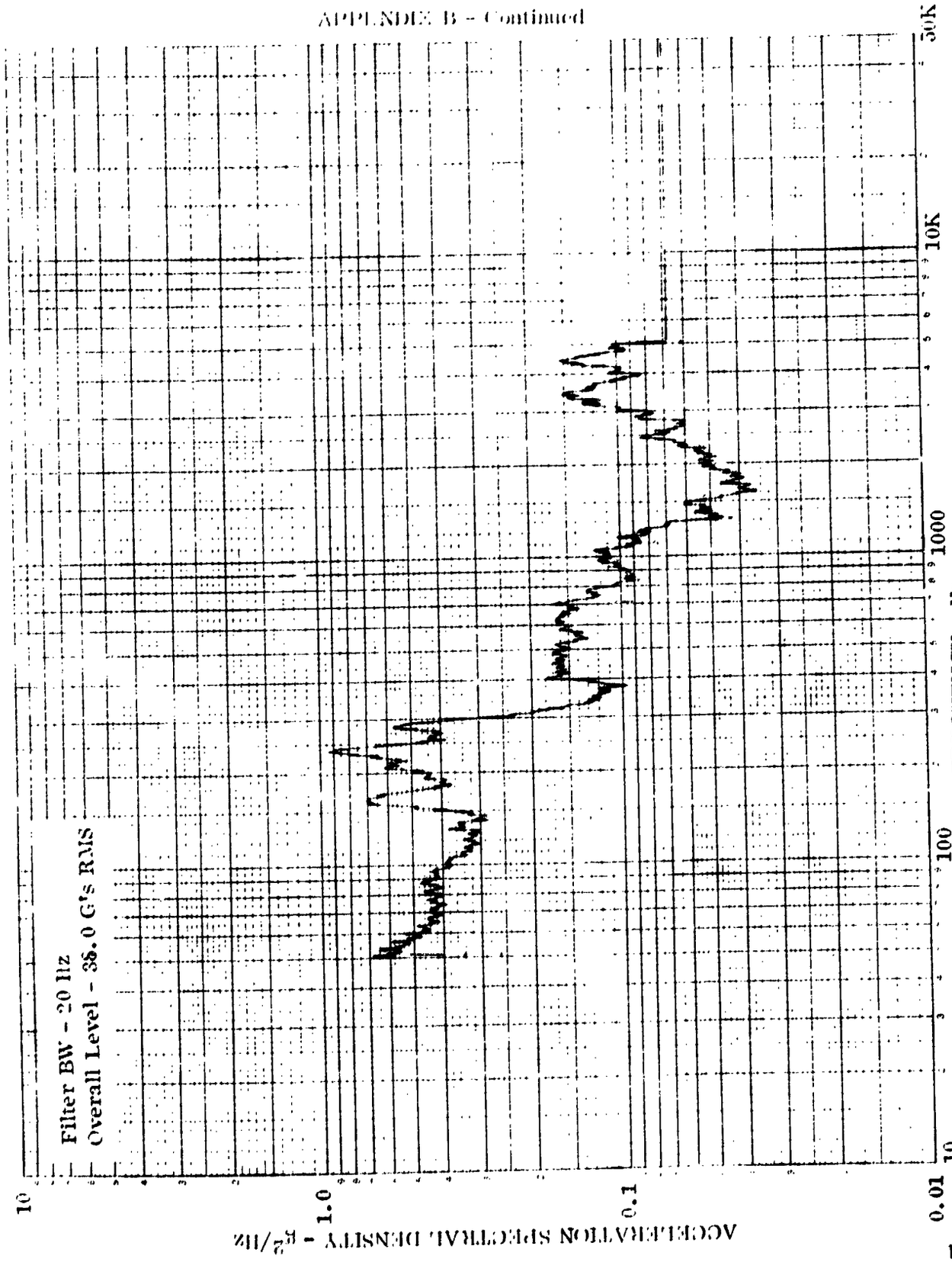

Figure B-8. Accelerometer No. 8, 158 dB OASPL, Cycle No. 1

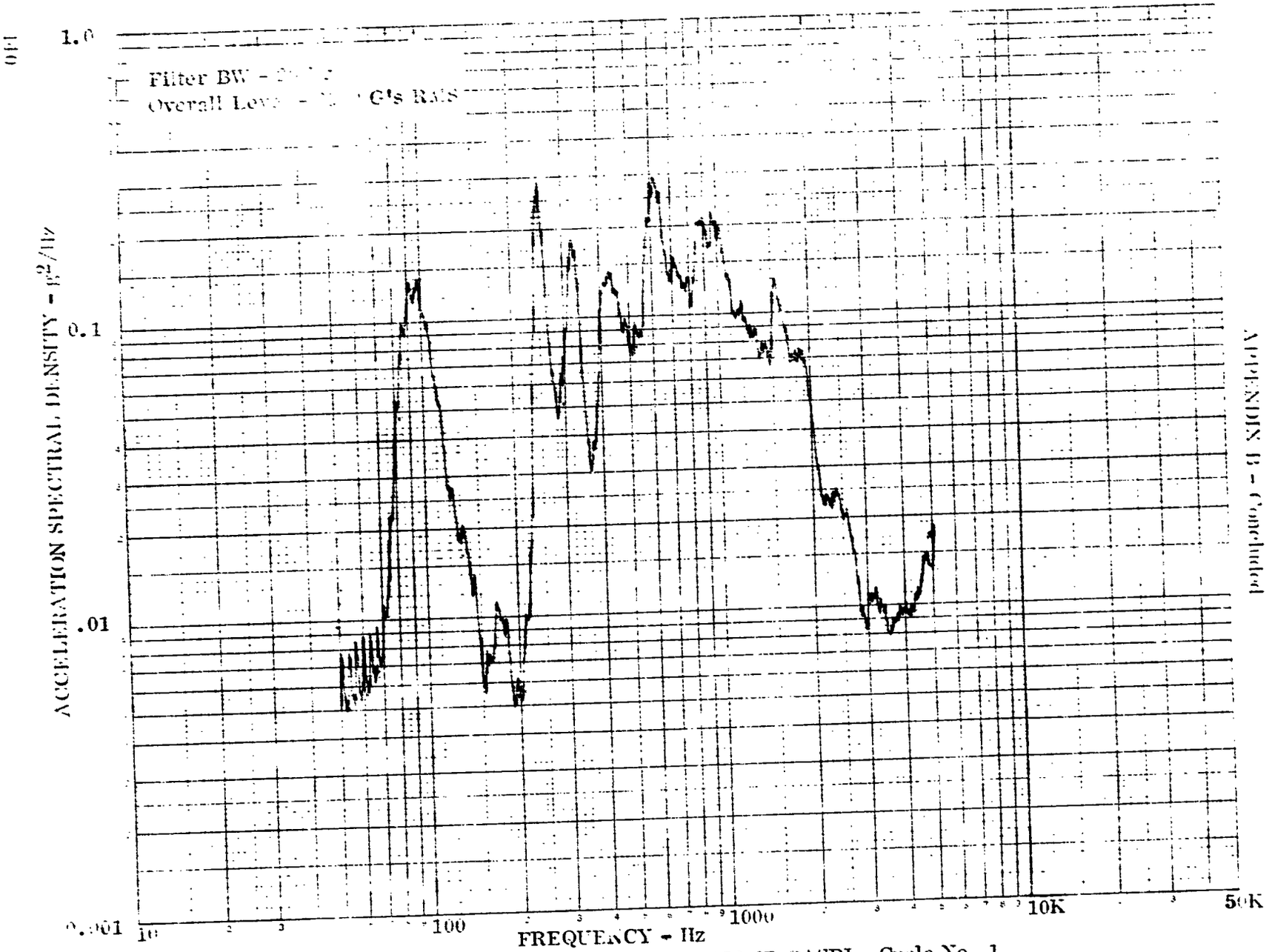

Figure B-9. Accelerometer No. 9, 138 dB OASPL, Cycle No. 1

APPENDIX C

RECOMMENDED TPSTF TEST PARAMETERS

The specimen described in Section 3.2 and shown in Figure 6-2 was designed for testing in the NASA Langley Research Center Thermal Protection System Test Facility (TPSTF). This tunnel is intended to provide a thermal environment at Mach 3.5 to 4.5 over a 2 by 3 ft. (61 by 91 cm) model surface. The expected maximum total enthalpy (H_T) in the test gas will be 3820 Btu/lb_m (8.88 MJ/kg). This is obtained by the combustion of methane (CH_4) with oxygen-enriched air. A schematic of the tunnel is shown in Figure C-1.

The recommended procedure is to establish supersonic air flow in the tunnel followed by ignition of a lean mixture of CH_4. This will provide an initial low heating rate over the test panel. [Based on previous thermal flow tests on columbium alloy specimens (References 1b and 13) the recommended maximum rate of rise is 25° F/sec. (16° K) sec).] A schedule of required heating with time will be programmed by controlling oxygen-enriched air mass flow and CH_4 ratios. The theoretical values of these components with combustor total enthalpy is shown in Figure C-2. Presented in Figure C-3 is the performance envelope of heat shield surface pressure and temperature that is expected to be obtained in the tunnel. The corresponding theoretical wall heating rates are presented in Figures C-4, C-5, and C-6. Shear forces are obtained from Figure C-7. Tunnel testing time will be limited by the supply of oxygen, air, and methane, and the transient heating rate schedule. A low heating rate schedule will give testing times up to 1500 seconds while it will be 400 seconds at a high heating rate schedule.

The entry history of panel surface temperature, heating rate and wall pressure desired for tunnel simulation is presented in Figure C-8, which shows a tunnel test time of 2500 seconds. It is noted that the high heating rates schedule that is required after 300 seconds will deplete the supply system very rapidly. Since the objective of the panel test is to simulate the high surface temperature and that only about 500 seconds of testing will be available for this test, a surface temperature schedule such as presented in Figure C-9 is recommended. As noted, the transient surface temperature rise and cooldown will be slightly less than 25° F/second (16° K/sec) and tunnel testing time within the available limit of 500 seconds. By staying within this limit it will assure control of the panel cooldown schedule. Also, the required heating rate and available pressure of the TPSTF tunnel is indicated. It is noted that the panel surface will radiate to the tunnel water-cooled wall which is expected to be at 1000° R (556° K) during tunnel operation at the high heating rates.

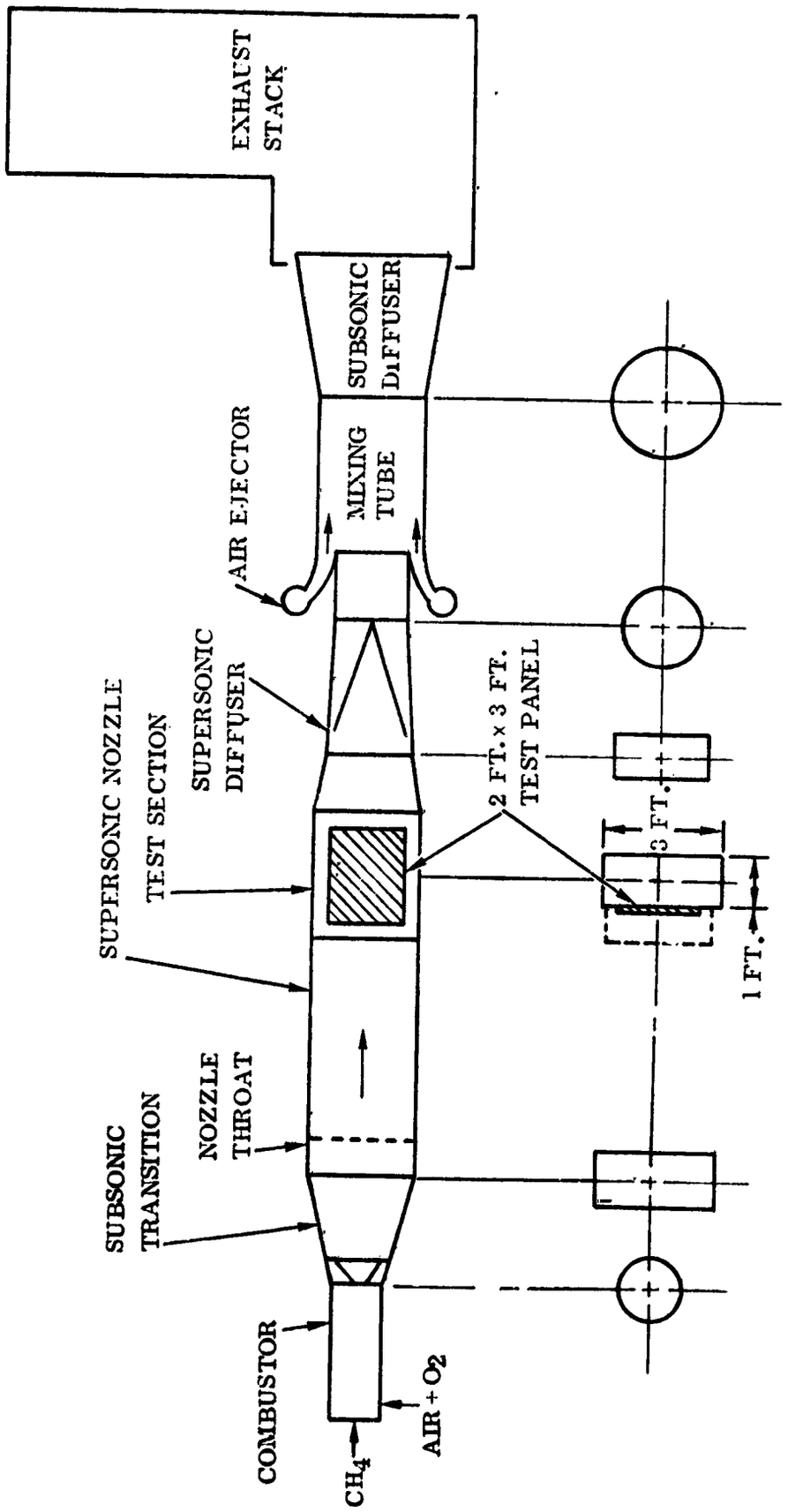

Figure C-1. Thermal Protection System Test Facility - TPSTF

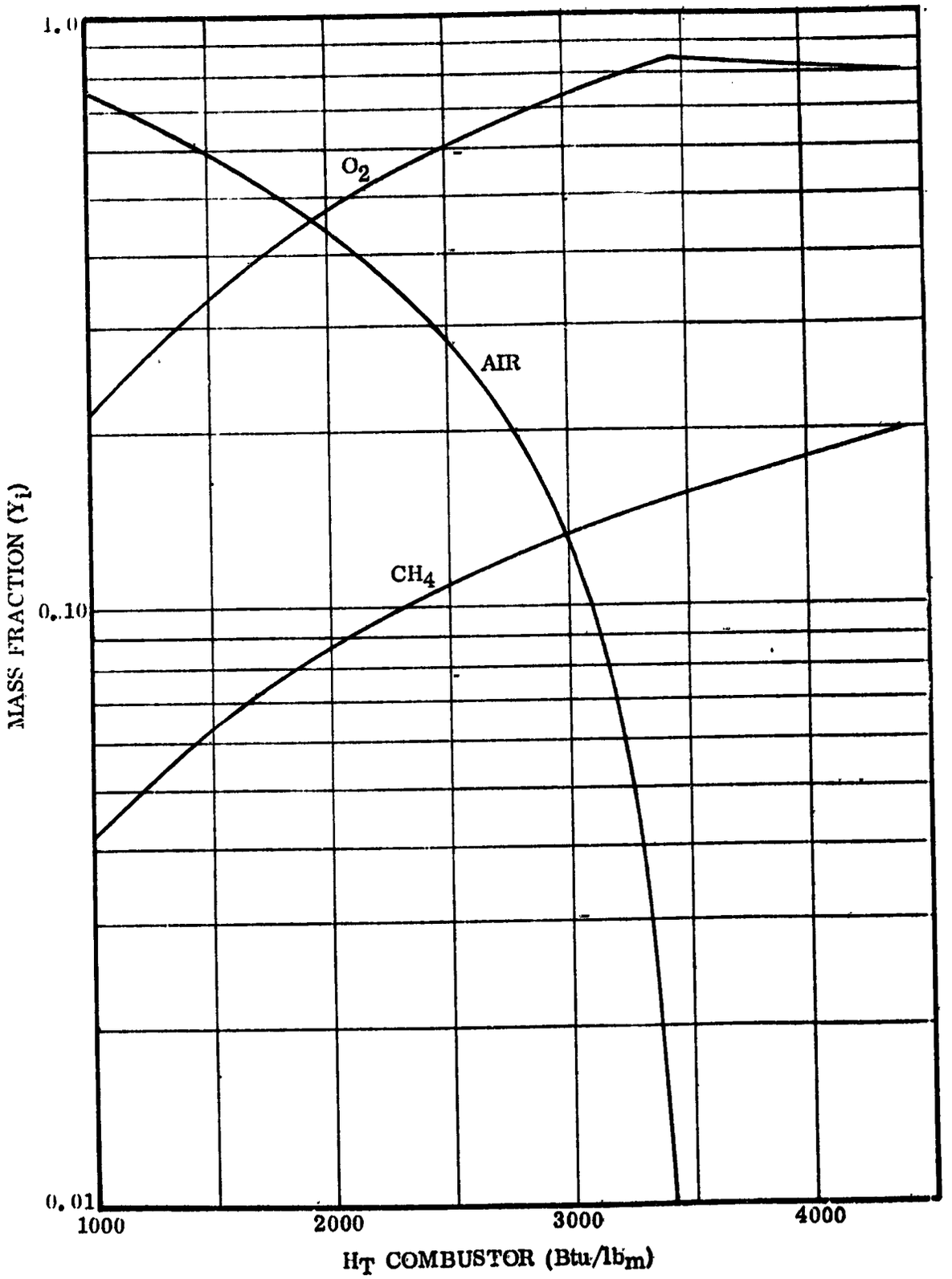

Figure C-2. Composition of Reactants in the TPSTF Combustor and the Resultant Enthalpies

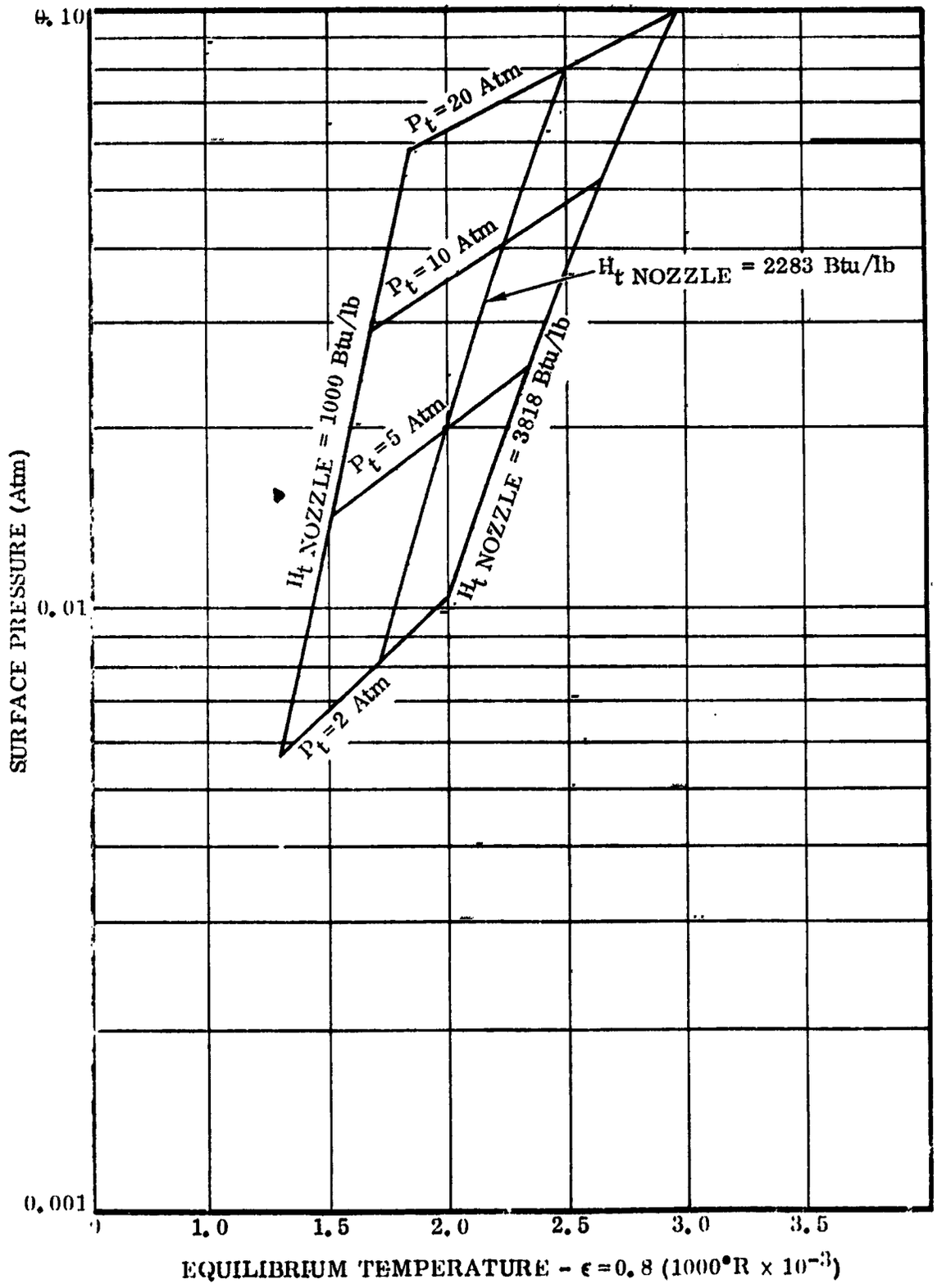

Figure C-3. NASA Langley TPSTF Capability for Structures – Panel Testing

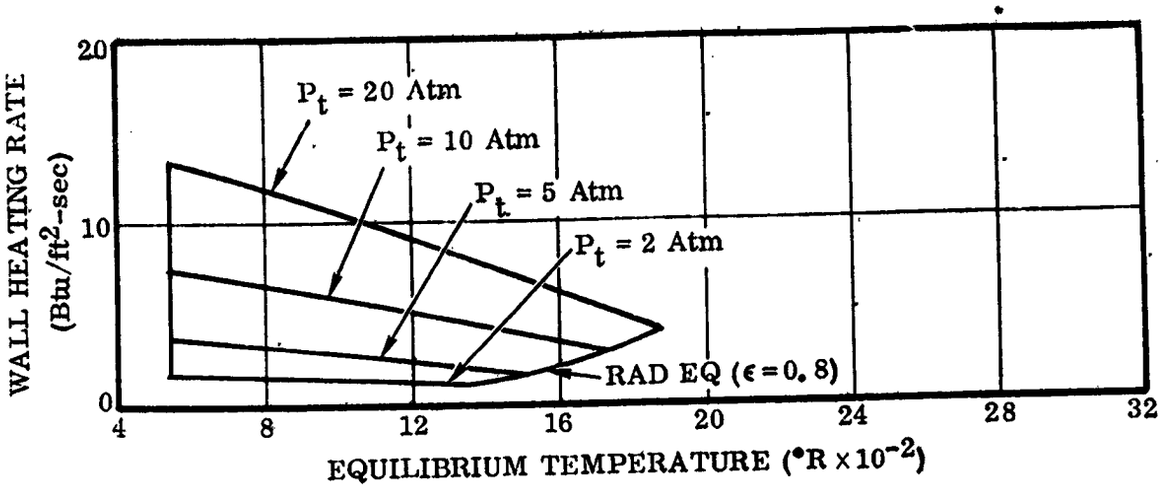

Figure C-4. Variation of TPSTF Heating Rate with Model Wall Temperature, H_T Combustor = 1200 Btu/lb_m

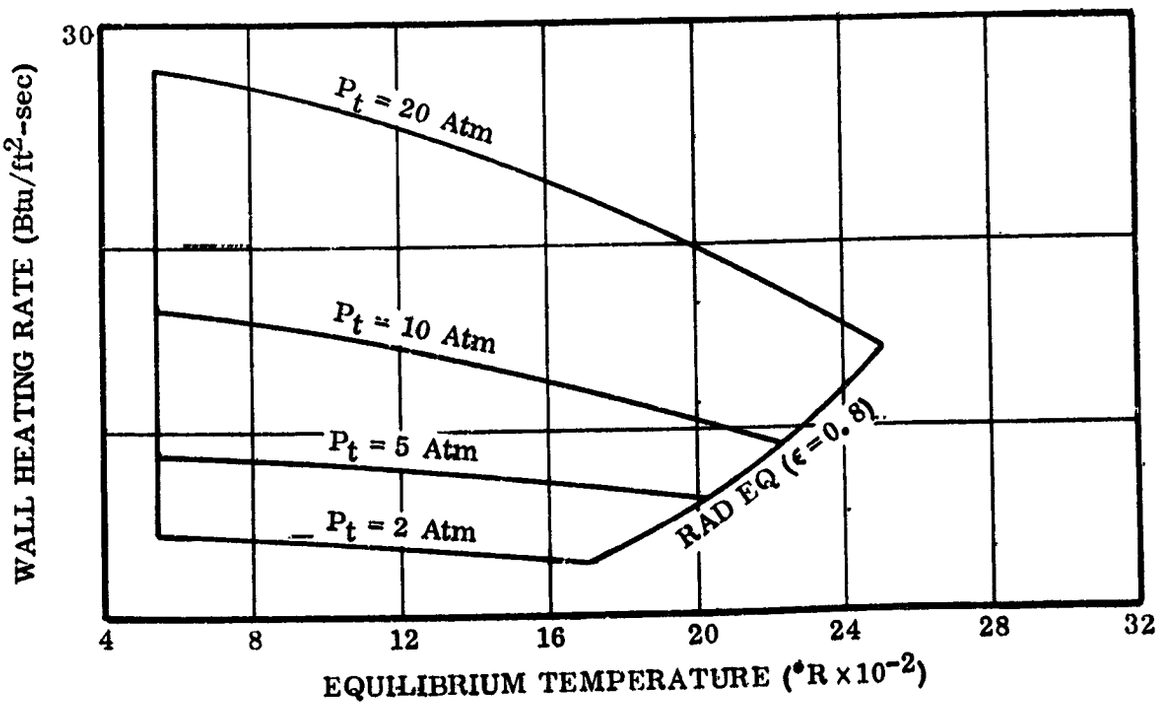

Figure C-5. Variation of TPSTF Heating Rate with Model Wall Temperature, H_T Combustor = 3000 Btu/lb_m

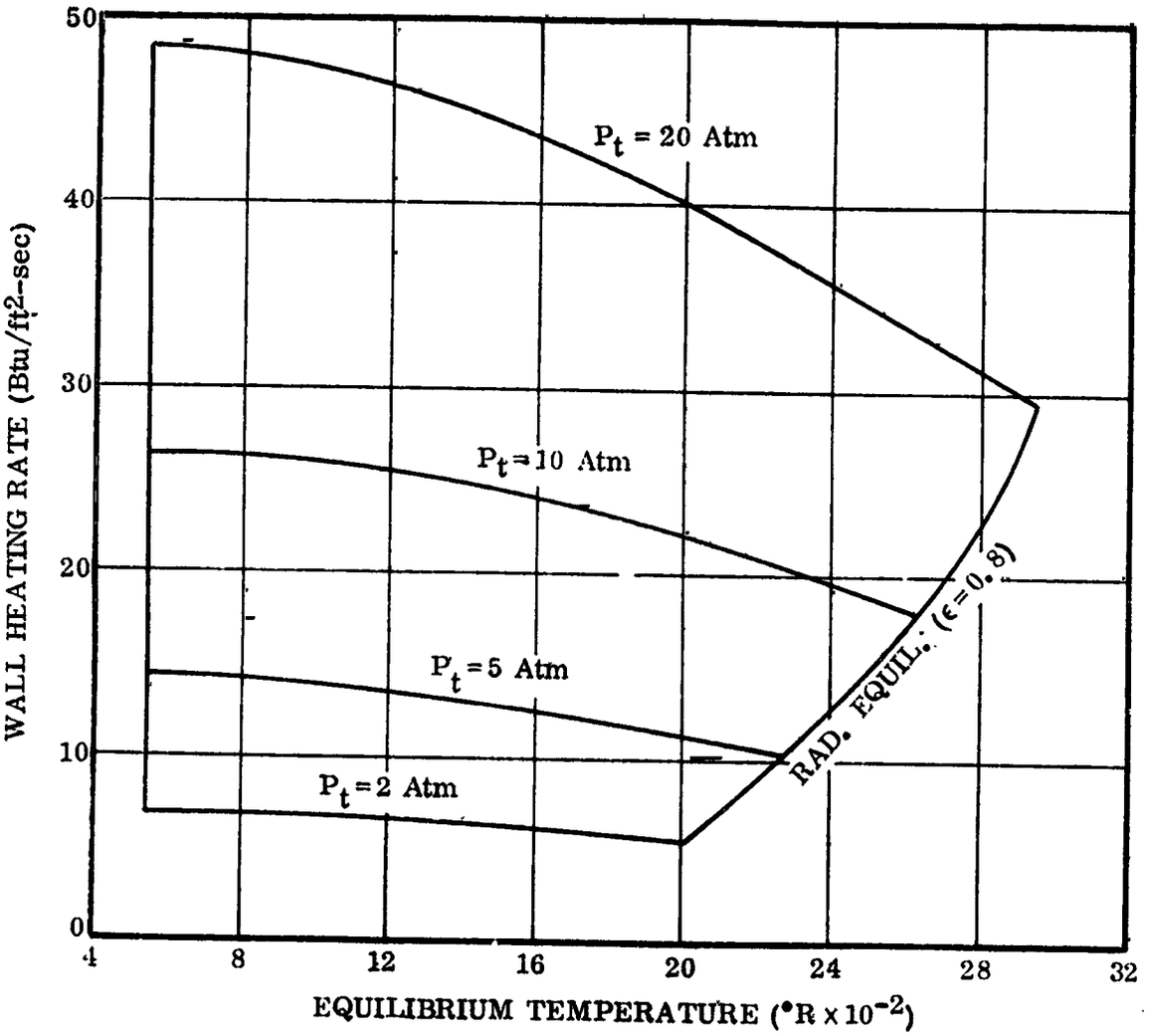

Figure C-6. Variation of TPSTF Heating Rate with Model Wall Temperature, H_T Combustor = 4400 Btu/lb_m

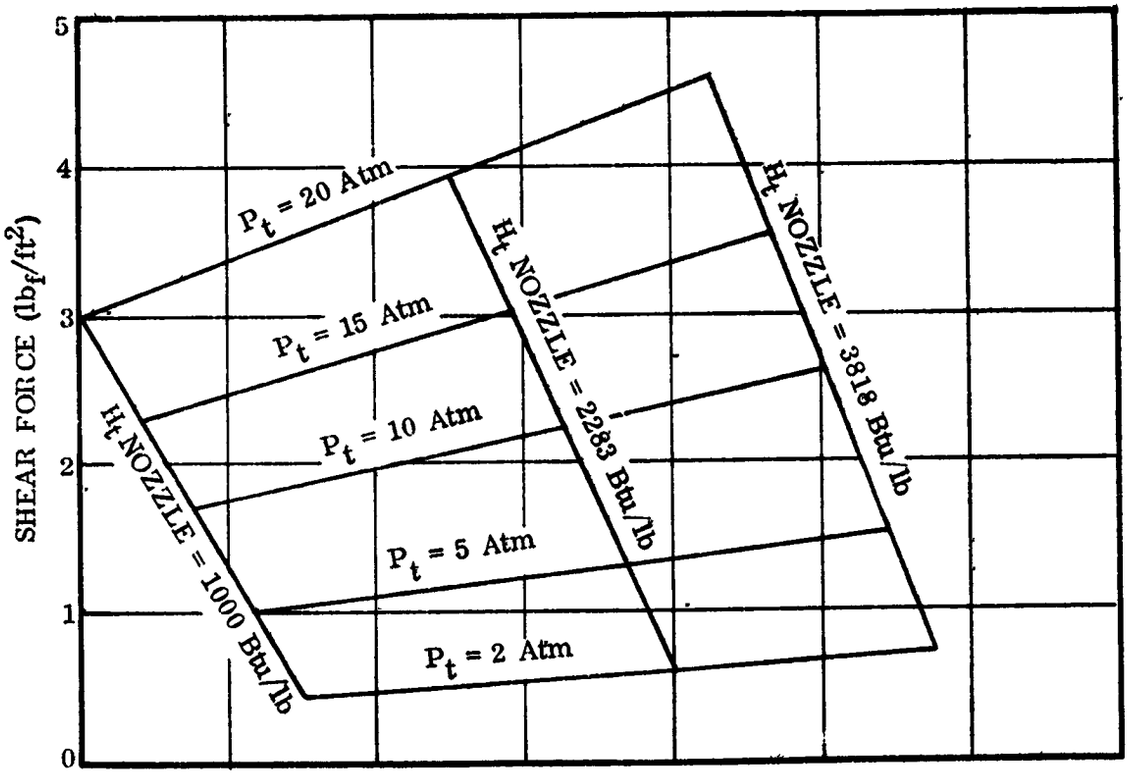

Figure C-7. Shear Forces on Walls of Test Panels in TPSTF

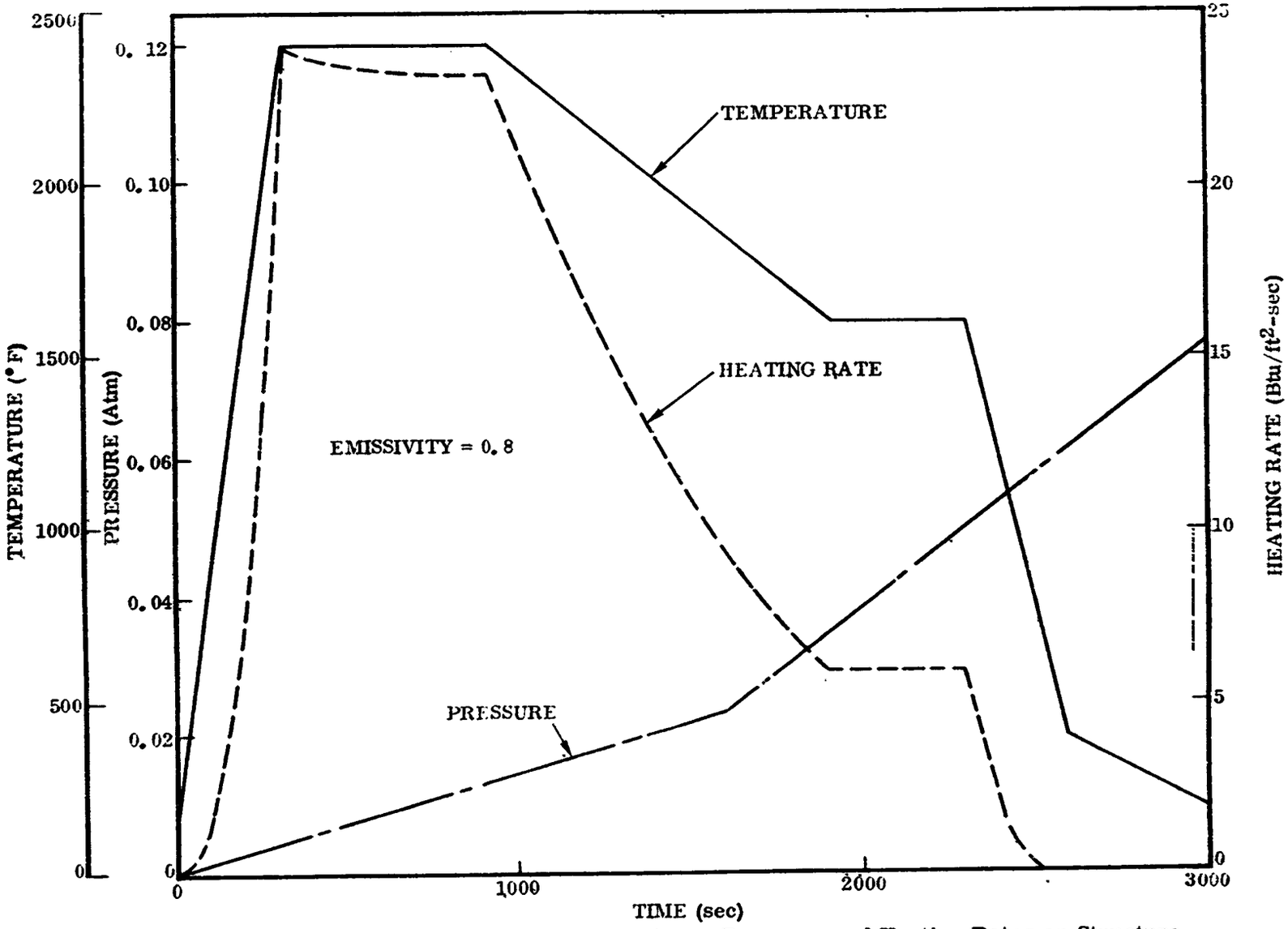

Figure C-8. Entry History of Surface Temperature, Pressure and Heating Rates on Structure

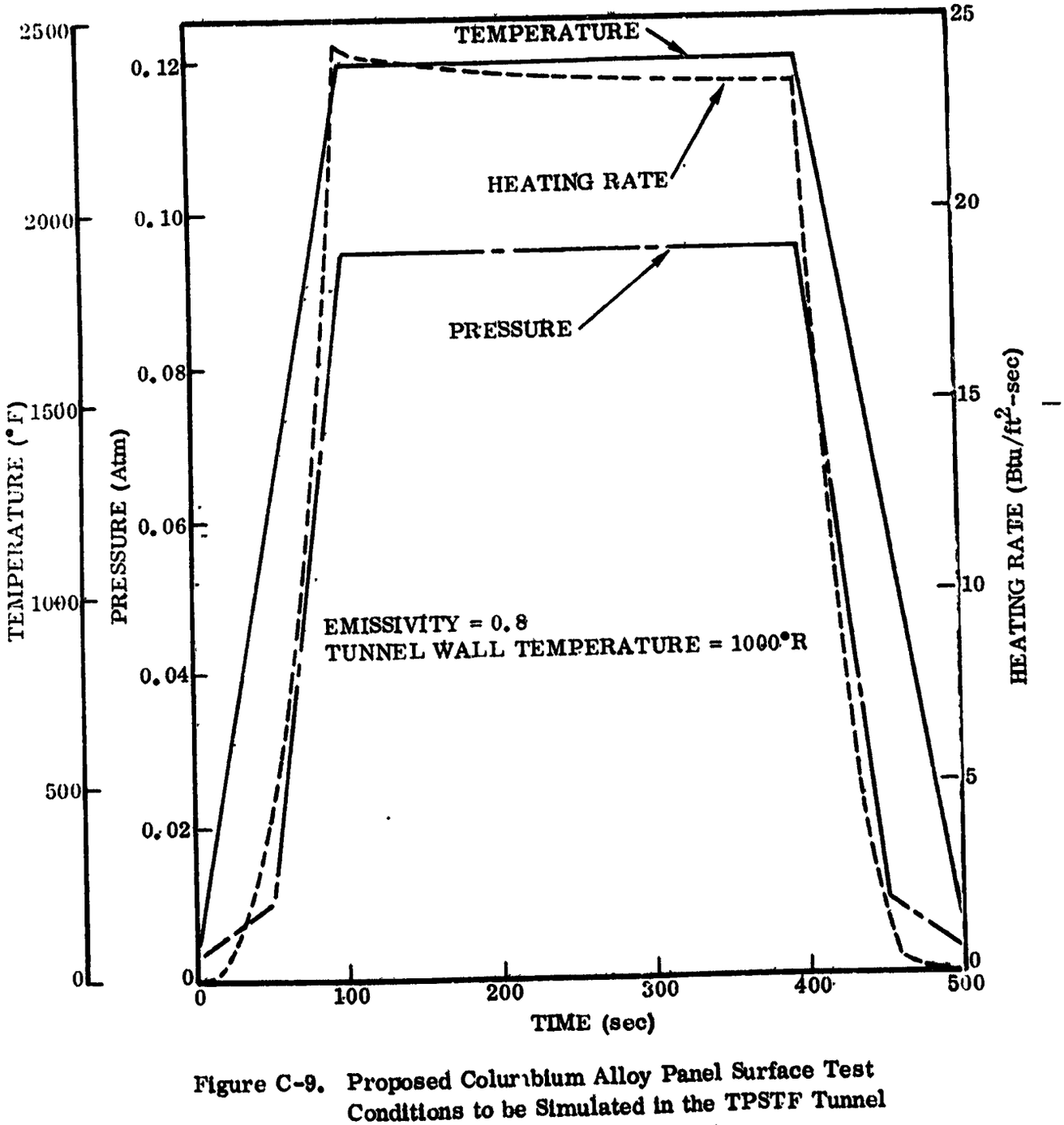

Figure C-9. Proposed Columbium Alloy Panel Surface Test Conditions to be Simulated in the TPSTF Tunnel

REFERENCES

1. Black, W. E., et al, Evaluation of Coated Columbium Alloy Heat Shields for Space Shuttle Thermal Protection System Application.
   a. Volume I, NASA CR-112119-1, June 1972.
   b. Volume II, NASA CR-112119-2, August 1973.

2. Hughes, T. A., High Temperature Insulation Materials for Reradiative Thermal Protection Systems, McDonnell Douglas Astronautics Company - East Report MDC E0666, Contract NAS8-26115, 19 July 1972.

3. Boren, H. E. and Campbell, H. G., Learning Curve Tables: Volume II, 86 - 99 Percent Slopes, The Rand Corporation, Memorandum RM-6191-PR (Volume III), April 1970.

4. Getline, G. L., Space Shuttle Booster Acoustic Environments, Convair Aerospace Division of General Dynamics Report 76-549-4-151/AD-71-28, May 26, 1971.

5. Cross, R. I., and Black, W. E., Optimization of Insulation and Mechanical Supports for Hypersonic and Entry Vehicles, AFML-TR-66-414, 4 April 1967.

6. Howard, J. L, and Torgerson, R. T., Techniques for Attaching Thermocouples to Disilicide Coated Refractory Alloy Materials, presented at the 1968 Annual Meeting of the American Society for Testing and Materials, June 23-28, 1968.

7. Toups, K. A., A General Computer Program for the Determination of Radiant-Interchange Configurations Factors, Technical Note ASD-TN-61-101, March 1963.

8. O'Neill, R. F., et al, Shadowed View Factors Program 3523, Convair Aerospace Division of General Dynamics.

9. Winiarski, L. D., et al, Computer Program to Evaluate Radiation Exchange Factors for Grey, Diffuse Surfaces (Script F), DDB64-003, Convair Aerospace Division of General Dynamics, 10 April 1967.

10. Anon., Thermal Property Data for Candidate Fibrous Blanket Insulation for Nuclear Reactors, General Atomic Company, February 1973.

11. Black, W. E., Lightweight Radiative Heat Shield Development, GDC-ERR-AN-1133, Convair Aerospace Division of General Dynamics, December 1967.

12. Culp, J. D., Field Repair of Coated Columbium Thermal Protection Systems (TPS). McDonnell Douglas Astronautics Company, - East Report MDC E0681, Contract NAS8-26121, 15 September 1972.

13. Black, W. E., Space Shuttle Vehicle High Temperature Load-Carrying Structure and Radiative Thermal Protection Systems, GDC-ERR-1497, Convair Aerospace Division of General Dynamics, June 1970.